UILU-ENG-81-2004

. ENGINEERING STUDIES

RAL RESEARCH SERIES NO. 490

RESPONSE OF REINFORCED CONCRETE PLATE-COLUMN CONNECTIONS TO DYNAMIC AND STATIC HORIZONTAL LOADS, VOLUME 1

By
DENBY G. MORRISON
and
METE A. SOZEN

A Report to the
NATIONAL SCIENCE FOUNDATION
Research Grant PFR 78-16318

UNIVERSITY OF ILLINOIS
at URBANA-CHAMPAIGN
URBANA, ILLINOIS
APRIL, 1981

RESPONSE OF REINFORCED CONCRETE PLATE-COLUMN CONNECTIONS TO DYNAMIC AND STATIC HORIZONTAL LOADS

By

Denby G. Morrison

and

Mete A. Sozen

A Report to the
NATIONAL SCIENCE FOUNDATION
Research Grant PFR-78-16318

University of Illinois
at Urbana-Champaign
Urbana, Illinois
April, 1981

50272-101

REPORT DOCUMENTATION PAGE	1. REPORT NO. UILU-ENG-81-2004	2.	3. Recipient's Accession No.
4. Title and Subtitle: RESPONSE OF REINFORCED CONCRETE PLATE-COLUMN CONNECTIONS TO DYNAMIC AND STATIC HORIZONTAL LOADS			5. Report Date 6.
7. Author(s): Denby G. Morrison and Mete A. Sozen			8. Performing Organization Rept. No. SRS 490
9. Performing Organization Name and Address			10. Project/Task/Work Unit No. 11. Contract(C) or Grant(G) No. (C) (G) NSF PFR 78-16318
12. Sponsoring Organization Name and Address			13. Type of Report & Period Covered 14.

15. Supplementary Notes

16. Abstract (Limit: 200 words)

The object of the investigation was to study the response of interior reinforced concrete plate-column connections. Eight specimens were tested, 5 "statically" and 3 "dynamically" (rate of loading significant). Other experimental variables were reinforcement ratio and the amount of superimposed vertical load. The specimens had certain common characteristics. Nominal slab dimensions were 1.8 by 1.8 m.; slab thickness was 76mm. The column was square with dimensions of 0.3 by 0.3m. The reinforcement layout in the slab was isotropic. The statically tested specimens provided information on the influence of the change in reinforcement ratio and the amount of superimposed vertical load on the response to horizontal loading. An analysis model (the "grid model") was developed to help interpret the results from the statically tested specimens. The dynamically tested specimens were used to obtain data on the response of the specimens, the observed hysteresis and calculated damping.

17. Document Analysis a. Descriptors

acceleration, beam, column, cyclic, damping, displacement, earthquake, frequency, hysteresis, linear, moment, plate, rotation, shear, slab, stiffness, strength, torsion

b. Identifiers/Open-Ended Terms

c. COSATI Field/Group

18. Availability Statement	19. Security Class (This Report) UNCLASSIFIED	21. No. of Pages 560
	20. Security Class (This Page) UNCLASSIFIED	22. Price

(See ANSI-Z39.18) *See Instructions on Reverse*

OPTIONAL FORM 272 (4-77)
(Formerly NTIS-35)
Department of Commerce

ACKNOWLEDGMENT

This study is part of ongoing research into the response of reinforced concrete structures at the Structural Research Laboratory of the Civil Engineering Department of the University of Illinois in Urbana. Research was funded by the Research Applied to National Needs program of the National Science Foundation under grant PFR-78-16318.

The dynamic tests were initiated by Fred Allen (Senior Lecturer, Swinburn College of Technology, Victoria, Australia), and the static tests by Prof. Ikuo Hirasawa (Dept. of Civil Engineering, Chubu Institute of Technology, Japan). Professor Hirasawa was responsible for the meticulous preparation and testing of the "statically" tested specimens and is sincerely thanked for his continuous advice.

Without the assistance of Professor V. J. McDonald and Mr. O. H. Ray -- ably supported by their laboratory staff -- the construction and testing of the specimens would not have been possible. Mr. G. Lafenhagen operated the testing equipment reliably and conscientiously, and his ready wit was refreshing.

Professors Gamble, Miller, Pecknold and Schnobrich were ready to help, and gave of their time unselfishly. Prof. Foutch also went out of his way to assist, and Prof. Scribner was most helpful in his comments.

The NSF advisory panel served to emphasize practical considerations. Members of the panel were M. H. Eligator of Weiskopf and Pickworth,

A. E. Fiorato of the Portland Cement Association, W. D. Holmes of Rutherford and Chekene, W. P. Moore Jr. of Walter P. Moore and Associates, and A. Walser of Sargent and Lundy Engineers.

Other researchers on the team managed to keep the working conditions cordial. Thanks are due to B. Algan, C. Wolfgram, P. Wilson, E. Schewe, J. Moehle and M. Kreger.

Mrs. P. Lane and L. Goode, and Miss J. Hubbard worked at the manuscript with good cheer and patience.

The CDC-Cyber 175 computing system of the Department of Computer Science was used for data reduction and analysis of the structures.

The reproduction and drafting sections of D. Jensen and R. Winburn were of a great help.

This report was prepared as a doctoral dissertation by D. G. Morrison with Professor M. A. Sozen.

TABLE OF CONTENTS

LIST OF TABLES

LIST OF FIGURES

FIGURE Page

FIGURE Page

1. INTRODUCTION

"Oh wonderful, when devils tell the truth!" (Richard III, Shakespeare). In the response of reinforced concrete plate-column assemblies to horizontal load, the "truth" may be hidden by the complicated nonlinear behavior of reinforced concrete sections, and the "three-dimensional" nature of response in a plate. In the paragraphs that follow the reasons for writing this report and what was attempted, will be introduced.

The flat-plate has a number of practical advantages. For example, formwork is simpler to erect and dismantle than for a beam-column design. The absence of protruding beams in flat-plate construction allows services to be routed with relative ease. In doubt is the relative flexibility of a plate-column connection compared with that of a beam-column joint--the result of which has marred the behavior of plate-column connections in earthquakes. The possibility of shear failure is also of concern. In some historically "earthquake-free" areas where flat-plate construction has been used extensively (such as New York) engineers are becoming aware of the need to consider seismic loading. Data on plate-column connections with dimensions more typical of those in tall structures are limited (column width to span ratio of about 1/6). This research document may provide guidance on these matters.

Eight specimens were tested, 5 "statically" and 3 "dynamically" (rate of loading significant). Other experimental variables were reinforcement ratio and the amount of superimposed vertical load. Designations of the test specimens used are as follows:

Designation	Rate of Loading	Reinforcement Ratio
S1	Static	0.65 %
S2	Static	0.98 %
S3	Static	1.31 %
S4	Static	0.98 %
S5	Static	0.98 %
D1	Dynamic	0.65 %
D2	Dynamic	0.98 %
D3	Dynamic	1.31 %

The statically tested specimens provided information on the influence of the change in reinforcement ratio and the amount of superimposed vertical load on the response to horizontal loading. An analysis model (the "grid model") was developed to help interpret the results from the statically tested specimens. The dynamically tested specimens were used to obtain data on the response of the specimens, the observed hysteresis and calculated damping. Much of the data, and experimental work, are described in detail in appendices. The relationship between chapters and appendices is as follows:

Chapters	Appendices
2. Outline of Experimental Work	C and D
3. Description of Experiments	C and D
4. Effect of Slab Reinforcement Ratio on Response to Increasing Load	E
5. Discussion of Observed Response of Specimens with Vertical and Lateral Load	E
6. Dynamic Tests: Discussion of Observed Response	F and H

Appendix A contains a description of the symbols used in the text; these symbols are also defined where they are used in chapters. Appendix B provides a literature survey. Owing to the large amount of raw data,

this report has been divided into two sections. Appendices E, F, G and H compose the second portion; it may be obtained from the University of Illinois at Urbana-Champaign.

The object of the research was: (1) To investigate the response of plate-column connections to horizontal loading, with emphasis placed on serviceability requirements. (2) To attempt to understand the strength of the specimens as a function of the change in reinforcement ratio. (3) To investigate the influence of the rate of loading on the strength of the specimens. (4) To provide information on the hysteresis of the moment-displacement relationships. (5) To obtain data on the equivalent viscous damping in the dynamically tested specimens.

2. OUTLINE OF EXPERIMENTAL WORK

2.1 Introduction

The overall configuration of the test structures was governed by equipment and modelling limitations, and the object of the tests. In all, 8 specimens were tested; 5 were tested "statically" and 3 "dynamically". A description of the specimens and the variables chosen follows. Appendix C has a detailed account of the specimens tested "statically," and Appendix D of those tested "dynamically".

2.2 Description of Specimens

There is a certain amount of ambiguity in the literature on investigation of slab-column connections because of the definitions of terms describing locations and directions. To reduce the causes of confusion, Fig. 2.1 is presented to define the terms relevant to the test specimen. This figure also serves to introduce the reader to the simple column-slab connection chosen to represent the structural system. All the specimens, whether they were tested statically or dynamically, had certain characteristics in common.

It was decided that the specimens would represent a third-scale interior column-slab connection. This scale was manageable on the Earthquake Simulator of the University of Illinois. The material properties in the specimens were expected to give a faithful representation of full-scale reinforced concrete.

Multiple-bay specimens were considered, but found to have some disadvantages. To test them successfully on the Earthquake Simulator they would have to be reduced further in scale to about 1/10th of full size; the material properties would be questionable because of their small scale. The simplicity of the single connection was attractive,

especially when considering "dynamic" testing. Furthermore, many researchers (Hawkins, Criswell, for example) have used the isolated column with profit for investigating flat-plate structures. The testing of multiple-bay specimens (Criswell 11, 12; Hawkins 20,21) provided information on the redistribution of load after failure of a single connection; this action was associated with large displacements that would violate serviceability requirements. The isolated column-slab connection was chosen.

Important features of the geometry of the specimens were kept constant in all the specimens; column length was different for the static and dynamic testing for practical purposes only. The slab was square, and had a length and breadth of 1829 mm (Fig. 2.2). Its thickness was also a "constant," and measured close to 76 mm. (Refer to Fig. D .3 for the as-built dimension.) The end boundary was simply supported, and the side boundary left free. (Refer to Appendix C and Appendix D for a detailed description of the supports.) The literature survey in Appendix B proved the boundary conditions on the side boundary to have a negligible influence on the behavior. The column, too, had a square cross section, and measured 305 by 305 mm. In relation to the slab it was very stiff. Thereby a reasonable modelling of the proportions of a high-rise flat-plate structure were achieved. The base of the column was hinged, and the top was loaded at the point indicated in Fig. 2.2. By these boundary conditions points of contra-flexure were modelled -- in the actual building at midspan of the plate and midheight of the column. This moment distribution, implied by the

choice of contraflexure-points, is also reasonable to expect in the lower levels of a plate-column structure.

The relative stiffness of the column with respect to the plate in the specimens was expected to realize a single degree of freedom; that of the rotation of the column about the base hinge. Resistance to the motion would be provided by an elaborate spring -- the deformation of the slab (refer to Fig. 2.3).

It should be pointed out that the "working" portion of the test specimen is the slab, the "output" being the moment-rotation relationship at the face of the column. In relating the model to the "full scale" structure, the parameters to be used are the slenderness of the slab and the relative size of the column (span/slab depth = 24; column width/span = 1/6). Lateral motion was restricted (see Appendix C and D).

Even though the reinforcement ratio in a particular specimen may be different from that of another specimen, the reinforcement layout was a further "constant" for the specimens. The steel was placed in a mat with the spacing of the reinforcing bars the same in the two principal directions (see for example Fig. C.4). A mat was positioned at the top and another at the bottom of the slab, providing an isotropic reinforcement configuration.

The materials were selected carefully to have as uniform a concrete-and-steel property for all the specimens as possible (Table 2.1).

2.3 Variables

Three major variables were envisaged: (1) the reinforcement ratio, (2) vertical load was applied to the plate and (3) rate of loading.

The bar-chart of Fig. 2.4 shows how the reinforcement ratio was varied in the statically tested specimens. These five specimens will be referred to as S1 to S5. Specimen S1 contained steel at a ratio of .65%, S2 had .98% and S3 had 1.31%. These three specimens (S1 to S3) were to be tested to investigate the influence of reinforcement ratio on the behavior of the connection. Specimens S4 and S5 had the same reinforcement ratio as S2 as they were to be used to investigate the effect of a further variable.

Figure 2.5 is a bar-chart indicating the superimposed slab load. The like reinforcement ratio of S2, S4 and S5, but differing superimposed vertical load carried by each, provided a comparison of the influence of vertical load to the plates. The reaction at the base of the column for specimen S5 (Fig. 2.5) was 28.6 kN, or about a shear stress of $.06\sqrt{f'_c}$ (f'_c in MPa) at a section one-half the depth of the slab away from the column face. This shear stress may be thought of as resulting from a total uniform load of 8.7 kPa (180 psf) for a column with a tributary area of 6 x 6 m (18 x 18 ft) and slab effective depth of 200 mm (8 in.). (Given a dead load of 5.4 kPa (110 psf), with a dead load factor of 1.2, the loading conditions may be considered as including a superimposed load of 2.3 kPa (48 psf).)

By having reinforcement ratios in the three "dynamically" tested specimens (D1, D2 and D3) comparable to those of S1, S2 and S3 respectively, the third variable was introduced: "static" versus "dynamic". For the "statically" tested specimens (S1 to S5) the horizontal load was applied by a hydraulic jack to the position on the column indicated in Fig. 2.2. The loading was cyclic, and at a rate that would exclude any significant inertial forces (Fig. 2.6). On the other hand the

"dynamically" tested specimens (D1 to D3) were subjected to a variety of base motions on the earthquake simulator. At the same point at which the jack provided horizontal load for the "static" tests, additional mass was placed to provide significant inertial forces in the "dynamic tests" (Fig. 2.2). Appendix C and Appendix D provide detailed descriptions of the specimens.

3. DESCRIPTION OF EXPERIMENTS

3.1 Introduction

The purpose of this chapter is to acquaint the reader with quantitites that will be used in the discussions to follow. A detailed character sketch of these participants is given in Appendix C (Static Tests) and Appendix D (Dynamic Tests).

The test procedure will also be discussed.

3.2 Characters

3.2.1 Static Tests

A load cell in the servo-ram kept track of the applied horizontal load at all times. This force was an important parameter used to correlate the other measured quantities with one another.

Horizontal displacements were measured at various heights on the column (Fig. C.9). From these, two important quantities were derived for the complete history of loading. One was the rotation of the column-slab connection. The measurements were made on the column close to the connection and possible column deformation was minimized. These measurements could identify deterioration that may take place in the plate close to the column face; damage at one face of the column could thus be compared with damage at the opposite face. The other important quantity obtained from the horizontal displacement measurements was the horizontal displacement at the level of the ram. In the dynamic tests the displacement at this level was also measured, enabling a direct comparison between the static and dynamic response.

Along the slab centerline in the direction of loading, vertical displacements were measured (Fig. C.10 and C.11). From these a profile

of vertical deflection was obtained at various loading times during testing. In the subsequent analysis of the response of the slabs, these profiles provided an important bench mark by which to evaluate calculations.

Further vertical slab deflection measurements along the longitudinal centerline were of importance in observing distress in the slab; a relative vertical parting of fiber, such as would be expected with punching failure in a slab, would be noticeable.

In the lateral direction, along two lateral parallel lines running past the front and back faces of the column, vertical displacements were measured at various times during testing (Fig. C.10 and C.11). By dividing the difference between two corresponding instruments by the distance between the two parallel lateral lines the twisting of the portions of the plate to the side of the column could be deduced. The value of this twist quantity was important in the analysis--particularly in obtaining torsional deformations.

Along about the same lateral line mentioned in the observation of twist in the plate, strain gauges were attached to the longitudinal reinforcing bars (Fig. C.4, C.5, and C.6). The gauges were placed along a single lateral line passing by the front face of the column; one gauge was positioned on the top bar and another directly below it on the bottom bar. These gauges provided invaluable information on how far yielding of the section had spread across the width of the plate.

For those specimens that had added vertical load (S4 and S5) the vertical reactions were measured. From these forces it was possible to know the average shear stress around the column.

The various response quantitites are exhibited in detail in Appendix E.

3.2.2 Dynamic Tests

Accelerometers and LVDT's (differential transformers) measured absolute accelerations and relative displacements at various heights on the structure (Fig. D.12). From these the response could be plotted by relating the moment of the horizontal forces (about the hinge at the base of the column) with the relative displacement at the position of the attached mass. This moment was resisted by the action of the slab at the slab-column connection.

The acceleration measured at the base during "steady-state" tests was also compared with that measured at the position of the idealized single degree of freedom system, and amplification information was obtained. From these amplifications, deductions could be made about the effective stiffness of the specimen (resonance) and the damping in the assembly.

Also forthcoming from the acceleration measurements were the "free-vibration" records. They too were of importance to deductions about the effective stiffness and damping.

A detailed description of the data is available in Appendix F.

3.3 Test Procedure

3.3.1 Static Tests

All specimens were tested by applying lateral displacement reversals. The maximum load for each cycle was controlled by the column rotation angle (practically, the displacement of the top of the column). Three load levels were applied, each consisting of 5 cycles, corresponding to a rotation angle of 1/400, 1/200, and 1/100, respectively. Thereafter, two large cycles were applied corresponding to the rotation angle

of 1/50. After that the specimens were loaded to failure. The loading pattern is shown diagrammatically in Fig. 3.1.

Displacements, loads, deflections, rotations and strains were measured after each increment or decrement of displacement during any cycle of load. Crack patterns for the slab were recorded at the first cycle to a given maximum level. The eighteen dial gages were also read at the first cycle to a new maximum load level, and during the last incremental loading to failure. The tests were monitored by plotting the applied load versus displacement at the top of the column level on an X-Y recorder.

Each test was completed within approximately seven hours.

3.3.2 Dynamic Tests

Response to three types of motion were recorded during the testing of a specimen: Simulated earthquake, steady-state and free-vibration.

The simulated base motion was the North-South component of the 1940 El Centro record. In the steady-state testing a sinusoidal base excitation with constant displacement amplitude was used; the input frequency was incremented to span the range of response from before the resonance of the specimen to after this occurrence. By connecting a wire to the steel capping plate on the column and hanging weights at the other end of the wire, a free-vibration motion was intorduced when the weights were released instantaneously.

As far as was possible, the described motions were performed in the same sequence for each of the dynamically tested specimens. This idealized test program is listed in Table 3.1. The actual sequence for each test is shown in Fig. 3.2 to Fig. 3.4. In these idealized diagrams, the ordinate is the maximum displacement measured at the position of the attached column-mass ("FV"=Free-Vibration and "SS"=Steady-State).

4. EFFECT OF SLAB REINFORCEMENT RATIO ON RESPONSE TO INCREASING LOAD

4.1 Introduction

In the statically tested specimens the two variables were the reinforcement ratios in the plates, and the amount of superimposed dead load. This chapter will concentrate on the first variable.

Comprehensive response information is available in Appendix E.

A "Grid-Analysis" will draw on observed force-displacement relationships, deflections on the longitudinal axis, twisting angles on the lateral axis to the side of the column, strain measurements and crack patterns to explain the relationships among observed quantities.

4.2 Effect of Reinforcement on Strength and Stiffness, General Remarks

4.2.1 Comparisons with Previous Research

One approach to evaluating the strength of the specimens is to compare the observed strength with that which could be achieved if the plate were to act as a wide beam. This mechanism--merely two-dimensional in character--is described in Appendix B with an illustration in Fig. B.3. The strengths calculated in this way are given in Table 4.1, and Fig. 4.1 shows the ratio of observed to calculated strength as a function of the reinforcement ratio. The lightly reinforced specimen, S1, came close to achieving this "wide-beam" mechanism; the more heavily reinforced specimen, S3, was well below this "possible" strength (Fig. 4.1). Specimen S2, with an intermediate amount of reinforcement, was consistent with the observed trend; it reached a strength closer to its possible "wide-beam" strength than the heavily reinforced specimen S3,

yet not as closely as the more lightly reinforced Specimen S1.

An alternative way to consider the plate-column connection is by calculating the limit that the column faces can carry if those plate portions framing into the column are taken as beams: called the "beam-analogy" by Park and Islam (39). A comprehensive description of this approach is provided in Appendix B (Section B.2.5, Fig. B.7). The more heavily reinforced specimen S3 had an observed strength 25% larger than the calculated "beam-analogy" value. A similar value calculated for the lightly reinforced specimen S1 underestimated the strength by 18% (Table 4.1).

The measured moment-rotation relationships of specimens S1 to S3 are compared with the two methods for strength calculation, "wide beam" and "beam analogy," in Fig. 4.2.

4.2.2 Observations on Shear

It is tempting to ascribe the inability of the more heavily reinforced specimens S2 and S3 to develop their potential "wide-beam" strength to a limit imposed by the shear strength of the connection. In the beam analogy this shear limit is introduced via torsion on the two lateral column-slab junctions and reactions on the remaining two faces.

No faulting was observed on the surface of specimens S2 and S3 to support the hypothesis of a shear failure as it was in specimens with superimposed vertical load. For specimens S4 and S5 faulting in the slab was conspicuous.

In all statically loaded specimens, continuous measurements were made of slab vertical deflection at a location four slab thicknesses away from the column face (Fig. 4.3 and Fig. C.9). To evaluate those measurements with respect to possible effects of shear failure, it is of

interest to compare readings made in specimen S3 with those in specimen S4 (that had superimposed vertical load).

Figure 4.4 shows two sets of measurements for each of specimens S4 and S3: force-displacement (vertical slab deflection as shown in Fig. 4.3a) and force-rotation curves (Fig. 4.3b).

The force-rotation curve for S3 (Fig. 4.4e) indicates that the load increased at a low rate as the rotation increased beyond the "yield" level up to the point where the specimen was unloaded. The force-displacement relationship for the same specimen (Fig. 4.4d) was qualitatively quite similar to the force-rotation curve.

For specimen S4, there was a reduction in force as the rotation was increased beyond approximately 5 percent, indicating a breakdown in the resistance mechanism (Fig. 4.4b). The force-displacement curve (Fig. 4.4a) shows that while rotation was increasing, after load 34.61, the vertical deflection decreased. This observation suggests that an inclined crack separated the zone within the immediate vicinity of the column from the rest of the slab. The column was torn away from the slab in that portion of the specimen.

Lack of similar observations for S3 indicates that its reduced strength (with respect to the flexural strength of the entire width) cannot categorically be ascribed to the full development of a critical inclined crack within the slab.

4.2.3 Crack Patterns

In general, crack patterns in specimens S1 to S3 were similar. However, there was a difference in the trajectories of the major cracks (shaded areas in Fig. 4.5). The inclination, in the horizontal plane and with respect to the lateral axis, increased with the amount of reinforcement (Fig. 4.5a to c).

4.3 The Grid Model

4.3.1 Introduction

The "wide-beam" and "beam-analogy" resulted in a wide range of calculated strengths for the same specimen. Besides, these methods are restricted to strength calculations -- they do not address the problem of stiffness.

A model is presented to help understand the observed force-displacement relationships in terms of geometric and material properties of the specimens. The model, built up of a grid of beam elements responding in flexure and torsion, is described in the following sections.

4.3.2 Description of the Grid

In matching the behavior of a portion of slab, the grid method replaces this portion by beams. Properties of the beams are derived by matching the curvature of the plate portion for a given force with that of the beams under a like force; this pairing considers the curvature due to pure flexure in two directions and the curvature due to pure torsion. A concise description of the procedure is available in Yettram et al (51).

A square grid pattern was used, with a square portion of plate represented by four beams along its boundaries. For a Poisson's ratio of zero a square pattern results in equal flexural and torsional rigidities for the beam members in a linearly elastic isotropic plate (Yettram et al (51)). A representation of a quarter of the specimen by the grid elements is shown in Fig. 4.6.

The model of the column-slab connection resists lateral load by three force quantities: flexure of the beams framing into the front

face of the column, torsion of the beams representing the plate to the side of the column, and eccentricity of shear reactions at the end of beams framing into the column from both directions (Fig. 4.7).

Considering the plate specimens as a grid of beams has a number of advantages: beam behavior may be easier to explain than plate action; bar-slip phenomenon may be easily incorporated; application to nonlinear behavior is possible with simple crack and yield criteria; the change in torsional stiffness after cracking can be handled conveniently.

4.3.3 Assumed Member Properties

Load-deformation properties of members were calculated from material properties. The relationship between the flexural and torsional stiffnesses in a beam before and after cracking was different. Certain assumptions regarding bar-slip were made for ease of calculation.

Steel and concrete properties were based on measurements (Table 2.1). To account approximately for the uncertain effects of shrinkage and construction stresses on cracking moments, moduli of rupture were reduced to one half of the mean measured moduli. A simple trilinear moment-curvature relationship was calculated for each beam using the simplified moment-curvature expressions given by Cardenas (6). These simplified curves are shown in comparison with curves calculated continuously (Appendix G.2) in Fig. 4.9.

The torsional moment was treated as two principal moments of opposite sign working at right angles to each other (Fig. 4.10a), at an angle of 45^{o} to the torsional moment. The isotropic reinforcement used also meant that flexural strength in any direction would be the same -- hence pure torsion and pure moment had like strength per

unit width (Fig. 4.10a). The flexibility of the beams representing a portion of plate in torsion was altered after cracking bearing in mind that the relative orientation of cracks to reinforcement orientation influences the stiffness in torsion (expressions in Cardenas (6)). Torsional flexibility is a function of the angle between the vector representing torsion and the direction of one of the reinforcement axes (the reinforcement axes were mutually orthogonal) (Fig. 4.10b). Even though this angle varied over the slab, it was assumed to be 45^{o} in determining torsional flexibility.

Reinforcement pullout at the column face was based on the model in Fig. 4.8a, and an assumed average bond stress of 4.0 MPa. For those beams that framed into the column face the rotation due to bar-slip was introduced into the analysis in the following way. Perpendicularly connected to a beam ("A" in Fig. 4.8b) running into the column face was another beam ("B" in Fig. 4.8b) which responded only in torsion. The "torsional" beam "B" shown in Fig. 4.8b is free to rotate (torque) at node "2" but cannot rotate (torque) at node "1". The torsional stiffness of the "torsional" beam is determined as follows. From equilibrium at node "2" (an expanded view of this node is given in Fig. 4.8c) the end-moment in the beam running into the column face is equal to the torsion in the beam introducing bar-slip. By restricting the axial rotation of the "torsional" beam at node "1", the rotation of this beam at node "2" is known as a function of the torsional stiffness and the torsion (end-moment). This rotation is equated to that of the bar-slip model shown in Fig. 4.8a. The end-moments are equal and cancel out of the equation to leave the torsional stiffness as a function of known physical quantities (Fig. 4.8c). The

"torsional" beam provided the required relative rotation due to bar-slip, and may be thought of as a spring connection for the "flexural" beam at the support boundary. The location in the grid of a "torsional" beam is indicated in Fig. 4.6.

4.3.4 Comparison of Calculated and Observed Response

The nonlinear response of the slabs was calculated by a routine "step-by-step" linear procedure. The "Polo-Finite" (33) system at the University of Illinois (Urbana-Champaign) was used for each step. The beam properties were changed when the moment exceeded the values shown for cracking and yielding moments (Fig. 4.9).

For each of the two specimens the calculated response of the slabs is compared with the following observed quantities: (1) Moment-rotation curves (4 figures); (2) the twist of the slab about the lateral centerline to the side of the column (1 figure); (3) the vertical slab displacement along the longitudinal centerline (1 figure); (4) the measured strain in bars to the side of the column monitoring the progress of yield across the plate (2 figures).

The comparison of measured and calculated moment-rotation curves for specimen S1 are given in Fig. 4.12 to 4.15. In Fig. 4.12 change of stiffness caused by initial cracking can be seen in the calculated points; the progressive reduction in stiffness seen in the calculated curve in Fig. 4.13 is due to spreading of cracking in the slab. In the calculations the torsional cracking moment was surpassed (to the side of the column) and this is indicated in Fig. 4.13; shortly after load cycle 21 was reached, yielding of the slab at the front column-face was calculated and is indicated in Fig. 4.14; in Fig. 4.15 the calculated yielding of elements across the width continued -- with the

points shown at which torsional yielding (to the side of the column) and yielding across the full width of the plate were calculated.

The next quantity compared was the measured twist of the portion of slab to the side of the column (Fig. 4.11). This twist was obtained from the difference in the vertical displacement of the slab measured along two parallel lines divided by the distance between the two lines. Matching of these calculated and measured twisting angles would enhance the credibility of the model used. Figure 4.16 shows the comparison of the observed and calculated values at various loads. (The positions of these loading stages are indicated on the moment-rotation curves of Fig. 4.12 to 4.15). A favorable comparison was obtained over a wide range of loads.

Figure 4.17 compares measured and calculated vertical displacements along the longitudinal axis for various loading stages. The measured slab deflection along the longitudinal centerline to the back of column (W) and those measurements to the front of the column (E) were the same for loading steps 1.0, 11.0 and 21.0. However, for loading step 31.0 the measurements to the back of the column (31W) were significantly larger than those measurements to the front on the column (31E). The calculated values compared well with the measurements to loading stage 21. At loading stage 31, calculation results corresponded closely to the average values (31 avg.).

As pointed out in Fig. 4.15, the lightly reinforced specimen S1 yielded across the full width of the plate. This statement is supported by the strain gauge readings that implied yielding of the bars across the full slab width (Fig. 4.19). At other loading points

the calculated spread of yielding was verified by the strain gauge readings; by loading 31 yielding had been calculated for elements to the front of the column as is also evident in the gauge reading in Fig. 4.18. By load step 34.57 the calculated extent of yielded elements had progressed to approximately the position of gauge No. 16, which -- by referring to Fig. 4.19 -- correlated well with measured values.

The calculated and measured moment-rotation curves for the heavily reinforced specimen, S3, are presented in Fig. 4.20 to 4.23. As was done with the calculations of specimen S1, the positions at which the various major changes in stiffness occur are noted (from cracking to yielding).

The calculated twisting angles, as presented in Fig. 4.24, bear a good resemblance to the measured values.

A favorable correspondence is also present in the measured and calculated vertical deflections along the longitudinal axis of specimen S3 (Fig. 4.25).

The strain gauge readings of Fig. 4.26 and 4.27 support the extent of yielding calculated in the grid model. The strain measurements on gauge No. 16 presented in Fig. 4.27 show that yielding had yet to reach this position by the conclusion of testing.

4.3.5 Comparison of Calculated Responses of S1 and S3

In the calculated response, the lightly reinforced specimen S1 utilized the full slab width, but the more heavily reinforced specimen S3 did not. In each case, a good correlation between calculated and measured values was obtained. The calculated response of each specimen is compared to investigate the factors causing the differences in the response of the two specimens.

As mentioned before, the applied moment at the slab-column connection was resisted by flexural moments and eccentric shear forces at the front face of the column, and torsion and eccentric shear forces at the side face (Fig. 4.7). In Fig. 4.28 the fraction of the applied moment resisted by "shear" and torsion at the side face is presented as a function of the rotation at the connection, for both specimens S1 and S3. As the connection rotation increased, various significant changes in the trends are apparent in the figure.

Initially, the calculated fraction carried by "shear" and torsion at the side face was 30% of the applied moment. Cracking of the beams representing the portion of slab to the front of the column decreased the relative stiffness of this part in flexure, and an increase in the percentage of moment carried by "shear" and torsion is noticeable in the figure.

At positions "A" and "A'" in Fig. 4.28 the abrupt drop in the amount of the applied moment carried by torsion and "shear" at the side face was due to the cracking of members to the side of the column in torsion. The relative stiffness of the plate to the front face of the column increased, and "flexure" became relatively more important. In the calculations the applied moment at which this occured was larger for specimen S1 than for S3 because S1 had a larger calculated cracking moment than S3.

The increase in the fraction of moment carried by "shear" and torsion at the side face for specimen S1 at "B" in Fig. 4.28 and at "B'" for specimen S3 resulted from the yielding of a grid-beam at the front face of the column. For both specimens the relative stiffness

of the beams representing the plate to the front of the column was reduced, and relatively less moment than before was carried by flexure at the front face of the column. The calculated spread of cracked members in both specimens up to this stage in the loading is shown in Fig. 2.29.

In Figure 4.28 the positions "C" and "C'" correspond to the stage at which the beams representing the slab to the front of the column had yielded. The side face continued to gain in relative importance because of its relative stiffness.

Positions "D" and "D'" in Fig. 4.28 represent the yielding in torsion of the beams at the side face of the column. For both specimens this yielding terminated the increase in the part of applied moment carried by the side face.

By referring to Fig. 4.28 the influences of the relative stiffness of portions of the plate on the moment quantities resisting the total applied load at the connection became evident. These quantities--flexure and shear at the column front face, and torsion and eccentric shear at the side face--are indicated as a function of connection rotation for the two specimens in Fig. 4.30 and 4.31. The contributions of the "front face" and "side face" to the overall stiffness of each specimen can be gathered from Fig. 4.30 (specimen S1) and Fig. 4.31 (specimen S3).

The changes in incremental stiffness also influenced the increment in moment carried by the grid beams across the width of the slab. The moments in defined beams across the width of specimen S1 and S3 are indicated for increasing column-slab connection rotation in Fig. 4.32

(specimen S1) and Fig. 4.33 (specimen S3). The key in each figure gives the position of the beams. For each beam the moment was normalized by its yield moment.

The shaded zones in the figures (4.30 to 4.33) are provided as a reference; the letters "A", "B", "C" and "D" correspond to the definitions given in Fig. 4.28. These figures allow insight into the portion of potential "wide beam" strength gained by each specimen at progressive loading stages. The history of the grid beams specified in Fig. 4.32 and 4.33 will be discussed in turn.

Position "B" in Fig. 4.32 and "B'" in Fig. 4.33 indicate the yielding in beam "30" at the front face of the column. For specimen S1 this occurred at a connection rotation of about 0.25%, and for specimen S3 at a connection rotation of about 0.5% as would be expected from a comparison of their strengths. Once the other beam at the front face yielded (positions "C" and "C'") the side face carried relatively more of the applied load.

Beam "32" in specimen S1 matured before the slab to the side face underwent a significant drop in stiffness. This took place at a connection rotation of about 1.0%, well before torsional yielding at the side face (position "D", Fig. 4.30). The stiffness of the slab to the side face in specimen S3 was reduced before beam "32" could yield, as is apparent just past the shaded zone in Fig. 4.31. As a result the beam "32" in specimen S3 yielded at a relatively large column-slab connection rotation of more than 2.0%. This yielding of beam "32" in specimen S3 happened at about the same time as torsional yielding at the side face of the column (position "C'", Fig. 4.31).

At the time of yielding in beam "30" the moment in beam "34" was about 40% of its yield moment in specimen S1, but only 20% of its yield moment in specimen S3. The overall stiffness of specimen S1 was sufficient to enable beam "34" to mature at about the same time that the plate to the side face of the column yielded in torsion. This happened at a connection rotation of about 2.5% (position "D", Fig. 4.32). When the portion of plate to the side face of the column yielded in torsion, the moment in beam "34" of specimen S3 had only reached 30% of the yield moment. The subsequent low stiffness of specimen S3 (Fig. 4.31) restricted the beam "34" from developing its potential strength within a reasonable connection rotation.

Shear stress calculated at the column from the shear reactions indicated that specimen S3 had an average stress of about $0.33\sqrt{f'_c}$, f'_c in MPa (or $4\sqrt{f'_c}$, f'_c in psi), whereas the lightly reinforced specimen S1 had a lower shear stress level of $0.25\sqrt{f'_c}$, f'_c in MPa. Modeling of both specimens by the nonlinear grid method was achieved without shear appearing as a limiting factor.

Figures 4.34 and 4.35 illustrate the difference in the ability of the two specimens S1 and S3 to propagate yielding across their respective widths. Even though specimen S3 could potentially resist more moment this could not be achieved without excessive rotation of the column-plate connection owing to the very low stiffness of the specimen.

4.4 Reflection on Stiffness

From the comparison of measured and calculated moment-rotation responses, it appeared that the slab-column elements were in a partially cracked condition before testing. The influence of cracking,

attributable primarily to shrinkage, was stronger for S3 (Fig. 4.20) than for S1 (Fig. 4.12).

A stronger influence on overall stiffness was the slip of the reinforcement at sections of maximum moment. Comparisons of measured and calculated curves suggest that this phenomenon was modeled satisfactorily. The calculated rotation at yield caused by bar-slip was 30% of the connection rotation (Specimen S3).

The success of the grid model was measured by comparing calculated and observed moment-rotation relationships, vertical slab displacements along the longitudinal axis, twist deformations along the lateral axis, and the progress of yield across the slab width.

The nonlinear-response model for the slab demonstrated that the major difference between the responses of S1 and S3 (that the yield moment of the full width of the slab was not developed for S3) could be explained in terms of flexural and torsional flexibilities of slab elements, and without invoking phenomena associated with shear failure.

5. DISCUSSION OF OBSERVED RESPONSE OF SPECIMENS WITH VERTICAL AND LATERAL LOAD

5.1 Introduction

This chapter will discuss the performance of three specimens with like reinforcement ratio (S2, S4 and S5) but with varying amounts of superimposed vertical load.

Criswell (11) distinguished between punching failure and flexural failure of a column-plate connection under vertical loading alone. Having obtained a shear value, V_f, from the flexural yield line mechanism he observed in relatively lightly reinforced slabs, he used this value to evaluate whether a specimen had failed in flexure or shear. When the observed shear strength, V_u, was less than the calculated value of V_f for the specimen he classified it to have failed in shear.

In a similar way one could appraise the performance of specimens S4 and S5, and compare their observed strength with the strength calculated from a likely yield-line pattern (that of the "wide-beam"). Remembering that even specimen S2--which had no superimposed vertical load--could not achieve the calculated "wide-beam" strength, immediately flaws the definition of V_f.

A comparison between the observed strength of the specimens S4, S5 (superimposed vertical load) and S2 (no superimposed vertical load) with their respective calculated "wide-beam" strengths may allow more insight than merely comparing their respective observed strengths with one another.

5.2 Crack Patterns

The trace on the surface of the inclined crack that caused the abrupt failure of specimen S4 was similar to that in S5. It was typical of those

recorded in punching shear tests by Criswell (11). In contrast to the punching of a slab subjected to only vertical loads, the inclined crack did not develop on all four sides of the column. The inclined crack could be seen at the center of the side faces of the column, spreading out in a fan pattern, like the wings of a grotesque fly, to the rear face of the column (Fig. 5.4).

As for specimens S1 to S3, both specimens S4 and S5 had well developed flexural crack patterns; in this respect the types of cracks in the specimens were similar (Fig. 5.5).

Judging the strength of specimens S4 and S5 by the crack patterns one could conclude that up to failure it was determined by the same mechanism as for specimens S1 to S3. In both specimens S4 and S5 this failure occured at relatively large connection rotations (about 4.5%).

5.3 Observed Response

Two trends are to be seen in Fig. 5.1: The lateral load achieved by specimen S4 appears less than that of S5 despite the fact that specimen S4 carried only a half of the superimposed vertical load of S5; the strengths of specimens S4 and S5 appear to fall below the strength of S2 (no superimposed vertical load).

As previously mentioned one may compare the strength of the specimens by how much of their respective calculated "wide-beam" strength they achieved. A prescience of the outcome of this comparison is likely if one observed from Fig. 5.2 that the moment-curvature relationships of S5 and S4 indicate that the flexural strength per unit of width was greater for specimen S5 than for S4. Figure 5.3 and Table 5.1 reveal that specimens S4 and S5 achieved about the same proportion of their respective "wide-beam" strengths. The implication of this comparison of

normalized strengths is that the different amounts of superimposed load did not make a significant difference. Also apparent in Fig. 5.3 is that in specimen S2 a larger proportion of "wide-beam" strength was obtained than for specimen S4 or S5.

Returning to Fig. 5.1 it is clear that in the initial loading range (say up to 20 kNm) specimen S2 responded in a significantly stiffer manner than did the other two specimens. This can be attributed to the effect of cracking caused by the vertical load. As the grid-analysis of specimens S1 and S3 indicated, the resulting reduction in initial stiffness would have a detrimental influence on the ability of the specimens S4 and S5 to develop their potential within a reasonable connection rotation. It does appear that connection rotations at maximum observed load in specimens S4 and S5 were greater than for specimen S2 (no superimposed vertical load).

From Fig. 5.1 it is also apparent that specimens S4 and S5 only failed abruptly after having achieved a significant deformation; not the type of behavior expected from a connection fettered by punching shear.

The conclusion is that both S4 and S5 reached a major portion (95%) of the strength of specimen S2 (when all are normalized by their respective "wide-beam" strength). The specimens S4 and S5 had to be deformed somewhat further than did specimen S2 to realize this strength. This must be borne in mind when making deductions with respect to stiffness from those specimens in which no superimposed vertical load was present.

Inclined cracks surfaced at excessive connection rotation of specimens S4 and S5. Up to this rotation the response mechanism was as for S1 to S3.

6. DYNAMIC TESTS: DISCUSSION OF OBSERVED RESPONSE

6.1 Introduction

This chapter will discuss the response of the specimens tested "dynamically" and will compare features of the static with those of the dynamic tests.

The reinforcement ratio was varied in specimens D1, D2 and D3 in the same way as for the static-test specimens S1, S2 and S3. The three ratios used were 0.65% (D1 and S1), 0.98% (D2 and S2) and 1.31% (D3 and S3).

The base motion during simulated runs was that of El Centro 1940, the North-South component. Steady-state runs of systematically varying frequency with constant base displacement were also conducted. By fixing the shake-table and releasing the top of the specimen suddenly --after having displaced it laterally a small amount--a free vibration was introduced.

Discussion will concentrate on the observed strength, stiffness and damping of the specimens.

The data represented here are documented in detail in Appendix F.

6.2 Response Similarities between the Dynamic and Static Specimens

The "wide-beam" action of the specimens may be assessed on the basis of their measured strengths. Without detracting from following comparisons between the static and dynamic test sets, Fig. 6.1 indicates the strength in the context of the "wide-beam" strength. (See also Table 6.1.)

The lightly reinforced specimen D1 did better than its potential strength, calculated assuming yielding across the full plate width ("wide-

beam" strength). This potential yield-line moment was calculated from static properties for the concrete and reinforcement. Both D2 (intermediate reinforcement ratio) and D3 (reinforced heaviest) failed to reach their potential "full-beam" strength. Referring to Fig. 6.1, the value indicated by DP is that of a pilot test documented in Appendix H. Its strength also follows the trend set up by the observed strength of D1, D2 and D3.

The observed crack patterns in the dynamically tested specimen were remarkably similar to those observed during the static test program (even though in the static tests the strength was achieved on a final loading cycle that resulted in some anti-symmetry). Generally, the crack patterns in the dynamic specimens were symmetrically located. The orientation of the major cracks was comparable to that of the major cracks in the static tests (Fig. 4.5). Specimen D1 had its major cracks spanning the full width of the slab (Fig. 6.2). This position was also observed in the statically tested specimen S1. Comparison of the cracking patterns for D1, D2 and D3 indicates a tendency for the major cracks to occur at an increasing angle to the edge of the column as the reinforcement ratio increases. No evidence of inclined cracking--associated with punching-shear--was seen on the surface of the slabs.

The influence of reinforcement ratio change was similar in the dynamically and statically tested specimens (D1 to D3 and S1 to S3): (1) The trend in strength variation as a function of reinforcement ratio was much the same. (2) The crack patterns provided evidence that a similar mechanism determined the behavior of the statically and dynamically tested specimens.

6.3 Strength

The increase in strength of a dynamically tested specimen over its statically tested counterpart is clearly visible in Fig. 6.1. By noticing that this increase is approximately constant with increase in reinforcement, it can be derived that the heavily reinforced specimen D3 had a relatively larger increase in observed strength over S3 than that of D1 over S1.

The purpose of Fig. 6.3 to Fig. 6.5 is to illustrate the range of the various runs for specimens D1 to D3. The ordinate represents the total moment applied to the plate-column connection. The displacement is that measured at the position of the attached column mass (Fig. 6.6). (In other diagrams dynamic-test runs are often referred to by the letter "R".)

Runs 2, 3, 5 and 6 (Specimen D1) are superimposed on the envelope obtained from the static test of S1 (Fig. 6.7). In runs 5 and 6, D1 reached an increased strength compared with the static envelope. Relative to the observed strength of S1 the increase does not appear to be substantial.

The shaded zone in Fig. 6.7 spans between a column-slab joint rotation of 1.5% to 2.0%, a range of significant joint rotation.

Three runs, 3, 9 and 10, are superimposed on the envelope measured from the statically tested specimen S2 (Fig. 6.8). A noticeable increase in strength of D2 over S2 was achieved.

Again, the shaded area indicates the extent of 1.5% to 2.0% joint rotation (Fig. 6.8).

Runs 2, 3, 4 and 5 from dynamically tested specimen D3 are compared with the envelope from statically tested S3 (Fig. 6.9). The "dynamic" strength of D3 had a clear edge over the "static" strength of S3.

The shaded zone spans in Fig. 6.8 between a column-slab joint rotation of 1.5% to 2.0%.

The smoothed envelopes--of the comparable specimens tested statically and dynamically--are presented in summary in Fig. 6.10. The observed strength of D2 was approximately 26% greater than that of S2. The increase of D3 over that of S3 was 38%. A comparison of the observed strengths in this way is misleading because of differences in the material properties of the specimens. By normalizing each specimen's observed strength by its calculated yield-line strength, the difference in material properties can be accounted for. This approach is presented in Fig. 6.1 and in Table 6.2. The comparison of normalized strengths results in less scatter: (1) the normalized strength of D1 had a 21% increase over that of S1; (2) the normalized strength of D2 had an increase of 27% over that of S2; (3) specimen D3 was 31% stronger than S3 if compared in this fashion. The effect of rate of strain on the material properties of concrete and steel will be explored in an attempt to explain the apparent differences between the dynamically and statically tested specimens.

An approximate strain rate can be calculated for the dynamically tested specimens: if one assumed a period for the specimens of about 0.2 seconds (see the frequency range in Fig. 6.23 beyond a displacement of 10mm) and assumes the time the steel takes to reach its yield strain as 1/6 of the period, a strain rate of 0.05/sec is plausible. Criswell (12) tabulated the findings of a number of researchers on the effect of strain rate on the lower yield stress of steel in tension. For intermediate grade steel

Criswell reported a 10% to 20% increase in lower yield stress for a strain rate range of 0.03/sec to 0.10/sec when compared with the yield stress of slowly tested steel. Bertero et al (5) measured a 28% increase in lower yield stress of deformed reinforcing bars (of intermediate grade steel) tested at a strain rate of 0.05/sec. Bertero et al noted that a strain rate of 0.05/sec did not increase the ultimate stress significantly when compared with the ultimate stress of bars tested at a low strain rate.

The strength of reinforced concrete sections in flexure is insensitive to variations in concrete strength. Shear strength, on the other hand, would be sensitive to changes in concrete strengths. The grid-analysis (of Chapter 4) explained the measured strengths of specimens S1 to S3 as being determined by flexural action. Adding to this the observation that the dynamically tested specimens D1 to D3 appear to have the same mechanisms as for S1 to S3 respectively, one can deduce that changes in concrete strength in the dynamic testing cannot explain the observed increase in strength of dynamically tested specimen D3 over that of statically tested S3.

Turning to the expected increase in lower yield stress (at larger strain rates) to account for normalized strength increases of 21 to 31% seems acceptable. It is possible that the lighter reinforced section of specimen D1 may be less sensitive to the rate of strain than D3 because of larger strains (Bertero et al (5)) in under-reinforced sections in flexure.

In conclusion it appears that the observed increase in flexural strengths of the dynamically tested specimens over those of the statically tested can be attributed to the increase in the lower yield point of the reinforcement associated with higher strain rates.

6.4 Stiffness

6.4.1 Methods of Evaluation

Guided by posts a pedestrian will keep to the sidewalk around a corner; remove the obstacle and one is tempted to take the short cut. In the response of the specimens tested a knowledge of the "outer" stiffness as well as the "short cut" stiffness is necessary.

Stiffness information is derived from free-vibration tests, steady-state tests, and moment-displacement plots obtained from earthquake runs. An idealized representation of the displacemet- history in these types of tests is shown in Fig. 6.11a. A unit displacement (Fig. 6.11a) has been used for illustrative purposes. For specimens D1 and D3 the steady-state testing was grouped (as described in Appendix D); a series of small-amplitude motions constituted a steady-state test prior to and after a steady-state test comprising large-amplitude motions (idealized in Fig. 6.11b).

The three types of tests (FV, SS, and Runs) cause different amplitudes of response, and this is illustrated in Fig. 6.12. The free-vibration test was limited to a very small amplitude of response. Steady-state tests caused both large and small amplitudes of response. Resonance frequency was taken as the measure of stiffness in the steady-state tests. The stiffness information obtained from moment-displacement relationships of the simulated earthquake runs spans small and large amplitudes of response. The secant stiffness to the point of maximum response is used in this case.

The previously experienced displacement of a specimen is a useful parameter by which the change in stiffness may be expressed. Generally the maximum amplitude of response during a simulated earthquake run increased as the testing sequence progressed. A summary of the sequence

of testing for specimens D1 to D3 is shown in Fig. 3.2 to 3.4.

The observed stiffness characteristics of each specimen will be discussed in turn in the following sections. In conclusion, general trends observed in the three specimens will be considered.

6.4.2 Specimen D1

For specimen D1 (ρ = 0.65%) frequencies at various stages in testing are shown in Fig. 6.13. A schematic representation of the testing sequence is also given in this figure. The displacement quantity referred to in Fig. 6.13 is the maximum top-level displacement experienced at the incident. Frequency values are plotted in Fig. 6.14 against the maximum previously experienced top-level displacement. The expected overall "softening" with increase in displacement, as gauged by an ever decreasing frequency, is quite evident in Fig. 6.14. Initially the stiffness dropped off rapidly for relatively small displacements, indicating extended cracking (Fig. 6.14). Quite significant softening still took place after a displacement of 10 mm (a column-slab rotation 0.9%). This implies that considerable "yielding" in the specimen occurred at a relatively large connection rotation.

In Fig. 6.15d one may observe a relatively soft response for the specimen at low amplitudes. The incremental stiffness increased as the amplitude of response increased. The soft-to-stiff type of response is present in Fig. 6.15c after the specimen underwent its maximum displacement (the inner loops).

The change in incremental stiffness of a specimen during a large-amplitude steady-state test will be discussed when using these tests to evaluate damping in the specimens.

The maximum response amplitude for specimen D1 during large-amplitude steady-state tests SS4.2 was close to that of the preceding simulated earthquake run, Run 5 (Fig. 6.13). The resulting softening during steady-state test SS4.2 can be inferred from Fig. 6.16d; there was a drop in frequency from the small-amplitude steady-state test SS4.1 (prior to large-amplitude test SS4.2) to SS4.3 (after SS4.2). Relatively less change in stiffness was encountered in SS3 (Fig. 6.16c). In these figures the amplification factor is the ratio between the base acceleration and the acceleration measured at the location of the mass in the equivalent single degree of freedom system.

6.4.3 Specimen D2

In Fig. 6.17 a record of the frequency at various stages in the testing of specimen D2 is presented. In the steady-state test there was no "sandwiching" of a large-amplitude test between two small-amplitude tests. As was the case for specimen D1, specimen D2 also underwent an overall softening as the experienced maximum response displacement increased. This trend is clear in Fig. 6.18. There was a rapid initial decrease in stiffness, and significant drops in frequency still occurred after 10 mm displacement.

The soft-to-stiff response of the specimen as it moves from low amplitudes to large amplitudes of response within a run (Fig. 6.4) is apparent in the latter stages of testing.

6.4.4 Specimen D3

The relevant frequency information for specimen D3 is compiled in Fig. 6.19 and Fig. 6.20. The mass on the specimen was increased on two occasions during the testing procedure; the masses were to cause additional moment to the relatively heavily reinforced specimen D3. This addition is

indicated in Fig. 6.20, and was monitored by the free-vibration tests. Changes in frequency resulted from this added mass, but do not distract from the general trend of decrease in stiffness. One may deduce from Fig. 6.20 that the specimen D3 yielded at a relatively large connection rotation as significant drops in stiffness occur after a displacement of 10 mm.

The moment-displacement diagrams (specimen D3) of the latter runs in Fig. 6.5 and those of the steady-state tests of Fig. 6.21 have a soft-to-stiff response. Without delving deeply into the response of nonlinear systems one may venture to say that the stiffening system in steady-state tests 3 and 4 should result in a large ("stiffer") resonance frequency (discussed further in Section 6.6) for a relatively larger amplitude test. In Fig. 6.22 the resonance frequencies from the large-amplitude tests bear out this observation, and these tests had larger resonance frequencies than the small-amplitude tests. This trend was not as obvious in the steady-state test of specimen D1. In steady-state test SS3.2 of specimen D1 (Fig. 6.16c) a lower resonance frequency than the preceding small-amplitude test was measured. Near resonance in this test the base amplitude changed abruptly from 1.5 mm to 1.0 mm, and caused a significant disturbance. An overall softening of the "short cut" stiffness could also disguise the stiffer response of the "short cut" stiffness at large amplitudes of response. This will be analyzed further in discussing damping of specimen D1.

6.4.5 Summary

In summary, Fig. 6.23 compares the change in frequency for three specimens D1, D2 and D3. The frequencies in this figure were calculated from the secant stiffness of the moment-displacement relationships for

the various simulated earthquake runs. There are important observations concerning all the specimens: (1) The specimens--as the grid analysis in Chapter 4 also indicated--appeared to be initially cracked, and a rapid drop in stiffness for relatively small displacements was apparent. (2) Significant changes in frequency after relatively large displacements (connection rotations of about 1%) imply that considerable yielding still took place at large displacements. (3) Initially the specimens responded quite linearly. For example, one may consider Run 2 and SS2.2 of D1 in Fig. 6.15. In the latter stages of testing the specimens tended to have a range of extremely low stiffness, followed by an incremental stiffening as larger response displacements were reached. This soft-to-stiff "short cut" stiffness was evident in Run 5 and SS4.2 of D1, Fig. 6.15 (the latter stages of testing of specimen D1). The range of low stiffness at relatively small displacements has been ascribed to bar-slip and the opening of cracks in the concrete. It is of importance as it affects the ability of the specimen to dissipate energy by hysteretic action.

6.5 Hysteresis

The area enclosed within a hysteresis loop in a force-displacement relationship is considered to be a measure of the energy dissipated in the system. Therefore, before discussing the calculated damping values of the dynamically tested specimens it may be informative to summarize the observed force-displacement relationships.

For reference purposes the area enclosed by hysteretic action in a moment-displacement relationship is given the label "hysteresis area."

Even before significant yielding occurred a considerable hysteresis area was observed in the moment-displacement relationships (Fig. 6.15a

and b). The extensive cracking of the plate across its surface can be expected to account for this.

The hysteresis area appeared relatively larger once yielding took place. This is quite evident in Run 5 of specimen D1 (Fig. 6.7), Run 10 in D2 (Fig. 6.8), and Run 4 in specimen D3 (Fig. 6.9). It is important to realize that these runs took place at relatively large rotations (a connection rotation of greater than 1.5%).

Furthermore, the shape of the hysteresis area was a function of the previously experienced maximum displacement. The hysteresis area of Run 5 in specimen D1 (Fig. 6.15c), enclosed by the "outer" loop is quite distinct from the hysteresis area in steady-state test SS4.2 (Fig. 6.15d) following Run 5. The previously experienced maximum displacement was not exceeded in SS4.2. The shape of the hysteresis area in Fig. 6.15d was pinched at large amplitudes of response. This shape was also evident in Fig. 6.15c after the specimen had exceeded the previously experienced maximum displacement (the inner loops in Fig. 6.15c).

In summary, the specimens appeared to dissipate considerable amounts of energy prior to yielding, and appreciably more after "yielding." The shape of the hysteresis area was sensitive to the amplitude of response, and the previously experienced maximum displacement.

6.6 Damping

6.6.1 Methods of Evaluation

In determining damping values for the specimens, certain simplifications were made regarding the type of damping and the system type. The damping factors referred to are equivalent linear viscous damping factors, usually expressed as a percentage of critical damping. The systems were assumed to have a single degree of freedom (SDOF system, Appendix G.1).

Linear as well as cubic stiffnesses were considered. The system with cubic stiffness was based on the well-known "Duffing equation" (Duffing (13)):

$$\ddot{x} + c\dot{x} + \omega_n^2 x + \mu x^3 = \ddot{z}$$

where

x = relative displacement of the SDOF system (a dot indicates a time derivative)

z = base motion

ω_n = natural frequency

$$= \sqrt{\frac{k}{\ell_e^2 m_e}}$$

k = linear spring stiffness [kNm/radian]

ℓ_e = equivalent length of pendulum (Table G.1)

m_e = equivalent mass (Table G.1)

c = viscous damping

$= 2\beta\ \omega_n$

β = damping factor as a percentage of critical damping

μ = cubic stiffness factor

$= k_c/(m_e \ell_e^4)$

k_c = cubic spring stiffness [kNm/radian^3](moment = $k(\theta)+k_c(\theta)^3$, θ=rotation of spring)

The damping values were calculated from free-vibration tests, simulated earthquake runs and steady-state tests.

A linear SDOF system was assumed to describe the response of the specimen in free-vibration tests. Damping factors were calculated using the logarithmic decrement method (Timoshenko et al (48)).

An evaluation of equivalent damping in the idealized SDOF oscillator

during the simulated earthquake runs was made as follows: the frequency of the system was calculated using the measured secant-stiffness (to the point of maximum response) in the specific run; the maximum relative displacement at the mass position of the equivalent SDOF system was measured; the calculated displacement response spectrum was entered at the aforementioned frequency, and by comparing calculated spectrum displacements with the measured maximum relative displacement a damping value was estimated. Damping values thus obtained are sensitive to changes in the assumed stiffness of the system; if the "FV stiffness" was used instead of the "secant stiffness" a maximum difference of 40% was obtained in respective damping values.

At the risk of emphasizing the steady-state tests to the detriment of the other methods of estimating damping, a detailed explanation of the "steady-state approach" follows.

The absolute acceleration of the equivalent SDOF system was measured during the steady-state test by taking the mean value for ten consecutive cycles (coeff. of variation typically 0.10). The amplification factor was the amplitude of response at each input frequency step divided by the amplitude of the base acceleration for that step. The resulting response spectra were compared with values calculated for linear or non-linear SDOF systems. In the latter case, the measured moment-displacement relationship of the specific steady-state test was approximated by a cubic stiffness expression (the "short cut" stiffness) that in turn was used to calculate response spectra. Damping values of 4, 6, 8, 10, and 12% of critical damping were used in calculations. Conclusions were drawn from comparing the calculated response spectra with the measured response data. Other researchers have evaluated measured response from steady-

state tests by other nonlinear means. For example, Ibanez (24) defined a nonlinear expression for damping. Iwan (25, 26) and Jennings (27) have calculated response spectra to steady-state motions by using various hysteresis models to describe their systems. Results from Iwan's studies are mentioned in the discussions to follow. The "Duffing equation," with the cubic stiffness for the SDOF system based on measured moment-displacement relationships, allowed further simplifications to be made. For example, the peak values of amplification of a linear system in a response spectra using the absolute acceleration of the SDOF mass as parameter is described by the following expression (Thomson (46)):

Max. Amplification factor =

$$\text{M.A.F.} = \sqrt{1 + \frac{1}{(2\beta)^2}} \quad \text{, if one assumes}$$

$$\omega_r = \omega_n$$

where

ω_r = resonance frequency

ω_n = natural frequency

β = viscous damping as a percentage of critical damping

$$\text{M.A.F.} \simeq \frac{1}{2\beta} \qquad (6.1)$$

for relatively small values of β.

The peak value in the nonlinear ("Duffing") system may be expressed as (Timoshenko et al (48)):

$$\text{M.A.F.} = \frac{1}{2\beta} \frac{\omega_r}{\omega_n} \qquad (6.2)$$

For the calculated response of the steady-state tests, using the nonlinear description, Eq. 6.1 and 6.2 gave similar estimates of damping. These

values are listed in Table 6.3. The simpler expression 6.1 will be used in discussions. Another advantage in using "Duffing's" equation was that a stiffening as well as a softening system could be investigated. Changes in "short cut" stiffness during a test could also be recognized, an important physical consideration.

The size of the response amplitude is important to place the various tests in perspective (Fig. 6.12): Free-vibration tests were small in amplitude; steady-state were both small and large in amplitude; the simulated earthquake runs were small and large in amplitude. The previous maximum displacement encountered by a specimen was usually exceeded in a simulated earthquake run, but the steady-state tests were generally kept below the maximum displacement experienced before the test.

The damping evaluated in the dynamically tested specimens follows. For each specimen an overall view of the damping evaluated is given at first, and then a more detailed discussion.

6.6.2 Specimen D1

The sequence of tests in specimen D1 and the estimates of damping during a test are shown in Fig. 6.24. The displacement value referred to in the figure is the maximum displacement in that particular test measured at the position of the attached mass on the column of the specimen. The maximum displacement encountered by a specimen before an evaluation of damping is another meaningful displacement parameter and is used in Fig. 6.25. This figure gives a summary of the damping values shown in the previous figure.

Some general observations may be made from Fig. 6.25. The damping values from the steady-state and free-vibration tests appear quite similar in Fig. 6.25. The different range of amplitudes in the two

types of tests do not seem to have had a significant effect. The large amplitude test in Run 5 produced the largest damping value of 13%. Significant increases in damping still took place after a displacement of 10 mm (1% column rotation).

The steady-state evaluation of damping appears to show a sharp increase early in the sequence of testing. By the time the specimen had encountered a maximum displacement of 10mm (about a 1% connection rotation) the large-amplitude steady-state test evaluated damping to be about 7%. The response in SS1 (Fig. 6.26) appears to be that of a linear system. As may be inferred by the decrease in amplification factor in Fig. 6.26, there was a sharp increase in damping between steady-state tests 2.2 and 3.2. Although the response in steady-state test SS1 (Fig. 6.26) resembles that expected from a relatively linear system, the response in steady-state tests SS3.2 shows an abrupt decrease in amplification factor after the resonance frequency was reached. To determine whether this jump was the result of the response of a system with nonlinear stiffness to steady-state motion, the response was calculated using the "Duffing equation" (Stoker (43)).

In Fig. 6.27a the assumed cubic stiffness is shown based on the observed moment-displacement relationship before resonance occurred. The "short cut" stiffness was used to generate the response curves marked "A" in the response spectra Fig. 6.27c. These curves are discontinued at the point of maximum amplification. The diamond shaped data points in this figure refer to observed values. The point of maximum measured response deviated from curves "A". As a result of malfunctioning of the equipment, the amplitude of the base-motion changed abruptly (1.5 to 1.0 mm) during this input frequency, and this would have influenced the measurements

significantly.

Before discussing the other portion of the response spectra in Fig. 6.27c it may be noted that a change in the "short cut" stiffness of the system seems to have occurred (the free-vibration test done prior to SS3 indicated a frequency of 5.7 Hz and that done afterwards resulted in a frequency of 5.0 Hz, Fig. 6.13). The cubic stiffness used to describe the response to a steady-state base motion after resonance in SS3.2 is indicated in Fig. 6.27b. Curves marked "B" in Fig. 6.27c were calculated using the stiffness shown in Fig. 6.27b. It seems that the observed maximum response point could have "belonged" to these curves; this is also in keeping with the type of "jumps" in response typical in a "softening" system. The decrease in stiffness is quite apparent in the relative shift of curves "B"; the broken line portion of curves "B" should have coincided with curves "A" if no change in frequency had occurred. If Fig. 6.27c is reconsidered in its entirety the abrupt change in measured response is the result of a change in the "short cut" stiffness. At the apparent damping level, the nonlinearity of the stiffness in SS3--as matched by the assumed cubic stiffness--is not severe enough to cause the observed jumps. The explanation of the response during SS4.2 is similar to that given for SS3.2. The assumed stiffnesses are indicated in Fig. 6.28a and b, and the calculated curves corresponding to these stiffnesses are plotted in Fig. 6.28c. An inferred shift in "short cut" stiffness is noticeable in Fig. 6.28c. The observed responses to steady-state tests SS3.2 and SS4.2 appear well matched by the calculated spectra assuming a soft-to-stiff "short cut" stiffness.

During the cycle of maximum response to earthquake run Run 5, the shape of the hysteresis appeared distinct from that of steady-state SS4.2 (Fig. 6.15 c and d). The response cycle in Run 5 followed the "outer" envelope, but SS4.2 did not surpass the previous maximum displacement experienced. Were these two tests judged by the concept of the energy dissipated being proportional to the area enclosed by the response cycle, Run 5 dissipated more energy. Even though the maximum damping value of 13% was evaluated from Run 5, the sensitivity of this evaluation to the assumed stiffness is considerable.

6.6.3 Specimen D2

The sequence of tests in Specimen D2 and the estimates of damping during a specific test are shown in Fig. 6.29. (The ordinate in this figure is the maximum displacement measured during a specific test.) The maximum displacement encountered before a damping evaluation is used as the abscissa in Fig. 6.30 to show the trend in damping values. The increase in damping after relatively large connection rotations (1%) suggests that significant yielding took place at a large rotation. A maximum damping value of 10% was evaluated for the simulated earthquake Run 10.

In the steady-state testing the damping obtained from SS6 appeared larger than that from the following steady-state test SS7. This may be inferred from the maximum amplification factors in Fig. 6.31. Steady-state test SS6 was unusual in that the previously experienced maximum displacement measured before the test was exceeded during SS6 (Fig. 6.29, sequence 28 and 29). Furthermore, the response to the base motion of SS6 was calculated using a cubic-stiffness approximation. The observed

moment-displacement relationship in Fig. 6.32a appears to have some softening at large amplitudes of response, as would be expected from the specimen in following the outer envelope of response. The assumed cubic stiffness in Fig. 6.32a follows a softening path rather than a stiffening one. The assumed cubic stiffness indicated in Fig. 6.32a was used to calculate the curves up to resonance in Fig. 6.32c (marked "A"). The assumed cubic stiffness used to calculate the response curves after resonance in Fig. 6.32c (marked "B") is shown in Fig. 6.32b. The calculated response appears to follow the trends in the observed values (Fig. 6.32c).

During simulated earthquake runs Run 8 and 9 the estimate of damping was appreciably lower than that from Run 7 (Fig. 6.29). In these runs the maximum previously encountered displacement was not surpassed.

6.6.4 Specimen D3

The relevant information on damping for Specimen D3 is shown in Fig. 6.33 and 6.34. From Fig. 6.34 it appears, as for the other specimens, that damping values increase markedly even after a top displacement of 10 mm.

In the evaluation of damping from small-amplitude tests (the free-vibration and small-amplitude steady-state) the estimates appear larger than the estimates from the other tests. A value of 16% was inferred from SS4.1 and 18% from SS4.3 (the two small-amplitude tests in steady-state test SS4).

The response to the large-amplitude steady-state tests is shown as amplification vs. input frequency in Fig. 6.35. Relatively sharp drops in amplification after resonance in SS2 and SS3.2 appear in this figure.

An attempt was made at matching the observed response up to resonance in each of these steady-state tests (SS2 and SS3.2). In Fig. 6.36a the measured moment-displacement and the assumed cubic stiffness is shown; Fig. 6.36b shows the calculated curves using this stiffness, and the observed data points. Figure 6.37 shows the results of similar calculations for SS3.2. A significant amount of high frequency disturbance can be seen in the measured response of SS4.2 (Fig. 6.21c); the filtered response (15Hz) is shown in Fig. 6.21d.

In the testing after a maximum displacement of about 10mm had been experienced by specimen D3, the evaluation of damping from the earthquake runs appeared somewhat larger than those obtained from the large-amplitude steady-state tests.

6.6.5 Summary

The damping values derived from the large-amplitude steady-state tests, small-amplitude tests (FV and SS), and simulated earthquake runs are discussed in turn. The calculated damping values at a reasonable connection rotation are discussed in the last paragraph.

The comparison of calculated response to steady-state tests, using an assumed cubic stiffness, with the observed response indicated that jumps in response could be explained in terms of changes to the overall stiffness properties ("short cut" stiffness) of the specimen. These jumps could not be ascribed to the incremental nonlinearity of the "short cut" stiffness, but rather to the change in "short cut" stiffness (Fig. 6.28a and b).

Small-amplitude tests (free-vibration and small-amplitude steady-state) appeared to lead to larger values for damping than did large-

amplitude tests (earthquake runs and steady-state) for specimens D2 and D3. In specimen D3 the small amplitude steady-state tests resulted in consistently larger values of damping than the large-amplitude steady-state tests (Fig. 6.22). This is in keeping with the theoretical results obtained by Iwan (25) for a system with limited slip at relatively small response amplitudes. At low amplitudes, before slip was completed, an elasto-plastic hysteresis relationship described the response for this model (Iwan). The response once slip had occurred allowed for no hysteresis relationship, merely a linear force-displacement relationship. This "wide" to "narrow" shape of the hysteresis area could be used as an idealization for the hysteresis of the steady-state tests of specimen D3, and the measured trends in Fig. 6.22 are consistent with the theoretical study by Iwan. The high amplification value obtained at resonance in SS4.3 (low-amplitude test) of specimen D1 (Fig. 6.16d) is also quite possible according to the study made by Iwan. Theoretically, "jumps" are conceivable as the specimen undergoes bar-slip phenomena, and the peak response would be a function of the lower "damping" of the larger response. The practical value of the small amplitude tests (FV and SS) seems questionable in the light of their erratic behavior. It is doubtful that the relatively high values of damping obtained in the latter stages of testing can be trusted.

Damping factors evaluated from the simulated earthquake runs appeared larger than those from comparable steady-state tests. This observation seemed to be sensitive to whether the maximum previously experienced displacement of a specimen was surpassed during that specific test (be it steady-state or earthquake run). The damping values obtained from large-amplitude tests (Runs and SS) appear to be consistent with the

surface contained by the observed hysteresis. For example, damping values from the latter runs in specimen D3 (Fig. 6.34) appear to reach a maximum at Run 4 which would be expected from the hysteresis areas in Fig. 6.5.

A summary of the tests is given in Fig. 6.38. The displacement quantity in these figures is the previous maximum displacement encountered by a specimen; the shaded zone indicates a connection rotation of 1.5 to 2.0%. The damping evaluated by the logarithmic decrement is shown in Fig. 6.38a for the three specimens D1, D2 and D3. Figure 6.38b is the data for the three specimens derived from the simulated earthquake runs, and in Fig. 6.35c the large-amplitude steady-state tests were used to evaluate the damping. For a connection rotation of 2% a typical value for a damping factor is 8%. A lower and upper bound for damping at this rotation (2%) seems to be 6% (Fig. 6.38c) and 11% (Fig. 6.38b).

7. SUMMARY AND CONCLUSIONS

7.1 Introduction

This chapter includes individual summaries of chapters 2 through 6,and a set of conclusions.

7.2 Outline of Experimental Work

In all, tests of 9 column-slab specimens are documented. Initially a pilot test was done (Appendix H), 5 specimens were tested statically (S1 to S5) and 3 dynamically (D1 to D3).

Certain geometric features were common to all specimens: they were 1/3 scale isolated slab-column connections of reinforced concrete; the slab and column dimensions were kept the same in plan, and were 1.8 by 1.8 m and 0.3 by 0.3 m respectively (Fig. 2.2); the relative size of the column made it much stiffer than the plate, thereby the column moved rigidly (Fig. 2.3); the span to depth ratio of the slab was 24, and the column to slab "spans" were in the ratio of 1 to 6; the reinforcement layout was isotropic.

There were three major variables in the experimental work: the reinforcement ratio, the amount of superimposed vertical load, and the rate of loading. The designation of the specimens follows:

Designations	Reinforcement Ratios	Superimposed Vertical Load
S1 (static)	0.65%	0
S2	0.98%	0
S3	1.31%	0
S4	0.98%	14.3 kN
S5	0.98%	28.6 kN
D1 (dynamic)	0.65%	0
D2	0.98%	0
D3	1.31%	0

The results from testing specimens S1, S2 and S3 were used to investigate the influence of the change in reinforcement ratio on the response of the specimens. Specimens S2, S4 and S5 were used to investigate the influence of superimposed vertical load. The superimposed vertical load on specimen S5 resulted in an average shear stress of $0.06\sqrt{f'_c}$ MPa (f'_c in MPa) at a section one-half the slab depth away from the column face. The specimens D1, D2 and D3 (tested dynamically) provided a comparison with specimens S1, S2 and S3 respectively, thereby the influence of the rate of strain on the response of the specimens was investigated.

7.3 Description of Experiments

In the statically tested specimens the load was applied cyclically (Fig. 3.1). The amplitude of the cycles was increased in 4 steps. At each of these levels a number of cycles of constant amplitude took place. In the final cycle the specimen was pushed to its limit, or the limit of the stroke of the jack (75 mm).

The dynamically tested specimens were subjected to three types of tests (Fig. 6.11a): simulated earthquake runs, free-vibrations, and steady-state tests. The maximum displacement caused by a simulated earthquake run was usually not exceeded by the steady-state and free-vibration tests that followed (Fig. 3.2 to 3.4).

7.4 Effect of Slab Reinforcement Ratio on Response to Increasing Load

The observed strengths of specimens S1 to S3 were compared with the calculated strengths assuming that yielding took place across the full width of the slabs (the "wide-beam" strength). The observed strength of specimen S1 was equal to its calculated wide-beam strength (Table 4.1). For specimen S2, the ratio of observed strength to calculated "wide beam" strength was 0.77. The ratio for specimen S3 was 0.61. No surface trace of inclined cracks was observed on specimens S1 to S3, and the measurements did not indicate the presence of an inclined crack. Therefore, the inability of specimens S2 and S3 to reach their full potential could not be categorically ascribed to the development of an inclined crack associated with a shear failure.

A model is presented to help understand the observed force-displacement relationships in terms of geometric and material properties of the specimens. This model is built up of a grid of beam elements responding in flexure and torsion. The analysis included the effects of cracking and yielding of elements, the effects of bar-slip, and the influence of cracking on the torsional stiffness of a reinforced concrete slab-member. The values of various quantities (moment-rotation relationships, displacements along the longitudinal centerline, angles of twist to the side of the column, yielding across the width

of the slab) calculated by the grid model are compared with the like observed quantities. Thereafter a comparison is drawn between the calculated response of specimens S1 and S3 to attempt to identify the reasons for the difference in the response of each specimen. The main conclusion derived from these comparisons is that the difference in the response of specimens S1 and S3 (that the yield moment of the full width of the slab was not developed for S3) could be explained in terms of flexural and torsional flexibilities of slab elements, and without invoking phenomena associated with shear failure.

7.5 Discussion of Observed Response of Specimens with Vertical and Lateral Load

The two specimens with superimposed vertical load developed inclined cracks at relatively large column-slab connection rotations (more than 4.5%). Up to failure, the crack patterns were similar to those observed on the slab surface of the specimens without superimposed vertical load.

The differences in material properties are accounted for by normalizing the observed strengths of specimens S2, S4, and S5 by their respective calculated "wide-beam" strengths (Table 5.1). The normalized strengths of specimens S4 and S5 (superimposed vertical load) were within 95% of that of specimen S2 (no superimposed vertical load), and it may be concluded that the superimposed vertical load used in the tests did not influence the response of the specimens significantly.

7.6 Dynamic Tests

The strength, stiffness, force-displacement relationships and inferred damping of the dynamically tested specimens D1 to D3 are

presented in Chapter 6.

The observed strengths of the dynamically tested specimens normalized by their respective calculated "wide-beam" strengths were larger than the normalized strengths of their statically tested counterparts (D1 vs. S1: 21%; D2 vs. S2: 27%; D3 vs. S3: 31%). A rate of strain in the reinforcing bars of 0.05/sec seems plausible, and at similar strain rates increases in lower yield stresses of up to 28% have been reported. It appeared that the observed increase in flexural strengths of the dynamically tested specimens over those of the statically tested could be attributed to the increase in the lower yield point of the reinforcement associated with higher strain rates.

Information on the frequency of the specimens at progressive stages in the testing were observed from free-vibration and steady-state tests, and calculated from the secant-stiffness observed in the moment-displacement relationships of the simulated earthquake runs. Initially, there was a rapid drop in stiffness, and considerable decreases in stiffness after relatively large connection rotations (1%) implied that significant yielding took place at large connections rotations. If the previously experienced maximum displacement was exceeded in a cycle by a specimen, the response could be described as stiff-to-soft (Fig. 6.15c). In response cycles that did not exceed the previously experienced maximum displacement, the behavior was soft-to-stiff (Fig. 6.15d).

The shape of the area enclosed by the hysteresis in a moment-displacement relationship also appeared to be dependent on the previously experienced maximum displacement, once the specimen had reached yielding.

If the previously experienced maximum displacement was exceeded in a response cycle, the area enclosed by the cycle appeared more uniform than an enclosed area resulting from response that did not exceed the previously experienced maximum displacement (compare Fig. 6.15c and d).

The calculated values of equivalent linear viscous damping were obtained from free-vibration tests, steady-state tests and simulated earthquake runs. The damping values derived from large-amplitude steady-state tests (those which resulted in a maximum displacement relatively close to the previously experienced maximum displacement) were calculated using assumed linear or cubic stiffnesses. A typical value for damping (expressed as a percentage of critical damping) at a connection rotation of 2% was about 8%. At a connection rotation of 1% the value for damping was about 5%. Within a range of reasonable connection rotations (up to a connection rotation of 2%) the small-amplitude and large-amplitude tests did not result in significantly different values of damping. At relatively large connection rotations the small-amplitude tests led to calculation of unreasonable high values of damping.

7.7 Conclusions

On the basis of the test results and the analyses reported, the following conclusions can be made about the reinforced concrete plate-column test specimens:

1. Nonlinear response of the plate-column specimens was well modelled by a relatively simple grid of beams responding in flexure and torsion. The "monotonic" moment-rotation curves calculated using this model matched closely the envelopes of the curves obtained under cyclic loading (static) in post-yield

as well as initial ranges of loading.

2. Difference in response of the specimens (inability of the relatively heavily reinforced specimens to achieve yielding across the full slab width) could be explained by flexural action, and without invoking the phenomena associated with shear failures.
3. Influence of the increase in reinforcement ratio in the isotropically reinforced slabs was to increase the strength of the column-slab connection significantly without a like increase in the connection stiffness. Though the relatively heavily reinforced specimens were potentially stronger, they could not fully achieve this potential within the same connection rotation as the lightly reinforced specimen.
4. The influence of reasonable amounts of superimposed vertical load (corresponding approximately to the slab dead load at a lower level of a multi-story structure) in addition to lateral loading was not significant. Those specimens with superimposed vertical load reached 95% of the strength of a specimen with like reinforcement ratio but no superimposed vertical load. Though failure was accompanied by the full development of an inclined crack (associated with shear failure), this failure took place at very large connection rotations (larger than 4.5%).
5. The rate of loading was observed to have caused an increase in the observed strength of the dynamically tested specimens of from 20% to 30% over that of the statically tested specimens. The increase in the lower yield stress of the reinforcement

at the larger rates of strain appeared to be compatible with the observed increase in strength.

6. On initial loading the stiffness of the specimens underwent a rapid drop for relatively small displacements (before yield).
7. Observed jumps in the response to steady-state base motion were found to be attributable to changes in the damage state of the specimen rather than to properties of a stationary moment-rotation relationship.
8. A representative value for the calculated equivalent viscous damping for the specimens at a connection rotation of 2% was 8% of critical damping, with 4% as the lower bound. At a connection rotation of 1%, the representative value of damping was 5%.

LIST OF REFERENCES

1. Aalami, B., "Moment-Rotation Relation Between Column and Slab," Journal of the American Concrete Institute, May 1972, p. 263.

2. ACI 318-77, Building Code Requirements for Reinforced Concrete, American Concrete Institute, December 1977, Detroit.

3. Allen, F., "Lateral Load Characteristics of Flate Plate Structures," Masters Degree Thesis, Monash University, Australia, June 1976.

4. Allen, F. and Darvall, P., "Lateral Load Equivalent Frame," Journal of the American Concrete Institute, July 1977, No. 7, Proceedings Vol. 74, p. 294.

5. Bertero, V.V., Rea, D., Mahin, S., and Atalay, M.B., "Rate of Loading Effects on Uncracked and Repaired Reinforced Concrete Members," Proc. 5th World Conference on Earthquake Engineering, Vol. 2, Rome, 1974, pp. 1461-1470.

6. Cardenas, A., and Sozen, M.A., "Strength and Behavior of Isotropically and Nonisotropically Reinforced Concrete Slabs Subjected to Combinations of Flexural and Torsional Moments," Civil Engineering Studies, Structural Research Series No. 336, University of Illinois, Urbana, May 1968.

7. Carpenter, J.E., Kaar, P.H., and Corley, W.G., "Design of Ductile Flat Plate Structures to Resist Earthquakes," Proc. 5th World Conference on Earthquake Engineering, Rome, 1973.

8. Clark, L.A., and White, I.G., "Test to Determine the Torsional Stiffness of Flexurally Cracked Slab Elements," Cement and Concrete Association, Wexham Springs, Slough SL3 6PL, 1978.

9. Collins, M.P., Walsh, P.F., Archer, F.E., and Hall, A.S., "Ultimate Strength of Reinforced Concrete Beams Subjected to Combined Torsion and Bending," Torsion of Structural Concrete, ACI Special Publication SP-18, ACI, Detroit, 1968, pp. 379-402.

10. Corley, W.G., and Jirsa, J.O., "Equivalent Frame Analysis for Slab Design," Journal of the American Concrete Institute, No. 11, Nov. 1970, Proc. Vol. 67, pp. 875-884.

11. Criswell, M.E., "Static and Dynamic Response of Reinforced Concrete Slab-Column Connections," Shear in Reinforced Concrete, ACI Special Publication SP-42, SP42-31, p. 721.

12. Criswell, M.E., "Strength and Behavior of Reinforced Concrete Slab-Column Connections Subjected to Static and Dynamic Loadings," Dec. 1970, U.S. Army Engineer Waterways Experiment Station, Vicksburg, Mississippi, Technical Report N-70-1 (Final Report).

13. Duffing, G., "Erzwungene Schwingungen bei veränderlicher Eigenfrequenz," Braunsweig, F. Vieweg u. Sohn, 1918.

14. Elias, Ziad M., "Sidesway Analysis of Flat Plate Structures," Journal of the American Concrete Institute, March 1979, No. 3, Proc. Vol. 76, p. 421.

15. Fraser, D.J., "Equivalent Frame Method for Beam-Slab Structures," Journal of the American Concrete Institute, May 1977, No. 5, Proc. Vol. 74, p. 223.

16. Gesund, H., and Goli, H.B., "Limit Analysis of Flat-Slab Buildings for Lateral Loads," Journal of the Structural Division, Proc. of the ASCE, Vol. 105, No. ST11, Nov. 79, p. 2187.

17. Ghali, A., Elmasri, M.Z., and Dilger, W., "Punching of Flat Plates under Static and Dynamic Horizontal Forces," Journal of the American Concrete Institute, Oct. 1976, No. 10, Proc. Vol. 73, p. 566.

18. Hanson, N.W., and Hanson, J.M., "Shear and Moment Transfer Between Concrete Slabs and Columns," Journal of the PCA Research and Development Laboratories, PCA, Vol. 10, No. 1, Jan. 1968, pp. 2-16.

19. Hartley, G., Rainer, J.H., and Ward, H.S., "Static and Dynamic Properties of a Reinforced Concrete Building Model," Division of Building Research, National Research Council of Canada, Ottawa, April 1979.

20. Hawkins, N.M., "Seismic Response Constraints for Slab Systems," Proc. of a workshop on Earthquake-Resistant Reinforced Concrete Building Construction, July 11-15, 1977, Berkeley, California, p. 1253.

21. Hawkins, N.M., "Seismic Response of Reinforced Concrete Flat Plate Structures," 7th World Conference on Earthquake Engineering, Istanbul, Turkey, Sept. 1980.

22. Hawkins, N.M., Mitchell, D., and Symonds, D.W., "Hysteretic Behavior of Concrete Slab to Column Connections," 6th World Conference on Earthquake Engineering, Vol. III, 1977, p. 2791.

23. Hsu, T.T.C., "Torsion of Structural Concrete--A Summary on Pure Torsion," Torsion of Structural Concrete, ACI Publication SP-18, ACI, Detroit, 1968, p. 165.

24. Ibanez, P., "Identification of Dynamic Structural Models from Experimental Data," UCLA-ENG-7225, School of Engineering and Applied Science, University of California, Los Angeles, March, 1972.

25. Iwan, W.D., "Steady-State Dynamic Response of a Limited Slip System," Journal of Applied Mechanics, Vol. 35, No. 2, June 1968, pp. 322-326.

26. Iwan, W.D., "Applications of Nonlinear Analysis Techniques," Applied Mechanics in Earthquake Engineering, Nov. 1974, Edited by the American Society of Mechanical Engineers, New York, p. 135.

27. Jennings, P.C., "Periodic Response of a General Yielding Structure," Journal of the Engineering Mechanics Division, ASCE, Vol. 90, No. EM2, Proc. Paper 3871, April 1964, pp. 131-166.

28. Jones, P.G., and Richart, F.E., "The Effect of Testing Speed on Strength and Elastic Properties of Concrete," Proc. ASTM, Vol. 36, (1936), pp. 380-391.

29. Kanoh, Y., and Yoshizaki, S., "Strength of Slab-Column Connections Transferring Shear and Moment," Journal of the American Concrete Institute, March 1979, p. 461.

30. Lampert, P., "Postcracking Stiffness of Reinforced Concrete Beams in Torsion and Bending," Analysis of Structural Systems for Torsion, ACI Special Publication SP-35, ACI, Detroit, Michigan, p. 385.

31. Lampert, P., and Thurlimann, B., "Torsionversuche on Stahlbetonbalken," Bericht Nr. 6506-2, 1968, Institute fur Baustatik, ETH, Zurich.

32. Lenschow, R.J., and Sozen, M.A., "A Yield Criterion for Reinforced Concrete under Biaxial Moments and Forces," Civil Engineering Studies, Structural Research Series No. 311, University of Illinois, Urbana, July 1966, 527 pp.

33. Lopez, L.A., Dodds, R.H., Rehak, D.R., and Urzua, J., "Polo-Finite: A Structural Mechanics System for Linear and Nonlinear Analysis," Civil Engineering Systems Laboratory, University of Illinois at Urbana-Champaign, and Department of Civil Engineering and the Academic Computer Center, University of Kansas, Lawrence, Kansas.

34. Mast, P.E., "Stresses in Flat Plates near Columns," Journal of the American Concrete Institute, Oct. 1970, p. 761.

35. Mehrain, M., and Aalami, B., "Rotational Stiffness of Concrete Slabs," Journal of the American Concrete Institute, Sept. 1974, p. 429.

36. Newmark, N.M., and Rosenblueth, E., Fundamentals of Earthquake Engineering, Prentice-Hall, Inc., Englewood Cliffs, New Jersey, 1971.

37. Oppenheim, A.V., and Schafer, R.W., Digital Signal Processing, Prentice-Hall, Inc., p. 211.

38. Park, R., and Paulay, T., Reinforced Concrete Structures, John Wiley, New York, 1975.

39. Park, R., and Islam, S., "Strength of Slab-Column Connections with Shear and Unbalanced Flexure," Journal of the Structural Division, ASCE, Sept. 1976, p. 1879.

40. Pecknold, D.A., "Slab Effective Width for Equivalent Frame Analysis," Journal of the American Concrete Institute, April 1975, p. 135.

41. Pecknold, D.A., "Effective Width of Orthotropic Plate," Journal of the Structural Division of ASCE, Vol. 104, No. ST5, May 1978, p. 867.

42. Seible, F., Ghali, A., and Dilger, W.H., "Preassembled Shear Reinforcing Units for Flat Plates," Journal of the American Concrete Institute, Title No. 77-5, No. 1, Proc. V. 77, Jan./Feb. 1980.

43. Stoker, J.J., Nonlinear Vibrations, Interscience Publishers, New York, 1950.

44. Sozen, M.A., and Otani, S., "Performance of the University of Illinois Earthquake Simulator in Reproducing Scaled Earthquake Motions," Proceedings, U.S.-Japan Seminar on Earthquake Engineering with Emphasis on the Safety of School Buildings, Sept. 1970, The Japan Earthquake Engineering Promotion Society, Tokyo, 1971, pp. 278-302.

45. Takeda, T., Sozen, M.A., and Nielson, N.N., "Reinforced Concrete Response to Simulated Earthquake," Structural Divison Journal, ASCE, Vol. 96, No. ST12, Dec. 1970.

46. Thomson, W.T., Theory of Vibration with Applications, Prentice-Hall, Inc., Englewood Cliffs, New Jersey.

47. Timoshenko, S., and Woinowsky-Krieger, S., Theory of Plates and Shells, McGraw-Hill Book Company, New York, 1959.

48. Timoshenko, S., Young, D.H., and Weaver, W., Vibration Problems in Engineering, John Wiley and Sons, Inc., New York, 1974.

49. Vanderbilt, D.M., "Equivalent Frame Analysis of Unbraced Concrete Frames," Paper submitted to the American Concrete Institute Conference, Nov. 1979, Washington, DC.

50. Warwaruk, J., "Torsion in Reinforced Concrete," Paper delivered at the American Concrete Institute Annual Conference, Nov. 1979, Washington, DC.

51. Yettram, A., and Husain, H.M., "Grid Framework Method for Plates in Flexure," Proc., ASCE, Journal of the Engineering Mechanics Division, June 1965, p. 53.

TABLE 2.1 Properties of Specimens

SPECIMEN	REINFORCEMENT RATIO ρ	TENSILE STRENGTH OF CONCRETE f_t [MPa]	COMPRESSIVE STRENGTH OF CONCRETE f'_c [MPa]	YIELD STRESS OF STEEL f_y [MPa]	YIELD STRAIN IN STEEL ε_y
S1	0.0065	2.9	45.8	323	0.0016
S2	0.0098	2.3	35.1	330	0.0016
S3	0.0131	2.2	33.9	335	0.0017
S4	0.0098	2.2	34.9	320	0.0016
S5	0.0098	2.4	35.2	340	0.0018
D1	0.0065	3.3	36.3	290	0.0015
D2	0.0098	2.3	33.9	327	0.0015
D3	0.0131	3.0	36.5	355	0.0015

TABLE 3.1 Idealized Testing Sequence: Dynamic

SEQUENCE	SIMULATED EARTHQUAKE RUN No.	FREE VIBRATION No.	STEADY STATE No.
1		1	
2	1		
3		2	
4	2		
5		3	
6			1
7		4	
8	3		
9		5	
10			2
11		6	
12	4		
13		7	
14			3
15		8	
16	5		
17		9	
18			4
19		10	
20	6		
21		11	
22			5

TABLE 4.1 Strength Comparisons

SPECIMEN	OBSERVED STRENGTH M_{OBS} [kNm]	WIDE BEAM CALCULATED STRENGTH* M_{YL} [kNm]	WIDE BEAM M_{OBS}/M_{YL}	BEAM ANALOGY CALCULATED STRENGTH** M_{BA} [kNm]	BEAM ANALOGY M_{OBS}/M_{BA}
S1	34.2	34.2	1.00	29.0	1.18
S2	38.8	50.5	0.77	30.0	1.29
S3	41.1	67.1	0.61	33.0	1.25

* Yielding across full width of slab.
Assumptions used given in Appendix G.2.

** Park and Islam (39) beam analogy.

TABLE 5.1 Comparisons of Strengths

SPECIMEN	OBSERVED STRENGTH M_{OBS} [kNm]	CALCULATED STRENGTH* M_{YL} [kNm]	M_{OBS}/M_{YL}
S2	38.8	50.5	0.77
S4	35.5	49.1	0.72
S5	37.5	51.4	0.73

* Yielding across full width of slabs.

TABLE 6.1 Comparisons of Strengths

SPECIMEN	OBSERVED STRENGTH M_{OBS} [kNm]	CALCULATED STRENGTH* M_{YL} [kNm]	M_{OBS}/M_{YL}
S1	34.2	34.2	1.00
S2	38.8	50.5	0.77
S3	41.1	67.1	0.61
D1	36.8	30.3	1.21
D2	48.8	49.6	0.98
D3	56.6	68.0	0.80

TABLE 6.2 Comparisons of Normalized Strengths

SPECIMENS	$\frac{(M_{OBS}/M_{YL})^{Dynamic}}{(M_{OBS}/M_{YL})^{Static}}$	% INCREASE
D1/S1	1.21/1.00 = 1.21	21%
D2/S2	0.98/0.77 = 1.27	27%
D3/S3	0.61/0.80 = 1.31	31%

* Yielding across full width of slab .

TABLE 6.3

Damping Values Calculated from the M.A.F.* of Steady-State Tests

SPECIMEN	STEADY-STATE TEST	DAMPING AS % OF CRITICAL DAMPING		
		β_1 **	β_2 ***	β_3 ****
D1	SS3.2	7.0	7.0	8.0
D1	SS4.2	8.0	8.0	8.0
D2	SS6	9.0	8.0	8.0
D3	SS2.2	6.0	6.0	7.0
D3	SS3.2	7.0	7.0	8.0

*M.A.F. = maximum amplification factor

**$\text{M.A.F.} = \sqrt{1 + 1/(2\beta_1)^2}$

***$\text{M.A.F.} = 1/(2\beta_2)$

****$\text{M.A.F.} = 1/(2\beta_3) \times \frac{\omega_r}{\omega_n}$

ω_r = resonance frequency

ω_n = natural frequency

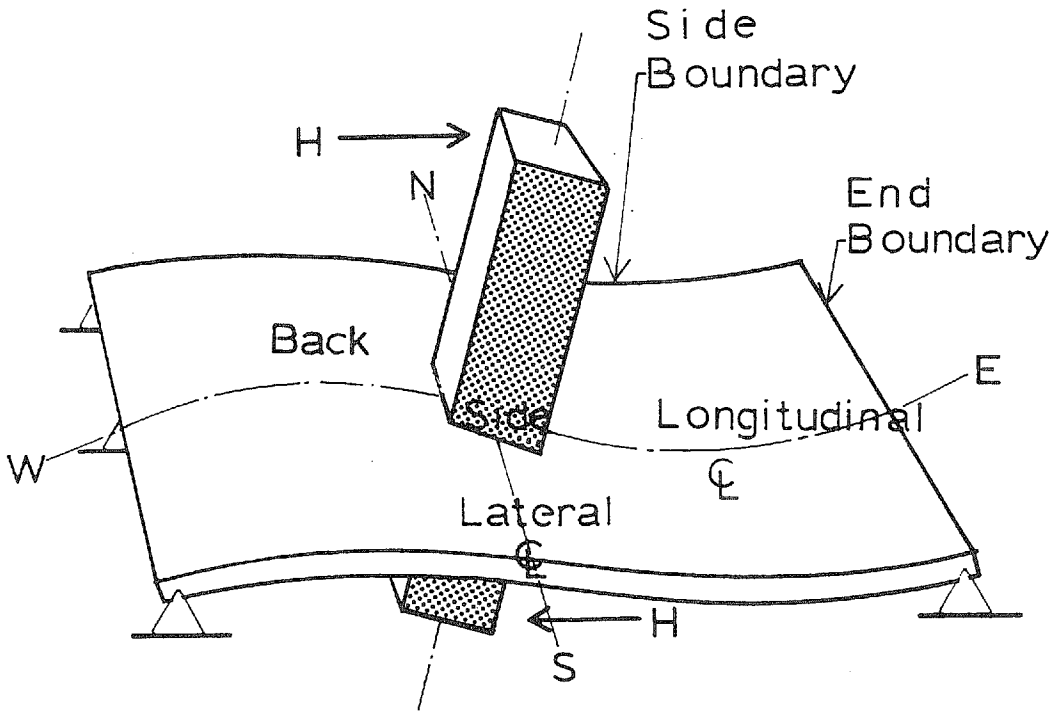

Fig. 2.1 Illustration of Terms Used to Describe Specimens

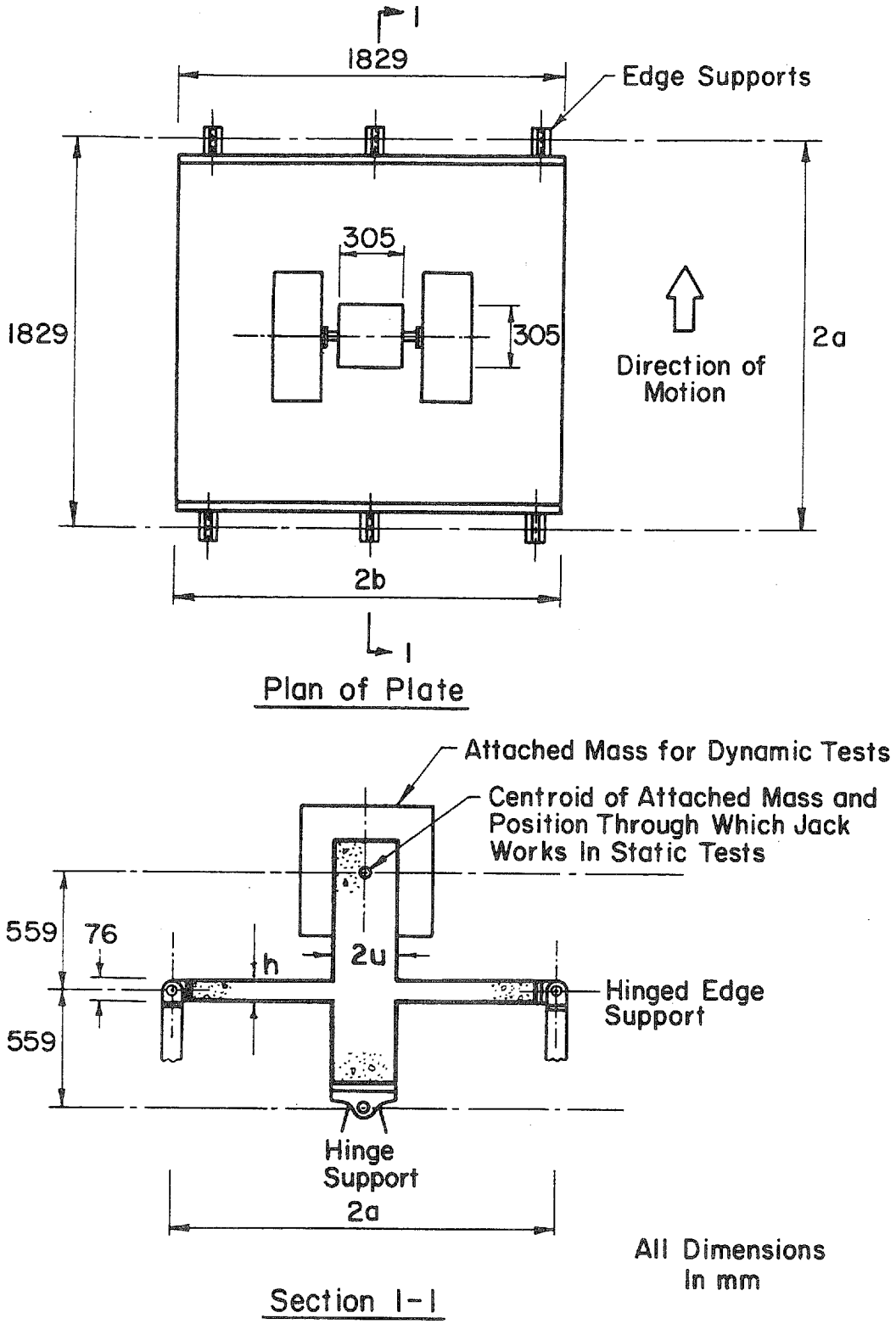

Fig. 2.2 Section and Plan of Assembly

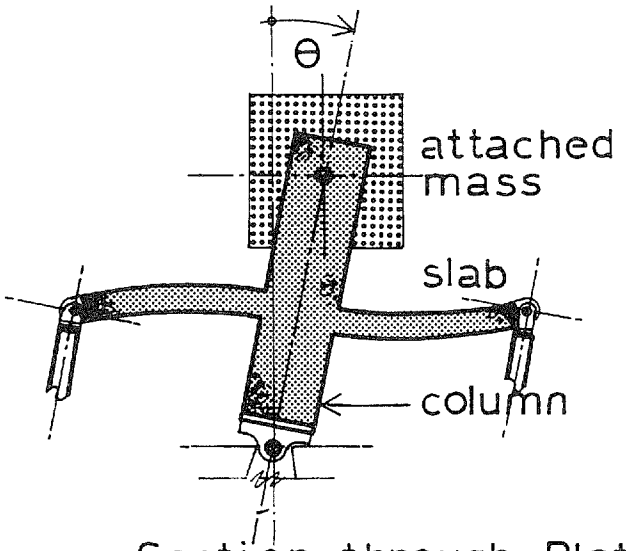

Section through Plate

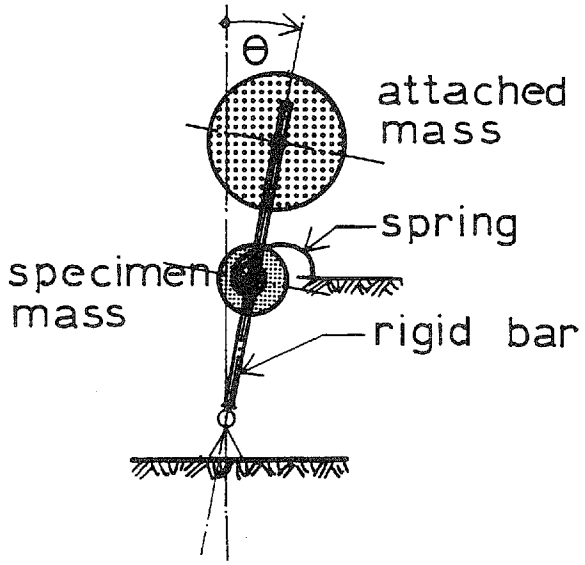

S D O F System

θ = s d o f.

Fig. 2.3 Idealized SDOF System

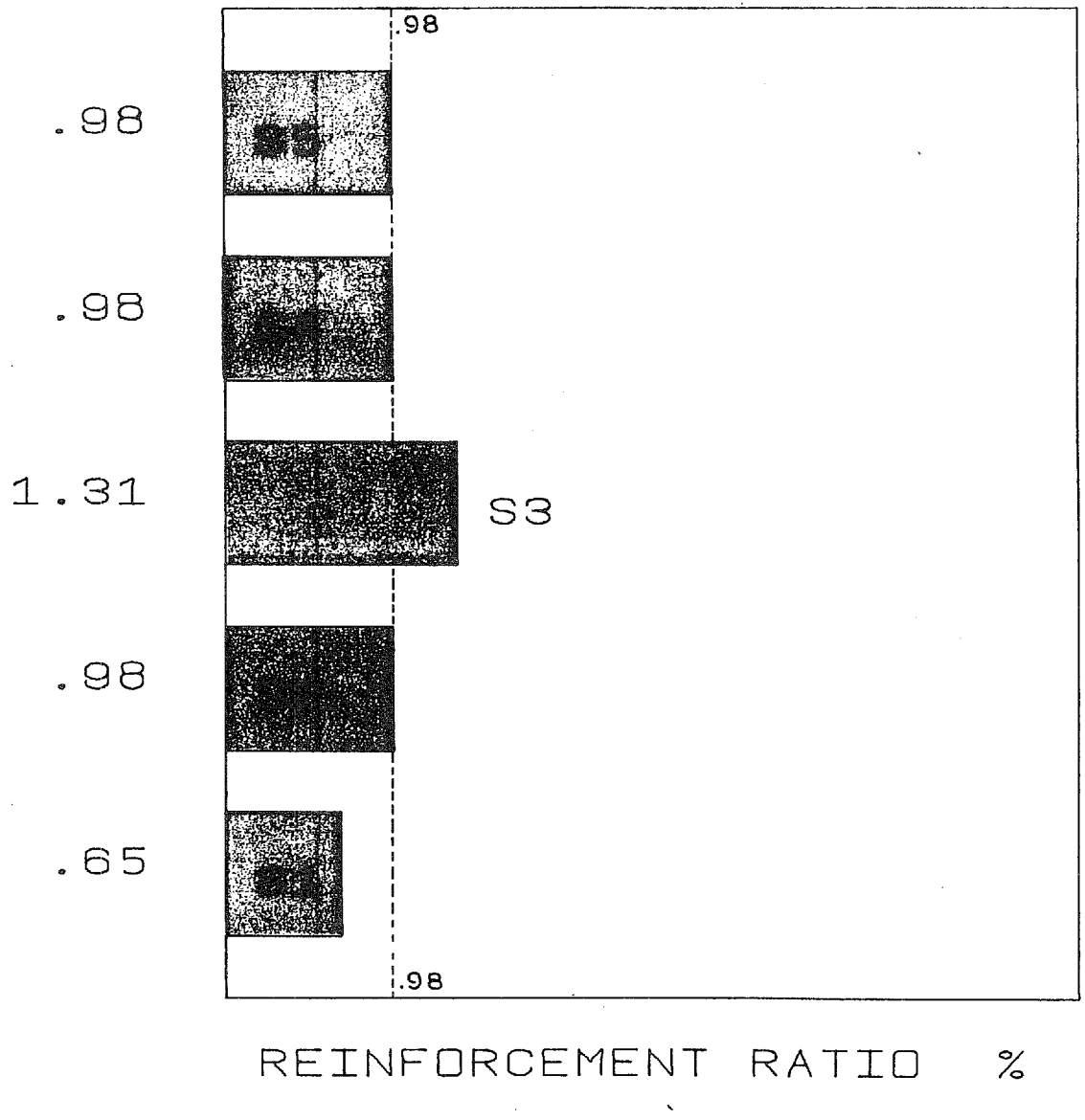

Fig. 2.4 Reinforcement Ratios in Static Specimens

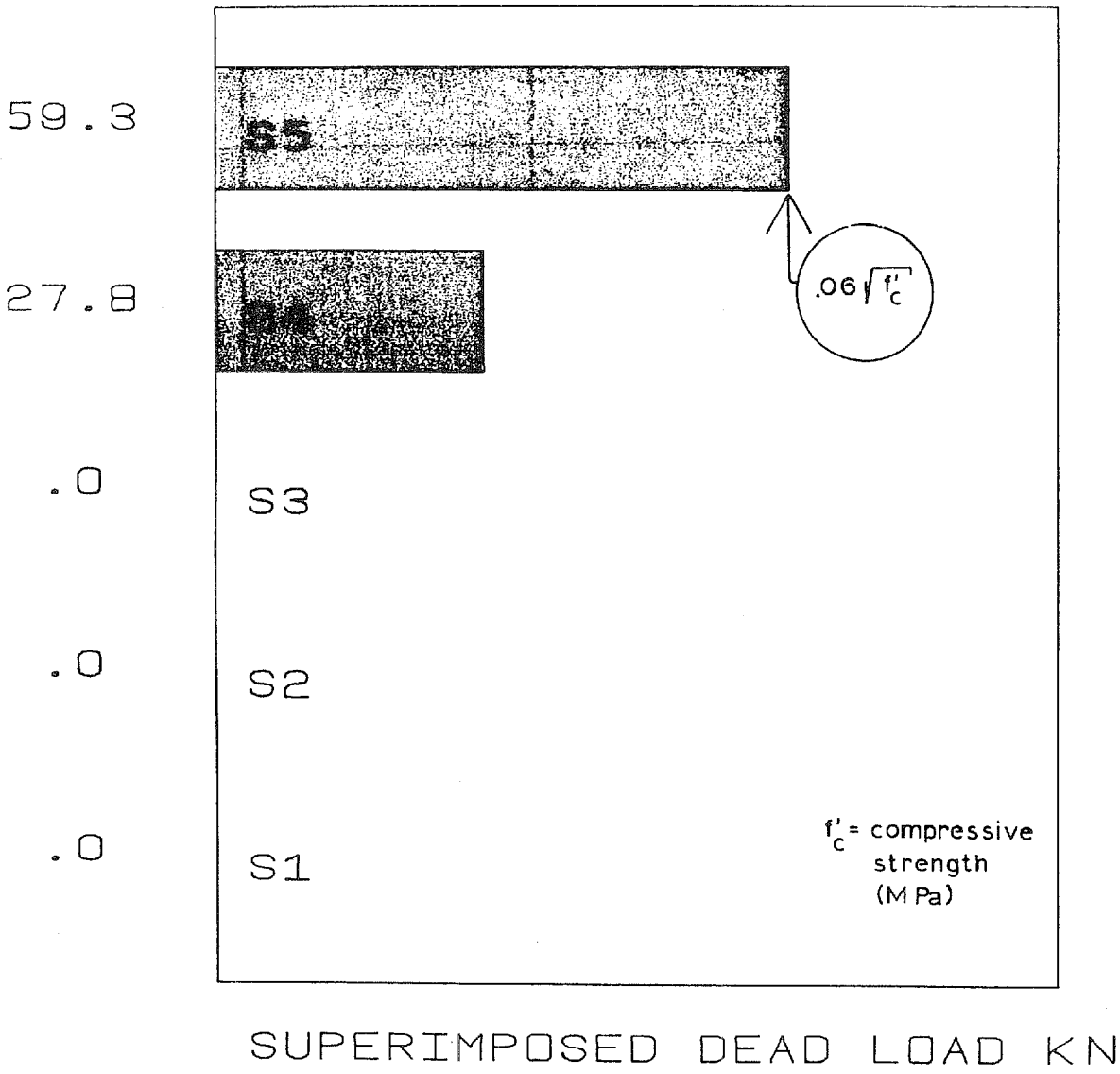

Fig. 2.5 Superimposed Dead Load in Static Specimens

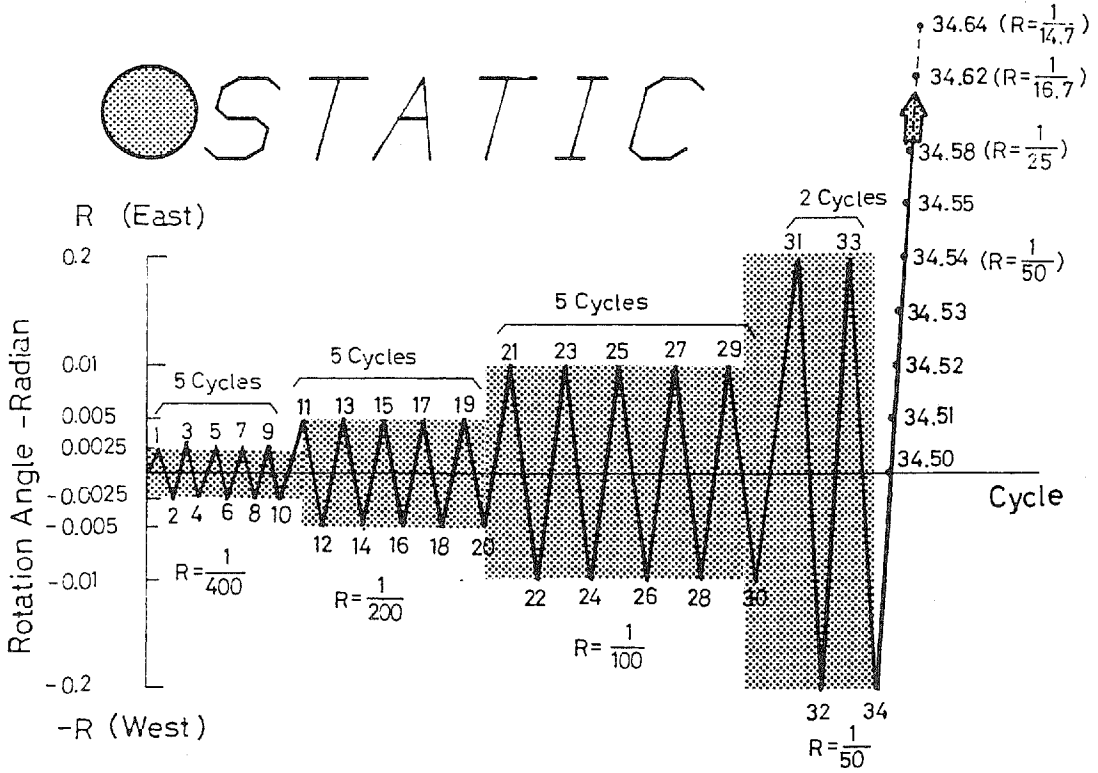

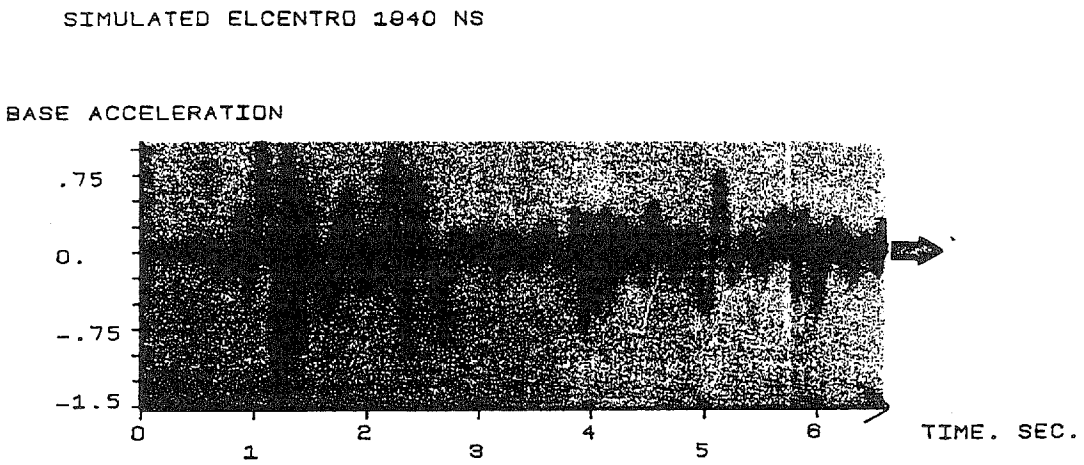

Fig. 2.6 Idealization of Static vs. Dynamic Variable

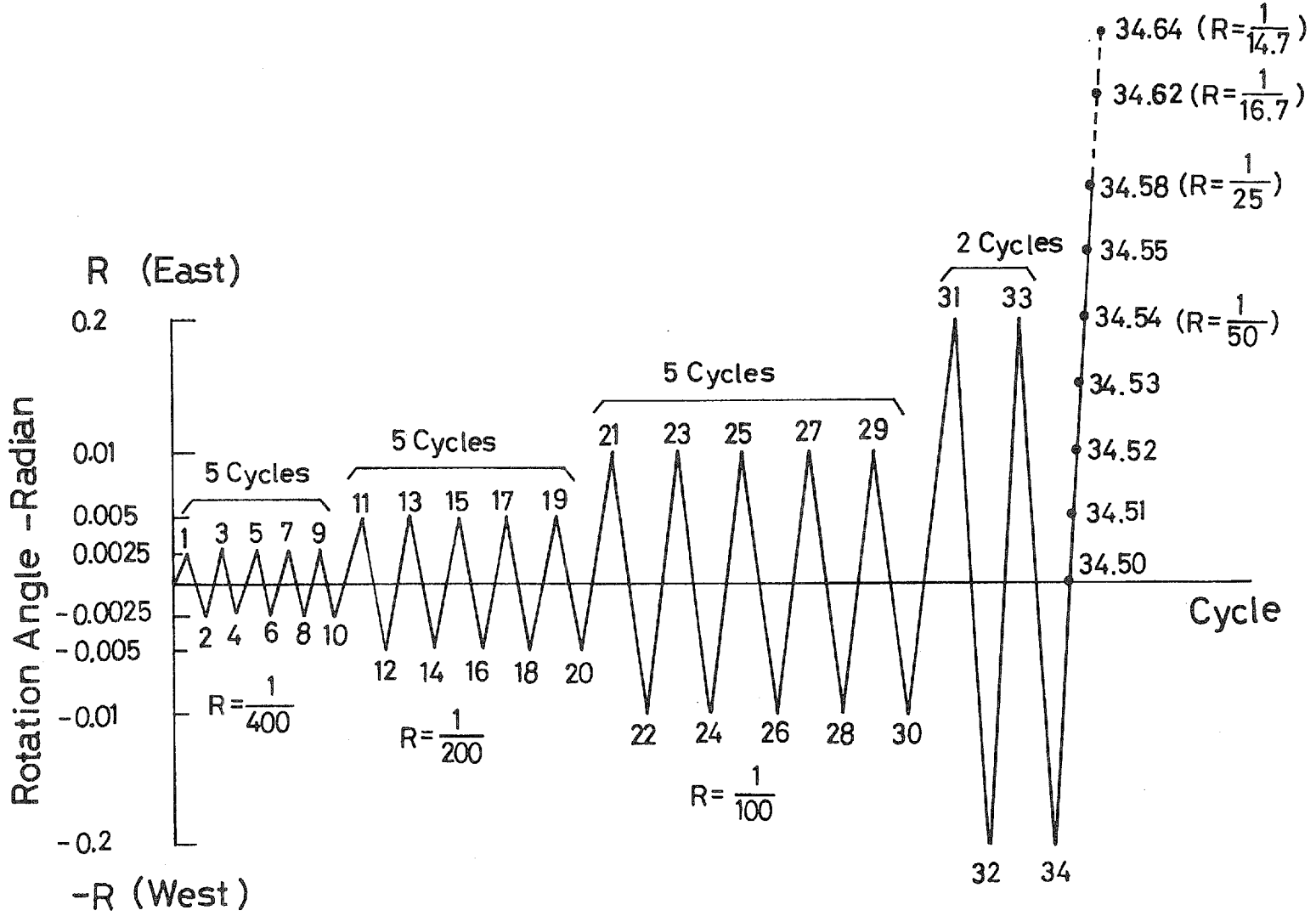

Fig. 3.1 Loading Pattern in Static Tests

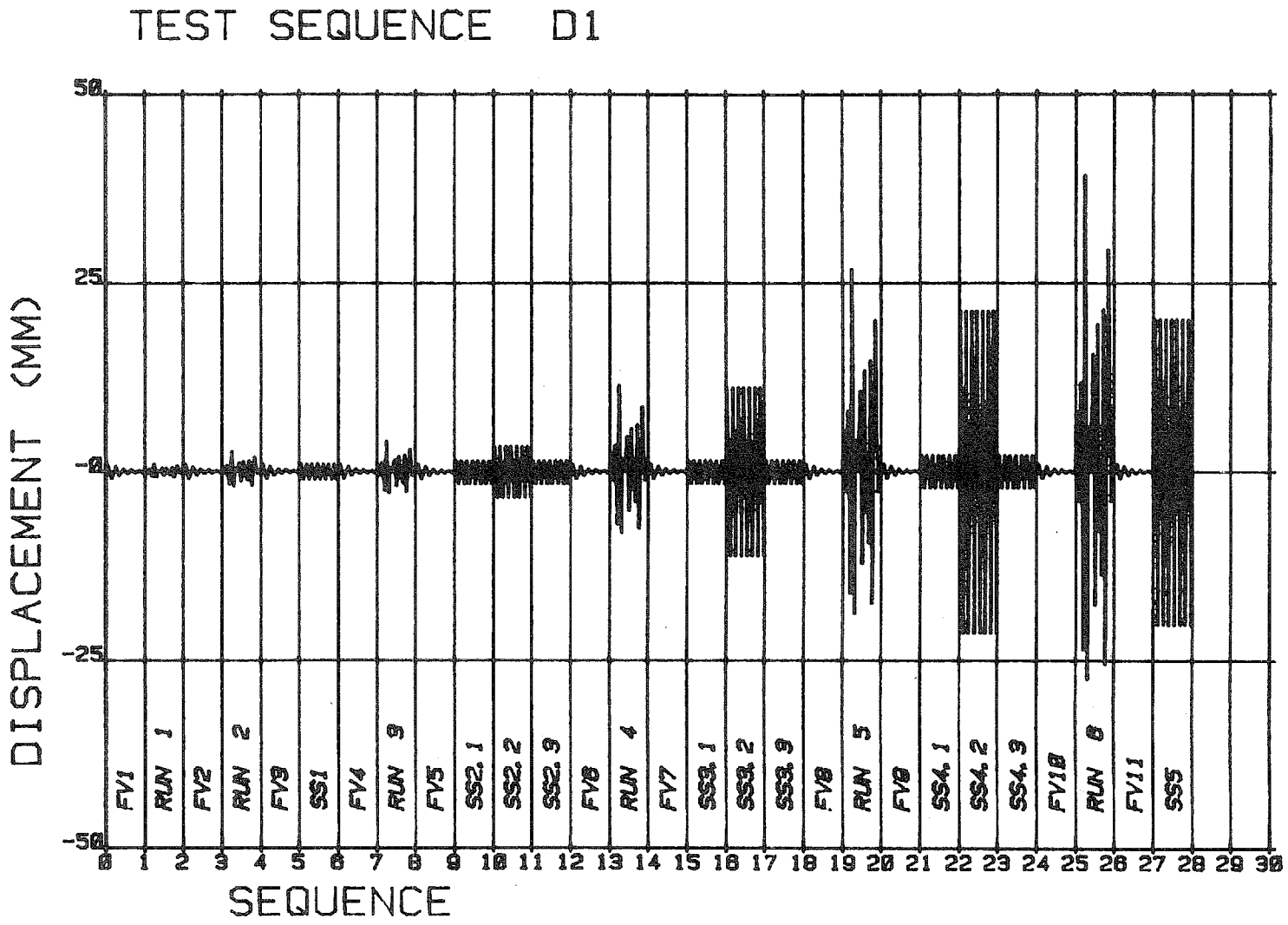

Fig. 3.2 Sequence in Testing of Dynamic Specimen D1

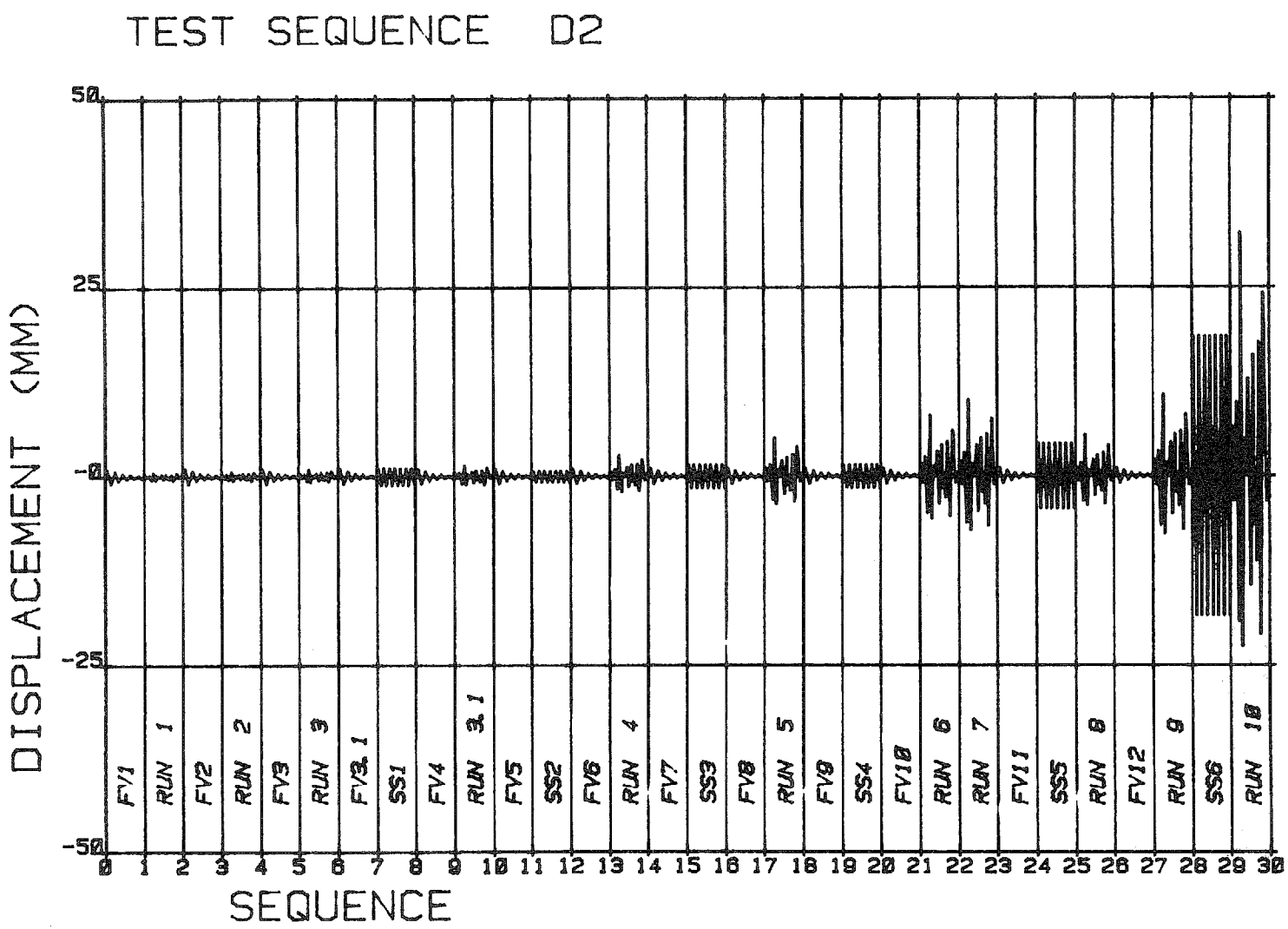

Fig. 3.3 Sequence in Testing of Dynamic Specimen D2

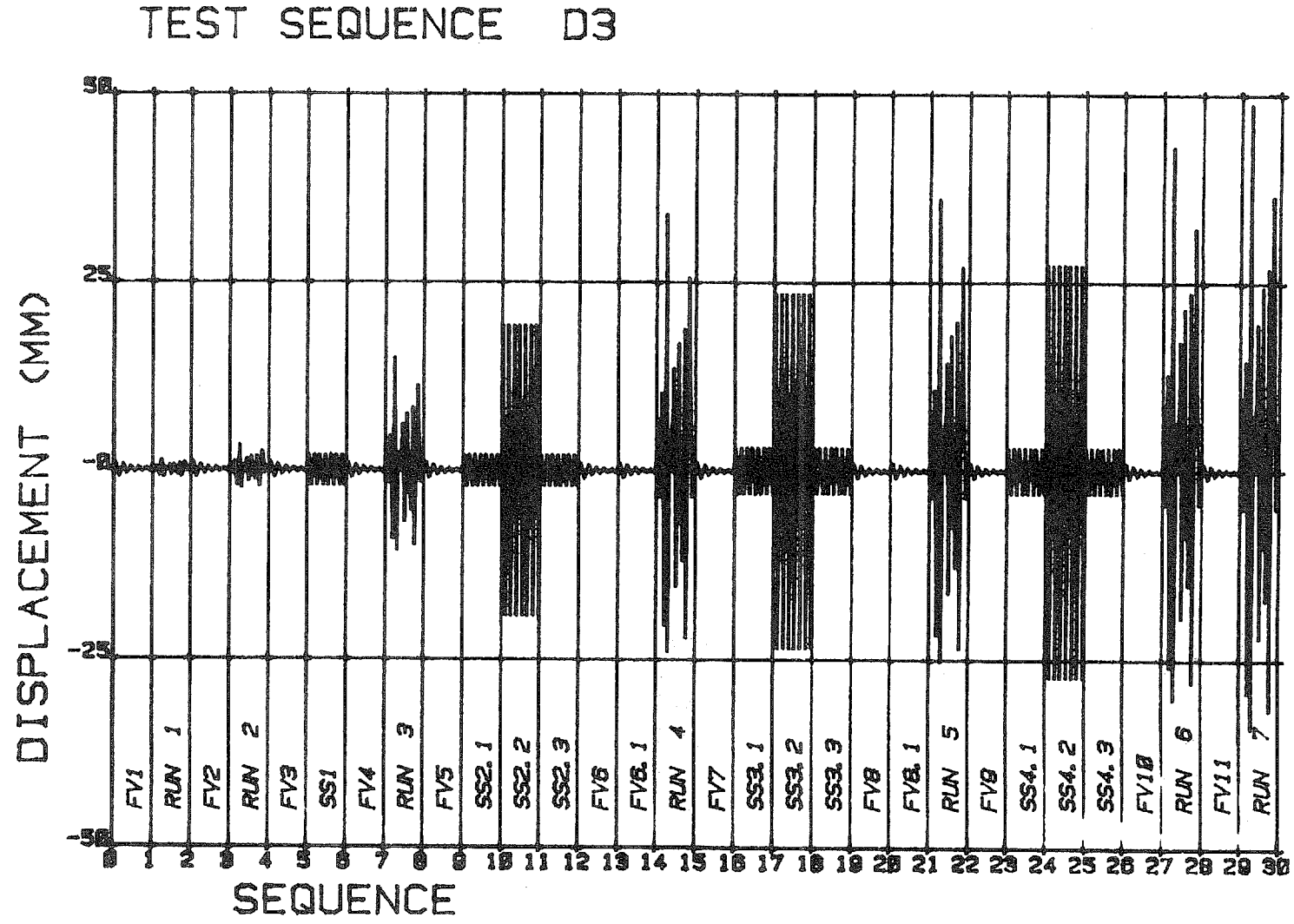

Fig. 3.4 Sequence in Testing of Dynamic Specimen D3

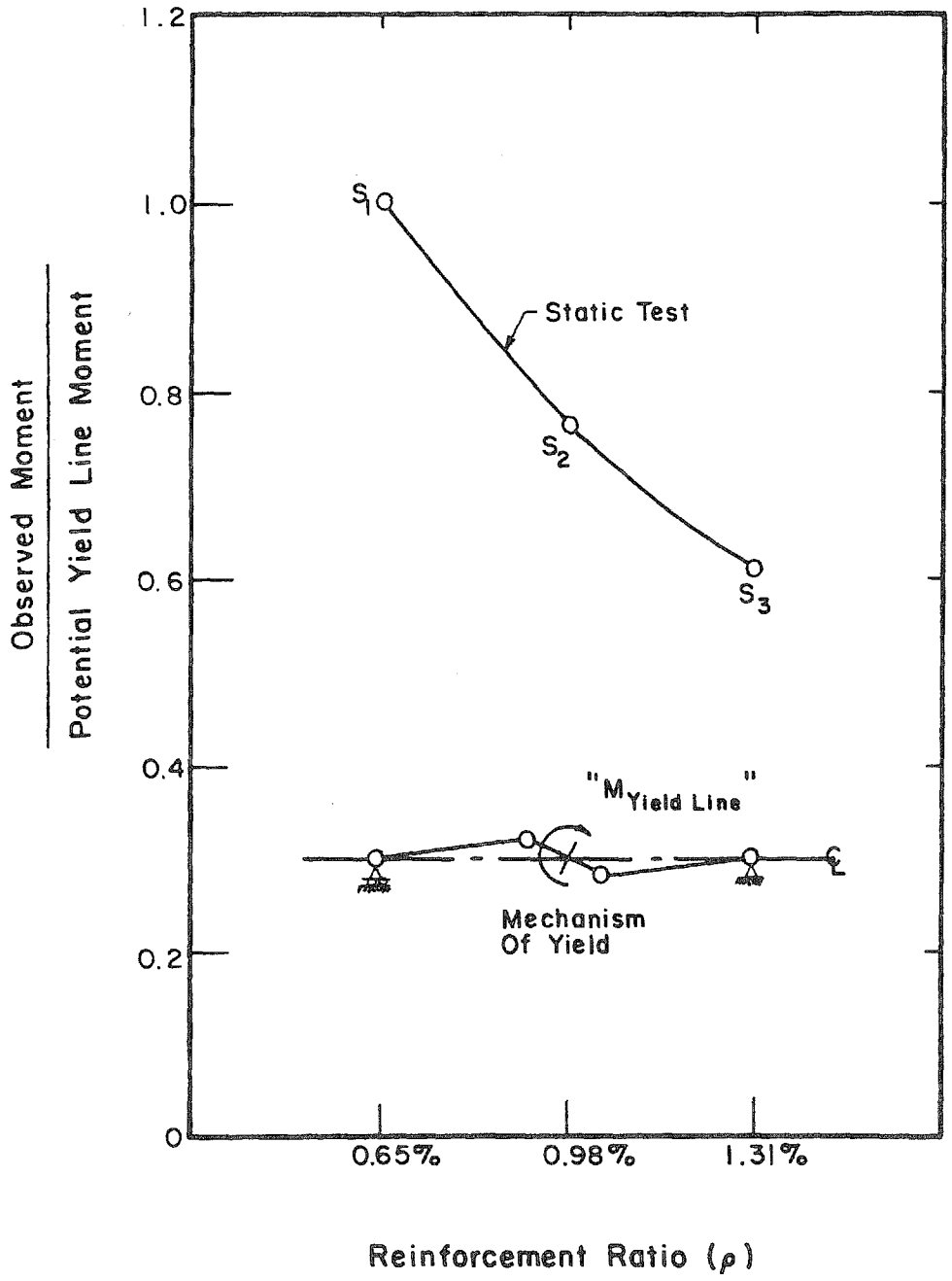

Fig. 4.1 Normalized Observed Strengths for Statically Tested Specimens S1 to S3

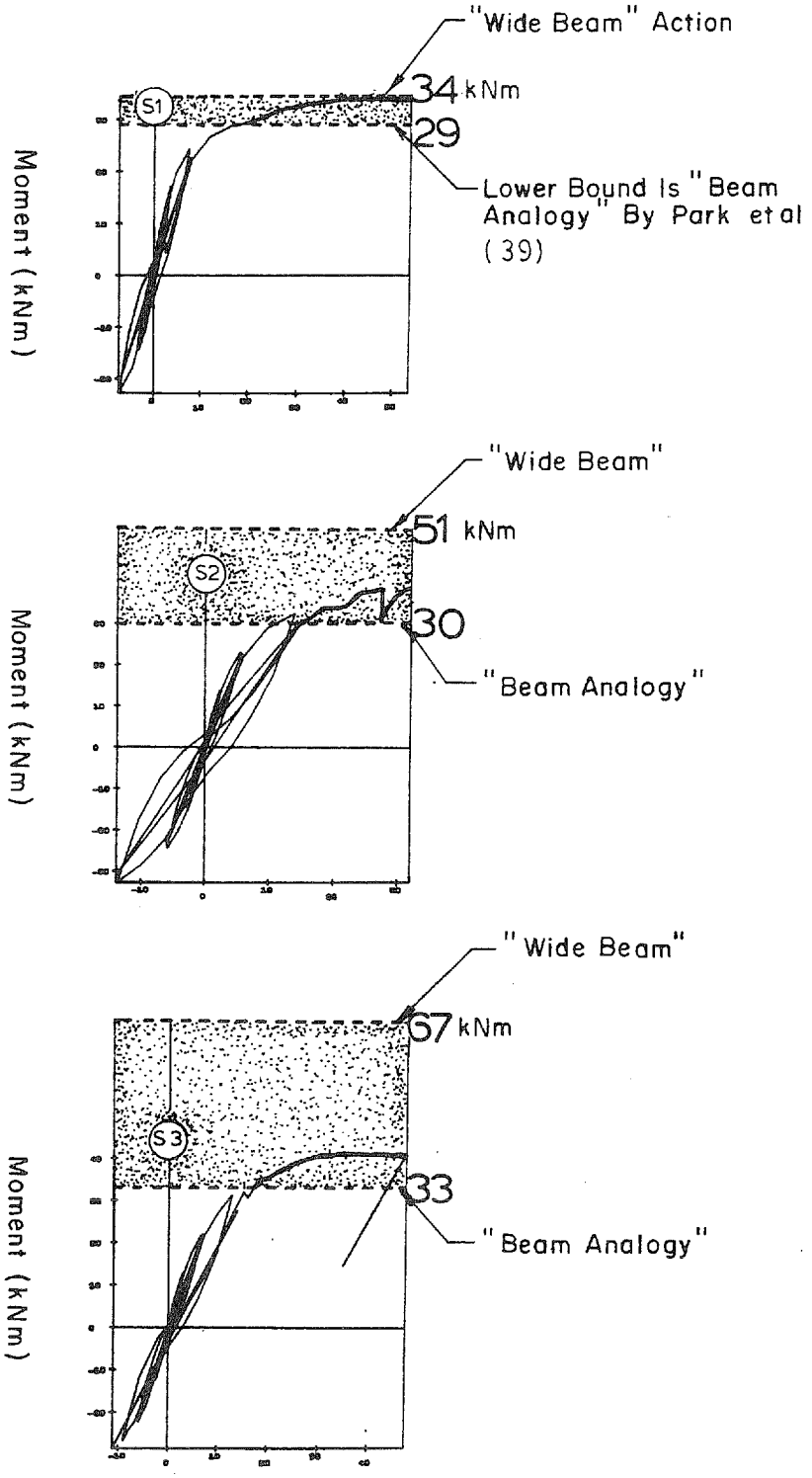

Fig. 4.2 Strength Comparisons for Specimens S1 to S3

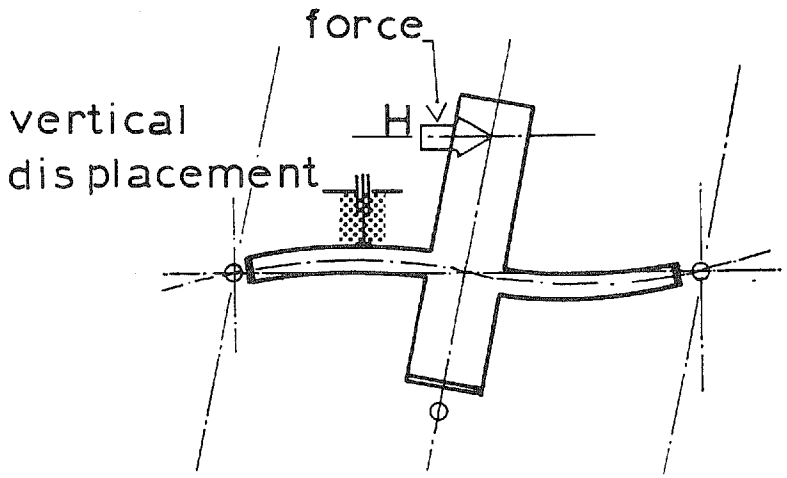

(a) Position on Slab of LVDT Measuring Vertical Displacement

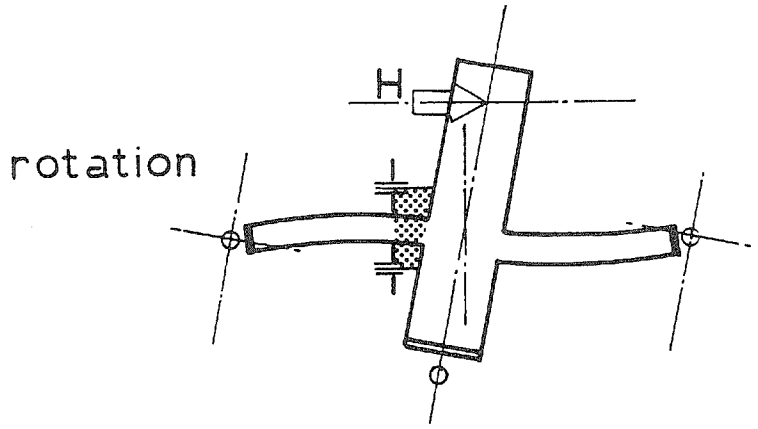

(b) Column Rotation Measured by Horizontal LVDT's

Fig. 4.3 Measurement Positions to Monitor Inclined Crack Formation

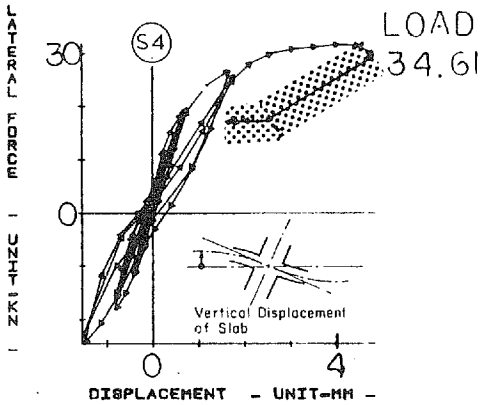

(a) Force vs. Displacement, S4.

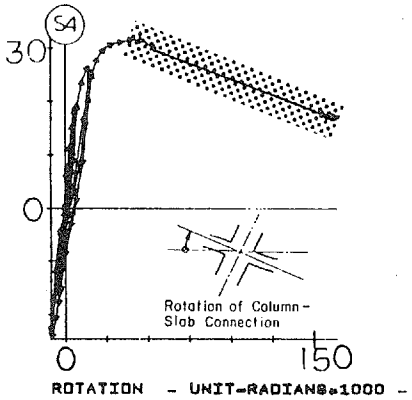

(b) Force vs. Rotation, S4.

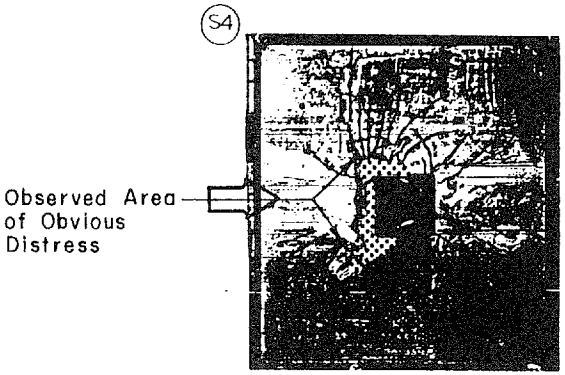

(c) Slab Surface, S4.

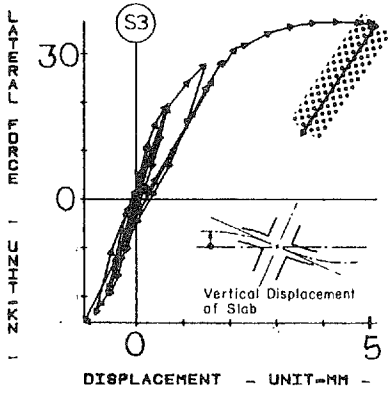

(d) Force vs. Displacement, S3.

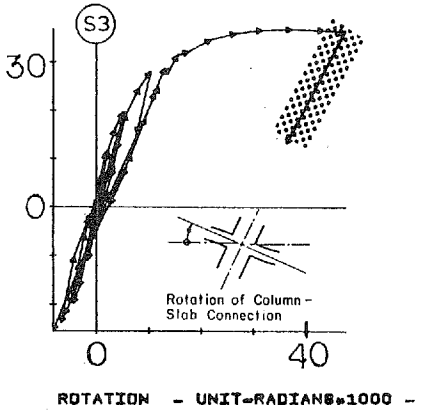

(e) Force vs. Rotation, S3.

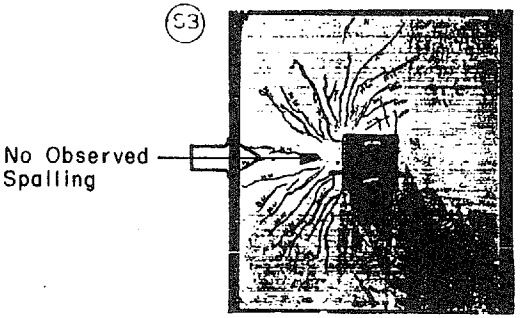

(f) Slab Surface, S3.

Fig. 4.4 Comparison of Vertical Slab Displacement and Column Rotation Measurements of Specimens S3 and S4

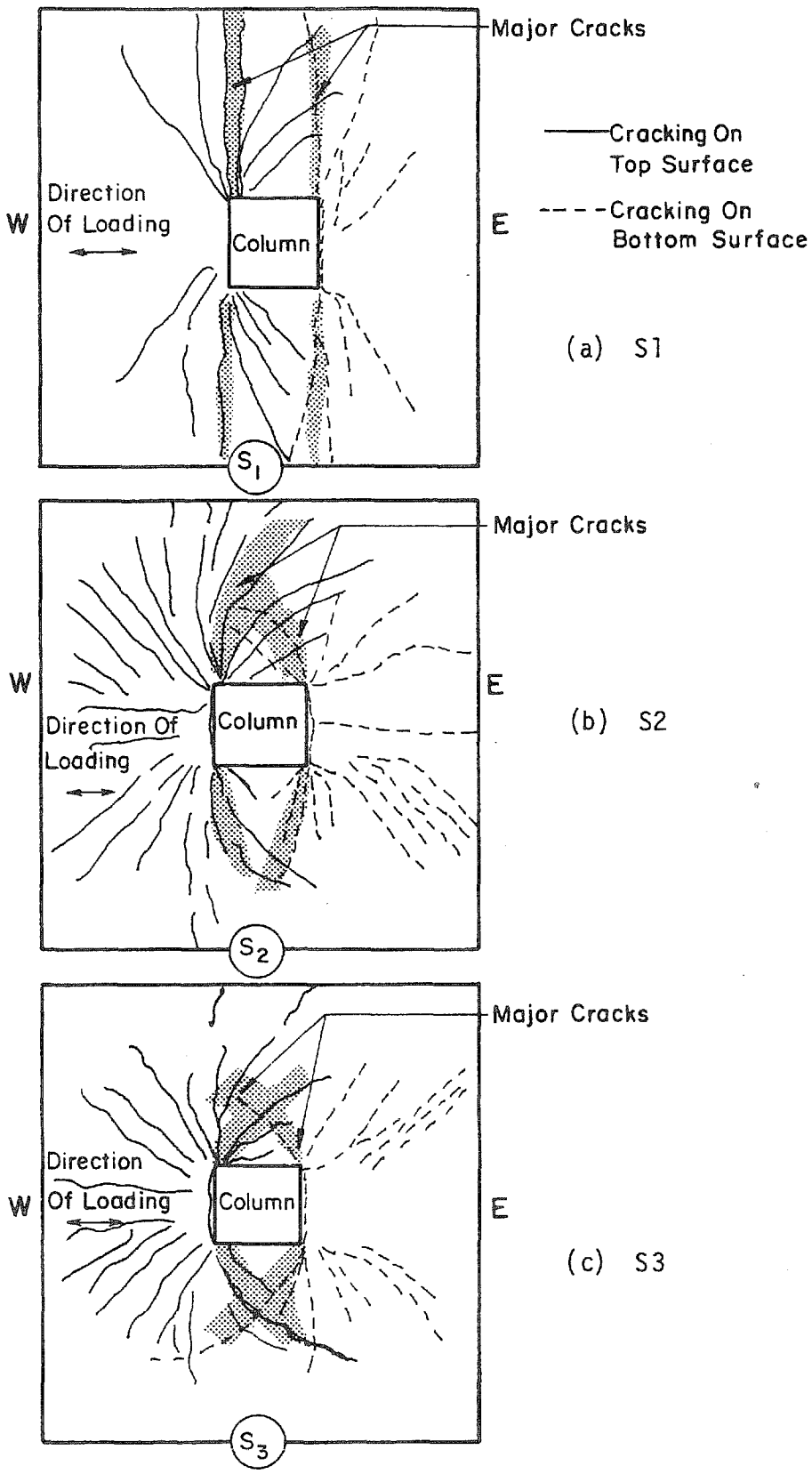

Fig. 4.5 Idealized Crack Patterns of Specimens S1 to S3

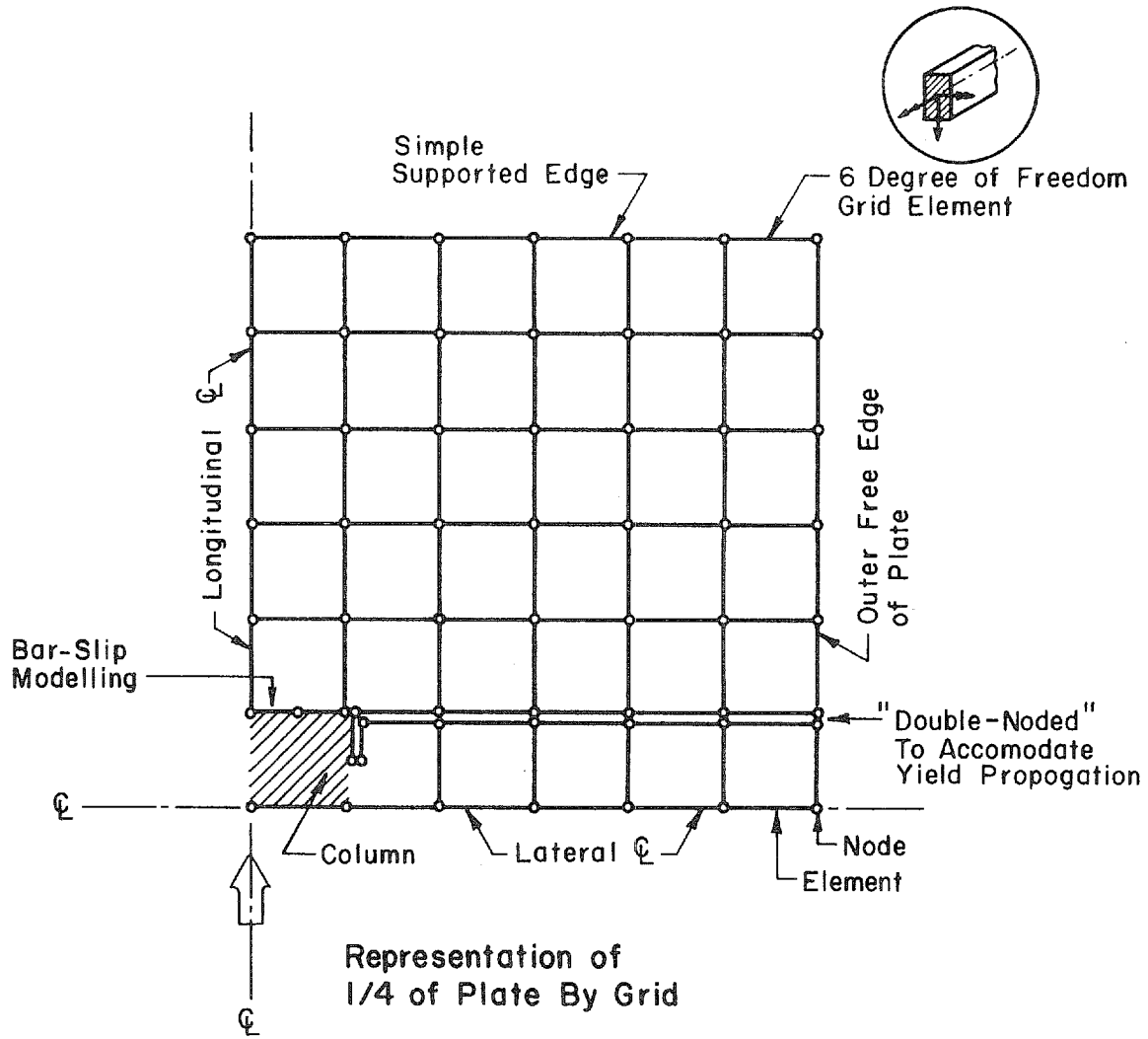

Fig. 4.6 Representation of a Quarter of the Plate by the Grid Model

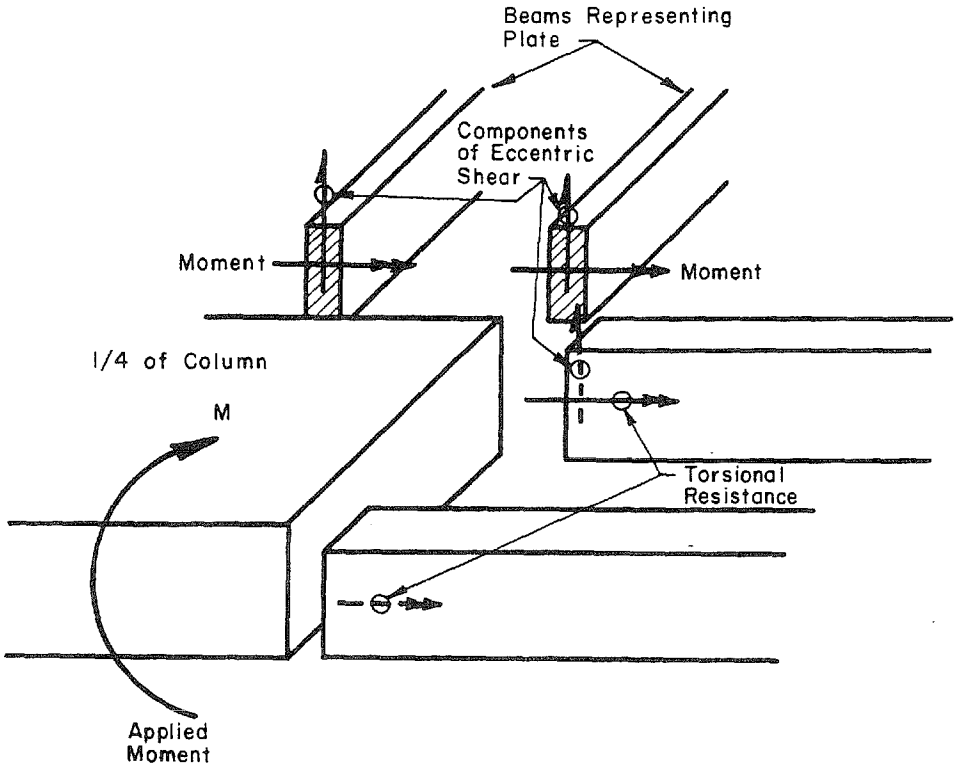

Fig. 4.7 Force Components Resisting Applied Moment at the Column-Slab Connection

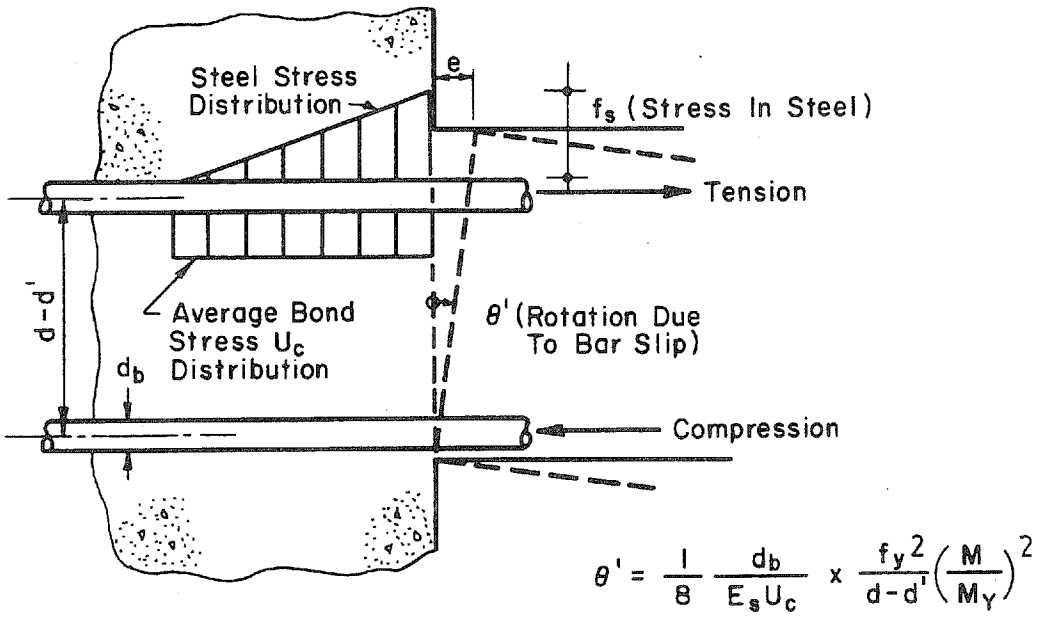

Bar-Slip Mechanism

(a) Bar-Slip Model

Fig. 4.8 Modelling of Bar-Slip

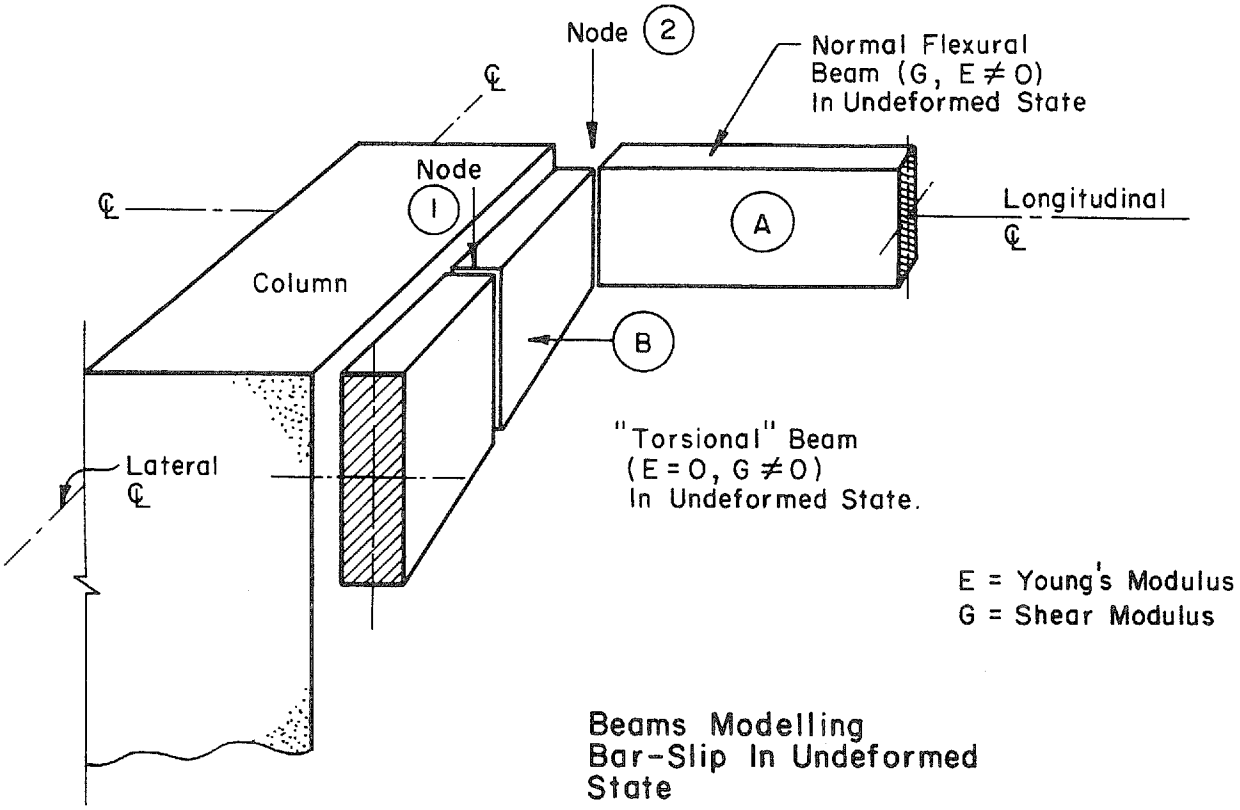

(b) Beams Modelling Bar-Slip

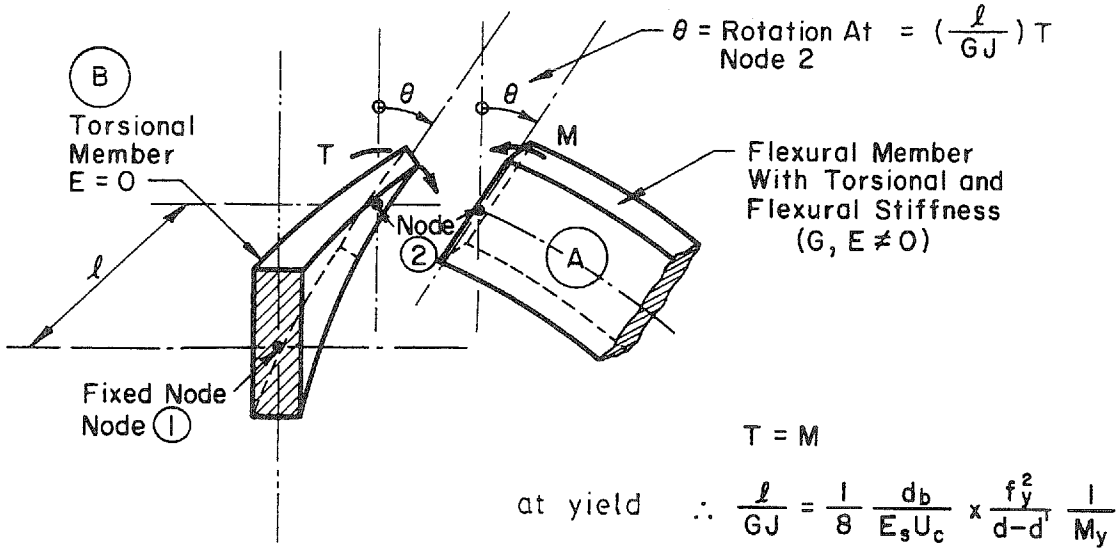

(c) Exploded View of Beams Modelling Bar Slip

Fig. 4.8 (contd.) Modelling of Bar-Slip

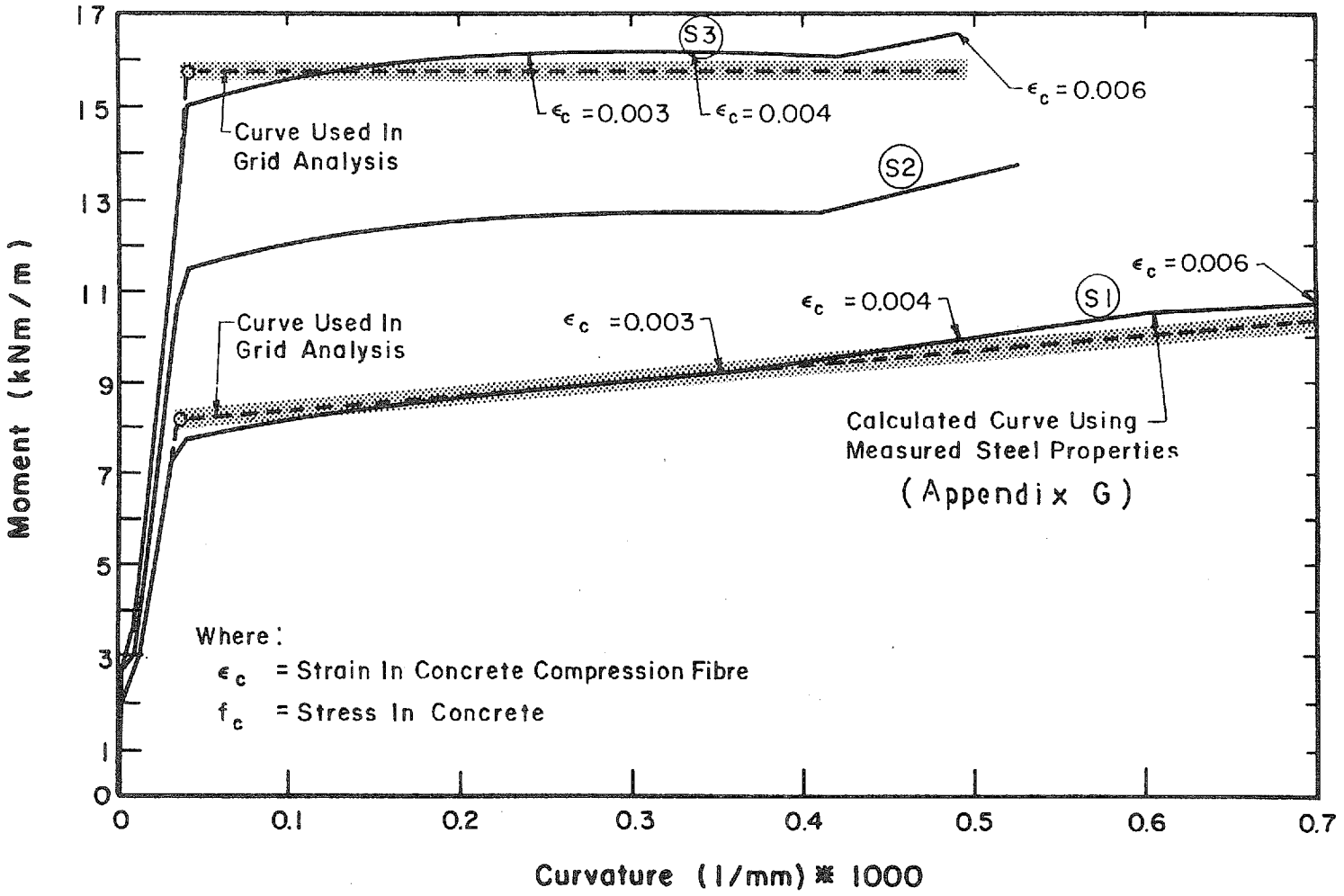

Fig. 4.9 Moment-Curvature Relationships for Specimens S1 to S3

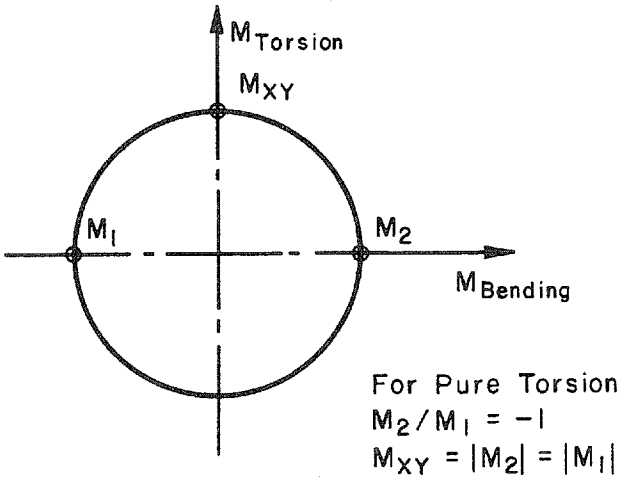

Mohr's Circle For Applied Moments
(a) Components of Torsion

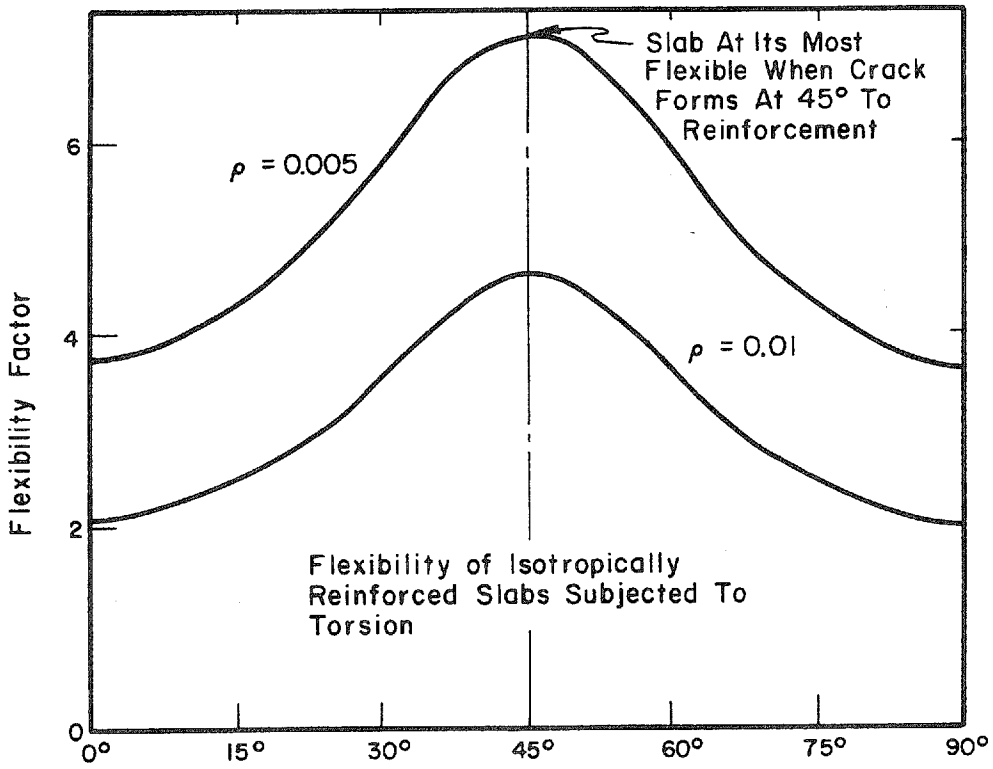

Example of Change In Stiffness With Relative Orientation of Reinforcement
(b) Flexibility in Torsion

Fig. 4.10 Torsion Relationships Used

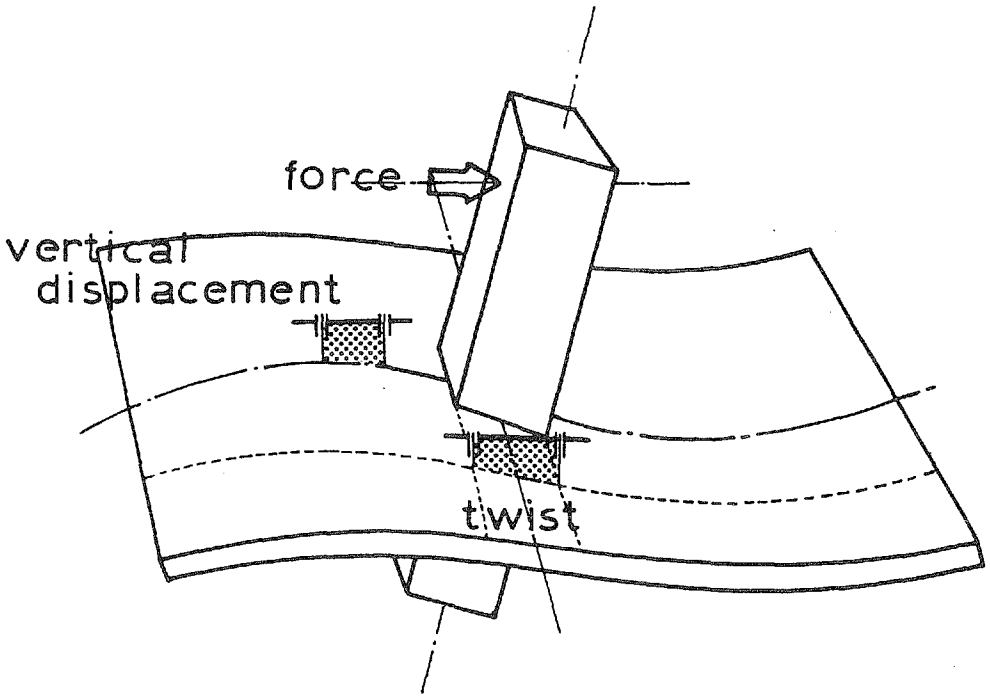

Fig. 4.11 Idealized Position of Vertical Displacement and Twist Measurements

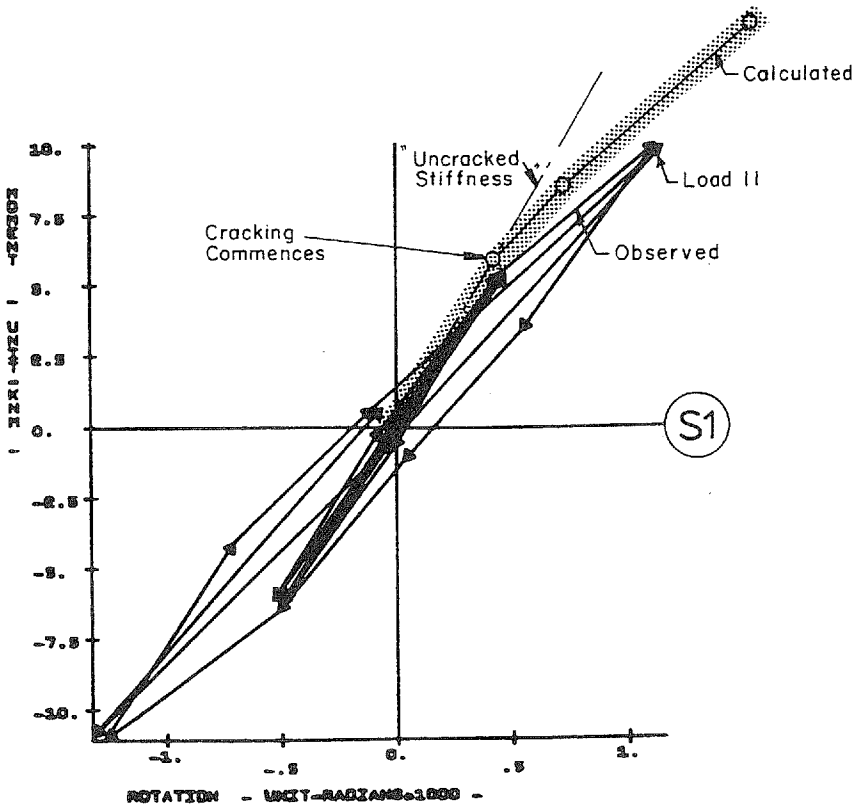

Fig. 4.12 Moment-Rotation Relationships up to Load 11, S1

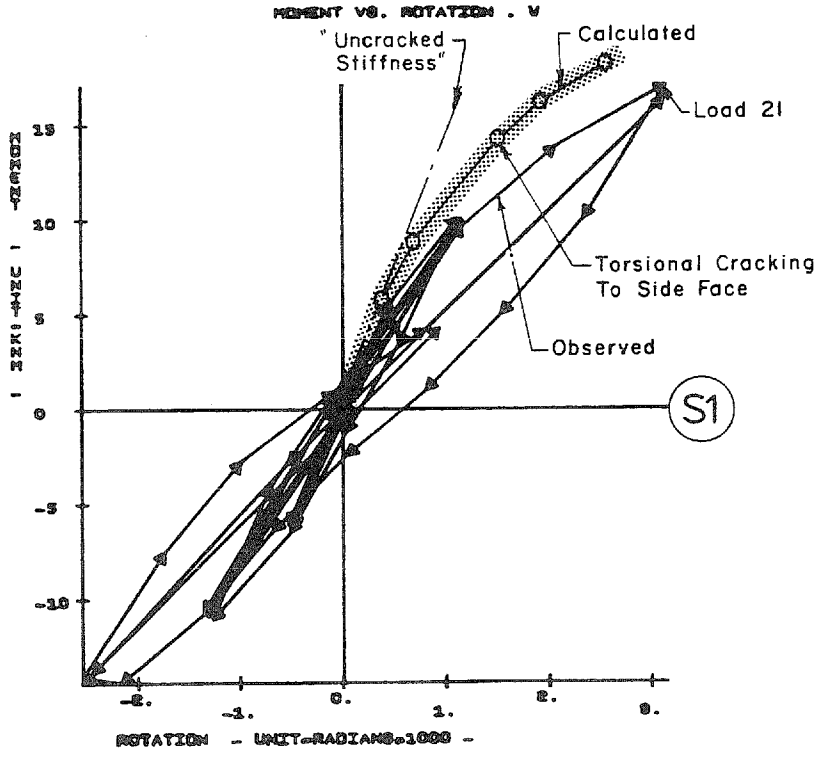

Fig. 4.13 Moment-Rotation Relationships up to Load 21, S1

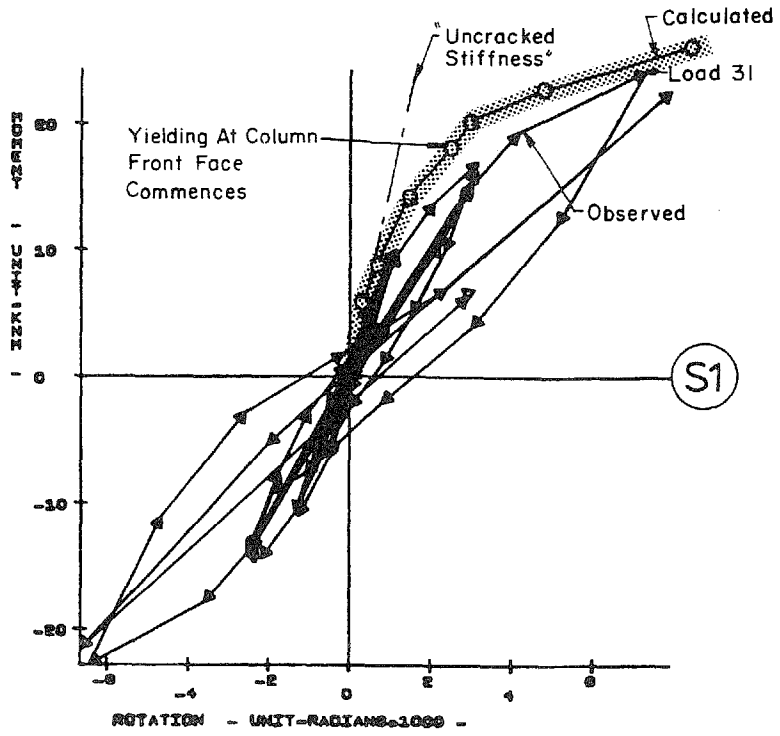

Fig. 4.14 Moment-Rotation Relationships up to Load 31, S1

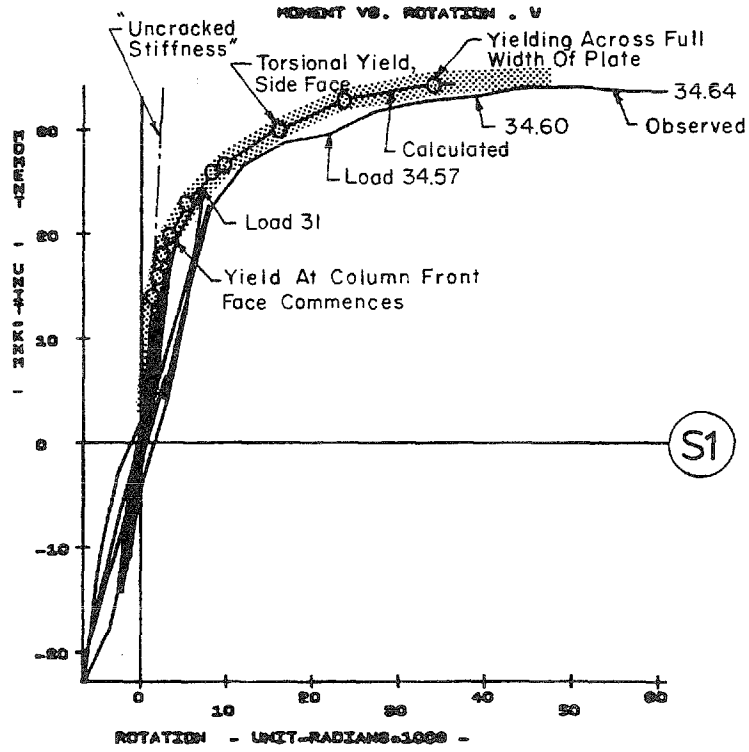

Fig. 4.15 Moment-Rotation Relationships up to Load 34.64, S1

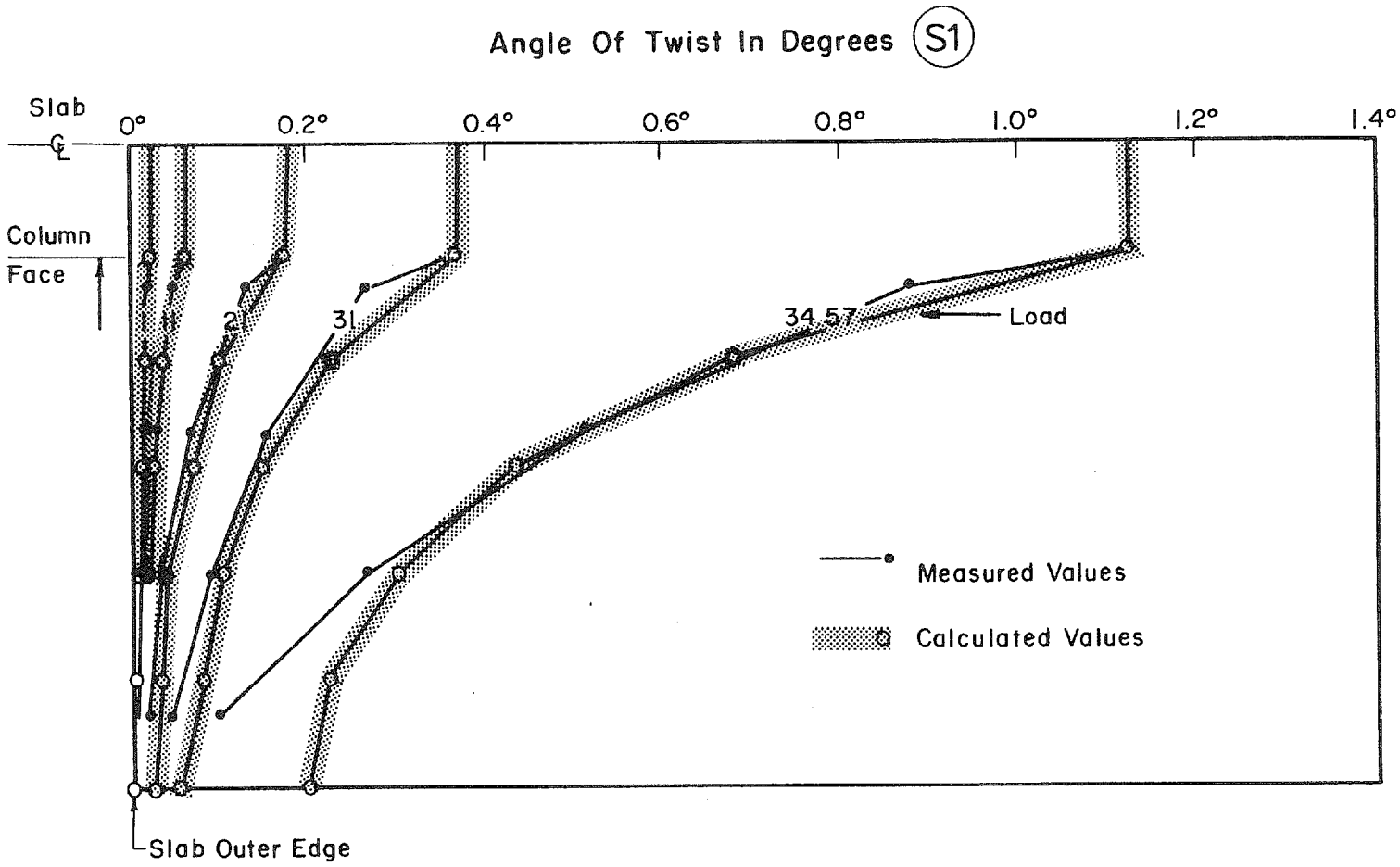

Fig. 4.16 Measured and Calculated Angles of Twist in Specimen S1

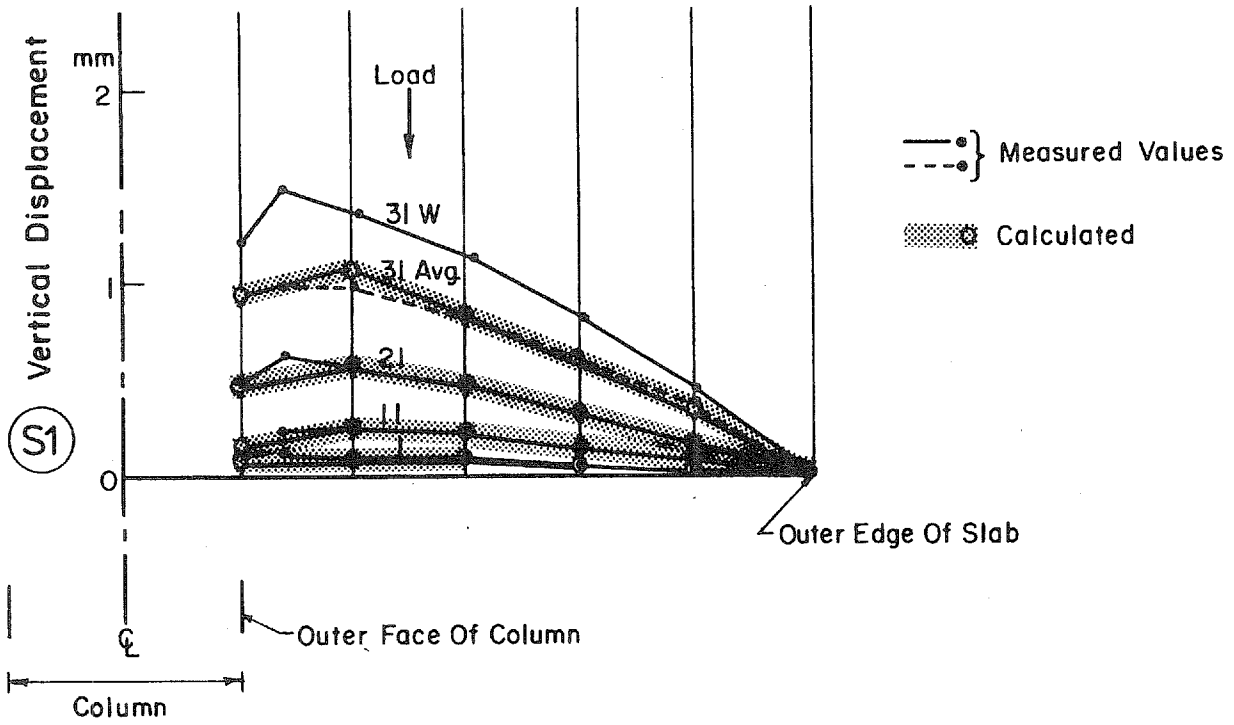

Fig. 4.17 Measured and Calculated Vertical Displacements along the Longitudinal Centerline in Specimen S1

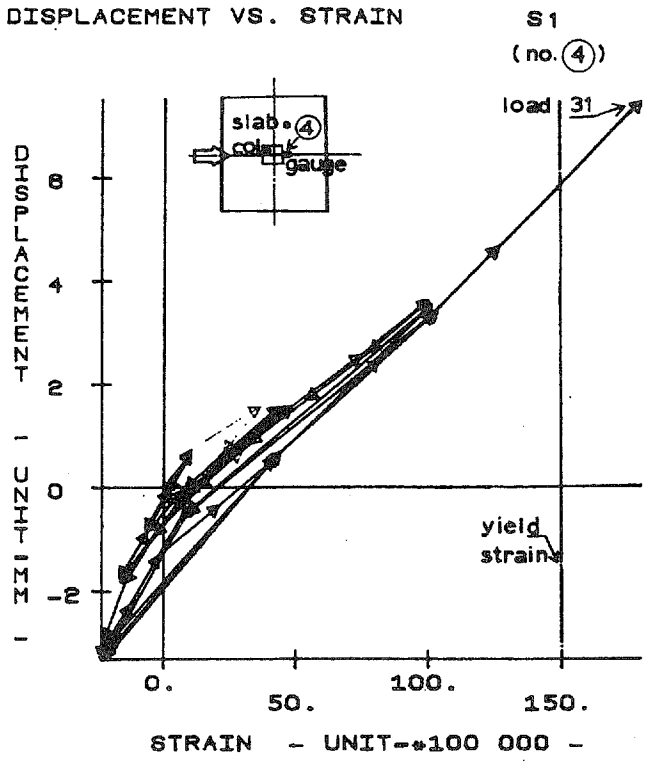

Fig. 4.18 Measured Displacement-Strain Relationship in Gauge 4 in S1

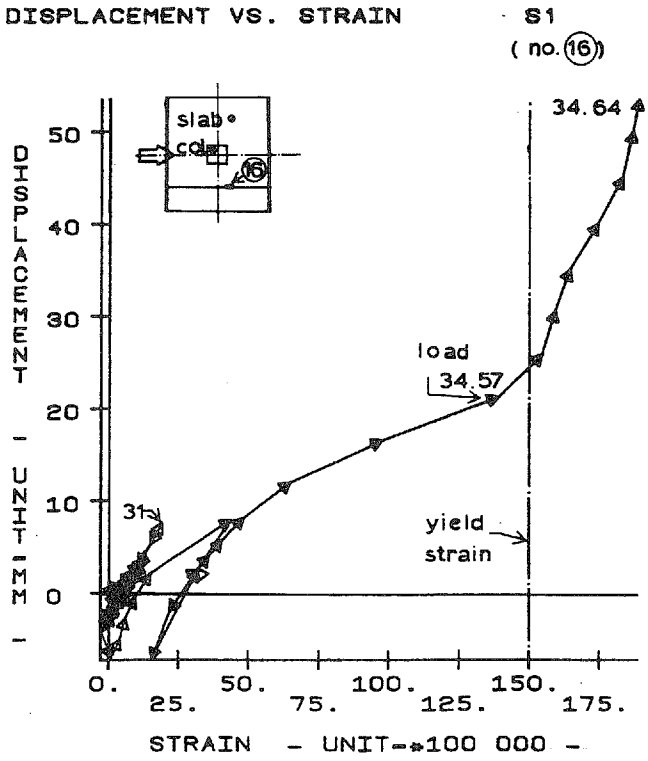

Fig. 4.19 Measured Displacement-Strain Relationship in Gauge 16 in S1

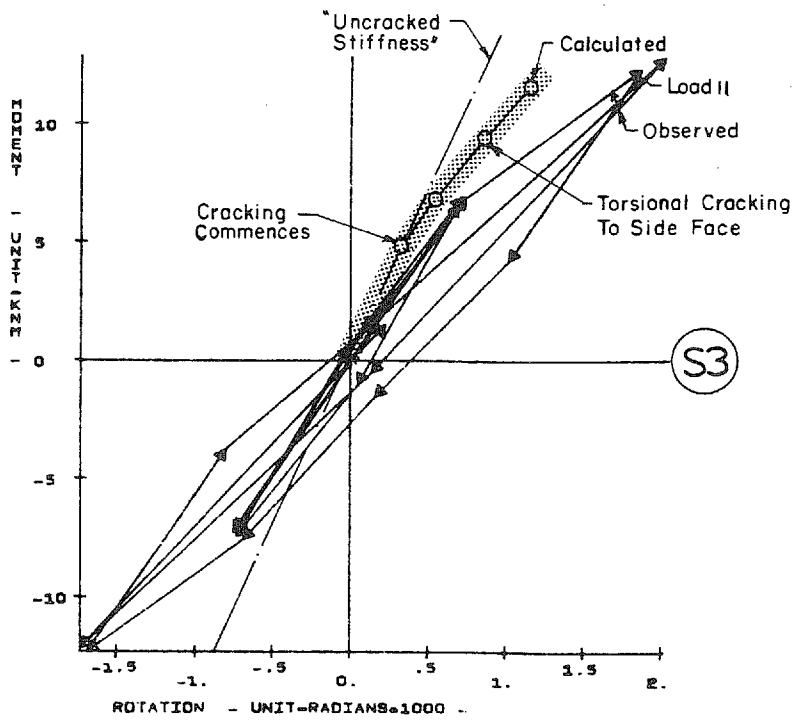

Fig. 4.20 Moment-Rotation Relationships up to Load 11, S3

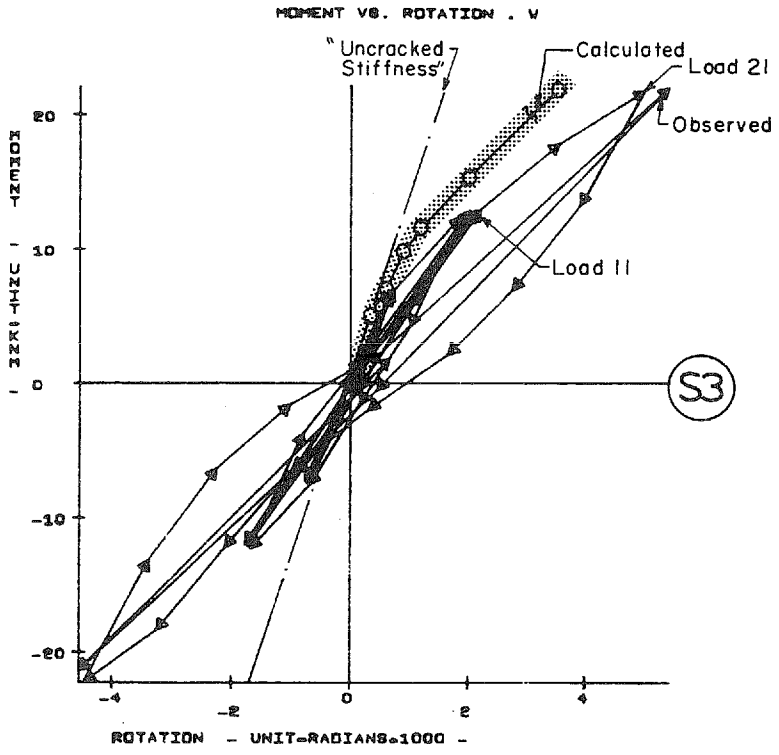

Fig. 4.21 Moment-Rotation Relationships up to Load 21, S3

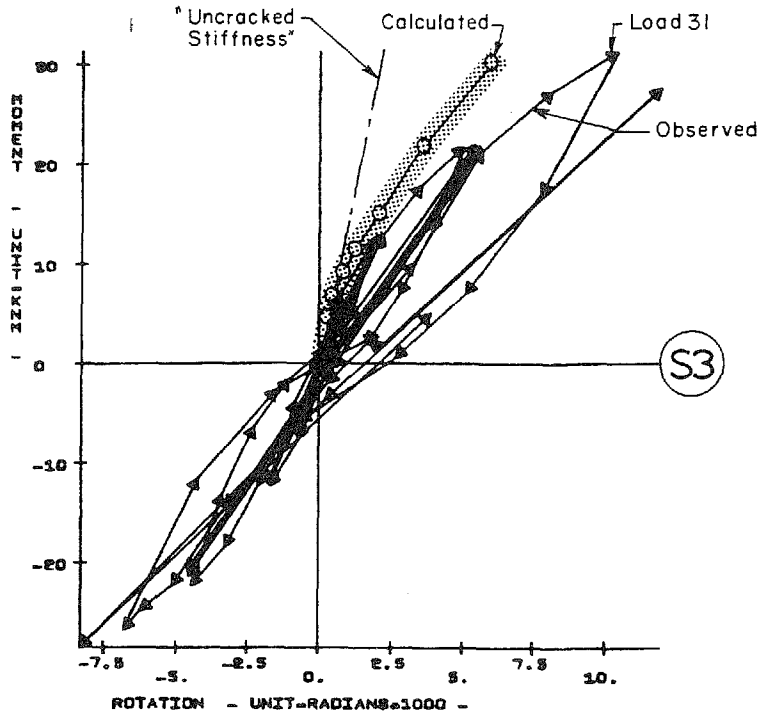

Fig. 4.22 Moment-Rotation Relationships up to Load 31, S3

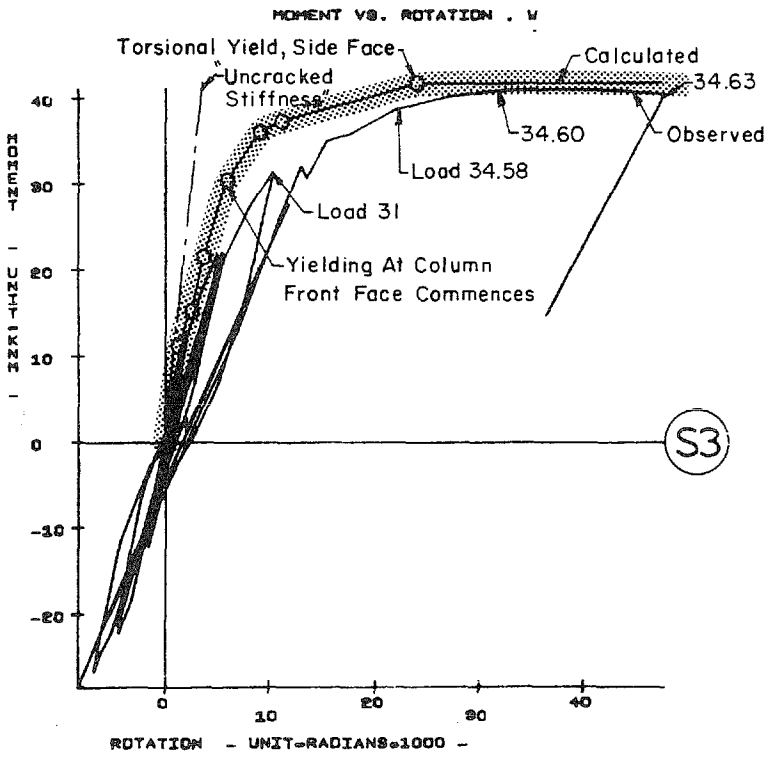

Fig. 4.23 Moment-Rotation Relationships up to Load 34.64, S3

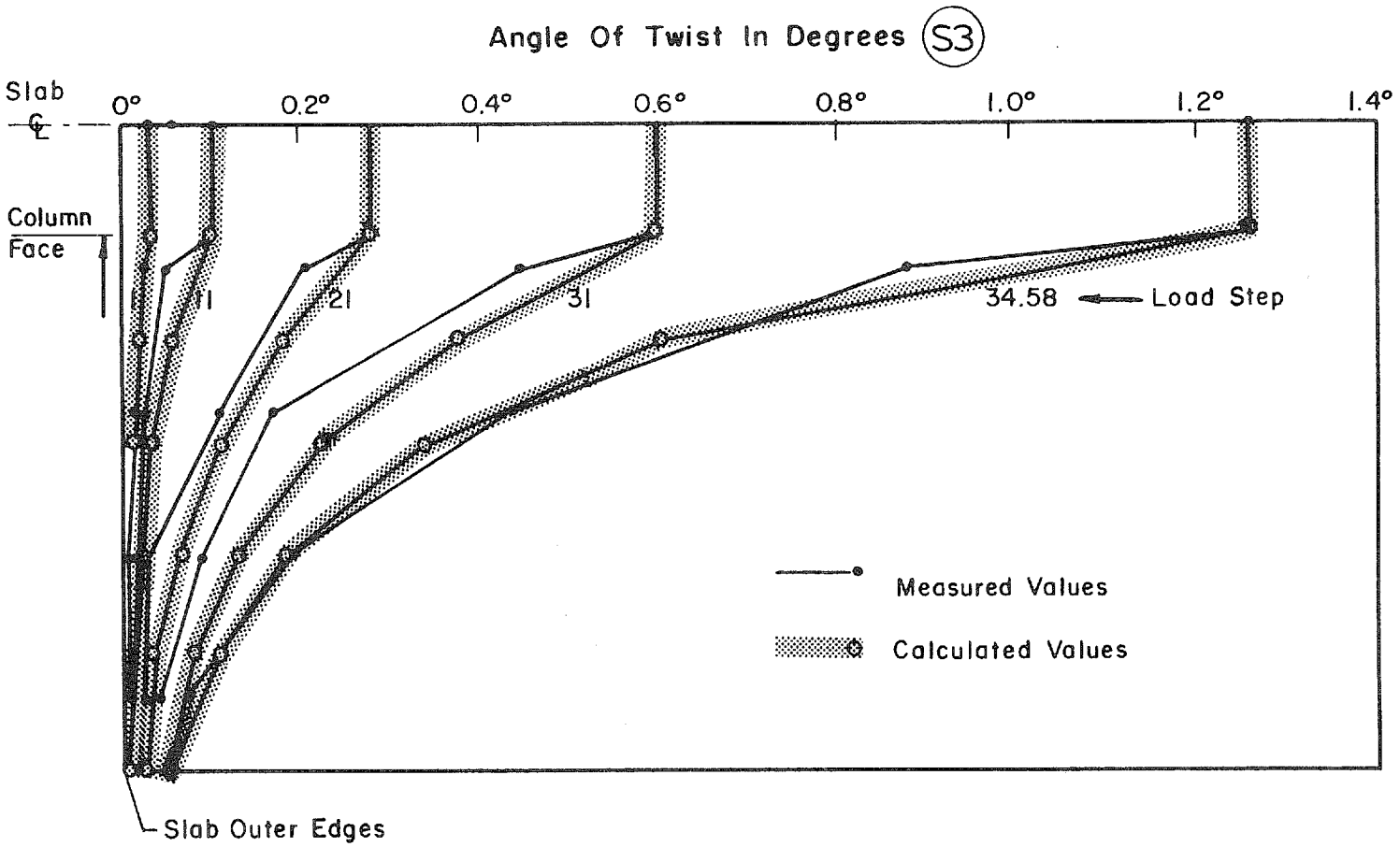

Fig. 4.24 Measured and Calculated Angles of Twist in Specimen S3

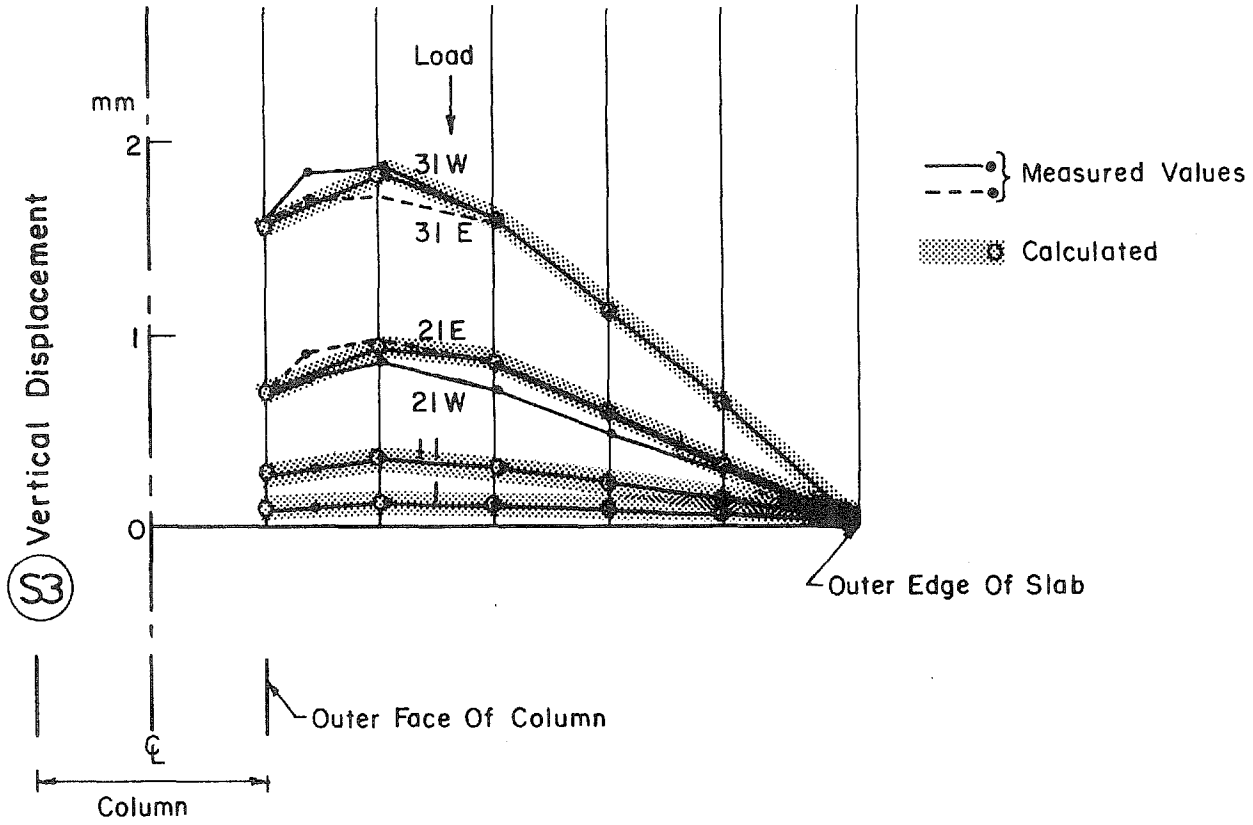

Fig. 4.25 Measured and Calculated Vertical Displacements along the Longitudinal Centerline in Specimen S3

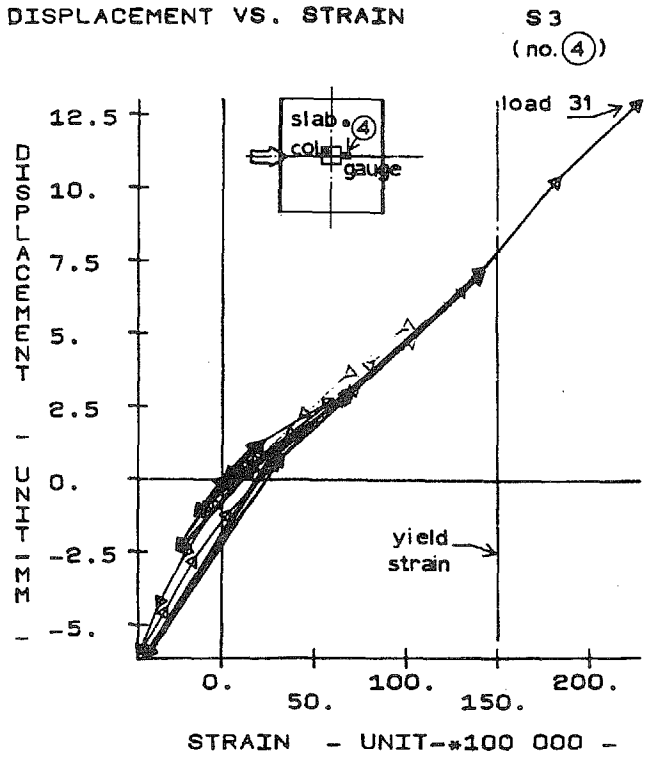

Fig. 4.26 Measured Displacement-Strain Relationship in Gauge 4 in S3

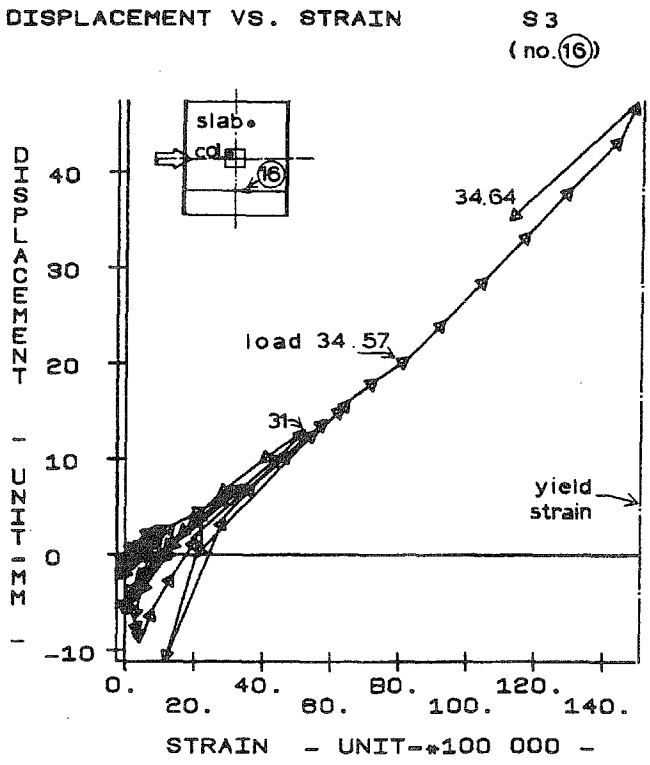

Fig. 4.27 Measured Displacement-Strain Relationship in Gauge 16 in S3

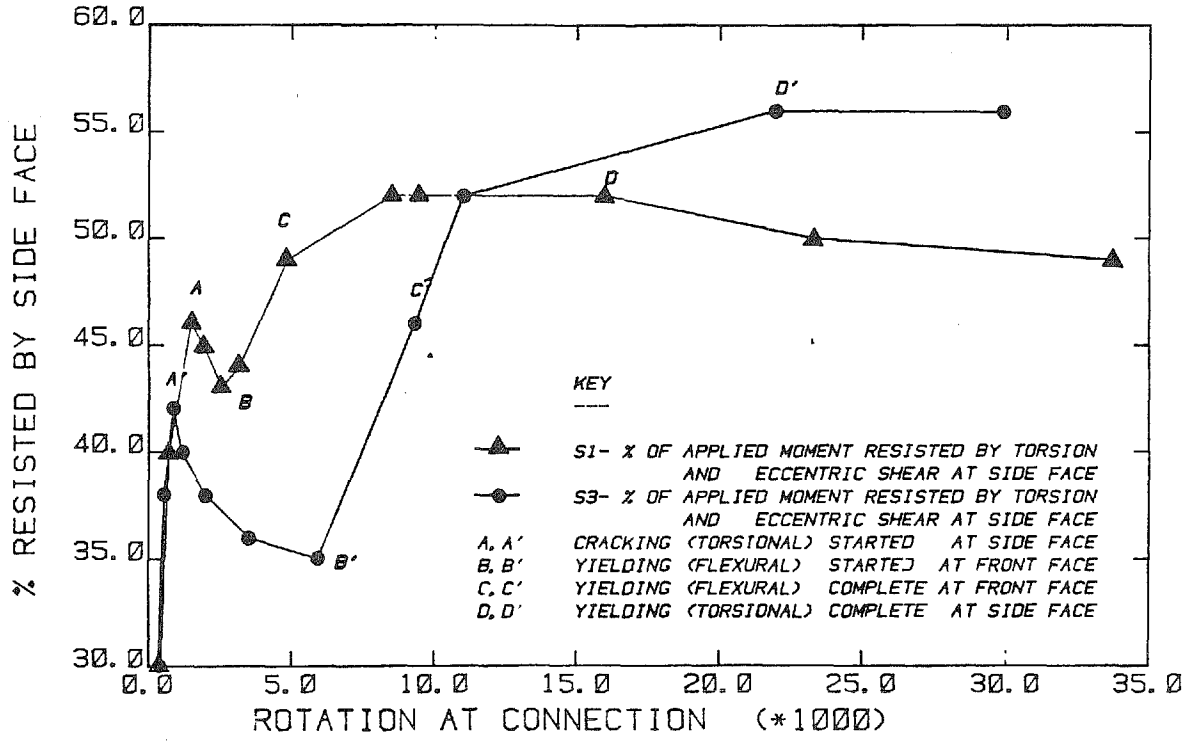

(a) Detail

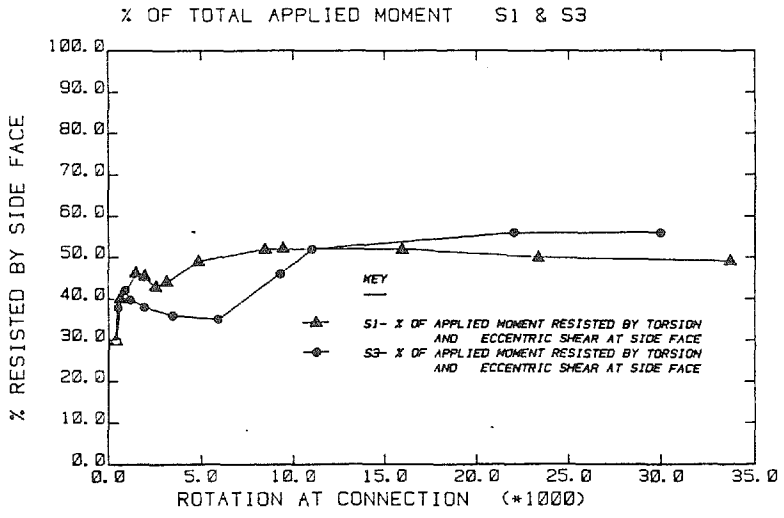

(b) Overall

Fig. 4.28 Percentage of Applied Connection Moment Resisted at Side Face of the Connection for S1 and S3

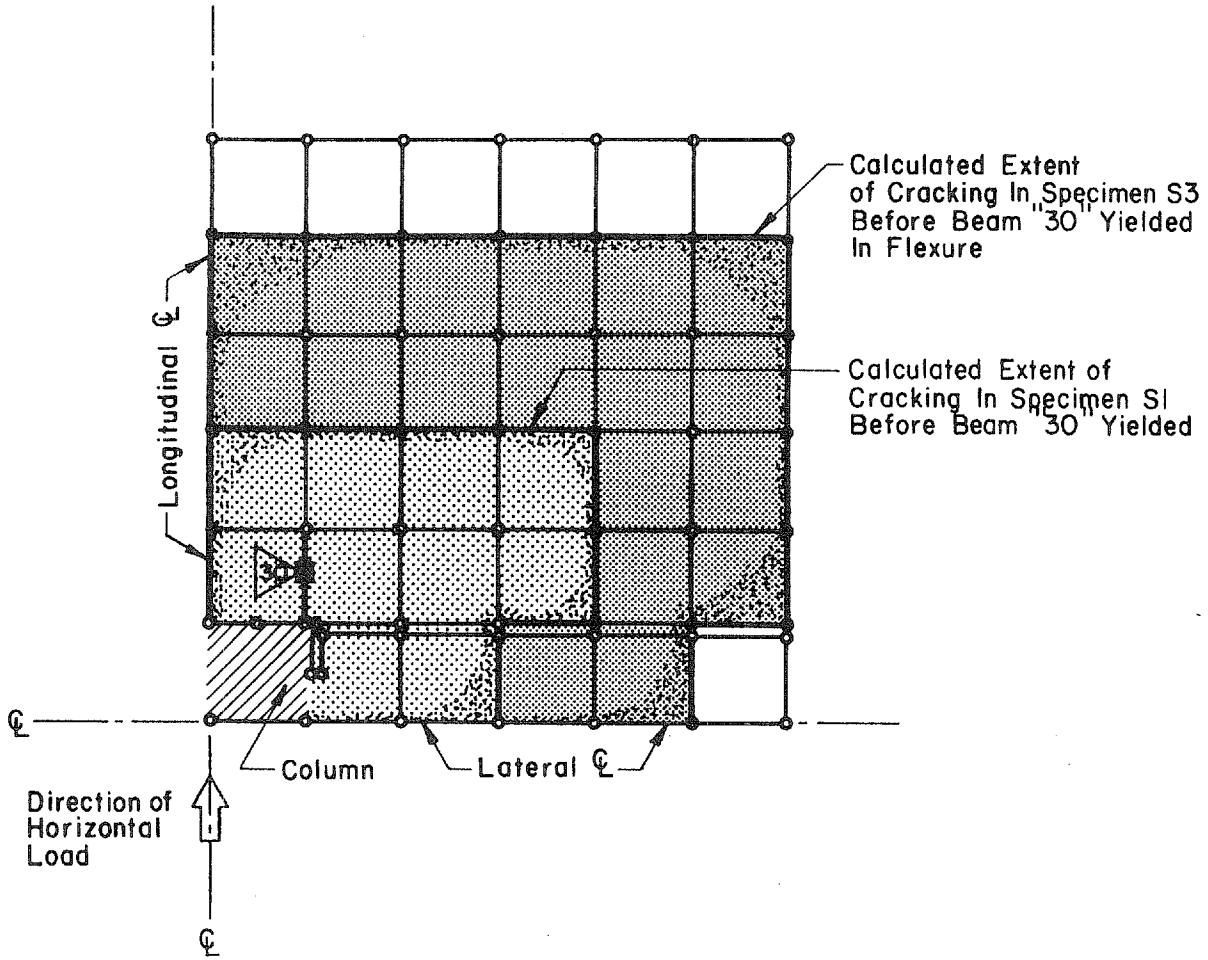

Extent of Cracking When
First Beam Yields

Fig. 4.29 Extent of Cracking When First Beam Yields for S1 and S3

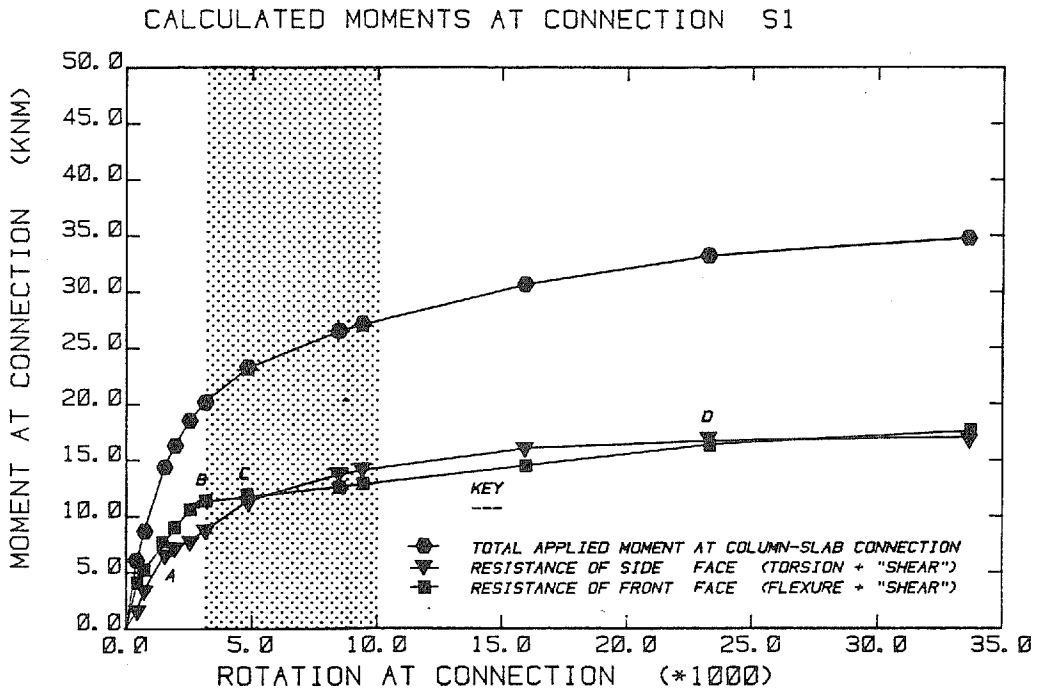

Fig. 4.30 Applied Moment, Moment at Side Face and Moment at Front Face vs. Connection Rotation in S1

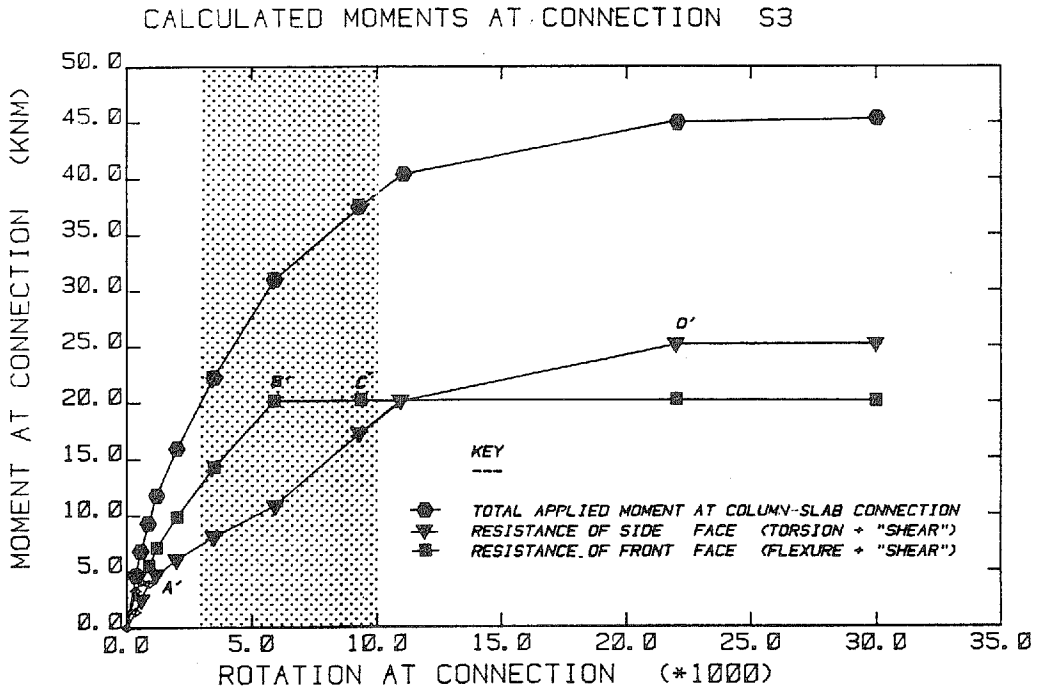

Fig. 4.31 Applied Moment, Moment at Side Face and Moment at Front Face vs. Connection Rotation in S3

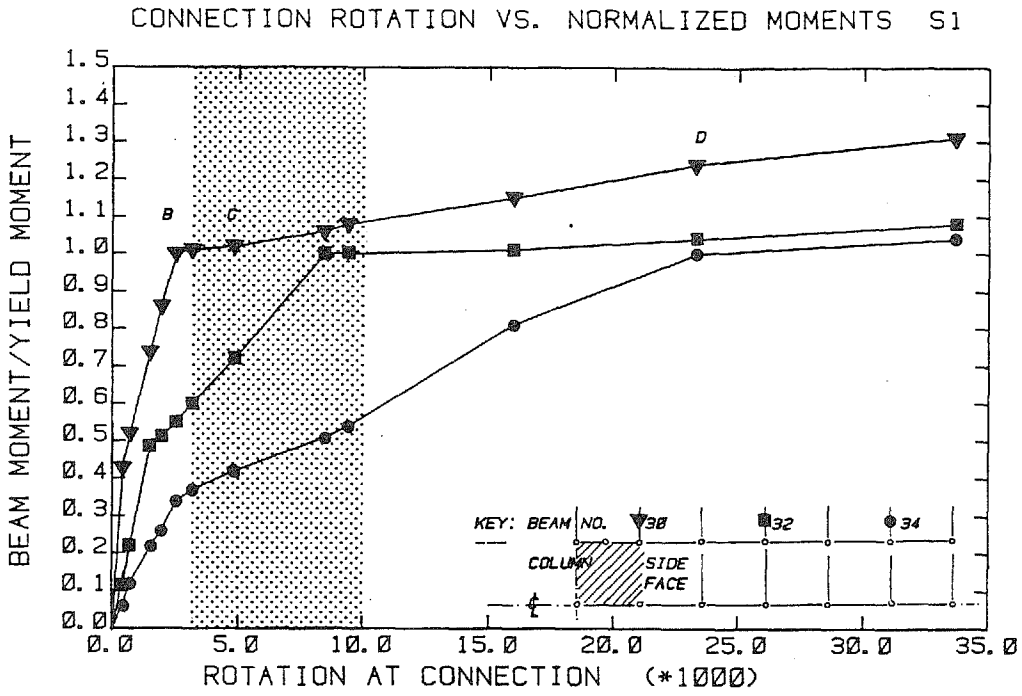

Fig. 4.32 Normalized Moments in Specified Beams across Slab Width vs. Connection Rotation in S1

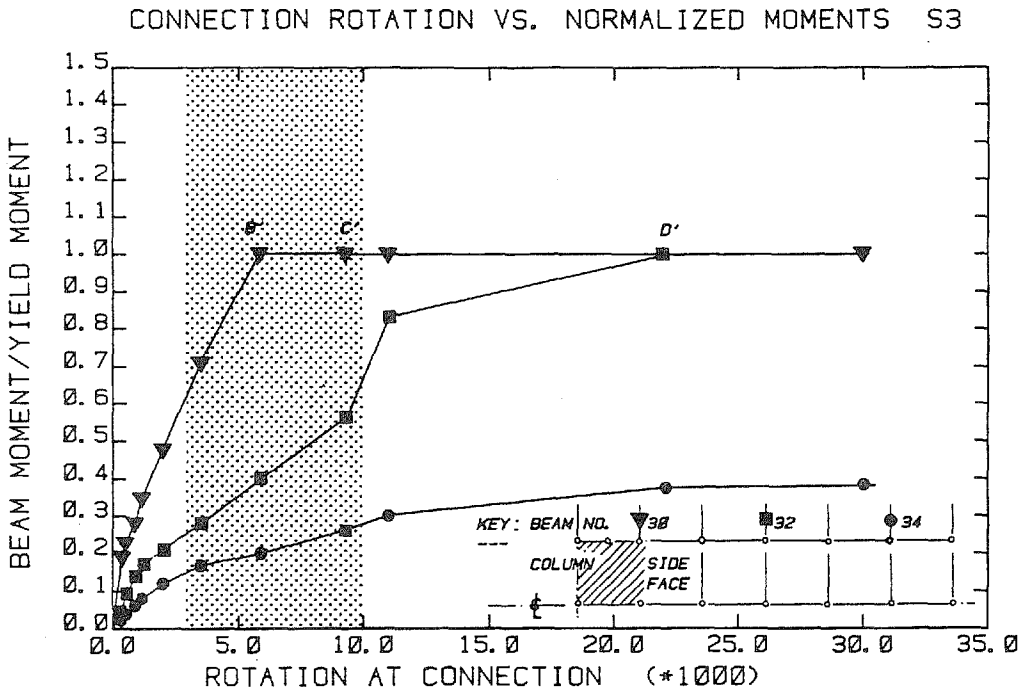

Fig. 4.33 Normalized Moments in Specified Beams across Slab Width vs. Connection Rotation in S3

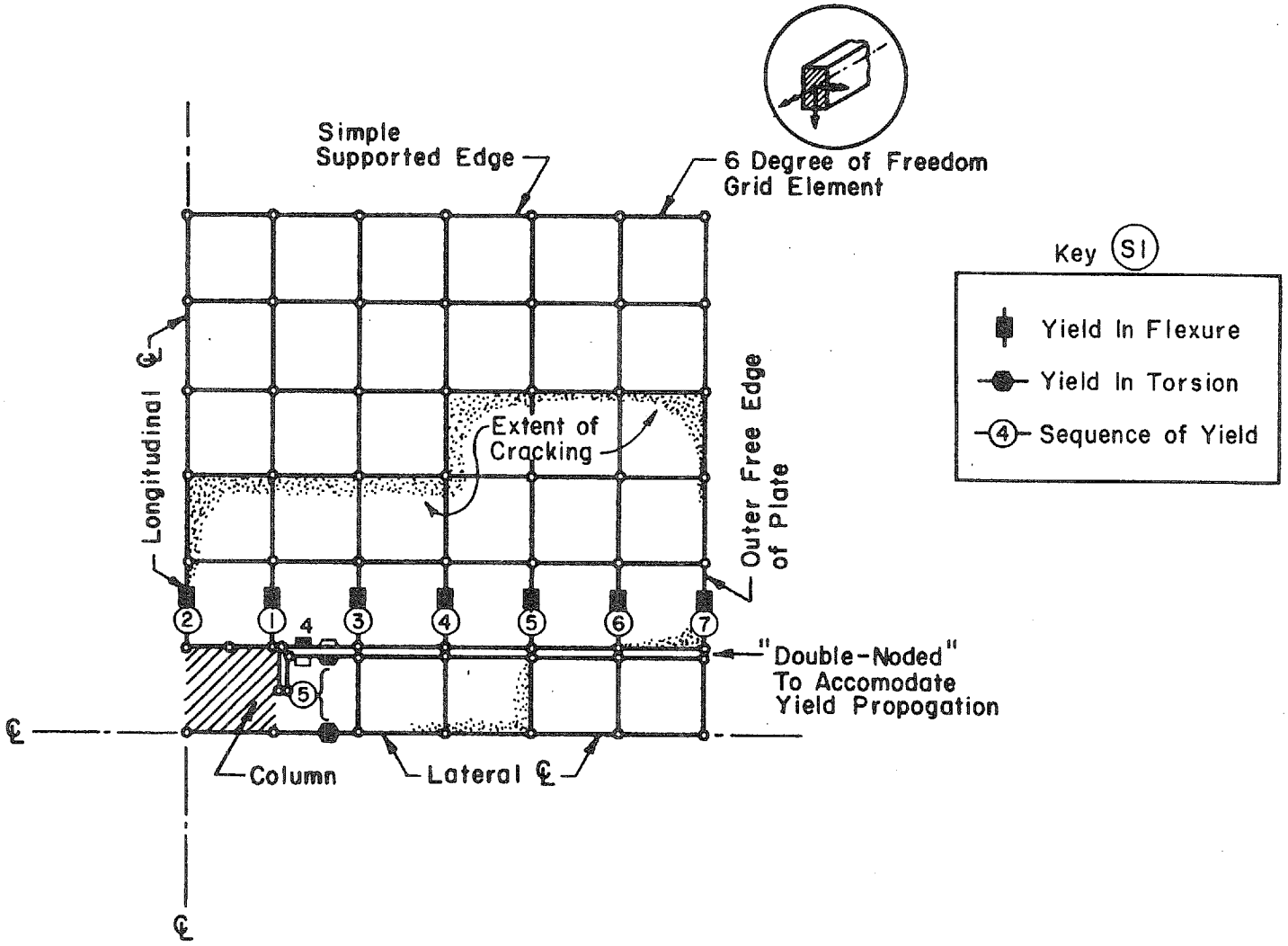

Fig. 4.34 Results of Grid Analysis on Specimen S1

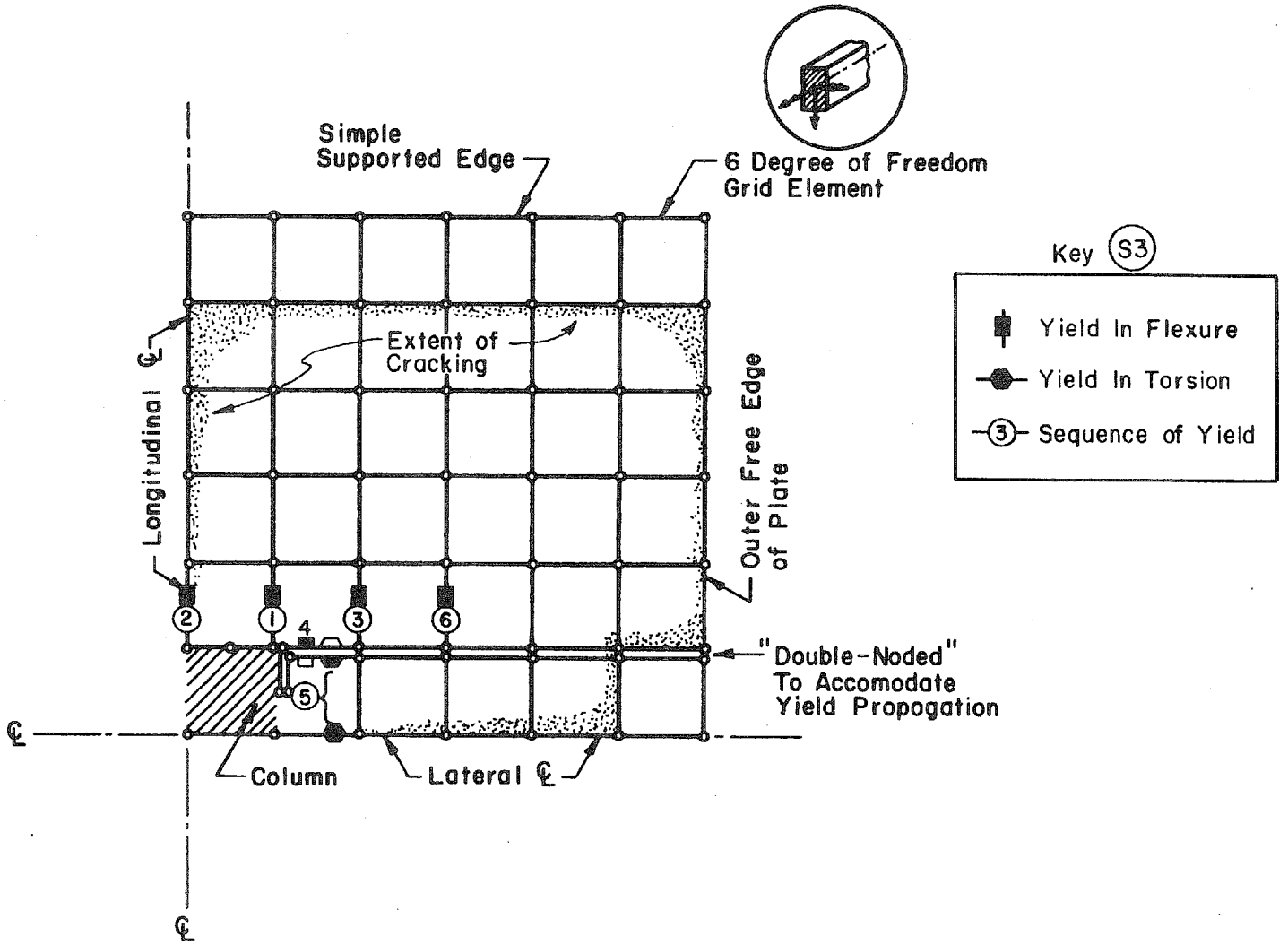

Fig. 4.35 Results of Grid Analysis on Specimen S3

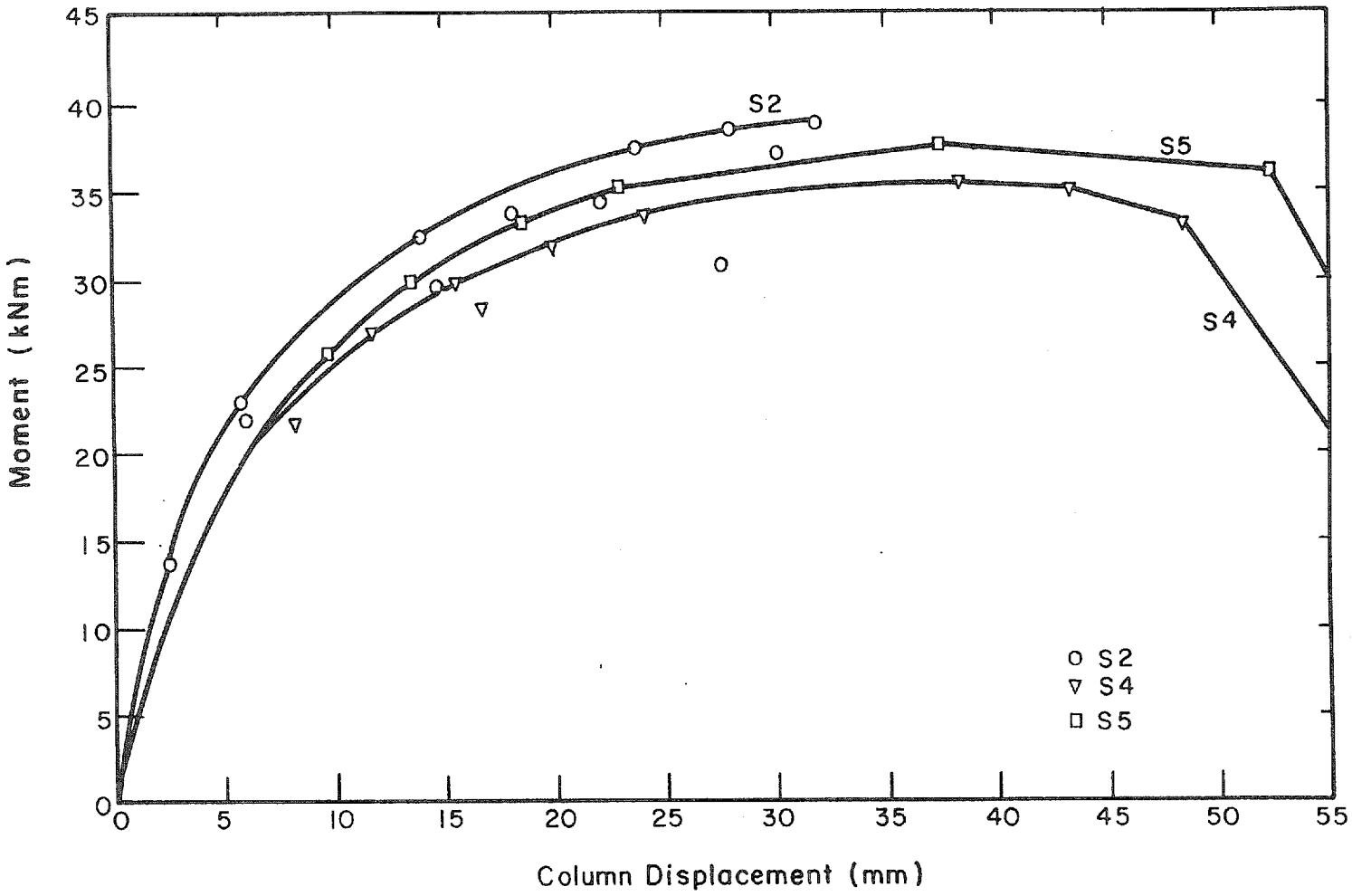

Fig. 5.1 Smoothed Moment-Displacement Relationships for Specimens S2, S4 and S5

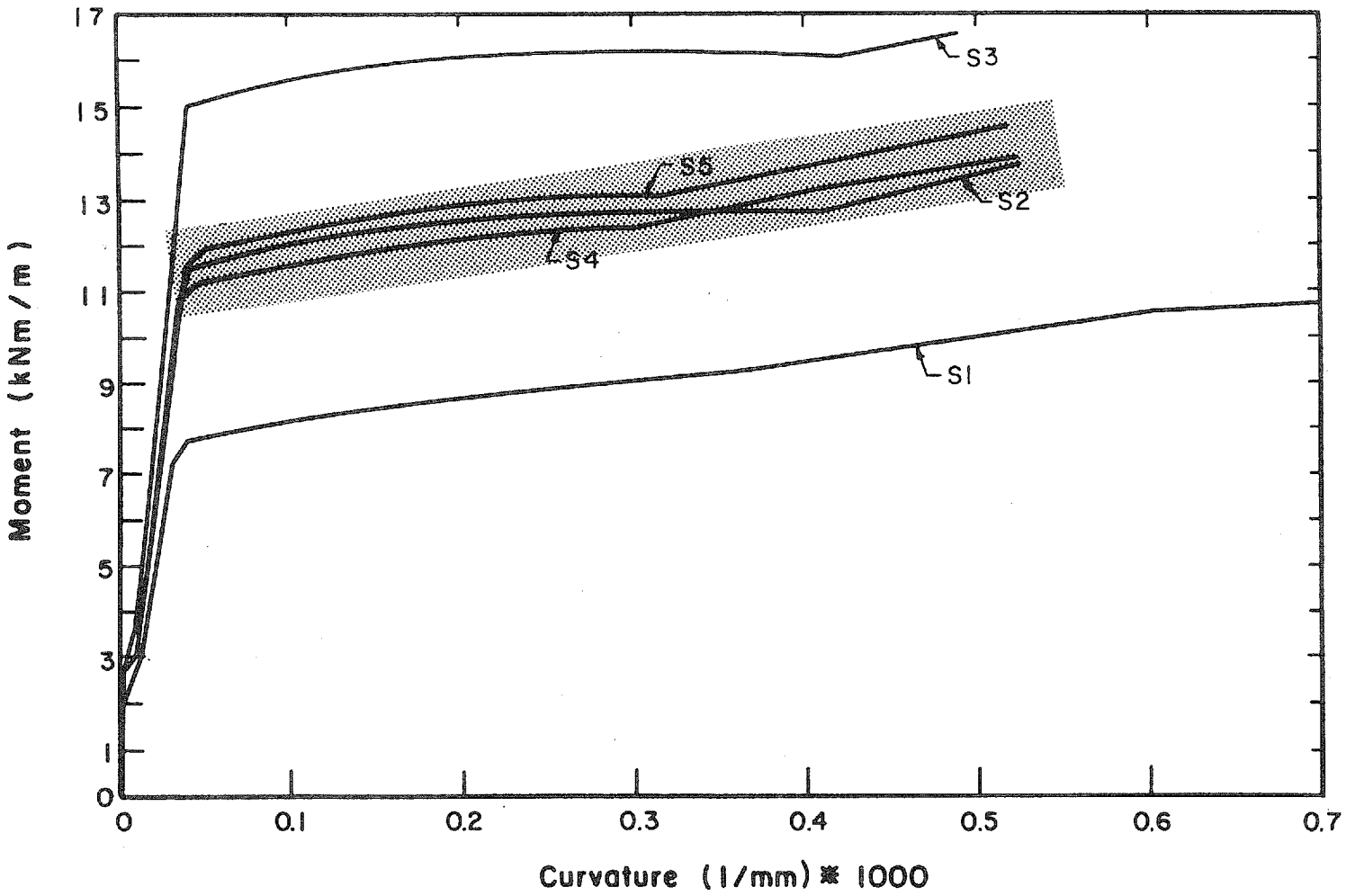

Fig. 5.2 Moment-Curvature Relationships for Statically Tested Specimens

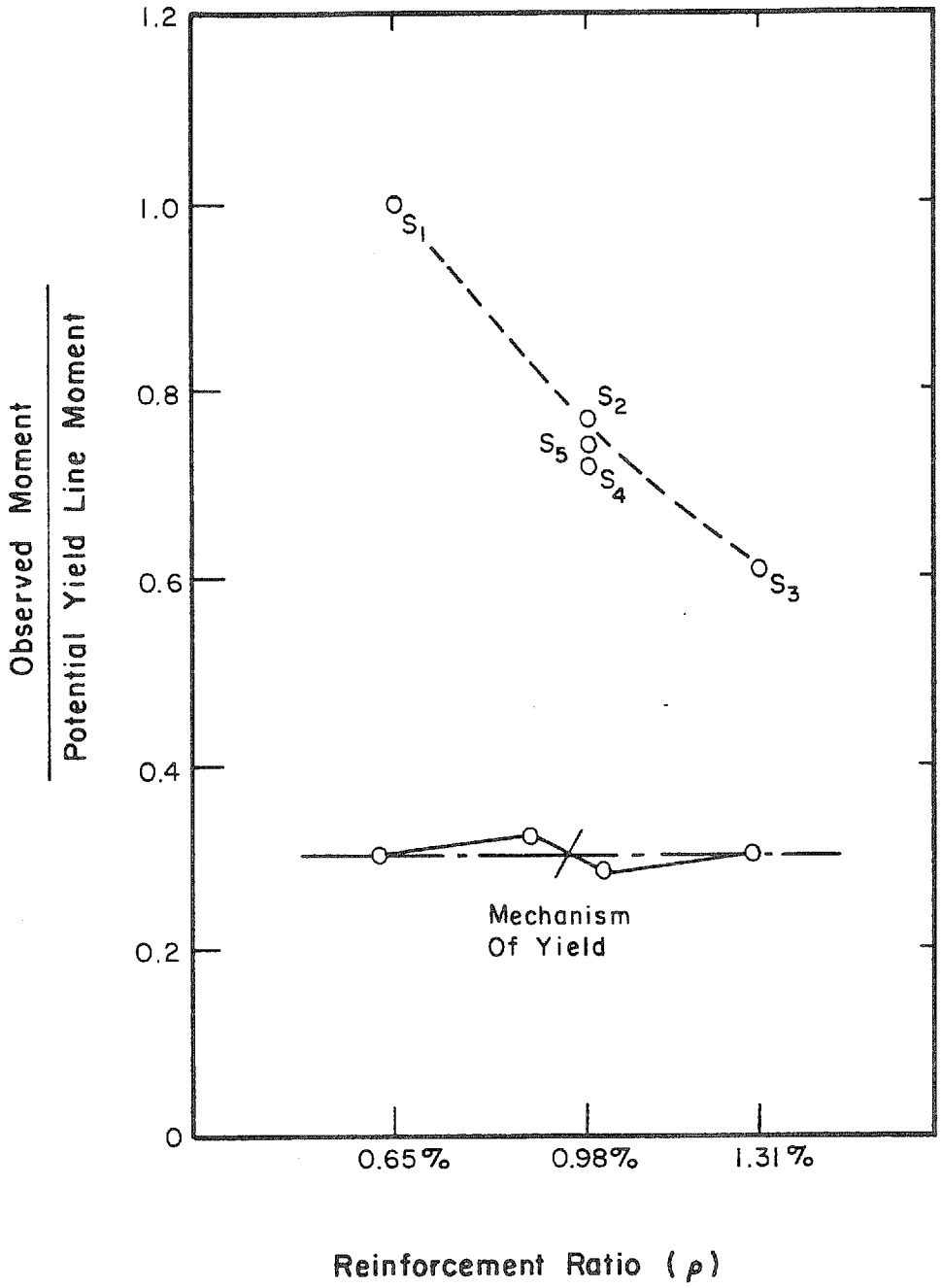

Fig. 5.3 Normalized Observed Strengths for Statically Tested Specimens

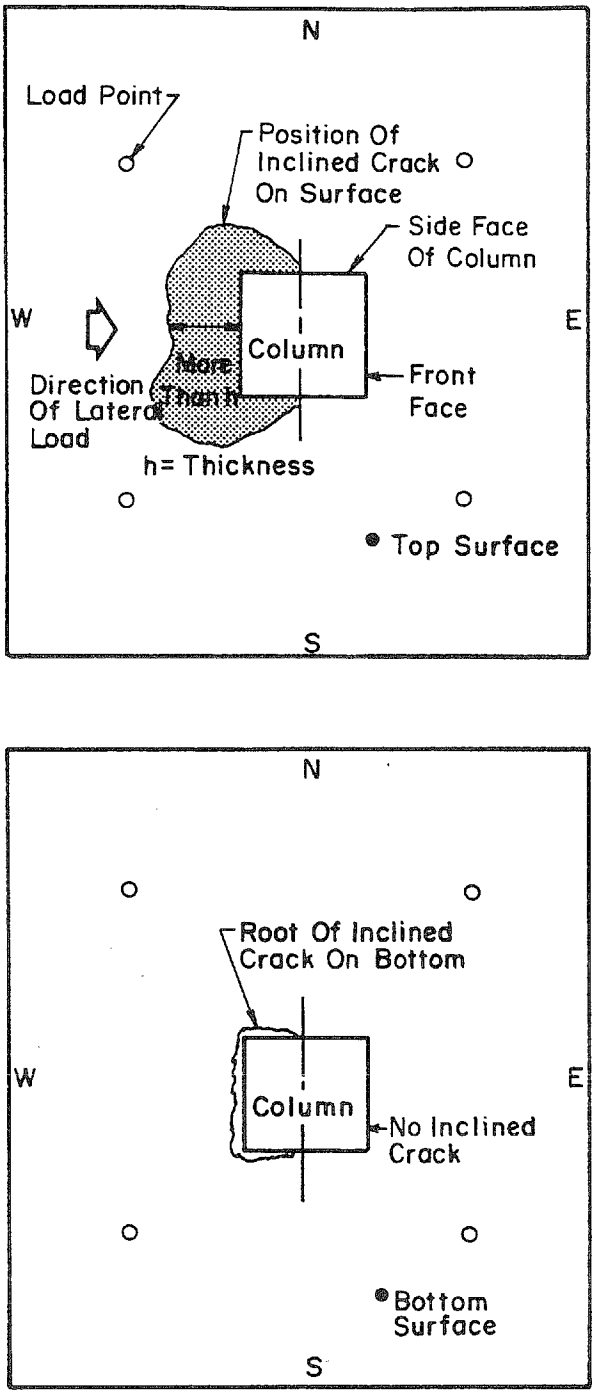

Fig. 5.4 Idealized Position of Inclined Crack in Specimens with Superimposed Vertical Load

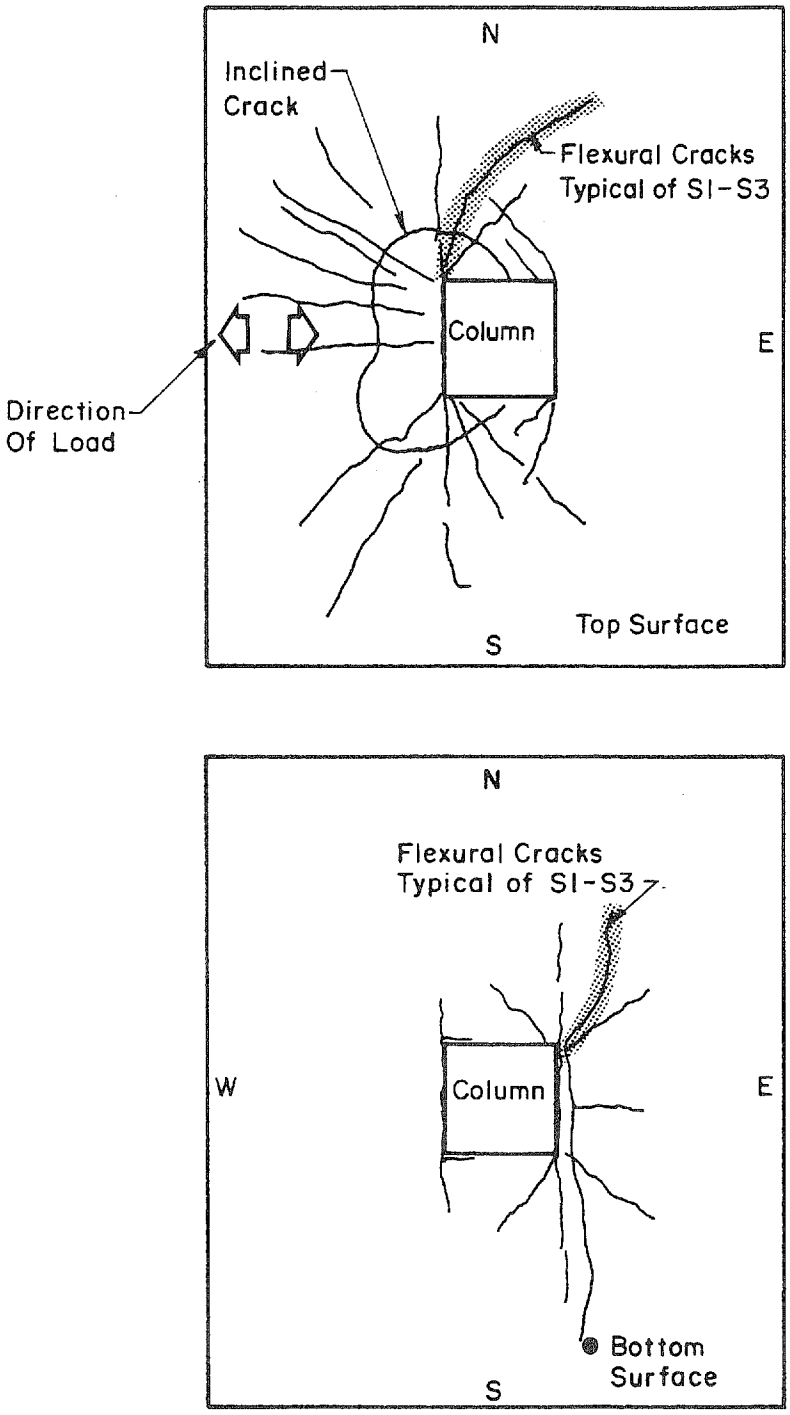

Fig. 5.5 Idealized Crack Patterns in Specimens with Superimposed Vertical Load

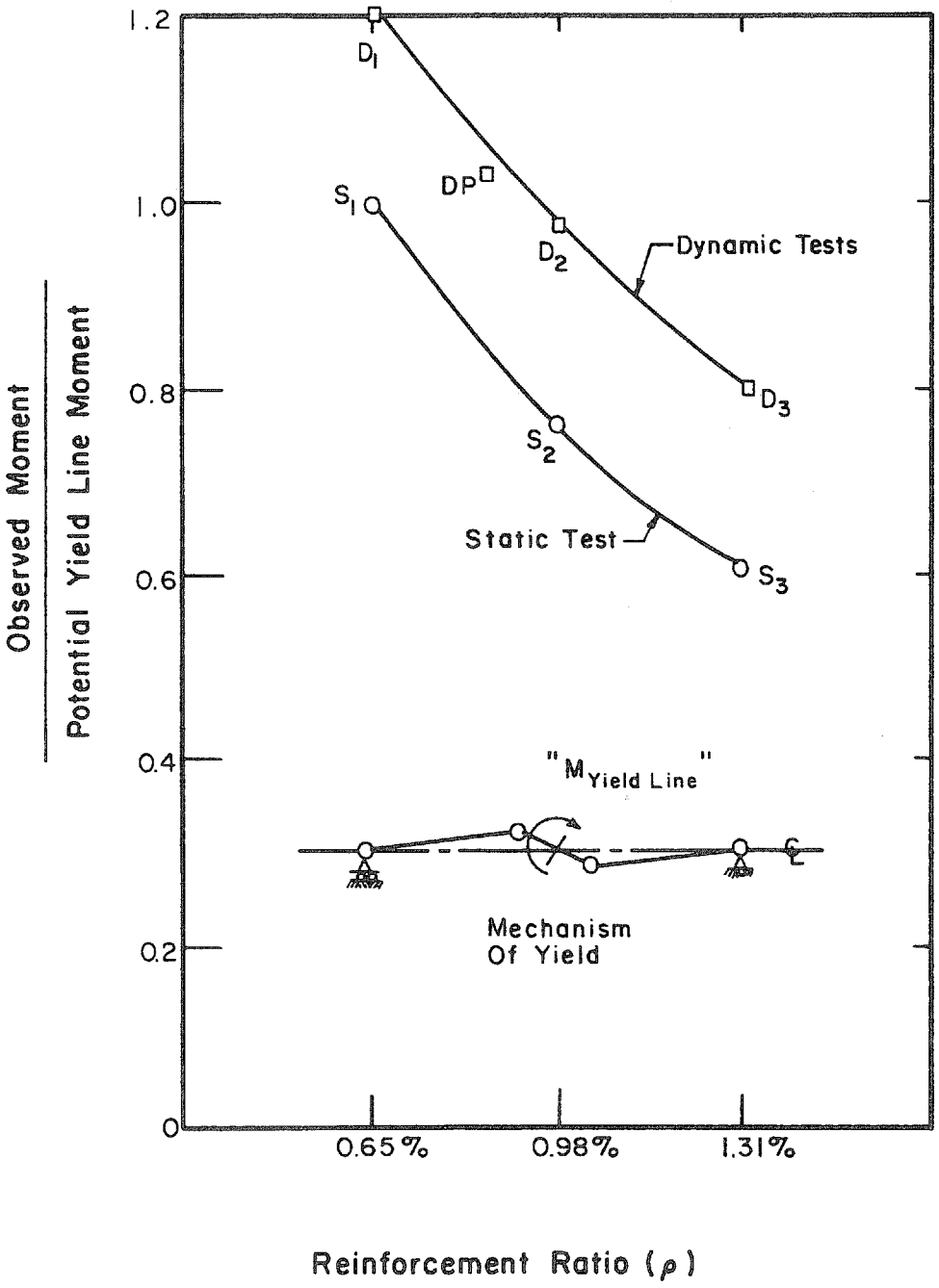

Fig. 6.1 Normalized Observed Strengths for Statically and Dynamically Tested Specimens

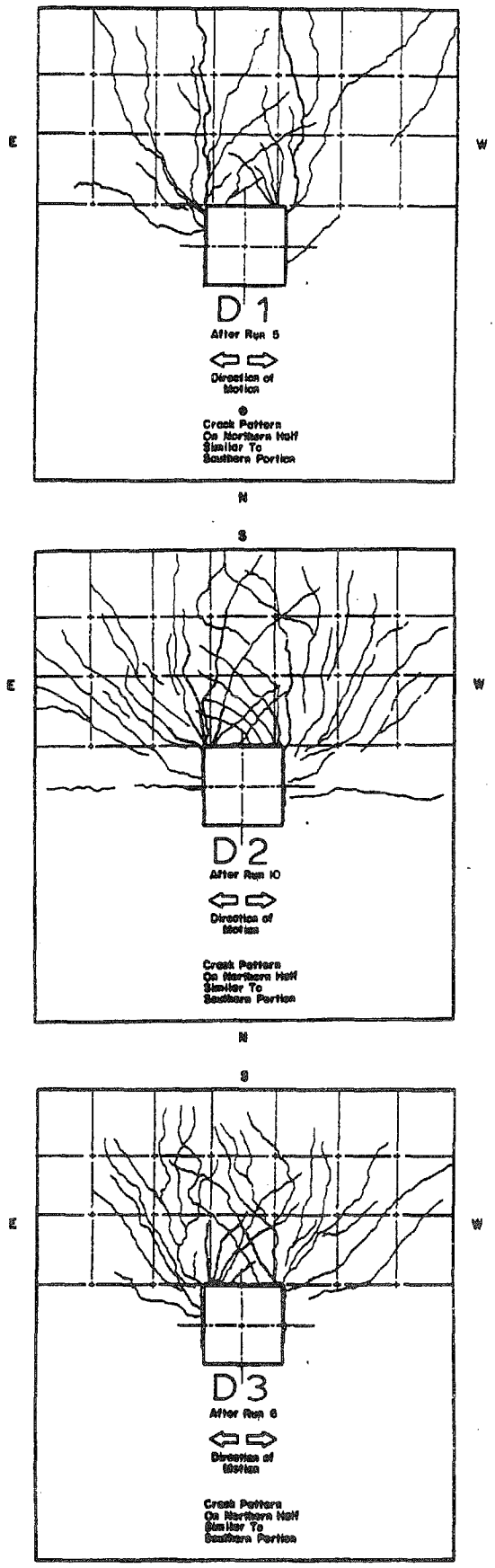

(a) D1

(b) D2

(c) D3

Fig. 6.2 Observed Crack Patterns in Dynamically Tested Specimens

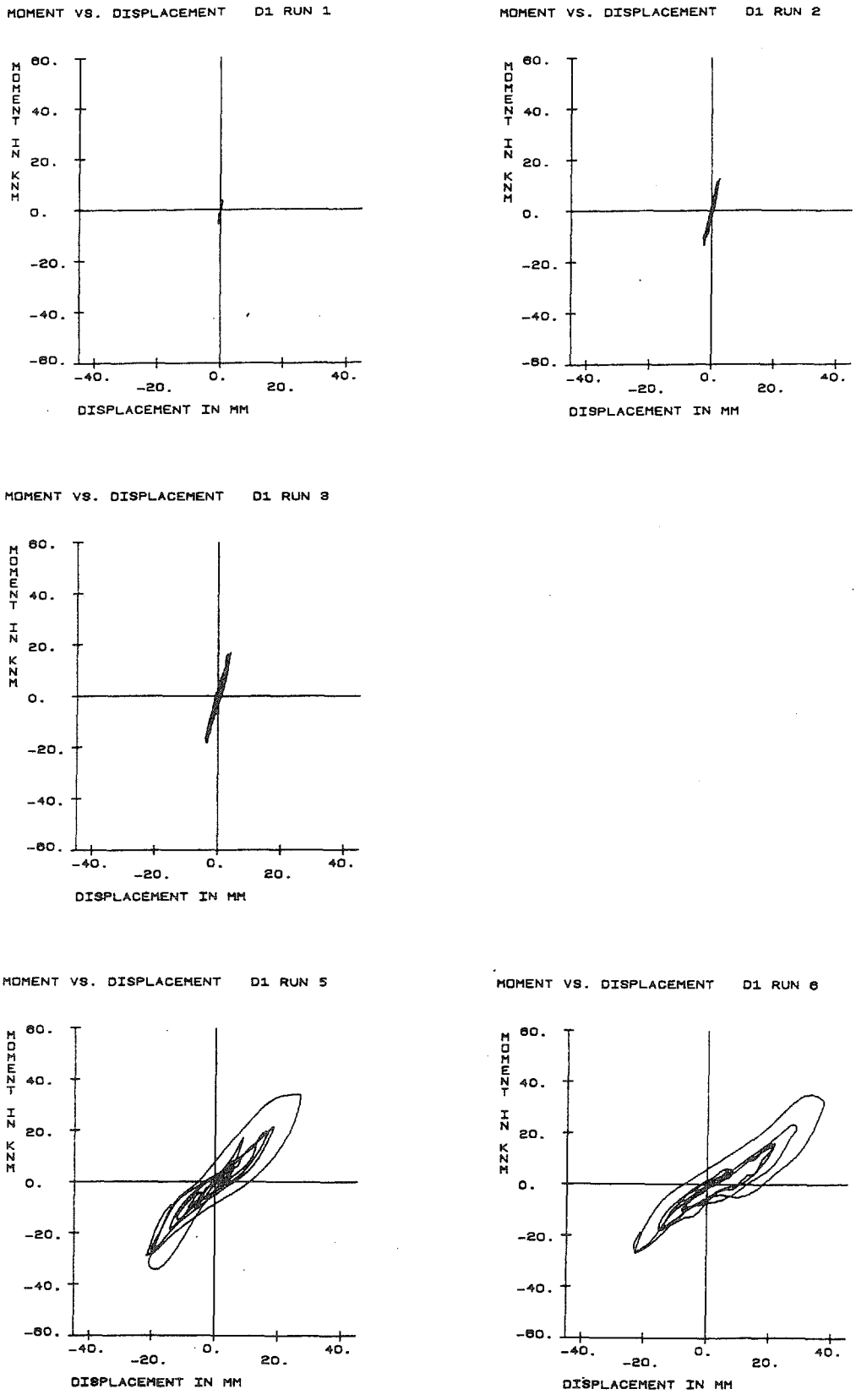

Fig. 6.3 Measured Moment-Displacement Relationships for Specimen D1

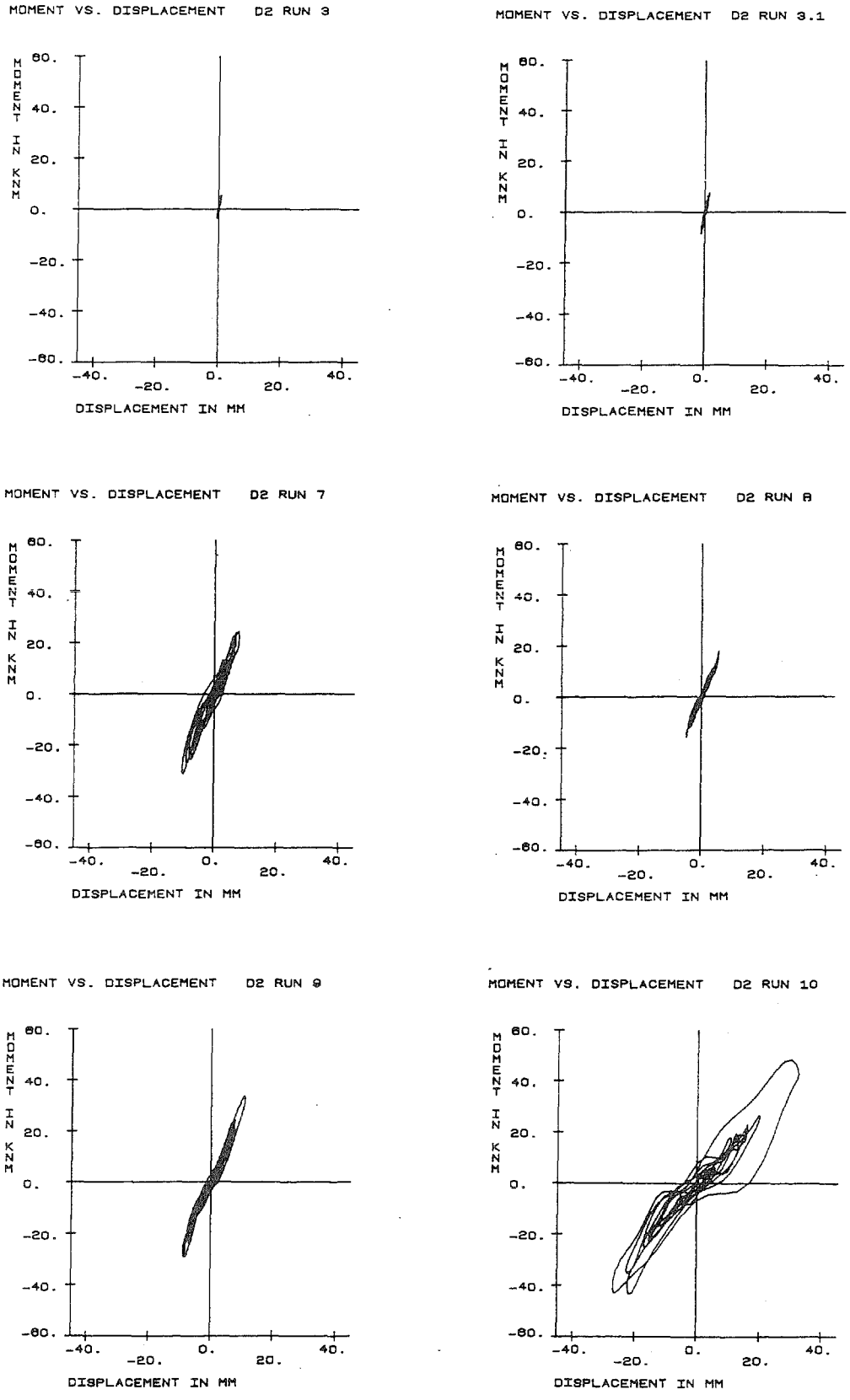

Fig. 6.4 Measured Moment-Displacement Relationships for Specimen D2

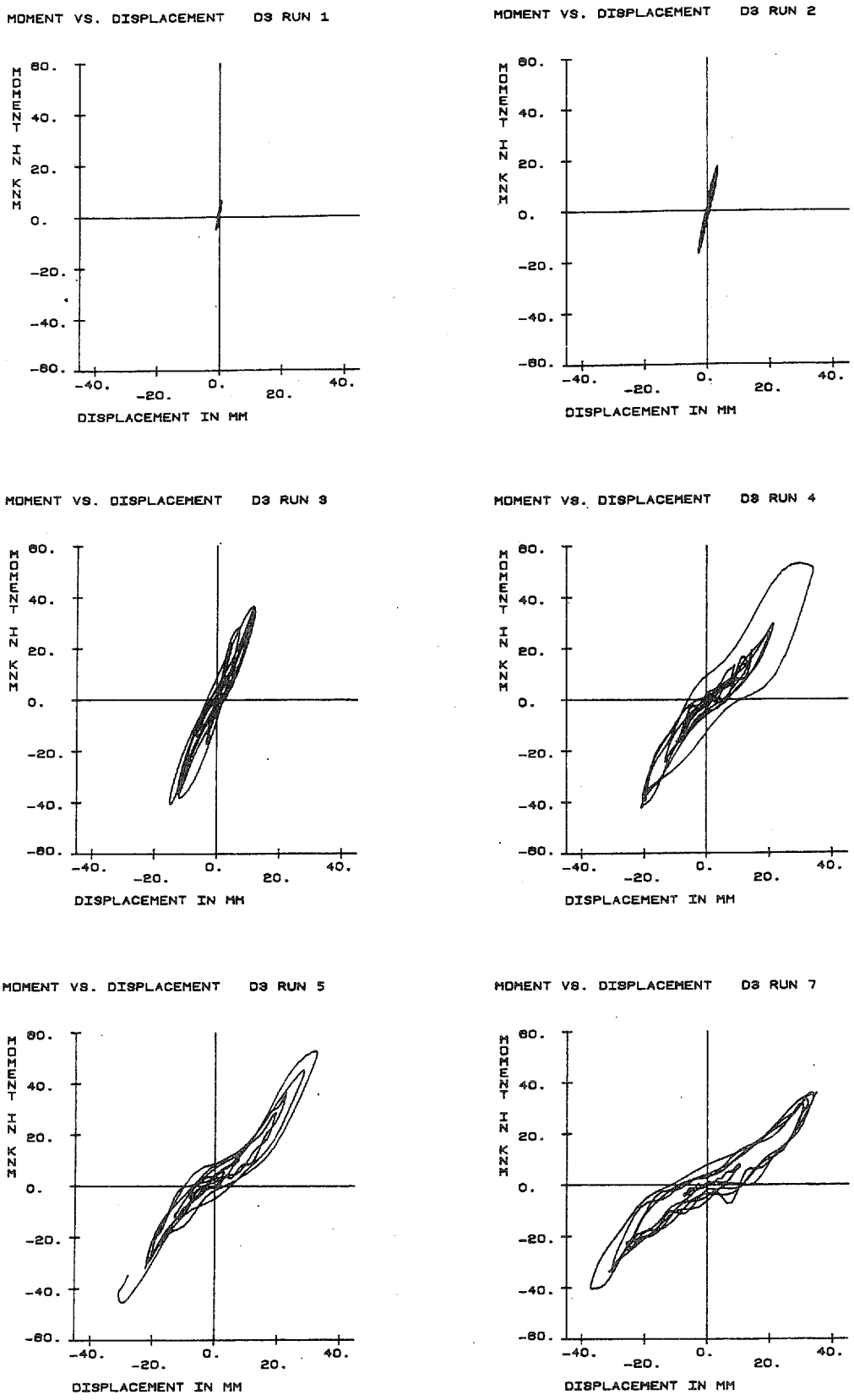

Fig. 6.5 Measured Moment-Displacement Relationships for Specimen D3

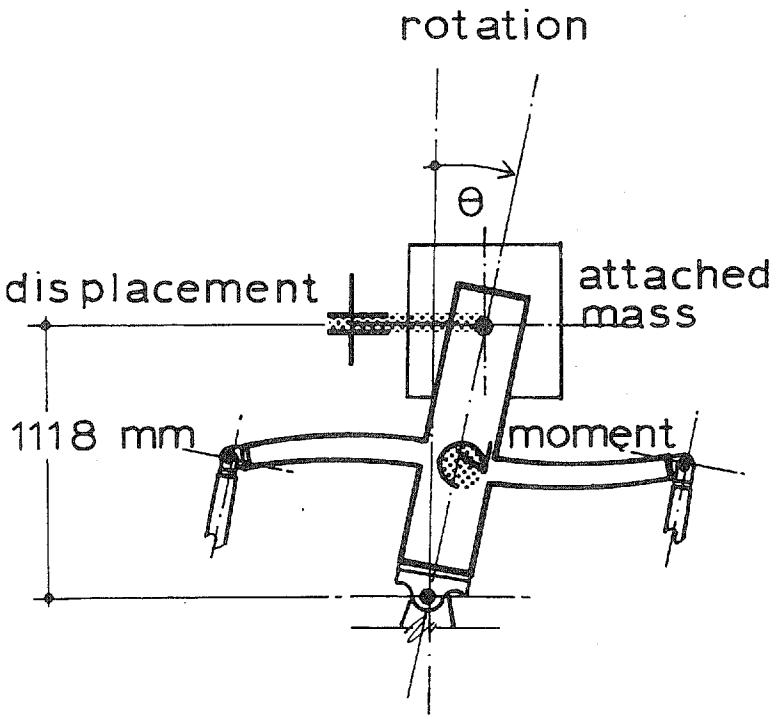

Fig. 6.6 Position of Displacement Measurement and Applied Connection Moment

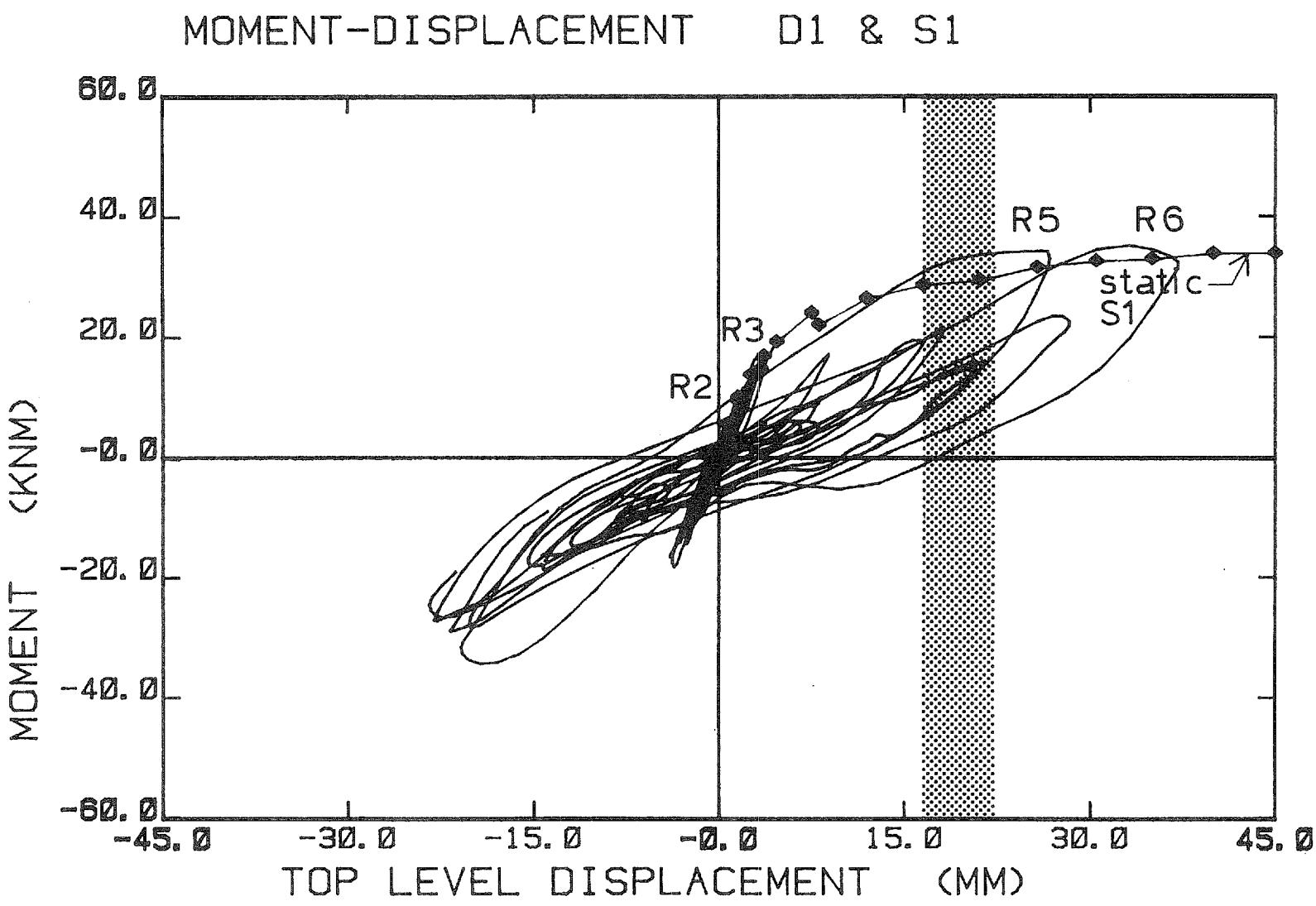

Fig. 6.7 Moment-Displacement Relationships for Statically Tested Specimen S1 and Dynamically Tested D1

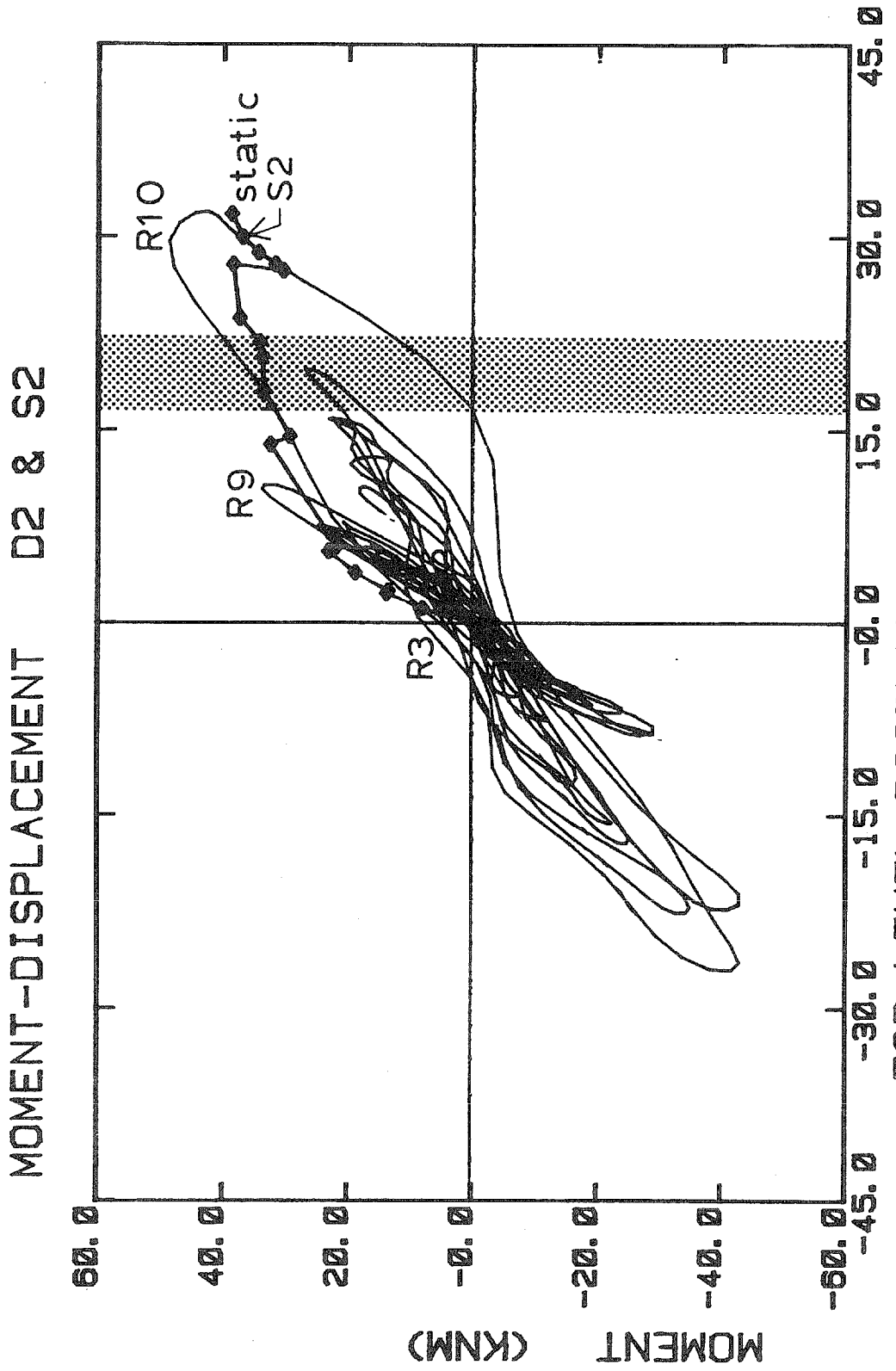

Fig. 6.8 Moment-Displacement Relationships for Statically Tested Specimen S2 and Dynamically Tested D2

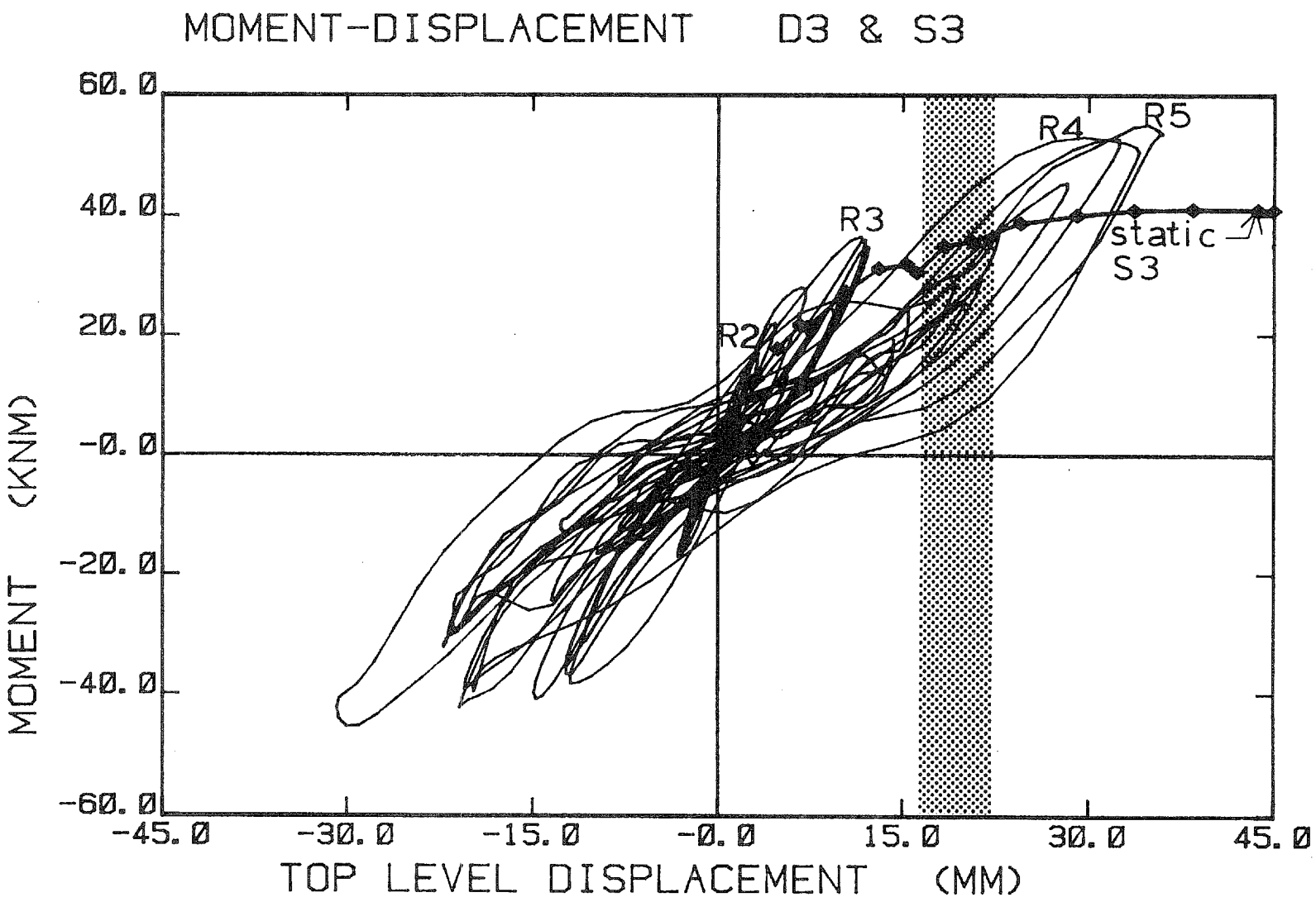

Fig. 6.9 Moment-Displacement Relationships for Statically Tested Specimen S3 and Dynamically Tested D3

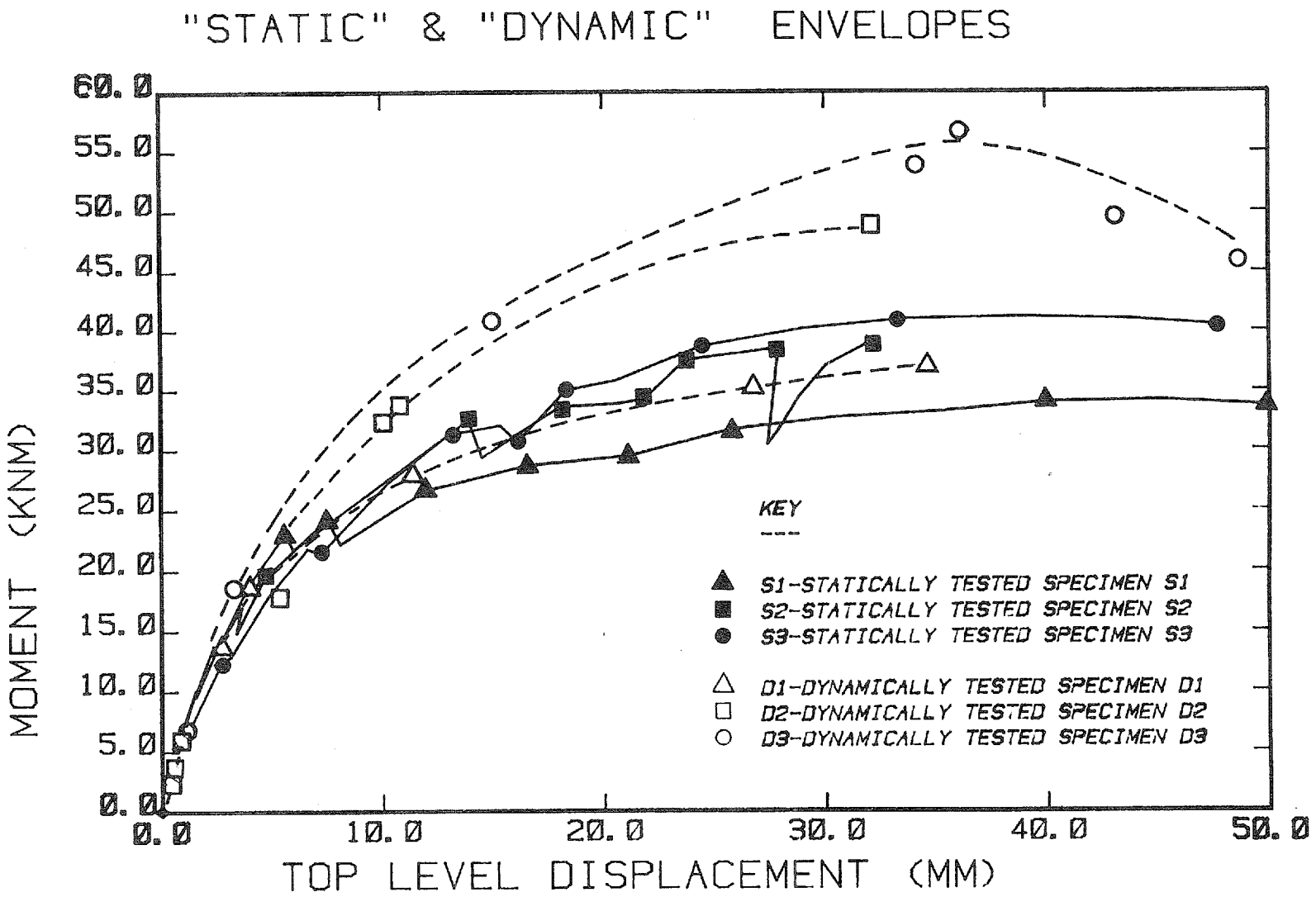

Fig. 6.10 Moment-Displacement Envelopes for Statically and Dynamically Tested Specimens

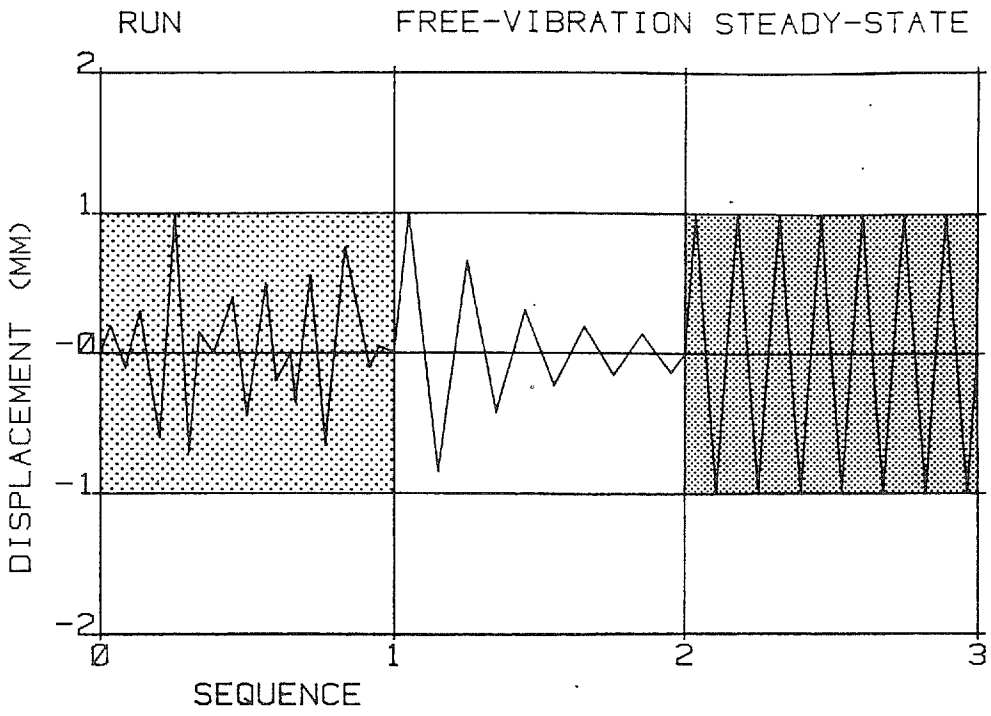

(a) Idealized Simulated Earthquake Run, Free-Vibration and Steady-State Displacement Response

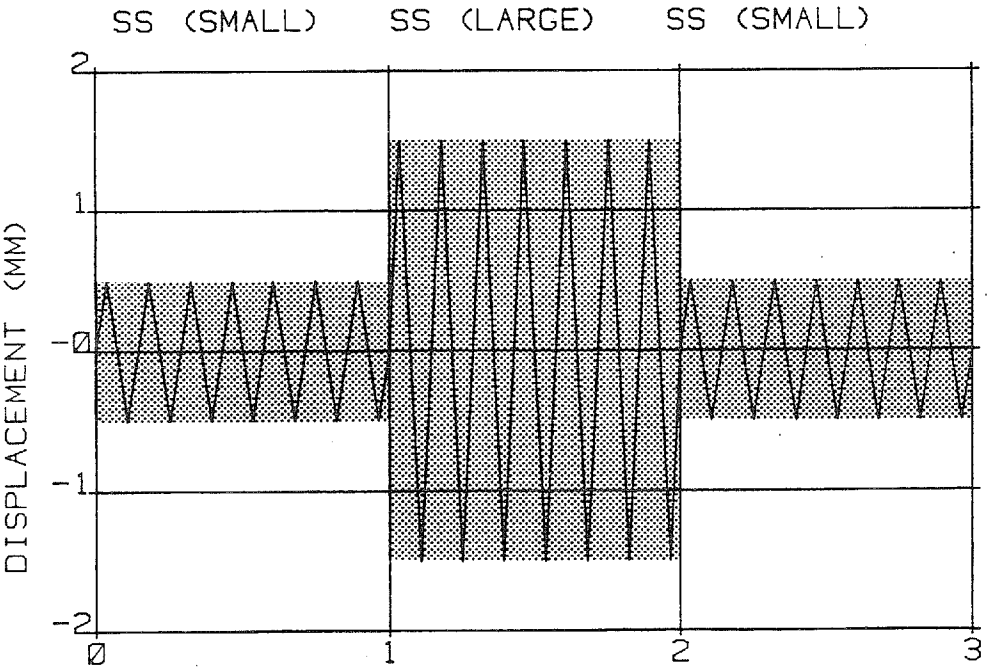

(b) Idealized Small-Amplitude, Large-Amplitude and Small-Amplitude Steady-State Tests

Fig. 6.11 Idealized Response to Various Test Motions

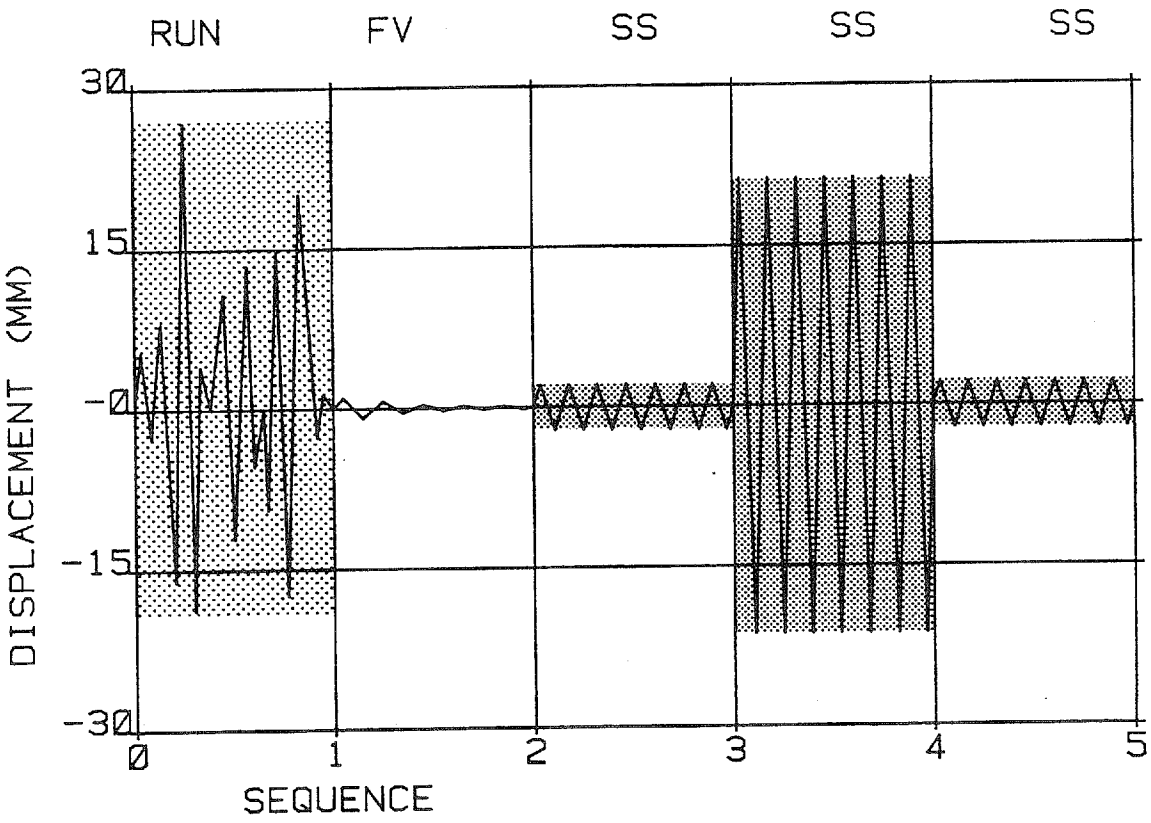

Fig. 6.12 Idealized Response Illustrating Amplitude of Response to Various Test Motions

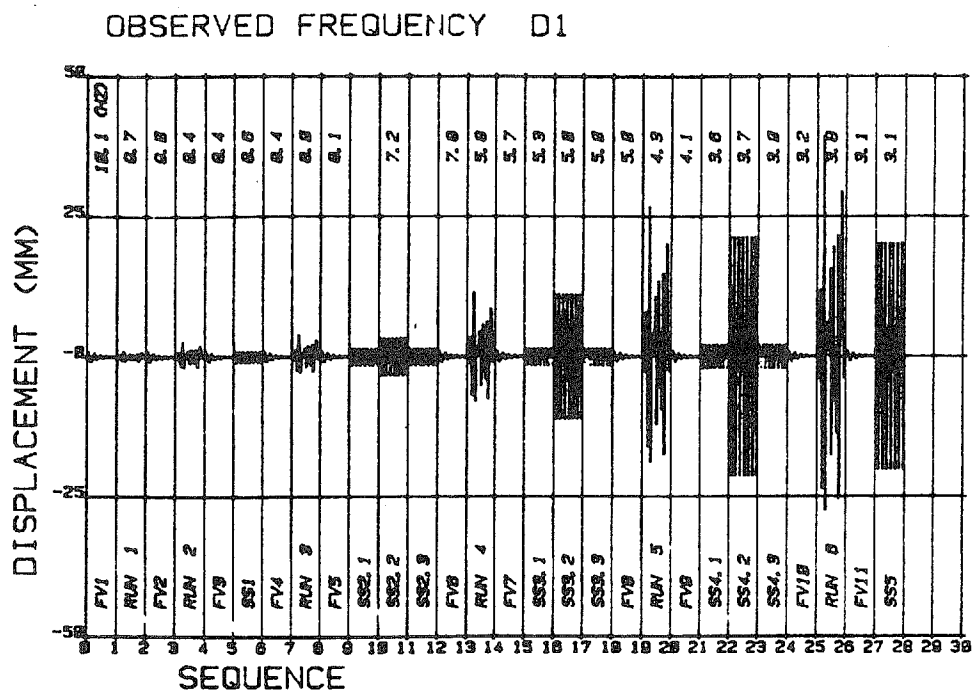

Fig. 6.13 Observed and Calculated Frequency Values for Specimen D1

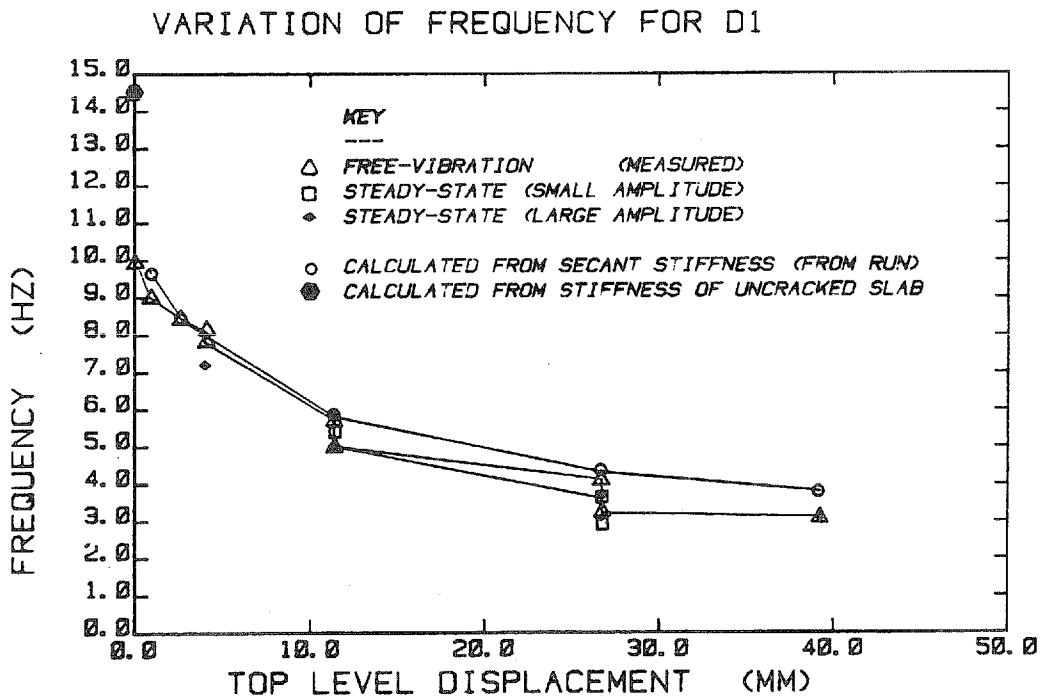

Fig. 6.14 Frequency vs. Previously Experienced Maximum Displacement for Specimen D1

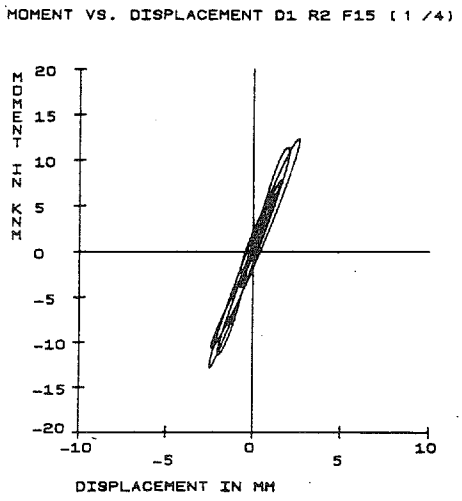

(a) Run 2

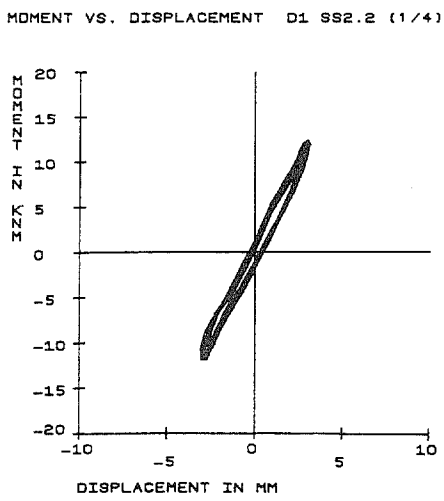

(b) SS2.2

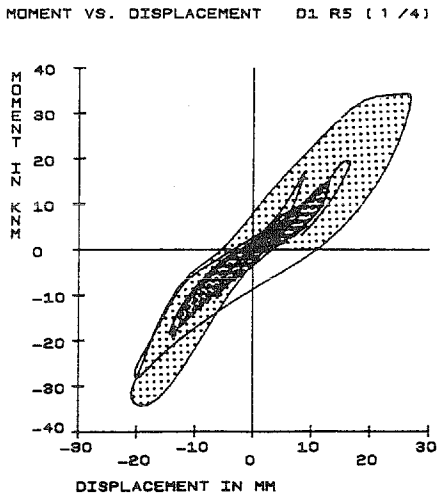

(c) Run 5

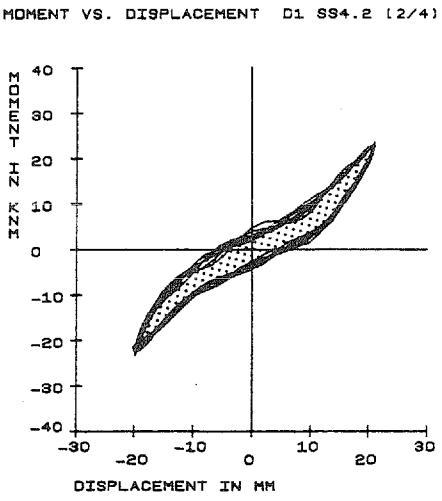

(d) SS4.2

Fig. 6.15 Representative Moment-Displacement Relationships for Specimen D1

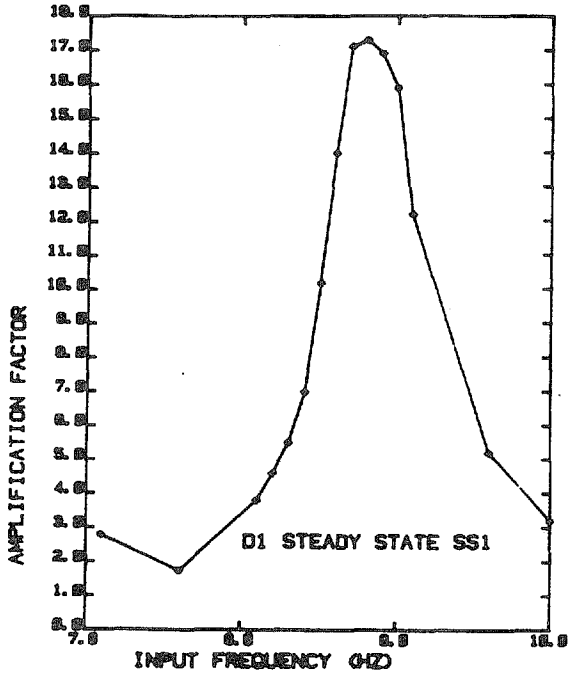

(a) SS1

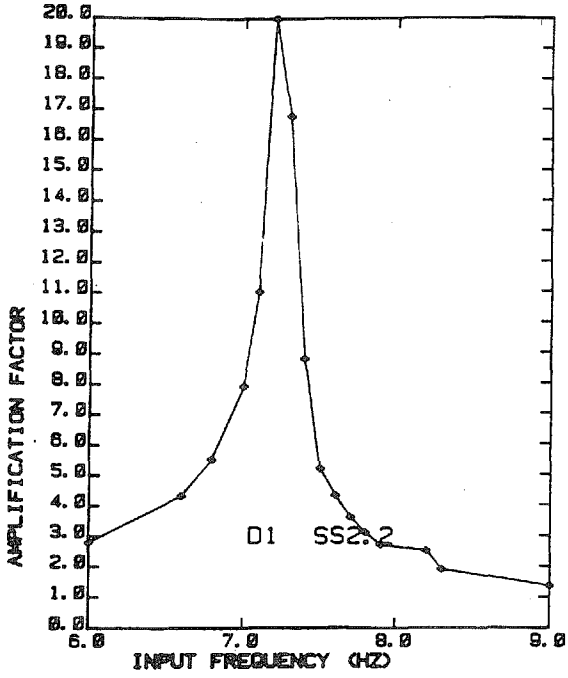

(b) SS2.2 (Large-Amplitude)

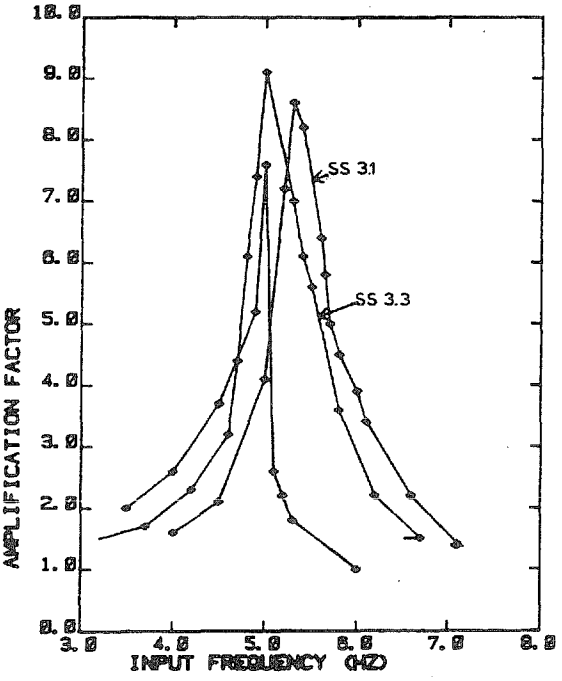

(c) SS3.1 and SS3.3 (Small-Amplitude), SS3.2 (Large-Amplitude)

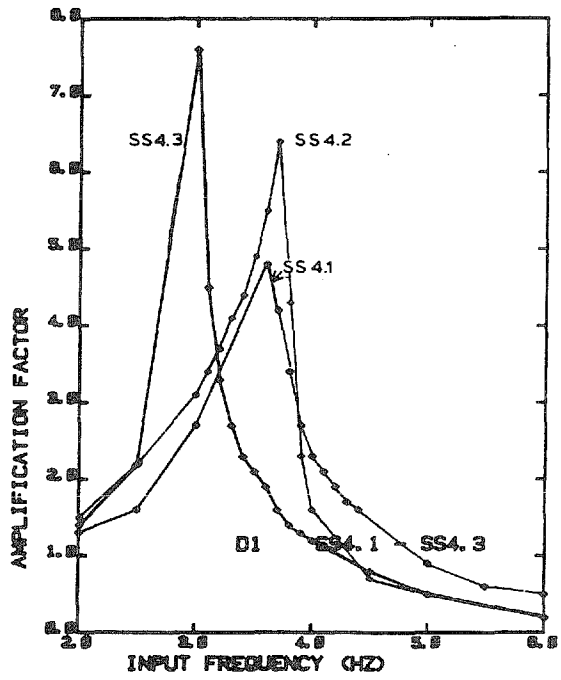

(d) SS4.1 and SS4.3 (Small-Amplitude), SS4.2 (Large-Amplitude)

Fig. 6.16 Measured Response to Steady-State Base Motion for Specimen D1

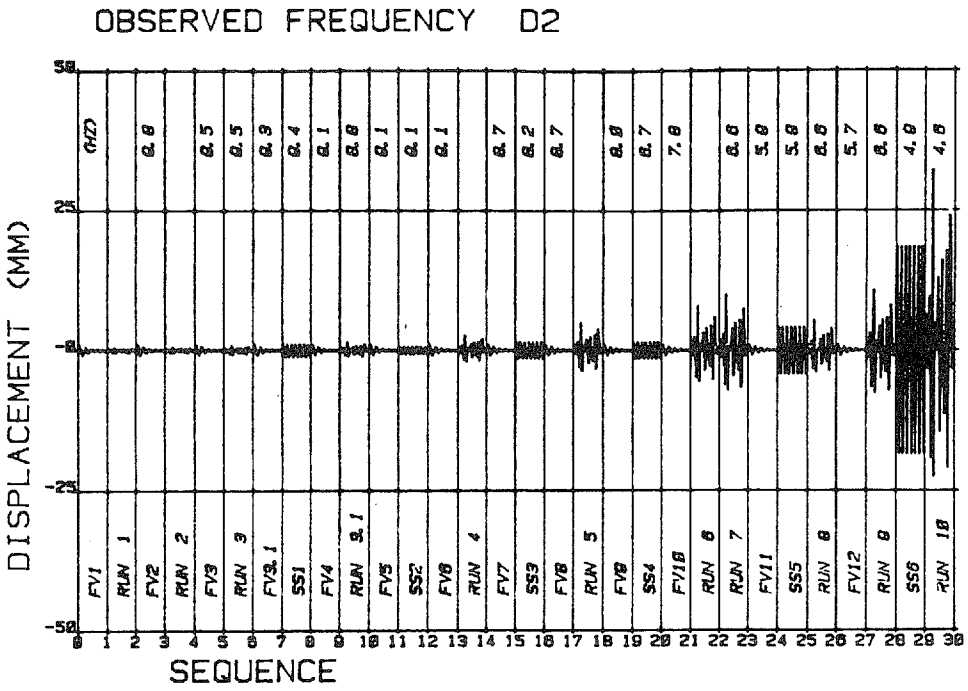

Fig. 6.17 Observed and Calculated Frequency Values for Specimen D2

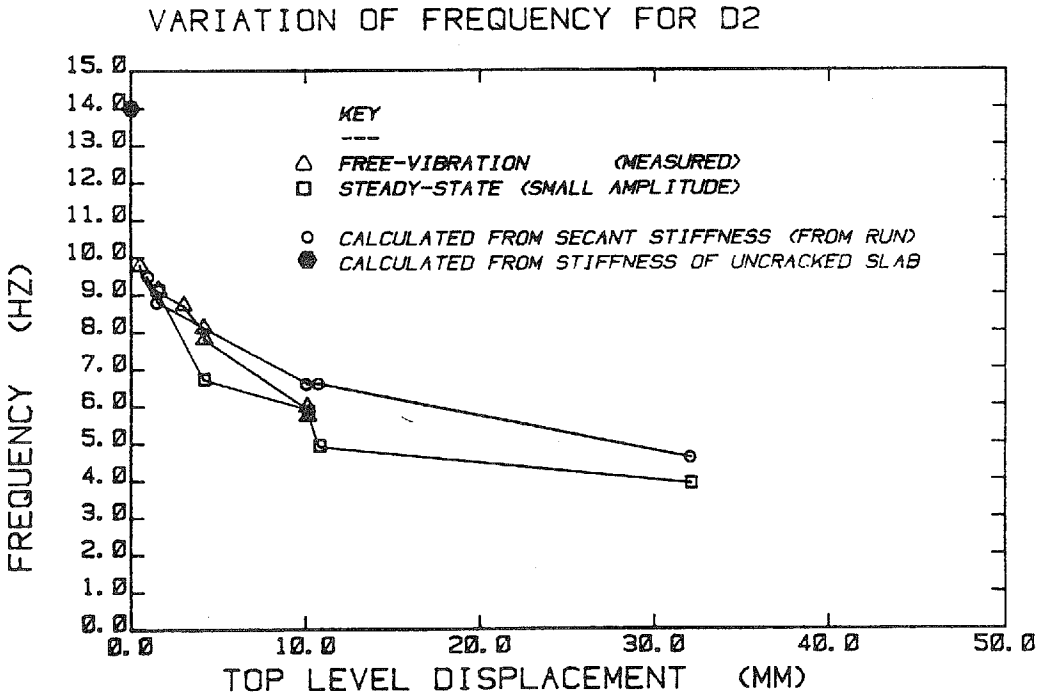

Fig. 6.18 Frequency vs. Previously Experienced Maximum Displacement for Specimen D2

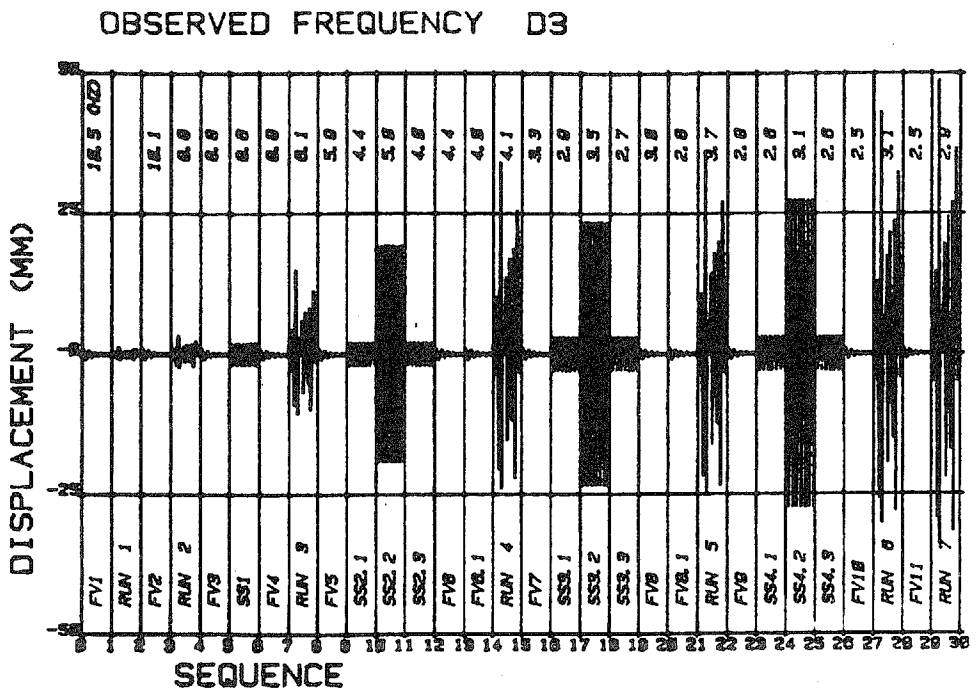

Fig. 6.19 Observed and Calculated Frequency Values for Specimen D3

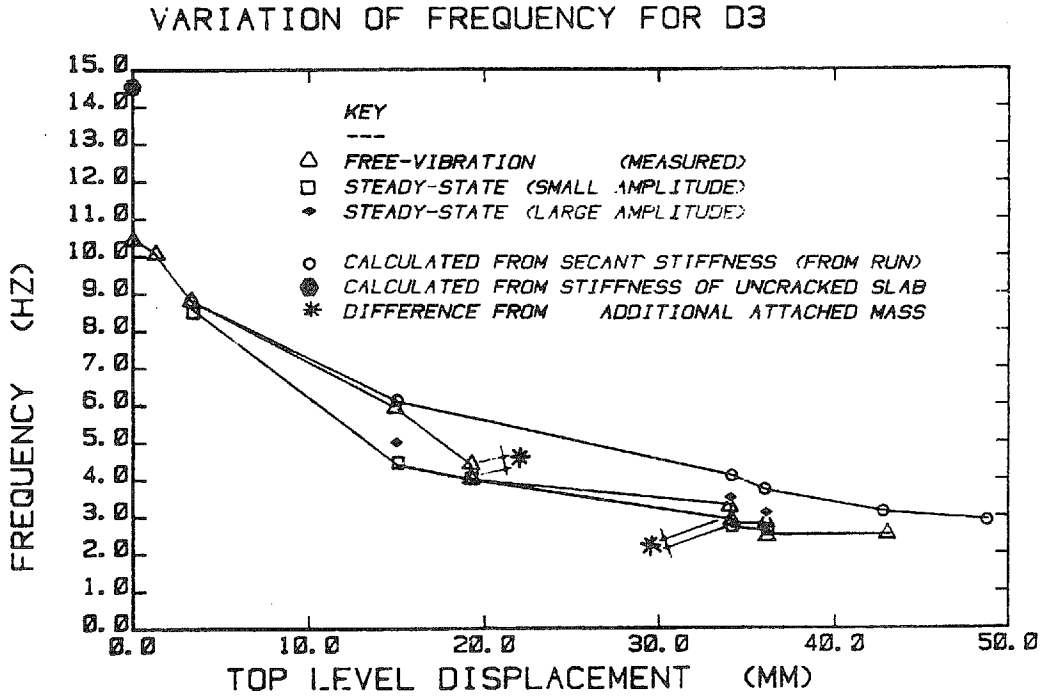

Fig. 6.20 Frequency vs. Previously Experienced Maximum Displacement for Specimen D3

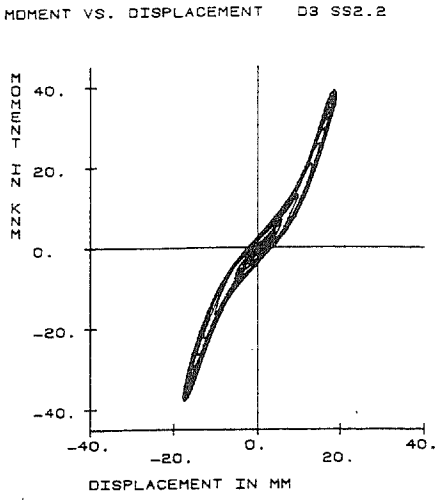

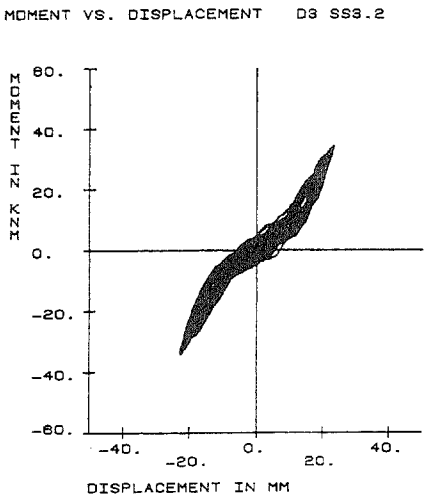

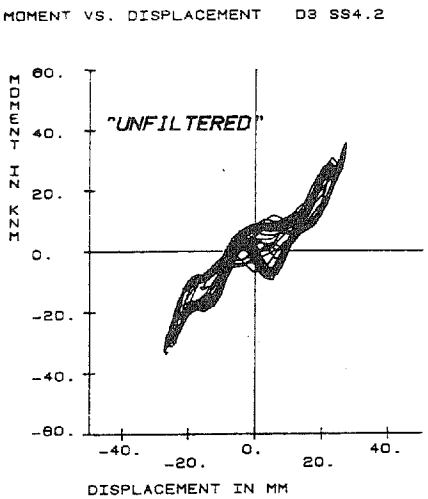

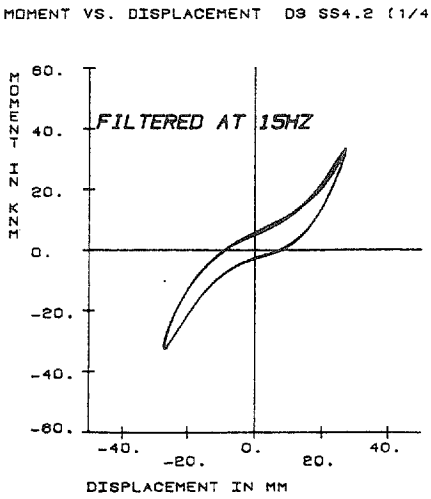

Fig. 6.21 Measured Moment-Displacement Relationships for Steady-State Tests of Specimen D3

(a) SS3.1 (Small-Amplitude),
SS3.2 (Large-Amplitude)
and SS3.3 (Small-Amplitude)

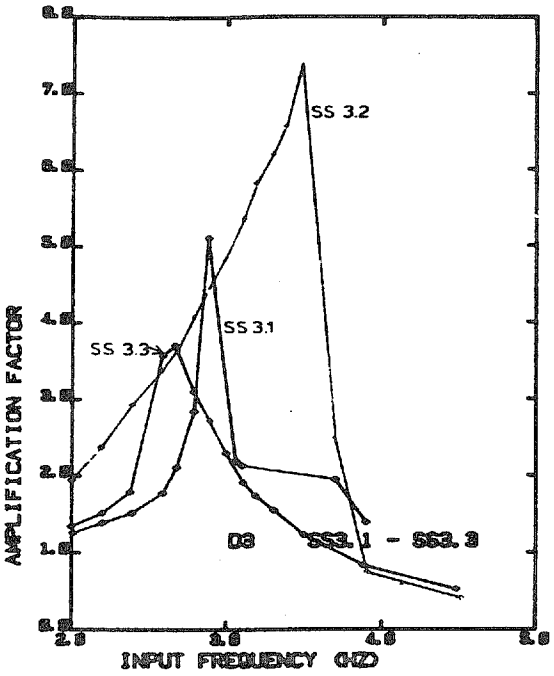

(b) SS4.1 (Small-Amplitude),
SS4.2 (Large-Amplitude)
and SS4.3 (Small-Amplitude)

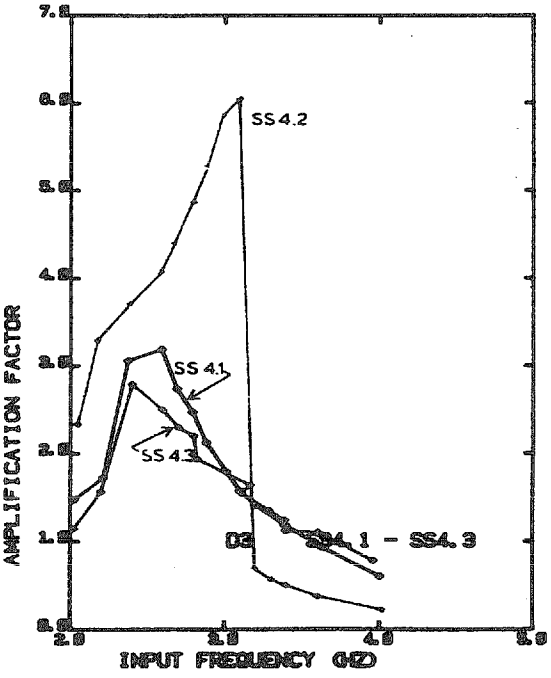

Fig. 6.22 Measured Response to Steady-State Base Motion for Specimen D3

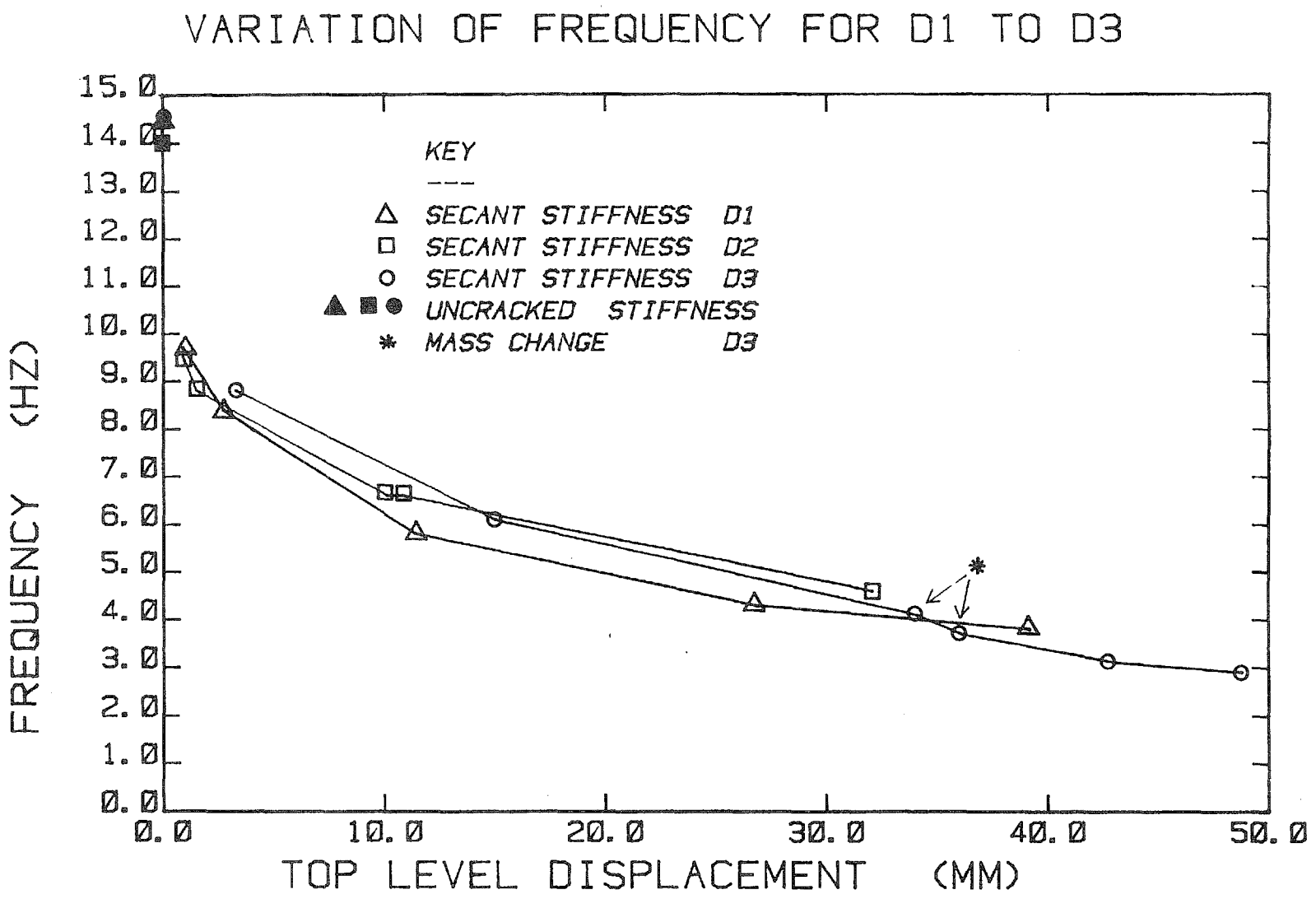

Fig. 6.23 Frequency vs. Previously Experienced Maximum Displacement for Specimens D1, D2 and D3

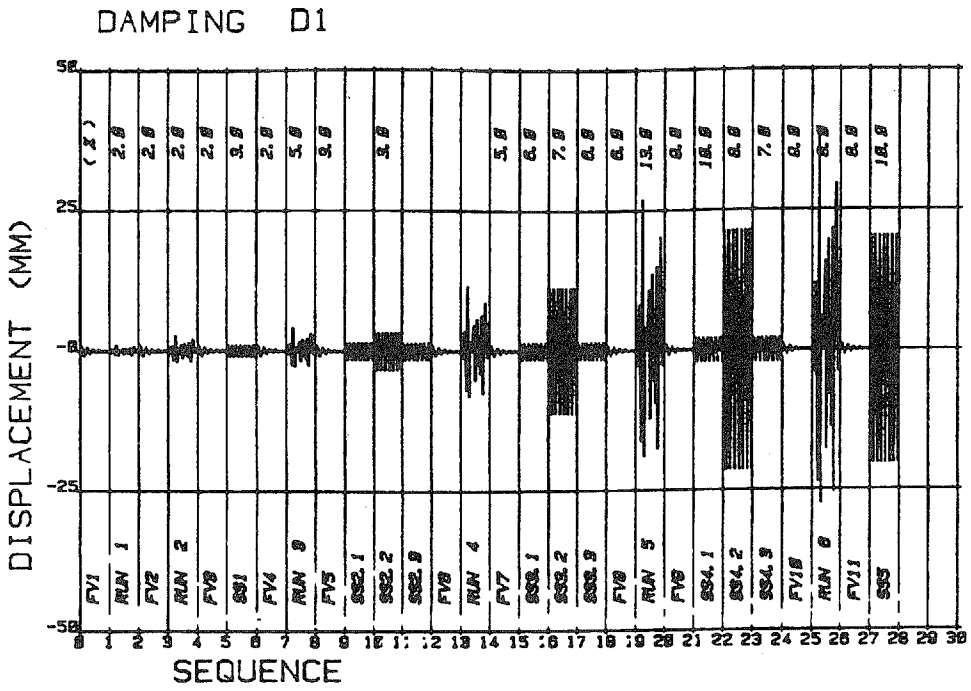

Fig. 6.24 Calculated Damping Values for Specimen D1

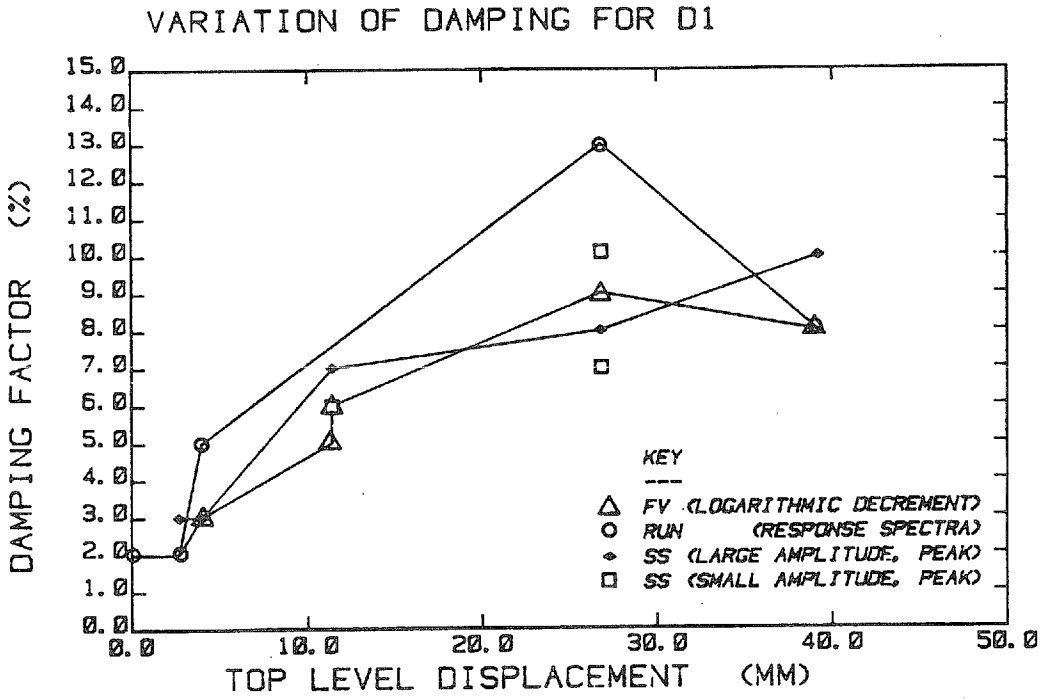

Fig. 6.25 Damping Factors vs. Previously Experienced Maximum Displacement for Specimen D1

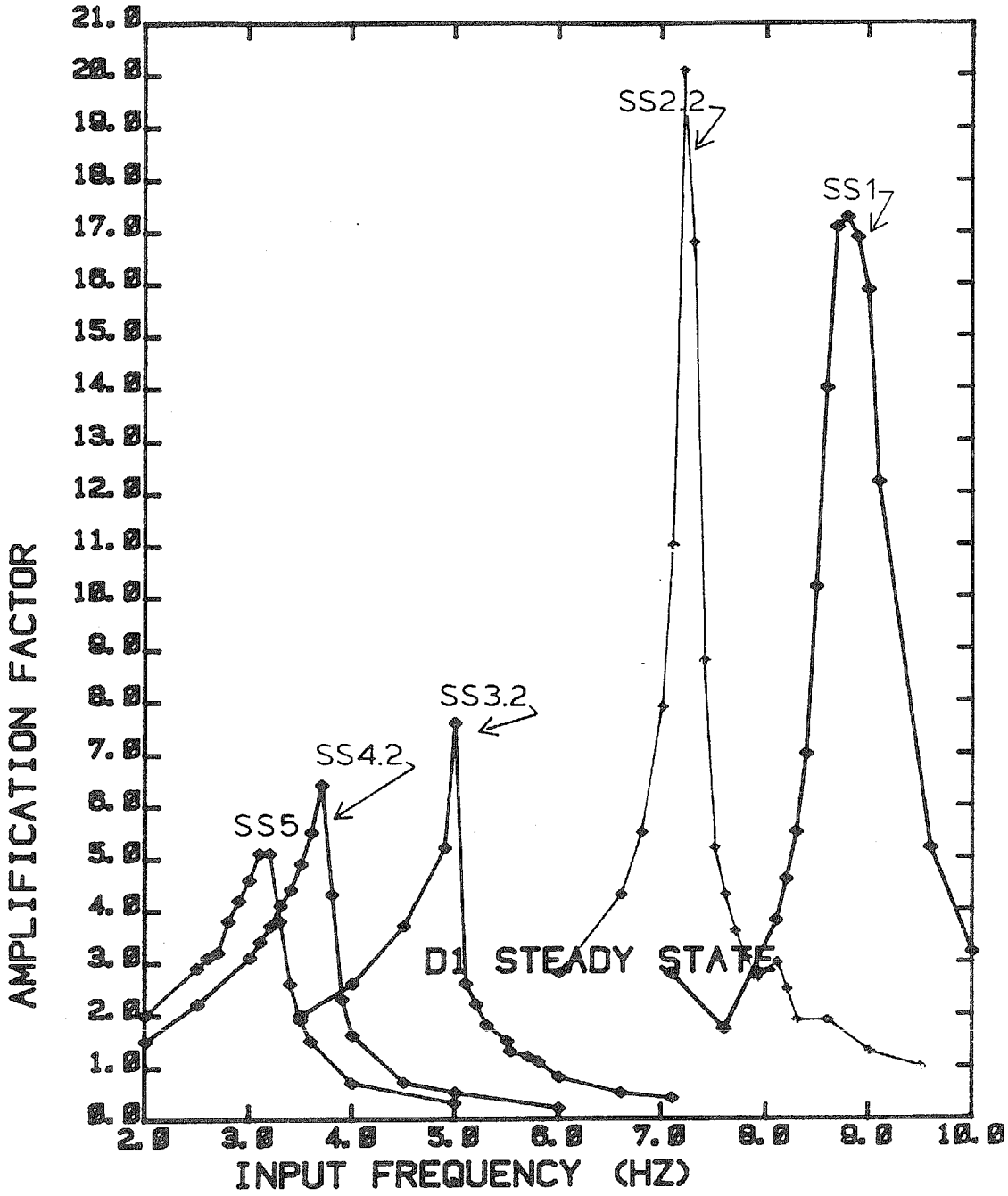

Fig. 6.26 Measured Response to Steady-State Base Motion for Specimen D1

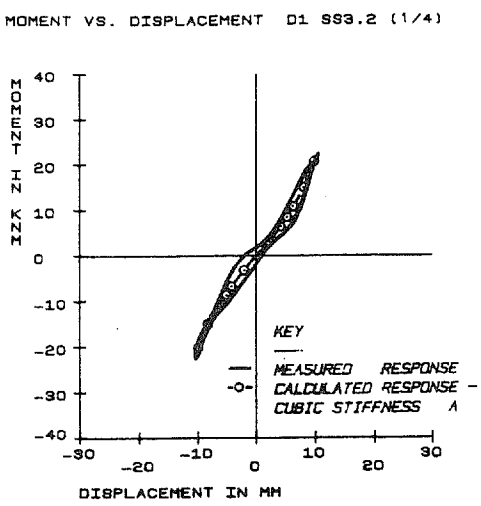

(a) Calculated and Measured Moment-Displacement Relationships Before Resonance

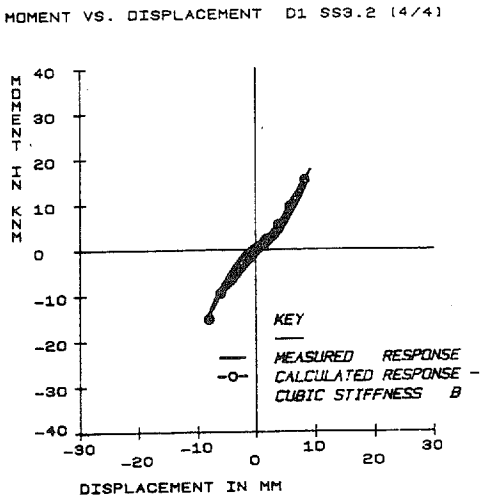

(b) Calculated and Measured Moment-Displacement Relationships After Resonance

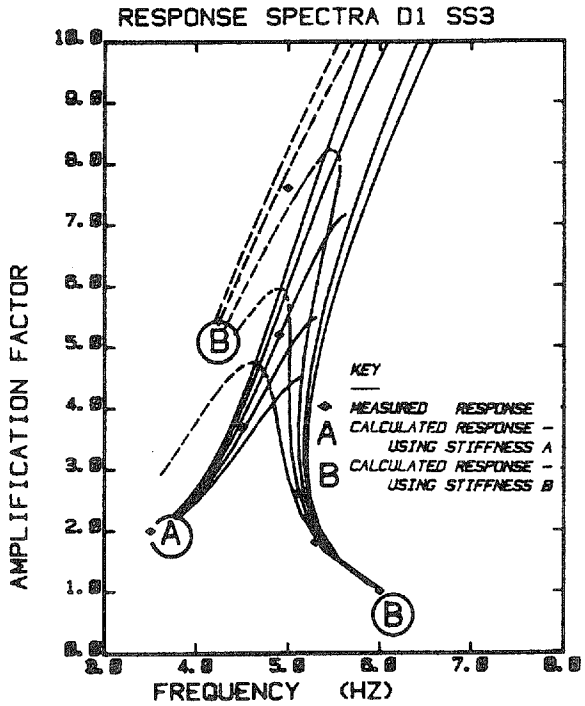

(c) Calculated and Measured Response

Fig. 6.27 Measured and Calculated Response to Steady-State Base Motion (SS3.2) for Specimen D1

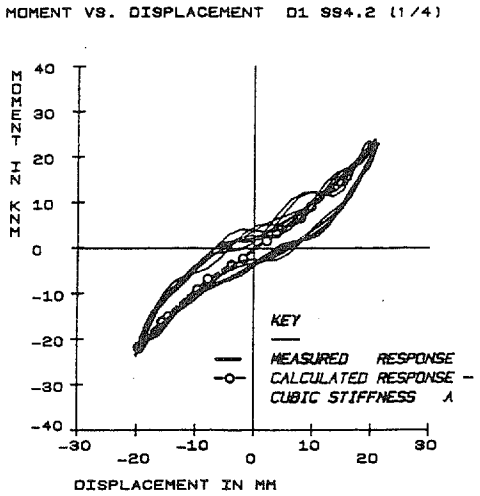

(a) Calculated and Measured Moment-Displacement Relationships Before Resonance

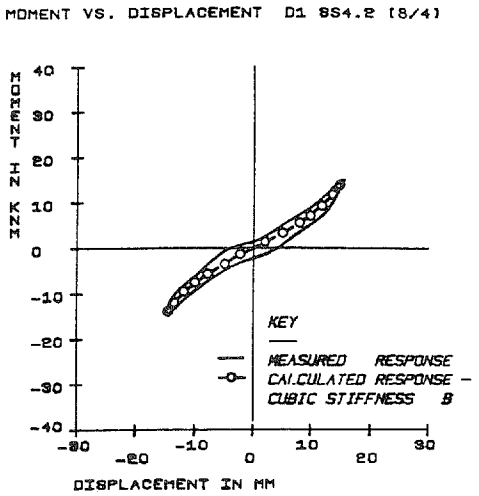

(b) Calculated and Measured Moment-Displacement Relationships After Resonance

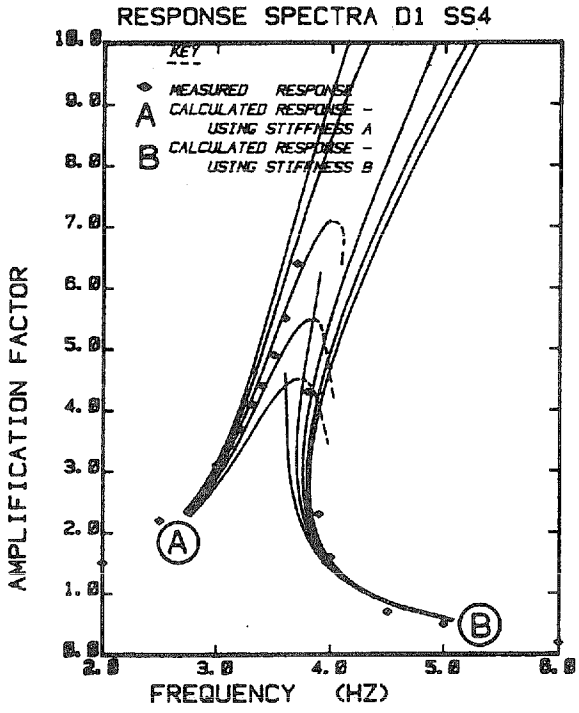

(c) Calculated and Measured Response

Fig. 6.28 Measured and Calculated Response to Steady-State Base Motion (SS4.2) for Specimen D1

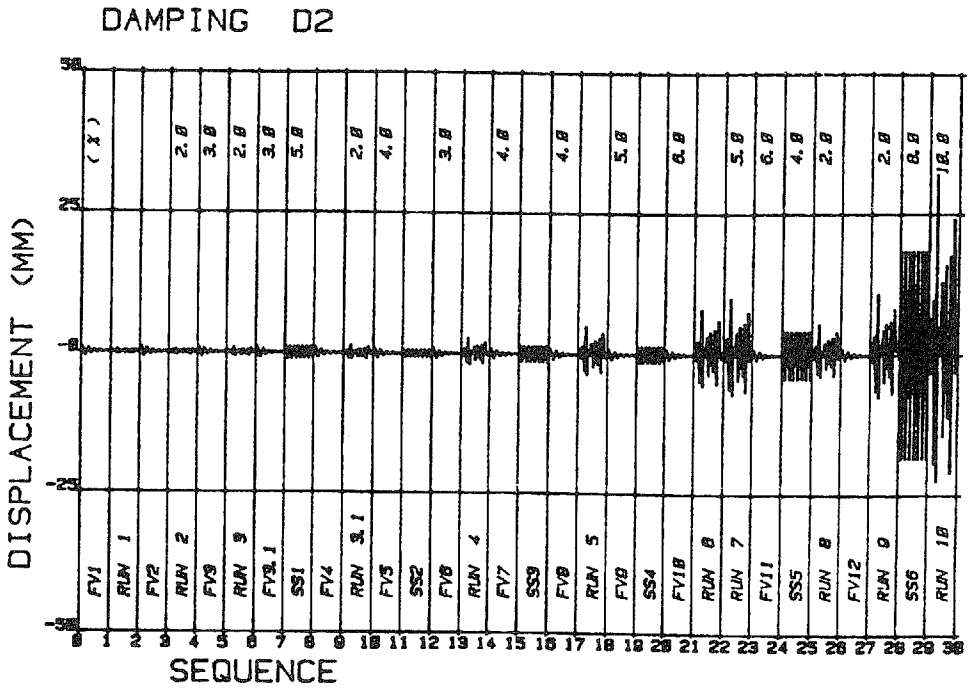

Fig. 6.29 Calculated Damping Values for Specimen D2

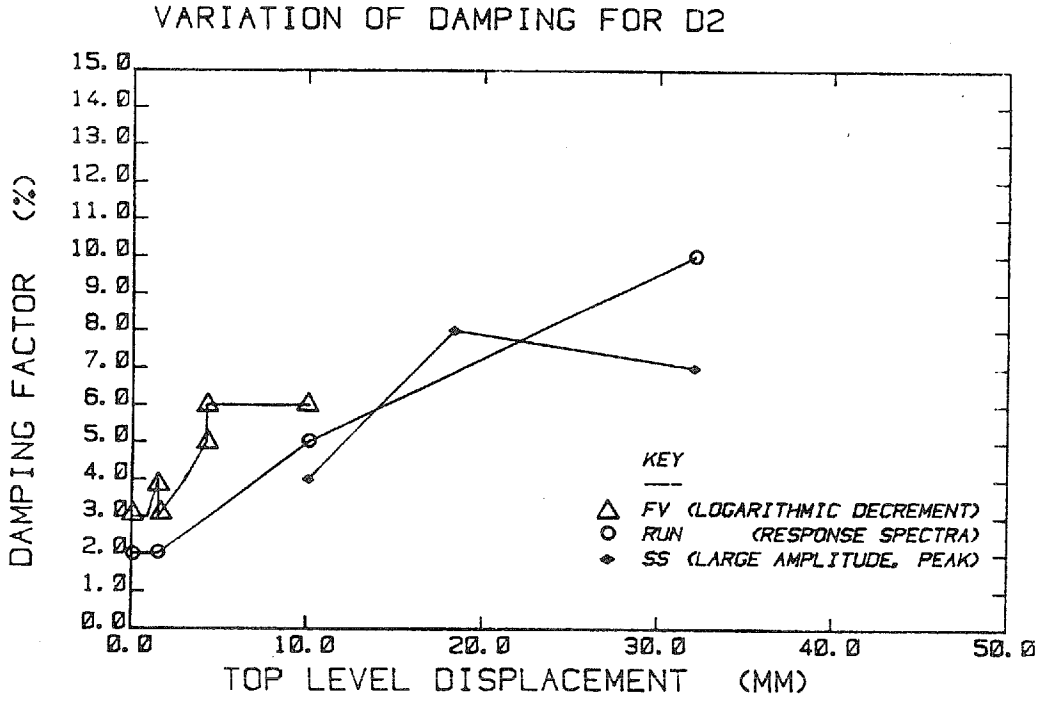

Fig. 6.30 Damping Factors vs. Previously Experienced Maximum Displacement for Specimen D2

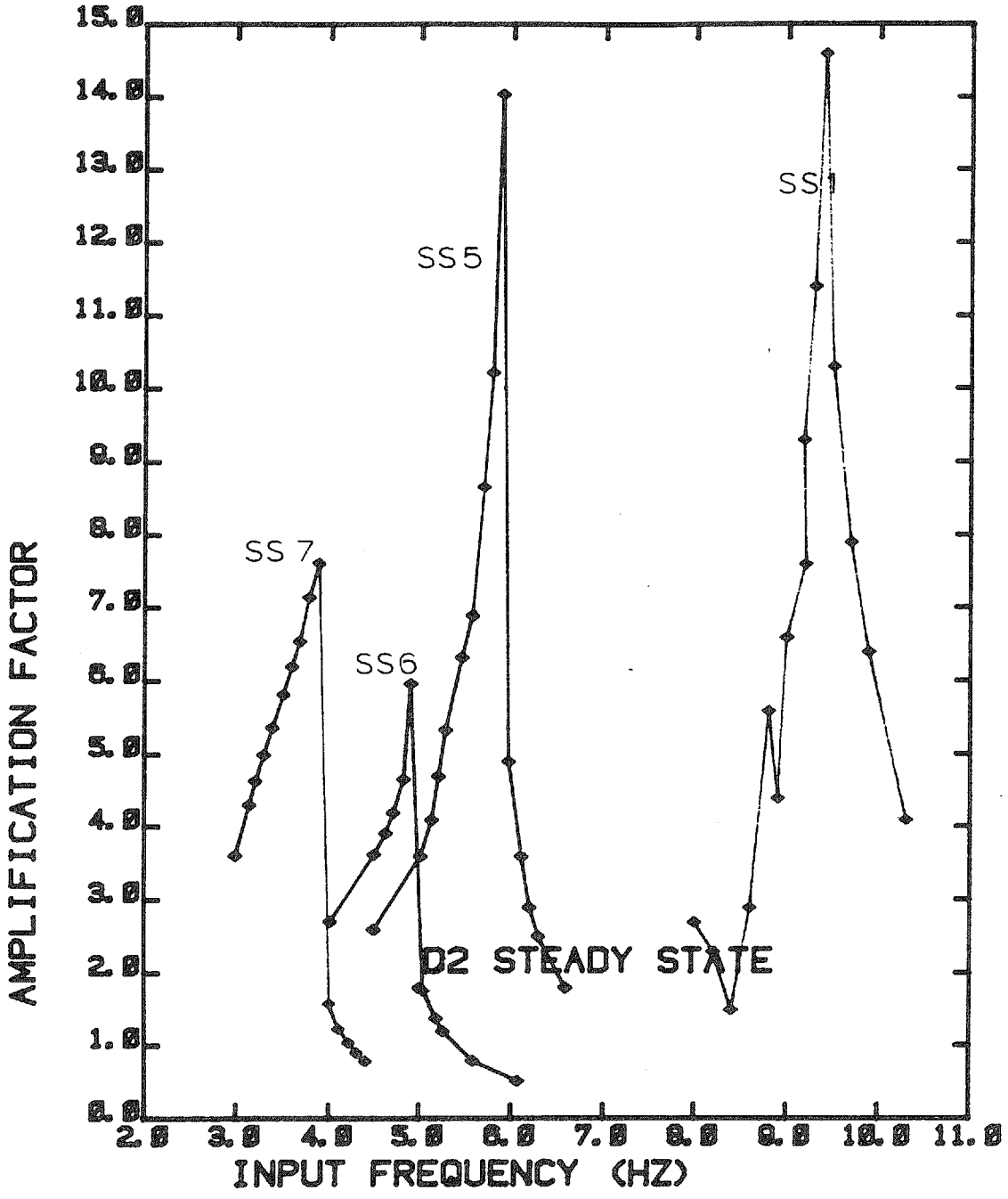

Fig. 6.31 Measured Response to Steady-State Base Motion for Specimen D2

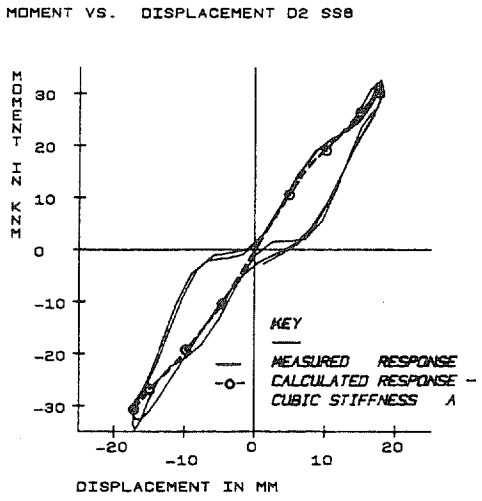

(a) Calculated and Measured Moment-Displacement Relationships Before Resonance

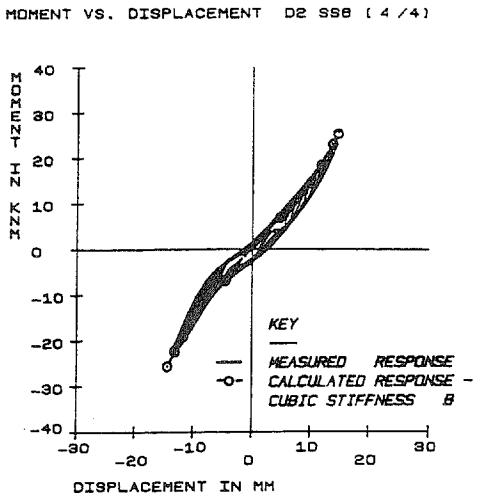

(b) Calculated and Measured Moment-Displacement Relationships After Resonance

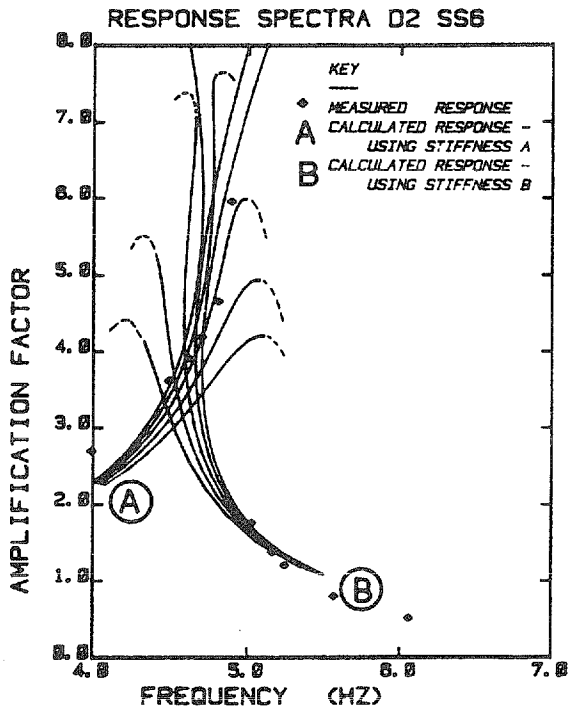

(c) Calculated and Measured Response

Fig. 6.32 Measured and Calculated Response to Steady-State Base Motion (SS6) for Specimen D2

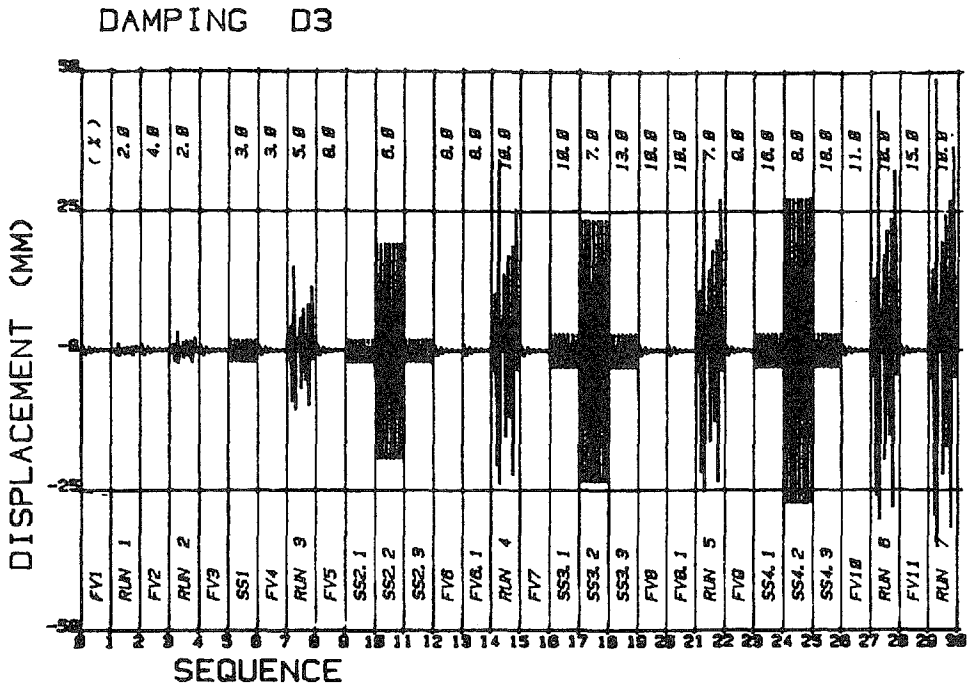

Fig. 6.33 Calculated Damping Values for Specimen D3

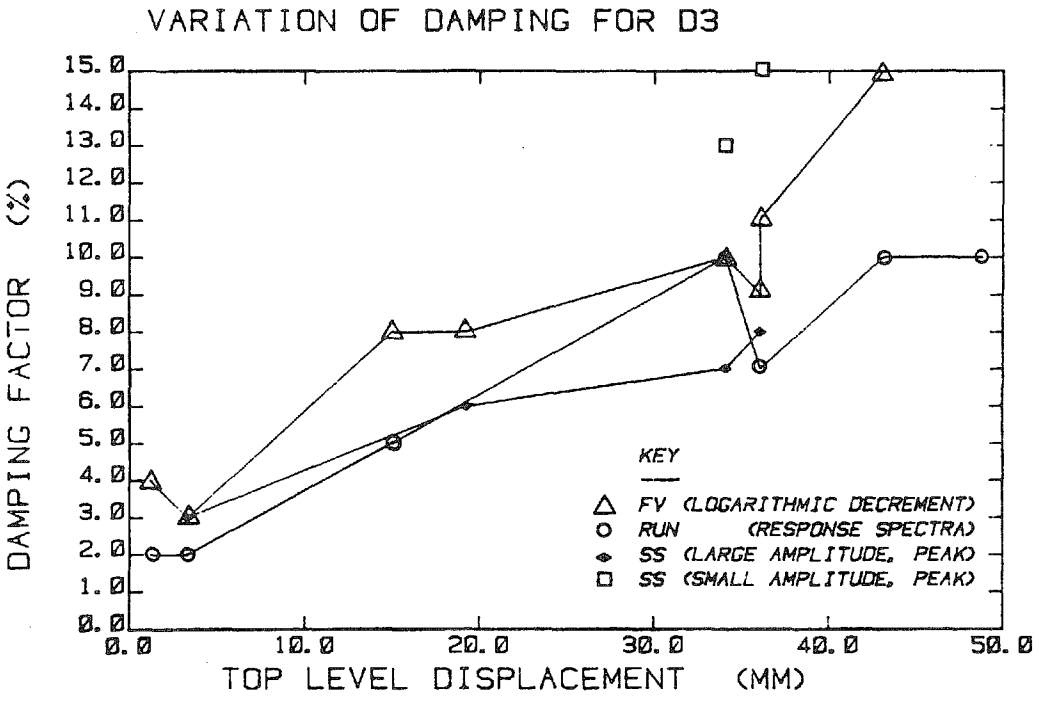

Fig. 6.34 Damping Factors vs. Previously Experienced Maximum Displacement for Specimen D3

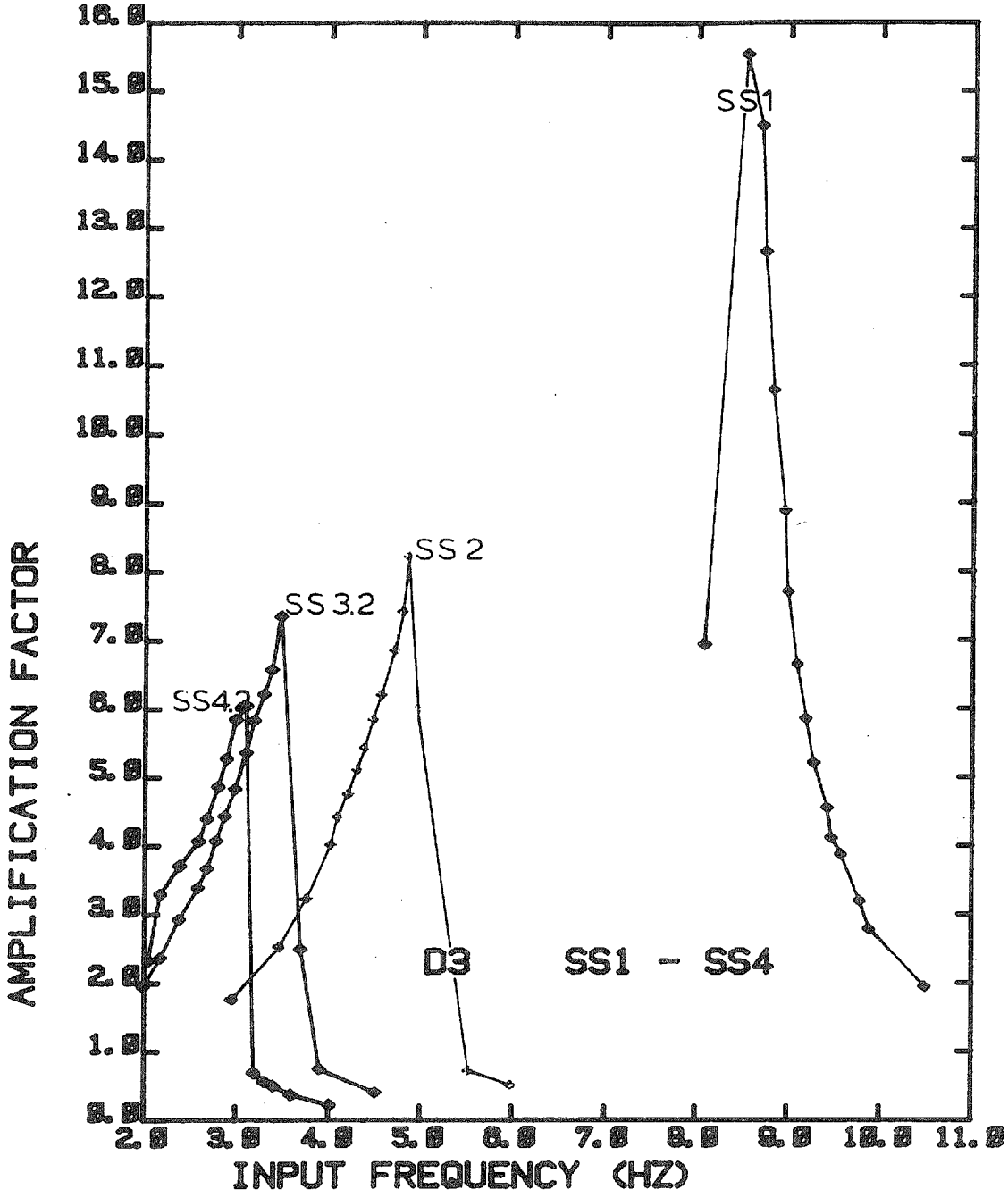

Fig. 6.35 Measured Response to Steady-State Base Motion for Specimen D3

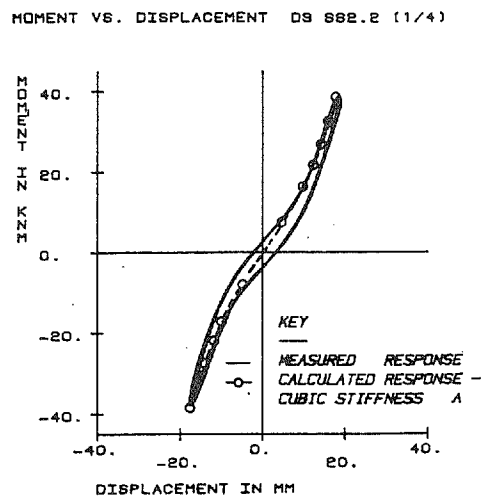

(a) Calculated and Measured Moment-Displacement Relationships Before Resonance

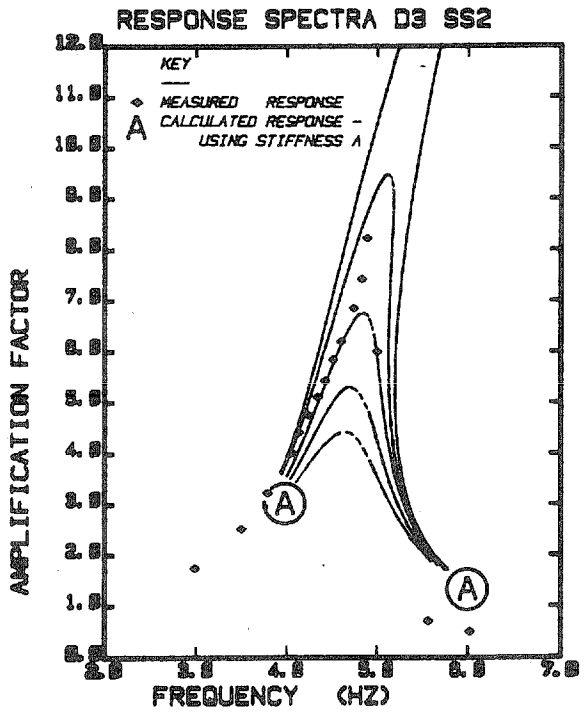

(b) Calculated and Measured Response

Fig. 6.36 Measured and Calcuated Response to Steady-State Base Motion (SS2.2) for Specimen D3

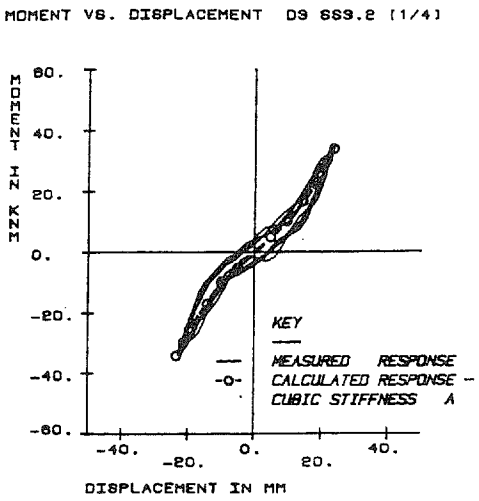

(a) Calculated and Measured Moment-Displacement Relationships Before Resonance

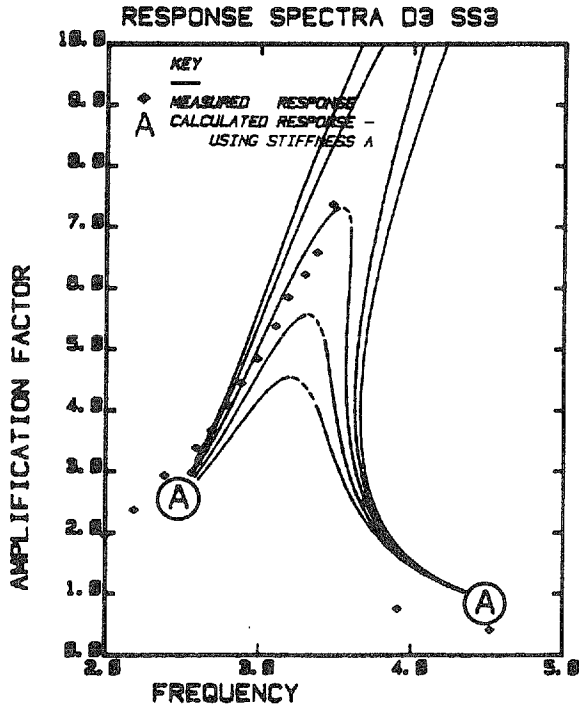

(b) Calculated and Measured Response

Fig. 6.37 Measured and Calculated Response to Steady-State Base Motion (SS3.2) for Specimen D3

(a) FV

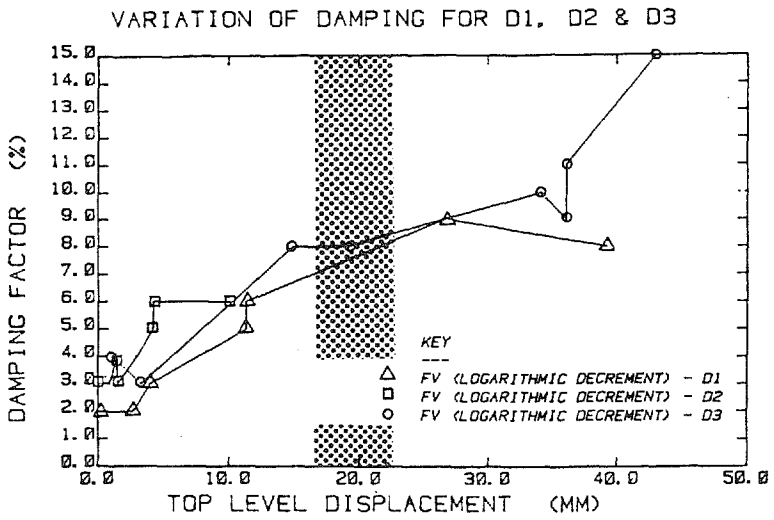

(b) Runs

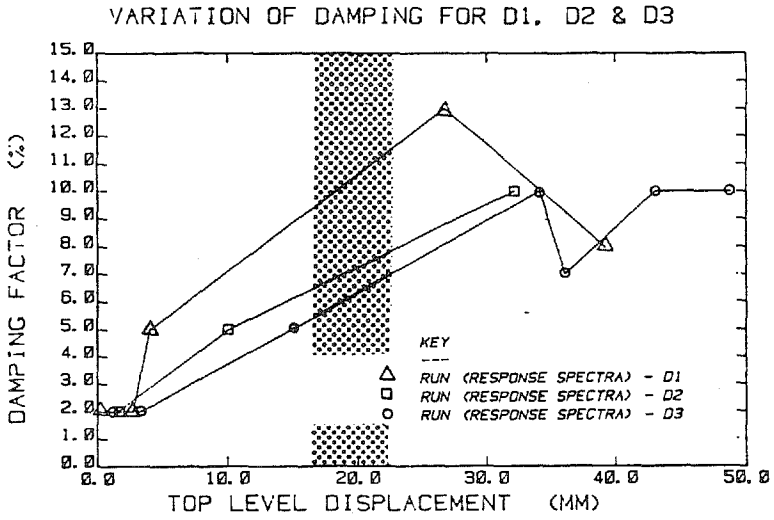

(c) SS

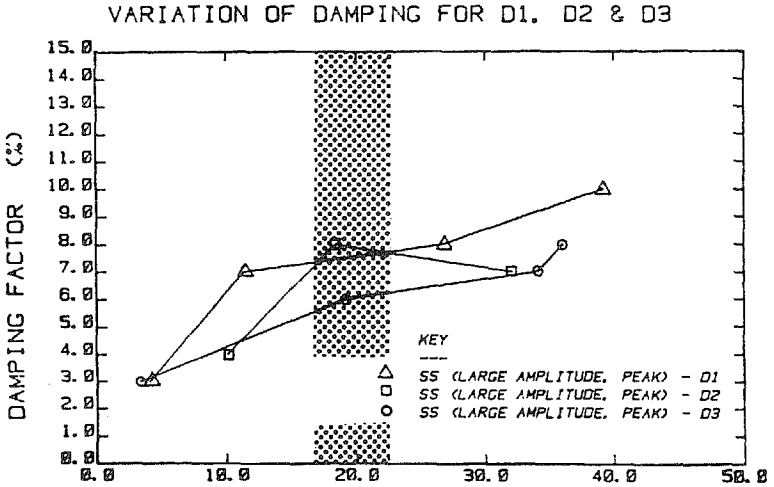

Fig. 6.38 Calculated Damping Factors vs. Previously Experienced Maximum Displacement for Specimens D1, D2 and D3

APPENDIX A

NOTATION AND DEFINITIONS

A.1 Notation

The notation is described when used in the text. For the convenience of the reader a list of the symbols is given for quick reference.

A = area

A_s = area of steel, reinforcing

a = span from column ℄ to inflection point in the direction of of horizontal load (full length of isolated column-slab. Slab specimen is 2a)

b = span from column ℄ to the inflection point in the direction transverse to that of horizontal loading. (Full width of the isolated column-slab specimen is 2b)

b = width of a beam section

c = viscous damping

D1 = Dynamic Specimen No. 1 ($\rho = 0.65\%$)

D2 = Dynamic Specimen No. 2 ($\rho = 0.98\%$)

D3 = Dynamic Specimen No. 3 ($\rho = 1.31\%$)

d = effective depth of a reinforced concrete section

d' = effective depth of top steel

d_b = diameter of the tensile and compressive reinforcement

E = east (In test setup)

E = Young's Modulus of elasticity

E_s = Young's modulus for steel

E_c = Young's modulus for concrete

e = steel elongation

F = external force

F_t = total external force

FV = free-vibration

FV1 = free-vibration Test No. 1

F15 = filtered at 15 Hz.

F35 = filtered at 35 Hz.

f'_c = concrete compressive strength (units are usually specified in the text)

f_c = concrete stress

f_s = steel stress

f_{sp} = tensile strength from splitting test

f_t = tensile strength of concrete

f_y = reinforcing steel yield stress

f_u = ultimate stress

G = shear modulus

g = gravity acceleration

H = horizontal force

h = overall depth of a section

I = moment of inertia

J_c = analogue to polar moment of inertia (ACI 318-77)

J = torsional moment of inertia

K = a minimized factor used in yield line analysis which depends on the degree of orthogonality of the reinforcement

K_c = column stiffness

K_{ec} = equivalent column stiffness (ACI "equivalent frame")

K_T = torsional stiffness of a member

K_{tcr} = cracked torsional stiffness

K.E. = kinetic energy

k = factor used in yield line analysis, beam analogy

k = spring stiffness

k_c = spring stiffness, cubic part

L_e = equivalent height

ℓ = length of member

ℓ_e = equivalent length

LVDT = linear voltage differential transformer

M = moment

M.A.F. = maximum amplification factor

M_{BA} = moment calculated from beam analogy

M_c = cracking moment

M_e = equivalent mass

M_{OBS} = observed moment

M_t = total mass

M_u = ultimate moment capacity

M_{YL} = moment calculated from yield line pattern

M_1, M_2 = principal moment

m = moment per unit length

m' = negative moment capacity per unit length

m_{xx} = moment according to elastic slab theory

m_{xy} = twisting moment accoridng to elastic plate theory

m_1 = mass at first level

m_2 = mass at second level

N = north (in test setup)

P.E. = potential energy

Q = load

Q_D = dead load

R = radius

R1 = simulated Earthquake Run No. 1

r = radius

SDOF = Single Degree of Freedom

S1 = Static Test Specimen No. 1 (ρ = 0.65%)

S2 = Static Test Specimen No. 2 (ρ = 0.98%)

S3 = Static Test Specimen No. 3 (ρ = 1.31%)

S4 = Static Test Specimen No. 4 (ρ = 0.98%)

S5 = Static Test Specimen No. 5 (ρ = 0.98%)

S = South (in test setup)

SS1 = Steady-state Test No. 1

T = torsional resistance, moment

u = half the column width in the direction of horizontal load (full width = 2u)

u_c = average bondstress in the concrete

V = force, usually shear force

V_u = ultimate shear force

V_f = shear force, obtained from a yield-line ("flexural") analysis

v = half the column width in the direction transverse to that of horizontal loading

v_u = ultimate shear stress

W = West (in test setup)

w = uniform distributed load

X = generalized coordinate

$\dot{X}$ = first time derivative of generalized coordinate

$\ddot{X}$ = acceleration of generalized coordinate

$\overline{x}$ = mean value

Z = slope of stress-strain curve at $\varepsilon_c > \varepsilon_o$

z = base motion

$\dot{z}$ = first time derivative of base motion; base velocity

$\ddot{z}$ = base acceleration

α = a factor of length

β = damping as a % of critical damping factor

β_s = equivalent critical damping

γ_v = fraction of total moment carried by shear (ACI 318-77)

ε_b = fracture strain; maximum measured strain

ε_c = concrete strain

ε_h = strain at which strain-hardening commences

ε_o = strain at $f_c = f'_c$

ε_u = ultimate strain; strain at which maximum stress occurs

ε_y = strain at which yield commences

η = factor to describe moment distribution in slabs

θ = rotation angle

θ' = rotation due to bar-slip

$\dot{\theta}$ = time derivative of θ; angular veolocity

$\ddot{\theta}$ = angular acceleration

λ = equivalent width factor in the equivalent beam approach to slabs

ρ = reinforcement ratio (A_s/bd)

ρ_t = total volume of reinforcement as a percent of concrete volume involved

ϕ = angle or curvature

Φ = mode shape

ω = circular frequency

ω_n = natural circular frequency

ω_r = resonance circular frequency

APPENDIX B

LITERATURE SURVEY

B.1 Introduction

Many contributions have been made in the attempt to understand the way in which the slab-column connection works; in discussion some are given detailed attention so that the reader may follow their application to the present study without undue cross-referencing.

In what follows, a division has been made between research on strength and stiffness. Stiffness aspects are further thought of in the range of relatively small displacements and that of large displacements.

The mood could not be set by neglecting strain rate effects, and the topic will receive attention.

B.2 Strength of the Column-Slab Connection

B.2.1 Strength: Introduction

Reinforced concrete design has progressed from an elastic outlook to that of limit design. In the development from elastic plate-theory to "beam analogies" the column-slab connection has followed a similar path.

Some strength criteria are obvious results of the importance of the three dimensions in plate behavior; yield line analysis, and punching analysis of slabs will remain important. Attention is also given to the design method shown in the ACI Code which assumes a linear stress distribution (its way of coping with the stress condition around a column-slab connection).

In simplifying, for example by beam analogies, behavior of the slab may be "misquoted." For this reason consideration is given to the incorporation of torsion in the "beam analogies."

In what follows the bias falls on what is considered an expected, and therefore reasonable, combination of loading.

B.2.2 Strength: Elastic Analyses

Much of the early research into the strength of the slab-column connection transferring moment and vertical shear used an elastic plate approach of small displacements. Analyses were reported investigating the moment, shear and twisting moment distribution at the column-slab interface.

The variation of plate forces for various boundary conditions of the plate were presented by Aalami (1) for example. He examined an isolated column-slab model representing an interior connection in a flat-plate structure; applying 3 different sets of boundary conditions to the side and end edges (refer to Fig. 2.1 for the definition of edges), varying from fixed to simply supported. He concluded that for an applied moment load at the column position the maximum plate moments did not differ by more than 3%. In his work he assumed a flexible column-slab connection, and commented that a rigid connection would tend to reduce the observed peaks in moment at the column. (The difference between a "flexible" and "rigid" column is explained in Fig. B.2.) Aalami (1) argued that if one were to impose a free support at the point of contraflexure for that analysis using a fixed end boundary condition, the same maximum moment would be achieved at the column-slab connection with a reduced longitudinal plate-span. This

appears to be a reasonable stand in the realms of elastic plate theory. Reflection is needed here as it has become apparent from experimental (39, 29) results that the ratio of the column to slab longitudinal dimension is indeed important to the strength of such an isolated column-slab connection.

Mast (34) attempted to compare results from an elastic Navier solution of the isolated slab-column connection with an applied moment at the column to experimental results reported by Hanson and Hanson (18). He did this in two ways: either by comparing the calculated elastic moment in the slab with those reported by Hanson and Hanson (18) or by drawing a comparison from the calculated shear on the front face of the column and the measured ultimate moment. The first comparisons of calculated moment to measured moment proved good at small displacements; the second method of comparison - using the calculated shear - gave very poor results for square columns.

B.2.3 Strength: Yield Line Patterns

The yield line approach is a useful way of obtaining the flexural capacity of a slab-column connection. In discussing yield line patterns for this connection authors (39,16) have distinguished between local patterns and those that extend to adjacent panels.

"Extended" Patterns: In the "extended" type Park and Islam (39) consider a mechanism made up of two parallel lines running across the full width of the slab passing the front and back column face respectively. For this pattern to dominate, horizontal loading must be the main contributor to failure, and gravity loads, therefore, should be negligible.

From the geometry of the mechanism a relationship between the angles of rotation and the plate dimensions may be obtained.

$$\theta_1 = \frac{1}{(a-u)}$$

$$\theta_2 = \frac{1}{u}$$

$$\theta = \theta_1 + \theta_2 \qquad \text{(See Fig. B.3)}$$

For the case of an isotropic reinforcement arrangement the negative and positive bending capacity of the plate may be expressed as "m" per unit length. Therefore, the internal resisting work done by the slab is $(m + m)(2b)\theta$. The external work done by the applied moment is $M_u \theta_2$. Furthermore, due to the antisymmetric yield pattern the work done by gravity loads will cancel out.

Equating the internal and external work one calculates the ultimate moment to be:

$$M_u = \frac{1}{\theta_2}(2m)(2a)\theta \qquad \text{(use 2a = 2b for a square plate)}$$

$$= 2m(2a)(1 + \frac{u}{a-u})$$

If the column to slab ratio, $\frac{u}{a}$, is 1:6, the expression for the ultimate moment, M_u, in a square plate becomes:

$$M_u = (2m)(2a)(1.2)$$

where m = negative or positive moment capacity per unit length,

2a = slab width, and the quantity of 1.2 is a result of the geometry of the slab-column joint.

Gesund and Goli (16) propose a further mechanism of the "extended" kind comprising a negative yield line spanning the slab width and passing next to the back face of the column, and a positive yield line at midspan between adjacent columns. The sawtooth appearance of a longitudinal section is illustrated in Fig. B.4.

Local Patterns: The alternative yield line pattern considered by Park and Islam(39) is referred to as a local mechanism. The components of the pattern are a rectangle immediately in front and at the rear of the column in the direction of loading, a triangle adjacent to either side face of the column, and, furthermore, a fan pattern radiating from each corner and connecting the rectangle and triangle (See Fig. B.5). To determine the critical configuration Park and Islam (39) calculate that angle ϕ, enclosed by the side triangles, which results in the minimum energy of resistance. Even though Gesund and Goli (16) use a complex expression for the radius of the corner fans, whereas Park and Islam (39) assume it to be constant, the angle ϕ resulting in a minimum position does not differ significantly for the two approaches.

The work done by a fan may be found from integrating between 0 and $(\pi - \phi)$.

$$\text{work} = \int_0^{\pi-\phi} [(m+m')(R d\gamma)](\frac{1}{R})$$

$$= (m+m')\ (\pi-\phi)$$

where $\frac{1}{R}$ is the angle of rotation.

m' = negative moment capacity per unit length

The work done by the two rectangles becomes:

$$\text{work} = [(m)(\theta) + m(\theta_1)]\ 2u + [m'(\theta) + m'(\theta_1)]\ 2u$$

$$= (m+m')(\theta+\theta_1)\ (2u)$$

The last component of internal work is obtained from the side triangles that undergo a rotation of θ_2 in the direction of loading. For a triangle: -

$$\text{work} = (m+m')(u \tan \phi)\ (\theta_2)$$

The angles θ_1, θ_2 and θ are obtainable from the geometry

$$\theta_2 = \frac{1}{u}$$

$$\theta_1 = \frac{1}{R}$$

$$= \cos \phi/u$$

$$\theta = (1 + \cos \phi)/u.$$

The external work is produced by the horizontal loading:

$$M_u\theta_2 = M_u(\frac{1}{u})$$

Once again the work done by the vertical dead load cancels out.

The total work expression becomes:

$$M_u\theta_2 = 4(m+m')\ (\pi-\phi) + (m+m')(\theta+\theta_1)(2u) + 2\ (m+m')(u \tan \phi)\ \theta_2$$

$$\therefore \quad M_u\ 1/u = 2(m + m')\ [2(\pi-\phi) + (1 + 2 \cos \phi) + \tan \phi]$$

$$\therefore \quad M_u = 2(m+m')(u)\ [2(\pi-\phi) + (1 + 2 \cos \phi) + \tan \phi]$$

From trial and error the critical ϕ can be found to be 59^o, and the expression becomes

$$m_u = 2(m+m')\ u\ 7.92$$

$$= 15.84\ (m+m')\ u. \qquad \text{for } m = m'$$

$$= 7.92\ (2u)(2m)$$

$$= 15.84\ (2u)(m)$$

After examining crack patterns reported by Ghali et al (17), Gesund and Goli (16) modified the local yield line pattern described by Park and Islam (39). The yield mechanism Gesund and Goli (16) proposed allowed for the gravity to contribute in that plate area, A_{slab}, outside the boundary of the dropped local mechanism. This was achieved by allowing fans to radiate from the corners of the back column face only. Rotation of the column still takes place about the center of the column, as in Park and Islam, however, to achieve compatibility without a fan at each of the front column faces the slab surrounding the local mechanism has to drop from its original position to the elevation of the front column face (See Fig. B.6).

Gesund and Goli considered a number of minor variations on their original local mechanism; after following a similar set of calculations as those shown for the local mechanism of Park and Islam they presented the following expression:

$$M_u/[(2v)\ \Sigma k] = K - \frac{\omega A_{slab}}{2m\ \Sigma k}$$

where M_u and 2v are as defined previously;

ω = uniform vertical plate load

A_{slab} = area of slab outside the local yield mechanism

$\Sigma k = k'_x + k_x + k'_y + k_y$

$k_x m$ = negative yield moment per unit length in the x-direction.

$k'_x m$ = positive yield moment, x-direction

$k_y m$ = negative yield mechanism per unit length in the y-direction.

$k'_y m$ = positive yield moment, y-direction

K = a minimized factor depending on the degree of orthogonality of the reinforcing.

The form of the expression differs, most markedly, from that of Park and Islam in the second term, the term that introduces the gravity loads. It is, furthermore, possible to obtain a "K - Park and Islam" and a "K - Gesund and Goli", and compare the resulting factors for various parameters. The ratio of "K - Gesund" to "K - Park" varies from .89 (for a column that has a front face 10 times that of the side face) to 1.08 (for a column that has a front face $\frac{1}{10}$ the size of the side face). From the ratio value of 1.08 Gesund and Goli deduce that their analysis may lead to the critical case as the second term in their expression could be larger than .08 for practical situations. It is apparent, nonetheless, that for cases with negligible gravity loads there is little to choose between the results of the two approaches.

From an analysis of yield line patterns, local and extended, it is possible to judge the behavior of a slab-column specimen. If it shows a value significantly below the strength of a measured value one will have to use a more complex approach to explain the behavior.

B.2.4 Strength: The ACI (318-77) Linear Shear Stress Design

Under the section dealing with special provisions for slabs in the ACI 318-77 Code[2] the allowance is made for a procedure assuming shear stresses to vary linearly in the design of the slab-column connection.

For an interior column slab connection, without the influence of openings in the slab, the critical section for shear is taken as being a distance of $\frac{d}{2}$ from the column slab interface (where d = effective depth of the slab).

A fraction of the total applied moment is used to determine a stress contribution in addition to that caused by vertically applied loads. This fraction is a function of the column geometry. The

fraction of moment thus determined is described as being transferred to the slab by the eccentricity of shear stresses on the critical section about the centroid of the critical section. The remainder of the applied moment is resisted in flexure at the front and back faces of the column.

The maximum factored shear stress may be calculated from

$$v_u = \frac{V_u}{A_c} + \frac{\gamma_v \, M_u \, r}{J_c}$$

γ_v = fraction of total moment carried by shear.

J_c = analogue to polar moment of inertia.

By the notation previously used to describe the column:

$$J_c = \frac{d\,(2u + d)^3}{6} + \frac{(2u + d)\,d^3}{6}$$

$$+ \frac{d\,(2u + d)(2v + d)^2}{2}$$

where $2u$ = column dimension in the direction of loading.

$2v$ = column dimension in transverse direction.

$$\gamma_v = 1 - \frac{1}{1 + \frac{2}{3}\sqrt{\frac{2u + d}{2v + d}}}$$

r = moment arm of critical section.

With the allowance of $4\sqrt{f'_c}$ (f'_c in psi) the expression may be solved to enable the designer to gauge the shear strength of the column-slab connection. (i.e. take $v_u = 4\sqrt{B'_c}$)

Kanoh and Yoshizaki (29) came to the conclusion that this approach --considering the geometry of section to determine γ_v--severely underestimates the contribution of torsion and shear.

B.2.5 Strength: Beam Analogies

Though the detail of one "beam analogy" and another may differ, the concept is the same; the assumption is that the slab portion given by the projection of the column acts as a beam.

Park and Islam: A very simple beam analogy design algorithm is described by Park and Islam (39). The beams frame into the column faces providing the bending, torsional and shear resistance. Calculations of the strength of such beams in torsion, bending or shear, or combinations of these, are based almost entirely on design methods set out in the ACI code (ACI 318-71). The difference in design lies in the ultimate stresses used, where the suggested stresses are often modified versions of those in the ACI code. The modifications come about due to factors neglected in the ACI code which are present in connections of columns and slabs, mainly the confinement provided by the slab.

Refering to Fig. B.7 the ultimate moment is comprised of: $M_{AB} + M_{CD} + T_{BC} + T_{DA} + (V_{AB} - V_{CD})\ (2u+d)\ \frac{1}{2}$, where M is a moment quantity, T is torsion and the last term acknowledges the shear as the faces AB and CD. The ultimate shear is the sum of the shear on all the faces: $V_{AB} + V_{BC} + V_{CD} + V_{DA}$.

A number of assumptions are made in the development of Park and Islams' design method:

1) The first is the location of the assumed critical freebody. It is taken as being situated at a distance of $\frac{d}{2}$ (d = effective depth)

away from the column faces.

2) The strengths achieved by the flexural action of equivalent beams framing into the connection as faces AB and CD are assumed to be passed yielding strengths. For face CD, which is under a positive bending effect due to the moment caused by lateral loads but under negative moment caused by gravity type loads, yield strength will be obtained if M_u/V_c is very large. A further simplification in determining the flexural resistance provided by the equivalent beams is the ommission of confinement effects provided by portions of the slab. The membrane forces just mentioned are expected to enhance the flexural strength and it is considered to be on the safe side to neglect their influence on flexure.

3) The shear capacity, however, is taken as being improved by such effects as confinement. For this reason a maximum shear stress of $4\sqrt{f'_c}$ (f'_c = in psi) is used which is twice that normally allowed for beams in the ACI code. The shear capacity is assumed to be unhindered by the presence of the ultimate bending moment at the section. The maximum shear stress is taken as occuring on that face on which gravity and lateral loading are in conjunction, in this case face AB. Using the maximum shear stress and assuming the proportion of the gravity load carried by the applicable face, the shear caused by the applied column moment can be determined. The total shear force on the face is $4\sqrt{f'_c}$ (2v + d) d, (f'_c in psi) from which the contribution of the gravity load can be subtracted to leave the lateral load's portion:

$$4\sqrt{f'_c}\ (2v + d)\ d - k_{AB}\ V_u$$

where $V_u = V_{AB} + V_{BC} + V_{CD} + V_{DA}$

and k_{AB} = that portion of total ultimate gravity load taken on face AB.

As the lateral loading is considered to cause equal but opposite shears on the faces AB and CD, the shear on face CE due to lateral load is found. On face CD, in contrast to face AB, the lateral load effect and gravity load effect oppose each other in shear. The shear on face CD is, therefore, deduced:

$$V_{CD} = k_{CD}\ V_u - [4\sqrt{f'_c}\ (2v + d)\ d - k_{AB}\ V_u]$$

4) The forces on the remaining faces AD and CB are provided by torsion of the equivalent beams framing into these faces, and the portion of gravity load carried by them. Once again the shear stress reached is assumed to be enhanced by similar factors influencing shear stress on the other 2 faces AB and CD, and it is taken as being $4.8\sqrt{f'_c}$ for the case where no vertical shear force is present; twice the ultimate torsional shear stress allowed by the ACI code for torsion of beams. The vertical shear is considered in the reduction of the torsional strength of the face. Furthermore, it is assumed that the two side faces under discussion can develop their ultimate torsional capacity at the same time the other two faces achieve their flexural capacity.

Applying the foregoing steps all the components in determining the ultimate total moment applied can be calculated. The resulting equation is:

$$M_u = \text{ultimate moment} = M_{AB} + M_{CD} + T_{BC} + T_{DA} + (V_{AB} - V_{CD}) \frac{2u + d}{2}$$

in which	V_{AB}, V_{CD} ------	Shear forces acting on faces AB, CD
	M_{AB}, M_{CD} ------	Bending moments acting on faces AB, CD
	T_{BC}, T_{DA} ------	Torsional moments acting on faces BC, DA
	$2u + d$ ------	Distance between faces AB and CD

Kanoh and Yoshizaki: The approach followed by Kanoh and Yoshizaki is another example of the beam analogy applied to the strength of column-slab connections. The method used is similar to that of Park and Islam, however a significantly higher shear stress is utilized by Kanoh and Yoshizaki to calculate torsional contributions.

The ACI 318-71 method used a factor "γ_v" which indicates how much of the applied anti-symmetric moment is carried by torsion and the eccentric shear along the critical section. Strain measurements were used by Kanoh and Yoshizaki in the calculation of the flexural component of resisting moment, and this permitted the calculation of "γ_v" for the observed strength in the test results. Additional punching tests allowed the researchers to obtain values of shear stress carried by the section, and in turn the moment resisted by the eccentricity of the shear could be established. The remaining unknown, the torsional moment contribution was, therefore, isolated. Using an expression for plastic torsion in terms of stress and geometry, the torsional stress was calculated. When compared to the permissable ultimate torsional shear stress value in the

ACI 318-71 code the stress determined from the experimental data was far in excess of that allowed for beams.

To substantiate the very high torsional stresses deduced from the application of moment to the slab-column connections Kanoh and Yoshizaki(29) extended their study, experimentally, to the torsional mechanism on the side of the column. This was achieved by applying a torque to the edge of a "half-slab" by means of a "column" stub. As the stub was cast to the edge of the slab with only the face of the column able to transfer load, the flexural and shear components of moment in the "complete" specimen type were effectively eliminated (see Fig. B.8).

From these follow-up torsional type test Kanoh and Yoshizaki concluded that a torsional shear stress of $24\sqrt{f'_c}$ (f'_c in psi) was in order -- a substantial increase over Park and Islams' value, which itself was double that allowed by the ACI 318-71 code for beams. A number of parameters were considered in the testing. The influence of different slab widths were considered, and another geometric variable was the width of the column stub. For the change in slab width there was no substantial increase in strength. In contrast to this last effect, there was a substantial difference in specimen strength for a larger column dimension in the longitudinal direction.

The inclusion of shear reinforcement in the form of stirrups did not result in any significant effects on the observed strength.

Furthermore, the same reinforcing spacing placed in strips of varying width did not result in substantially different behavior. This seems to indicate, as was supported by the very localized slab rotations

Kanoh and Yoshizaki reported, that the load carrying mechanism was affected by parameters close to the column.

Besides the column width, the other factor having a marked effect on the observed strength was the amount of transverse reinforcement passing through the column face.

The results of the testing left the researchers with the impression that even higher torsional stresses could be obtained in "complete" slab and column connections as the confinement, and steel continuity, would be greater in that case when compared to the "half slab" specimens.

Torsion: To ponder for a few moments on torsion in rectangular beams seems appropriate after this, rather vigorous, attempt by Kanoh and Yoshizaki to harness torsional effects in the slab-column connection. As Warwaruk (50)points out, the two commonly used torsion models for beams -- the skew bending mechanism (Collins et al (9)) and the space truss analogy (Lampert and Thurlimann (31),Park and Paulay (38) p. 362) --result in similar calculated torsional strengths. The role of stirrup reinforcing in the respective strength expression does differ. In the truss analogy the stirrups help resist the compression in the cracked concrete side faces of the beam. As such they appear explicitly in the expression for torsion resisted by the section. For the skew bending mechanism the stirrup horizontal legs, in the same plane as the longitudinal steel, contribute to the internal resisting moment. It is interesting, therefore, to remember that the stirrup reinforcement in the Kanoh "torsional" tests had little effect on the "torsional" strength, an unexpected result if reasoning in terms of the space truss analogy.

B.2.6 Strength: Punching

Owing to the very substantial punching shear stresses applied to connections in conjunction with applied moment, concern has been expressed about punching failure of the column-slab connection. Hawkins (20) has applied vertical loads amounting to vertical shear stresses on the critical slab section from $2\sqrt{f'_c}$ (f'_c in psi) to close to $4\sqrt{f'_c}$ (f'_c in psi). Ghali et al applied a vertical load to their column slab tests subjected to applied moment and shear of close to $\sqrt{f'_c}$ (f'_c in psi).

With the fetters of such high vertical shear stresses it is no wonder that punching becomes a main concern in column slab connections that must also resist an applied column moment. Referring to Fig. B.9, Hawkins (20) describes a simplified force displacement relationship as containing three points of abrupt change: the first is at the point that ends the initial linear response and indicates yielding the reinforcement through the column width; the next possible change occurs on yielding of the reinforcement across the full width of the slab; the third point is the culmination of the force displacement relationship and occurs on punching. As the slabs Hawkins tested were more heavily reinforced the last two points described move closer together. In other words for relatively heavily reinforced slabs punching is possible before the slab can reach its full flexural capacity. Expanding on this rather simplified force displacement representation of Hawkins for cases with less severe vertically applied load than the foregoing, the role of the villanous punching may be surplanted by a "beam analogy" type of limitation. The beam analogy, one may recall, reaches its maximum as a result of a combination of torsion, shear and flexure in the equivalent beams.

Reverting back to the punching dominated design, Hawkins (20)provides guidelines for shear reinforcement to resist punching. Seible et al (42) provide some alternatives to stirrups as reinforcement. One may recall that both research efforts involved very severe vertical loads.

B.3 Response in the Predominantly Linear Elastic Range

B.3.1 Elastic Response: Introduction

In the discussion that follows the emphasis will be on the behavior of the slab component in the column-slab connection; the response is assumed to be mainly linearly elastic. Following a description of some of the geometric variables involved, a few analysis approaches will be discussed and compared. Experimental results will also be related to various analysis methods.

B.3.2 Elastic Response: Geometric Variables

In modelling the load transfer from the column to the slab--for a column with an applied horizontal force--two extreme mechanisms can be used. On the one end of the scale the column may act as a rigid element, and on the other as a flexible conveyor (Refer again to Fig. B.2). The rigid element approach is correct when noting that the horizontal column slab interface will remain plane on rotation of the connection only if the column is perfectly axially rigid; finite element analyses support this statement (Pecknold (40)). The response of the slab has been shown by Mehrain and Aalami(35) and Pecknold(40) to be very sensitive to the stiffness of the carry-over mechanism of the column slab connection (in a practical $\frac{u}{a}$ range).

In sharp contrast to the observation by Aalami (1) that the peak moment in the slab at the column face was relatively independent of the

end boundary condition, this boundary condition becomes important when considering the stiffness of the column-slab element. On the other hand Mehrain and Aalami concluded that the side boundary condition was not of importance to the stiffness. A further insensitive parameter is the interplay of the column's dimensions; Pecknold (40) examined the effect of a change in a $\frac{v}{u}$ ratio of $\frac{1}{2}$ to 2 and found it negligible.

Especially in experimental modelling these geometric variables have been recognized in the idealization of boundary conditions.

B.3.3 Elastic Response: The Equivalent Beam Concept

As was the case with "beam analogies" in calculating the strength of the column-slab connection, the equivalent beam transfers a three dimensional problem into a two dimensional one.

Using the elastic theory of plates for small deflections one may investigate the slab slopes for a column-slab element with moment being transferred from the column to the slab. It is evident that the rotation of the slab is a maximum at the column slab connection and peters out on either side of the column toward the side boundary. A beam, on the other hand, has a constant slope at a specific cross section (Refer to Fig. B.10). As two dimensional analyses are cheaper than three dimensional, an opportunity to transform the slab into an "equivalent beam" was grasped by numerous researchers. Working on these lines it becomes clear that a beam of smaller width than a slab of like span and depth would result in an equal rotation at the midspan position (the position of the column-slab connection). This ratio of widths is called the "equivalent width" factor (refer to Fig. B.11).

To obtain rotation of the slab, at the interface of load transfer by the column, a plate analysis applying the Navier method (Timoshenko and Woinowsky-Krieger) is performed. Such an analysis is discussed by Pecknold (40) and expanded to the case of an orthotropic plate (Pecknold(41)). The orthotropic plate analysis by Pecknold allows consideration of orthotropic conditions resulting from cracking. Both Pecknold (40,41) and Allen and Darvall (4) use identical Fourier analyses to determine the plate slope, however Pecknold uses a simple beam to derive his "equivalent width" factors, whereas Allen and Darvall use a beam with a rigid portion at midspan.

The rigid insert of Allen and Darvall models the effect of the finite size of the column. For this reason values of "equivalent beam" widths tabulated by Pecknold (40,41) are larger (the beam used is more flexible) than those of Allen and Darvall (rigid insert). A simple relationship exists between the two factors:

$$\lambda_{Allen} = \lambda_{Pecknold} * (1 - \frac{u}{a})^3$$

where λ_{Allen} = equivalent width factor listed by Allen and Darvall (4)

and $\lambda_{Pecknold}$ = equivalent width factor listed by Pecknold (40)

B.3.4 Elastic Response: The Equivalent Frame Approach

Following the same rationale behind the "equivalent beam approach" --simplifying a three dimensional structure into a plane frame--

Corley and Jirsa (10) described the "equivalent frame analysis" for slab design. It should be emphasized, at the outset, that the type of load the analysis was catering for was a vertical gravity type and not horizontal loads.

The equivalent frame comprises two main parts: an equivalent column and a beam portion. In establishing the properties of the beam portion, the full slab width is employed with allowance made for cracked properties and the rigidity in the column region. The stiffness of a lateral torsional member is linked, in series, with that of the actual column in the structure to compose the "equivalent column". This linkage was a way of accommodating the ability of the three dimensional slab to distribute load around an even rigid column. Such a "flow" of load had been noticed in the occurrence of appreciable positive slab moments caused by "checker" type load. Therefore, the origin of the "lateral torsional member" is traced to the transfer of moment from the slab to the column. The moment along the front face of the column, 2v, goes directly into the column, whereas the moment in the slab outside of this "column strip" (of width 2v) is transmitted—by a "lateral torsion member"—as a torque to the side column face (of width 2u). Furthermore, to determine the stiffness of the "equivalent column" the stiffness of the "lateral torsion member" is required. For this purpose Corley and Jirsa (10) assume a linear moment distribution of applied moment to the "lateral torsion member" rising from zero at the edge of the slab to its maximum value at the centerline at the column grid such that the area under this distribution is unity; thereby representing a unit applied total moment. The applied moment distribution causes a

parabolic twisting moment distribution along the "lateral torsion member". Dividing this diagram by GC, where G is the shear modulus and C a torsional constant resulting from a St. Venant approach to rectangular sections (see Park and Paulay p. 349), results in the twisting diagram for the torsional member. As Vanderbilt (49) notes, some confusion results from the derivation by Corley and Jirsa (10) as they take, without explanation, $\frac{1}{3}$ of the twisting diagram to arrive at a total rotation in the "lateral torsion member". The factor of $\frac{1}{3}$ is used to align experimental observations with the analytical approach. The expression for K_T, the stiffness of the "lateral torsion member", becomes:

$$K_T = \frac{1}{2} \left(\frac{1}{3} \int_0^b \phi_x \, dx\right)$$

$$= (18\ EC) \left((2b) \left(1 - \frac{v}{b}\right)^3 \right)$$ for a square panel of width 2b, where ϕ_x = twist in the torsional member, and 2v = front face of the column.

Therefore, $\frac{1}{K_{ec}} = \frac{1}{\Sigma K_c} + \frac{1}{K_T}$, where

K_{ec} = equivalent column stiffness

ΣK_c = sum of column stiffnesses

The "equivalent frame" approach appealed to researchers considering analysis methods for structures resisting horizontal load. Carpenter, Kaar and Corley (7) proposed using the "equivalent frame" method of the A.C.I. 318-71 code for the design of "ductile" flat-plate structures to resist earthquakes; others were less enthusiastic. Fraser (15) doubted

whether the "equivalent frame" method should be applied to flat-plate structures resisting horizontal load. Even Carpenter et al (7) caution the designer about the significant drift that is to be expected, leading one to wonder whether their approach to stiffness may be too simple.

B.3.5 Elastic Response: Other Approximate Methods

A complementary energy approach, such as the representation by Elias (14), also must address the quandary of the role of torsion in a column slab sturcture. Once again, Elias (14) seeks to simplify a three dimensional problem to two dimensions. Similar to the treatment of torsion by the "equivalent frame" method, Elias (14) restricts the influence of torsion to a strip on either side of the column. However, Elias permits the width of this strip to vary. He assumes a moment distribution which is linear in the longitudinal direction, in the transverse direction and constant in line with column front face but hyperbolic outside of this column projection. (Refer to Fig. B.12.) The assumed maximum longitudinal moment does not necessarily occur at the column face for a transfer of moment from the column to slab, a clear departure from elastic plate theory. Moreover, the position of the assumed maximum moment depends on the width of the torsional zones that, in turn, are determined from his analysis. After finding the contribution of the longitudinal moment, m_{xx}, and the twisting moment, m_{xy}, his analysis boils down to determining two parameters, α and η. Where α = defines the zone of influence of m_{xy} (or "torsion") and η is used to define his assumed moment distribution function in the transverse direction.

Energy methods do permit a relatively easy extention to structural systems other than the simple flat plate, and, for example, edge beams

could be incorporated. Although Elias (14) may claim a good correlation between his method and more expensive finite element results for ratios of column-longitudinal to slab-longitudinal dimension, $\frac{u}{a}$, of less than $\frac{1}{50}$, marked discrepancies occur for ratios larger than this value. The ratios of $\frac{1}{50}$ and less may be a restriction on the wider application to more rigid connections.

B.3.6 Elastic Response: Comparison of Methods

Admittedly the "equivalent frame" applications are more general than an "equivalent beam", which is restricted to simple flate plates, but the performance of the "equivalent frame" subjected to horizontal load is hampered by the treatment of the lateral torsional member.

Allen and Darvall (4) analyzed three hypothetical buildings of practical dimensions, by four variations of a plane frame. They subjected the frames to a triangular horizontal load. Properties used for the four frame variations were: #1) full column stiffness combined with the full plate width acting as a beam; #2) for the interior columns full stiffness was assumed, but an equivalent column for outer columns, combined with the full plate width acting as a beam; #3) the "equivalent frame" of the ACI 318-71; #4) the full column stiffness combined with an "equivalent beam" to transform the slab to a two dimensional element. Allen and Darval (4) reported the analysis using full section properties as columns and beams #1) to be the stiffest, with the "equivalent frame" analysis #3) resulting in the largest drifts. These two extremes were significantly different with the horizontal displacements roughly doubled from one to another. The authors promoted the performance of the full column and "equivalent beam" properties--case number 4--as the most reasonable.

Experimental support for this judgement was provided by work conducted by Allen (3) on thin steel and micro concrete isolated plate specimens with a column induced moment.

Experimental work on more complete assemblies entailing multi-story and multi-panel scaled models is not common, as Vanderbilt (49) noted. Nonetheless, an impressive correlation was reported by Vanderbilt (49) for the results of an analysis using an "equivalent beam" and full column approach, and the measurements from an experimental study by Hartley, Rainer, and Ward (19) of a 7-story, approximately tenth scale, flat-plate model. Vanderbilt (49) could not provide a good matching between the experimental (19) results and an analysis using properties derived from an "equivalent frame" method. He investigated an arbitrary reduction of the "lateral torsional" member's length to align results, which led him to raise the possibility of yet another "equivalent" - the "equivalent length factor" for the "lateral torsional member". A stiffening of the "lateral torsional member" had been previously suggested by Mehrain and Aalami (35) who proposed using a wider width for the "torsional" member. Yet, the same authors did expect cracking to cause the unadulterated "equivalent frame" to be more attractive.

Diverting for a moment from the comparisons drawn by Vanderbilt (49) from the experimental measurements of Hartley et al (19), it is of interest to the dynamic behavior of flat plate structures to take note of findings by Hartley et al with respect to their free vibration tests. Flexibility measurements were made by loading the floors one by one in the following three ways: 1) longitudinally, 2) laterally and 3) torsionally. These measurements enabled the development of a structural stiffness

matrix which was analyzed to provide natural frequencies. The fundamental frequencies thus obtained, in the three directions mentioned, were remarkably close to the measured frequency from free vibration tests. This led Hartley et al (19) to believe in the validity of free vibration testing of structures in the range of linear elastic response.

The substantially larger deformations required of a structure in resisting forces caused by earthquake loading require very different approaches than those discussed in the preceding paragraphs.

B.4 Large Displacement Response of Flat-Plate Structures

B.4.1 Introduction

The isolated slab-column element has been tested extensively to resolve nagging doubts about the ability of flat-plate structures to undergo large displacements. The relative flexibility of the connection, nonetheless, poses the question as to whether the element is an efficient energy "absorber" in the range of displacements that will still be acceptable to other non-structural elements. Very little has been done to investigate the serviceability aspect of the flat-plate-column structure; however, some approaches to framed structures will be discussed for possible application to that flat plate.

B.4.2 Experimental Investigations of the Isolate Interior Flat-Plate-Column Connection

A large variation in parameters has been considered by Hawkins (21,22) and his research associates, and a summary is given in Table B.1. Two types of specimens were used, one with a cyclic lateral load application and one other with a cyclic vertical shear load (refer to Fig. B.13).

More specifically, Hawkins, Mitchell and Symonds (22) isolated the influence of the increase in the top reinforcing ratio in their slabs subjected to lateral loading. The trends they observed were an increase in the pre- and post-yielding stiffness, where Hawkins (22) defines the yield of the bars through the column face as indicating "yield". Furthermore, shear and flexural strength was enhanced and the deflection at failure also increased. They (Hawkins et al (22)) urged the use of "strip reinforcement", that is the concentration of reinforcement within the "column projection". The relatively under-reinforced assemblies were more efficient as damping mechanisms; this statement by Hawkins et al (22) is undoubtedly linked to the flexurally dominated behavior of the relatively lightly reinforced slabs. Hawkins et al (22) also indicate that an increase in reinforcement results in the increase in stiffness degradation noticeable in the low load range of a specific loading cycle. This could very well be the result of shear playing a more dominant role than flexure in the overall behavior.

Hawkins et al (22) imply that stirrup shear reinforcement controls the flexibility of the column slab joint-- they report 10% to 20% stiffer joints than those without shear reinforcement. Shear reinforcement is also accredited with the more stable hysteresis behavior of the joint. Crushing of the concrete was observed at 5 times yield displacement, and, it is claimed, good behavior was observed for displacements even passed this point. The implications of the extremely large deflections --to which Hawkins et al (22) refer here --are questionable from a serviceability criterion ($2\frac{1}{2}^{\circ}$-5° in connection rotation).

Calculating damping coefficients as indicated, Hawkins et al (22) list the following values as representative: 10% in the elastic range when loaded to a new peak with 8% for subsequent cycles, and 14% in the inelastic range when loaded to a new peak with 12% for a subsequent equal cycle.

Hawkins et al (21,22) suggest a model for analysis of the response of the interior column slab connection that allows for concentrated deformation by flexure and torsion. At the front and back face of the column - slab interface they prescribe a flexural element that links the column to the rest of the slab, while at the side faces a torsional linking element is assumed. (Refer to Fig. B.14.) The flexural link described by Takeda et al (45), and the rest of the slab, presumably, acts as a beam. The torsional link has a stiffness obtained from experimental results of Hsu (23), and is an empirical formula meant for the post cracking stiffness of beams. It is evident from this relation by Hsu (23), $K_{tcr} = (0.021)\ \rho_t\ K_t$ (where K_{tcr} = torsional stiffness of reinforced concrete after cracking; p_t = total volume of reinforcement as a percent of the concrete volume involved; K_t = stiffness before cracking) that the post cracking stiffness for beams with torsion is almost insignificant. Even a more rigorous presentation by Lampert (30) leads to a similar conclusion. By contrast, when considering the post cracking stiffness observed in the torsion experiments of Kanoh and Yoshizaki, (29) and Clark and White (8) -- where relatively stable post cracking stiffness was noted-- one wonders whether the Hawkins et al (22) torsional approach is not carrying the beam analogy too far. The slab constraint, it would appear, is a significant contributor to the

enhanced post cracking stiffness of slabs above that of beams. Rather surprisingly, when recalling the emphasis on stirrup reinforcement by Hawkins et al (22), Kanoh and Yoshizaki (29) found that stirrup shear reinforcement did not influence the post cracking stiffness or strength in their torsion "half-slab" tests. The transverse reinforcement and the longitudinal column dimension were, by a long chalk, the significant parameters for post cracking "torsional" stiffness in the Kanoh and Yoshizaki (29) experiments.

B.5 Strain Rate Effects

B.5.1 Introduction

The exact effect of rate of strain on material properties is not easy to determine. In the following sections the effect of higher rates of strain on the stiffness and strength of reinforced concrete sections is discussed.

B.5.2 Strain Rate: Beams and Column-Slab Tests

The phenomenon that concrete and steel strengths and stiffnesses are dependent on strain rates at which they are tested has been known for some time. Jones and Richart (28) reported a logarithmic relationship for concrete compression strengths tested at different strain rates as far back as 1936. That research, done at the University of Illinois, showed how concrete strengths were considerably enhanced when tested at relatively higher strain rates. The observed increase in strength spanned the full practical range of strain (see Fig. B 15a).

In stark contrast to the extent of differences at various strain rates in concrete, steel had a far more restricted zone of dissimilarity (see Fig. B 15b). As Bertero et al (5) illustrated, when comparing reinforcing

tested at strain rates of 0.05/sec., 0.005/sec. and quasi-statically, the steel has a markedly different yield strength. Significantly, however, the differences were quickly reduced within the zone of the yield plato, and were almost indistinguishable by the stage the various tests entered the strain hardening range. Newmark and Rosenblueth (36) reported a similar observation. The fact that the only significant difference in steel behavior was its yield strength led Bertero et al to conclude that strain rate effects would have a negligible influence on the response of a structure to seismic loads. Thereto is attached a most important qualification that the response of the structure must be dominated by flexural behavior of its elements such that the steel behavior dictates. An under-reinforced beam with adequate shear strength and ductile response would fit this requirement.

Criswell (11) tested a series of 19 slab-column connections for punching strength at loading rates that varied from extremely rapid to those that could be expected in seismic loadings. For the very rapid loadings he observed a distinct difference between the time at which the maximum puncing shear force was experienced by the connection, and the time at which the maximum flexural forces were generated by displacements in the slab. This difference in "critical load" occurrence helped the slab to reach an increase in strength of 2.25 times the "static" strength, a strength increase not possible by strain rate effects alone. For those loads with a rise time of 9.32 m sec. (a period of .04-.125 sec.), which are possible loading times for seismic loading, an increase in punching strength of 25% to 50% over the statically loaded specimen was observed. Strain rate related increases in concrete strengths are most likely the reason for these increases.

The results presented by Bertero et al (5) contrast further with those of Ghali (17) et al when consideration is given to the effects of different strain rates on energy dissipation and ductility. The beams tested by Bertero et al were only significantly influenced in the immediate range of yielding, therefore, the energy dissipated by the beams and the ductility reached were not markedly different for like beams tested at different strain rates. On the other hand, the dynamically tested slab-column connections reported by Ghali et al had improved ductility and energy dissipation characteristics in comparison to their counterparts tested statically. Bearing in mind that the slabs tested by Ghali et al were loaded by an applied couple to the column stub and a vertical punching shear, the slabs tested by Criswell (11) with a dynamic vertical punching shear alone registered deflections at failure of 25% to 50% more than statically tested slabs.

In order to attempt to use the observed failure crack patterns as an indicator of the influence of different strain rates on the various specimens, it is important to have a feeling for the failure mechanisms involved. The crack patterns noted by Bertero et al are in keeping with the other observations regarding strength, ductility and energy dissipation in that they exhibit the same failure mechanism for like beams tested at different strain rates. Owing to the dominance of flexure in these beams the observations are consistent. The slab-column connections tested by Ghali et al (17) also showed little difference between the failure modes of statically and dynamically tested specimens. For a difference to have occurred it would have been necessary for the shear and torsional resisting components to have been enhanced by strain rate effects to the extent that a flexure mechanism may have been possible. This argument is founded on the conclusion

of Bertero et al (5) that strain rate effects do not influence flexural strength significantly. Owing to the very high punching stress applied by Ghali et al ($\simeq \sqrt{f'_c}$, with f'_c in psi) no such difference in static and dynamic failure mechanism is suspected. Much the same observation may be made with respect to failure mechanisms when considering the pure punching load applied by Criswell (11) to the slabs he tested at strain rates comparable to those used by Ghali et al (17). The punching mechanism as explained by Criswell (11), starting with radial principal moment cracks from each column corner, the formation of secondary moment cracks radially around the column, and then the propagation of the inclined crack in the slab close to the column slab interface, does not lend itself to a different failure mechanism. No difference in failure mechanism was observed by Criswell (11) in "statically" tested slabs and those tested at load applications with a rise time of 9.32 m sec.

One is confronted by what is meant by "strain rate". The question being that of how to determine the "istantaneous" strain rate. If we assume, for purposes of illustration, that the "material" is subjected to a harmonic cycle, at the point at which a maximum displacement and acceleration occur the velocity is zero. Assuming strain rate to be directly linked to velocity this would imply that at the point of maximum displacement the strain rate is zero; but, if we assume the "material" to be ductile and perfectly elasto-plastic, it may well have yielded before the point of zero velocity. The example in Park and Paulay (p. 568), therefore, where that part of the cycle from no load to yielding is used to calculate an "average" strain rate, seems quite acceptable as they consider an appreciable portion of the cycle as yield plato.

In summary, considering the discussed literature which cover pure bending of beams (Bertero et al (5)), column-slab connections with a couple and a vertical punching force applied to the column (Ghali et al (17)), and column slab connections with pure punching applied (Criswell (11)), it appears that the influence of strain rate on the behavior of reinforced concrete is dependent on the mechanism involved for the specific assembly.

TABLE B.1 Test Programs (Hawkins et al)

Series	Ref.	Specimen Type	No. of specimens	Concrete Strength	Top ρ	Bottom ρ	Gravity Load	Stirrups	Variables
	(20)	See Fig. B.13		[MPa]	[%]	[%]	kN		
I		A	5	22-35	.6,.9,1.3, 1.9+.6*	$\frac{1}{2}$ top ρ	129-151	None	Reinforcement ratio load history
II		A	5	25-32	.9,1.3, 1.9+.6*	$\frac{1}{2}$ top ρ	125-133	All	Reinforcement ratio, stirrup strength & extent, load history.
III		A	5	23-31	.6,.9, 1.9+.6*	$\frac{1}{2}$ top ρ	236-271	2 specimens	Reinforcement ratio, stirrup strength & extent.
IV		A	6	23-30	1.9+.6*	$\frac{1}{2}$ top ρ	129-271	All	Column size shape, gravity loads, stirrup strength & extent.
V		B	5	22-31	.9,1.9+.6*	$\frac{1}{2}$ top ρ	187	3 specimens	Reinforcement ratio, stirrup strength & extent.

NOTES: Type A : Moment reversal
Type B : Shear reversal

* 1.9% in column strip,
0.6% in the rest of the slab

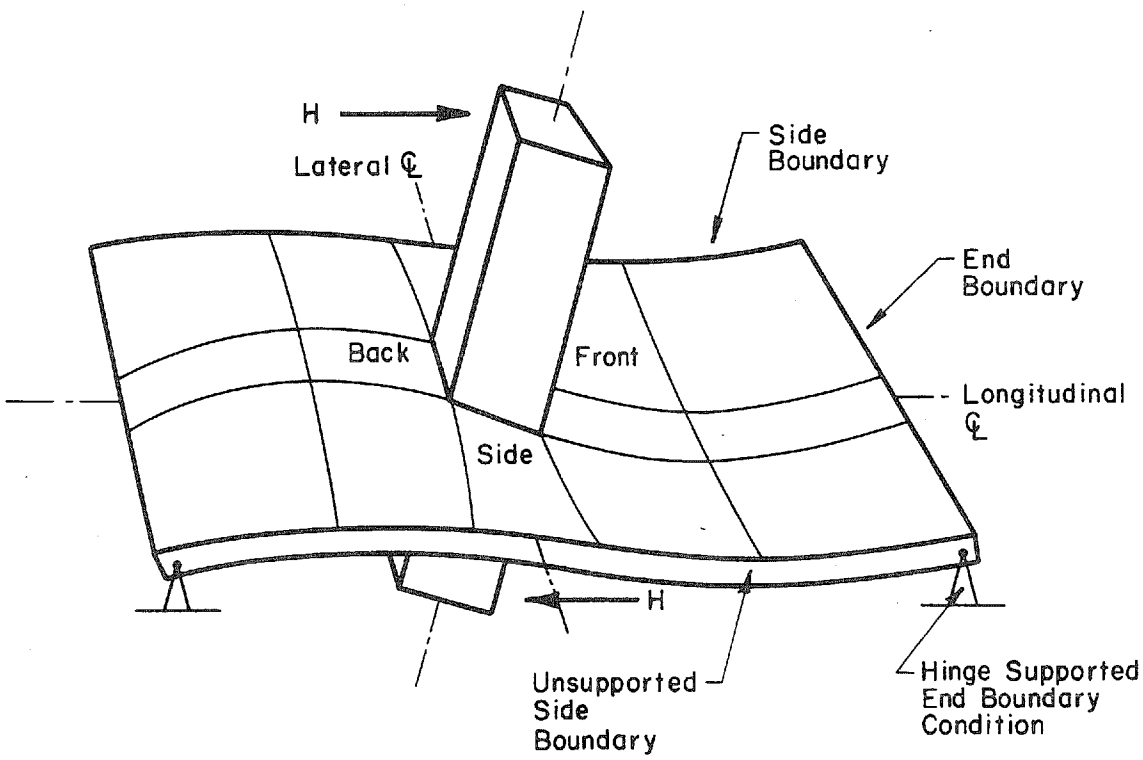

Fig. B.1 Definition of Terms used to Describe Slab-Column Connection

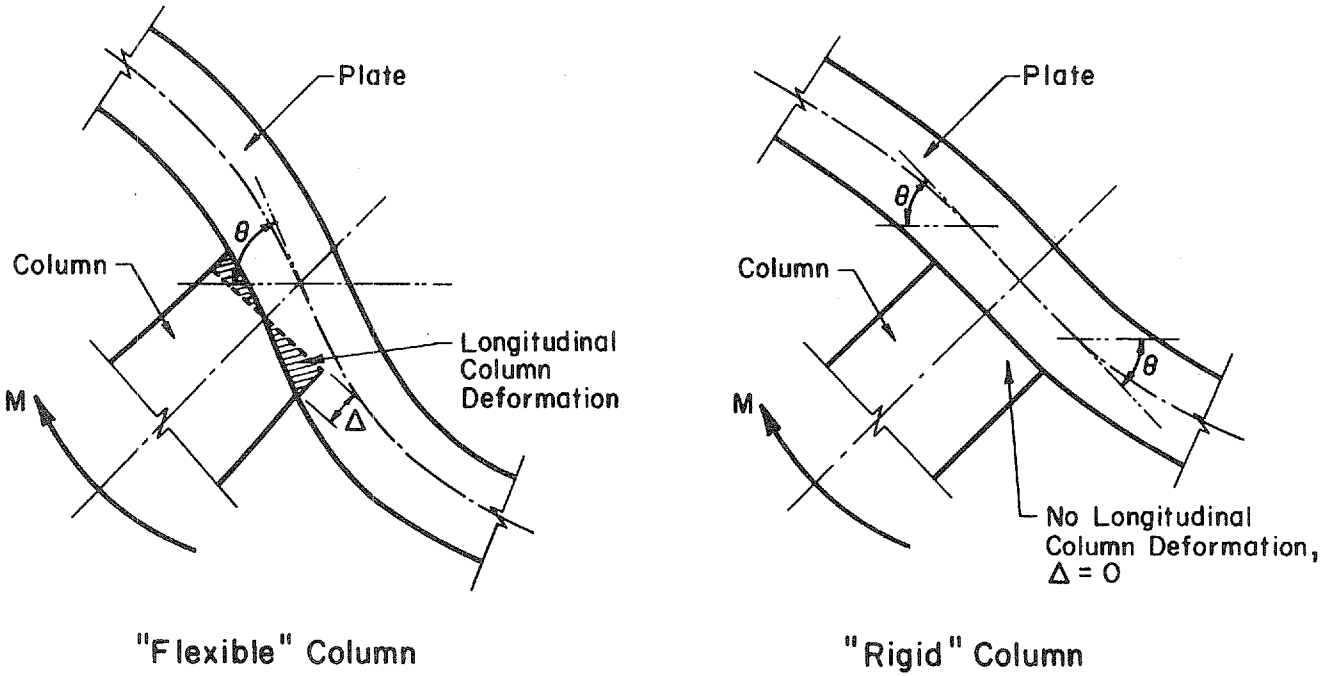

Fig. B.2 Description of "Flexible" and "Rigid" Columns

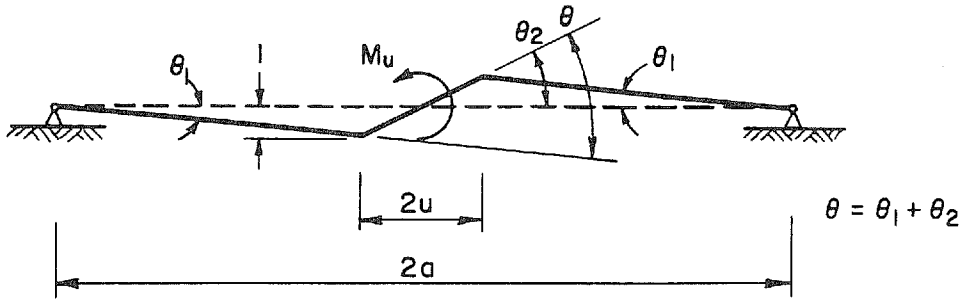

Section X-X

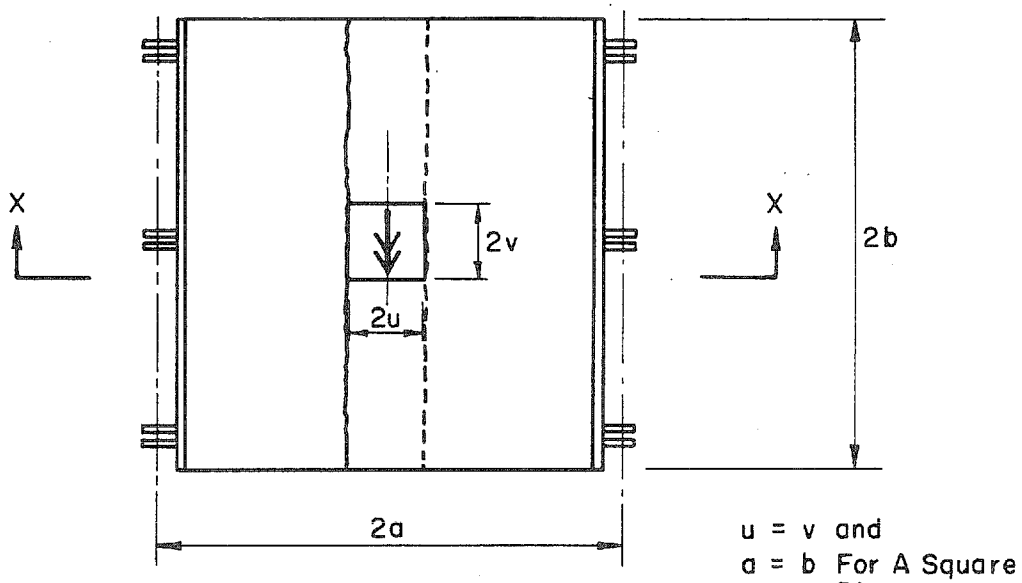

Plan of Assembly

Fig. B.3 "Wide-Beam" Mechanism

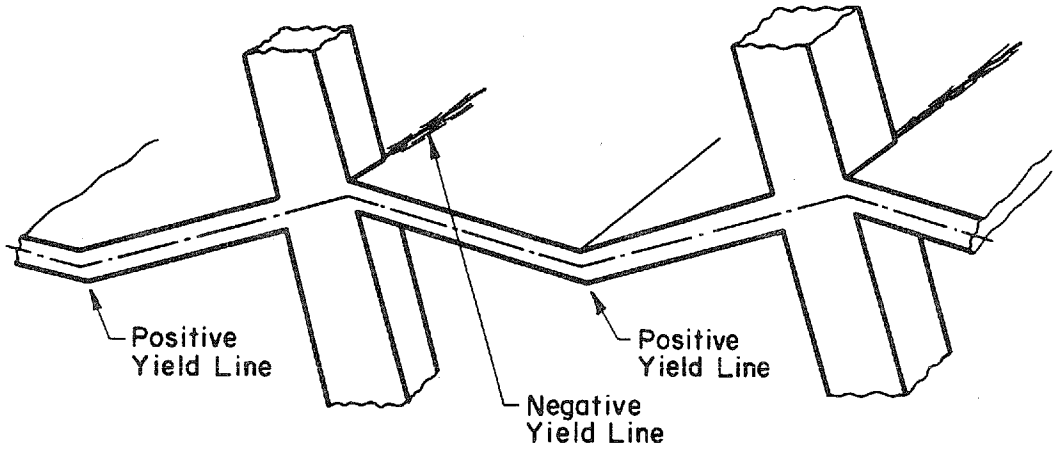

Fig. B.4 Yield Mechanism of Connection and Midspan

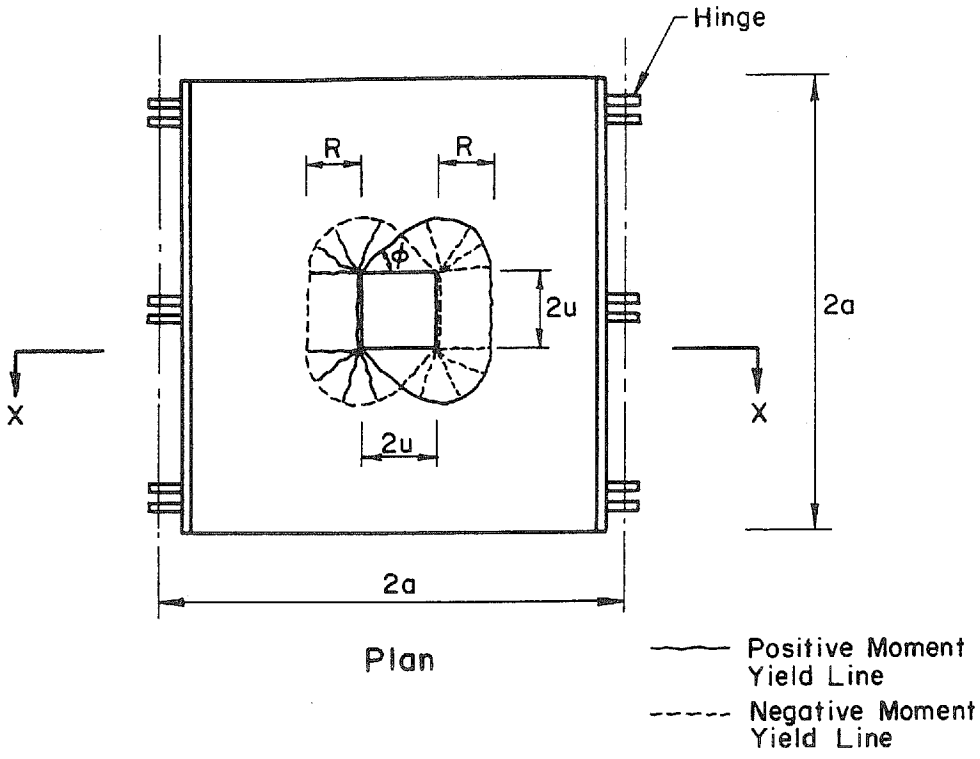

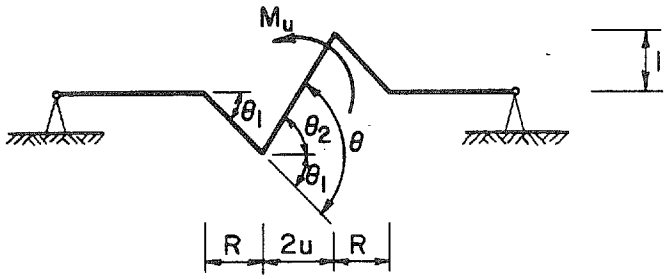

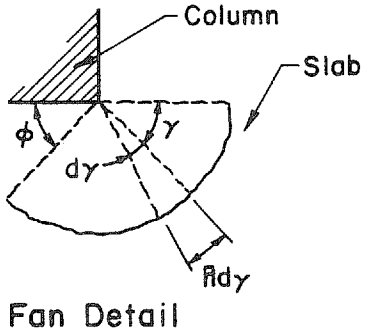

Fib. B.5 Local Yield Line Pattern
(Park and Islam)

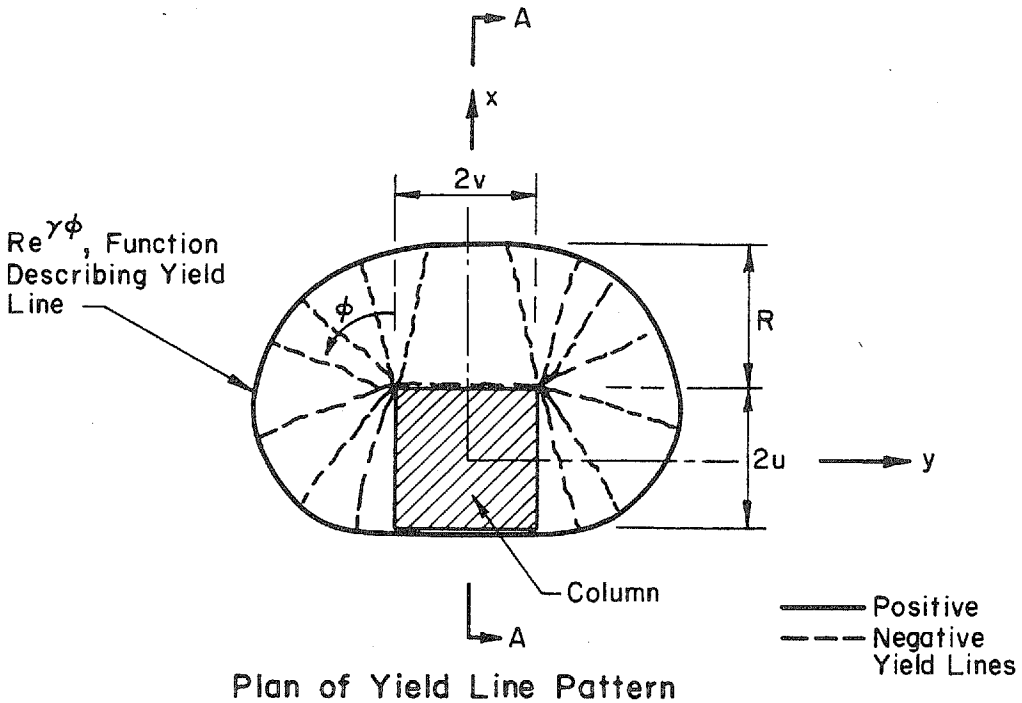

Plan of Yield Line Pattern
(After Gesund and Goli, 1979)

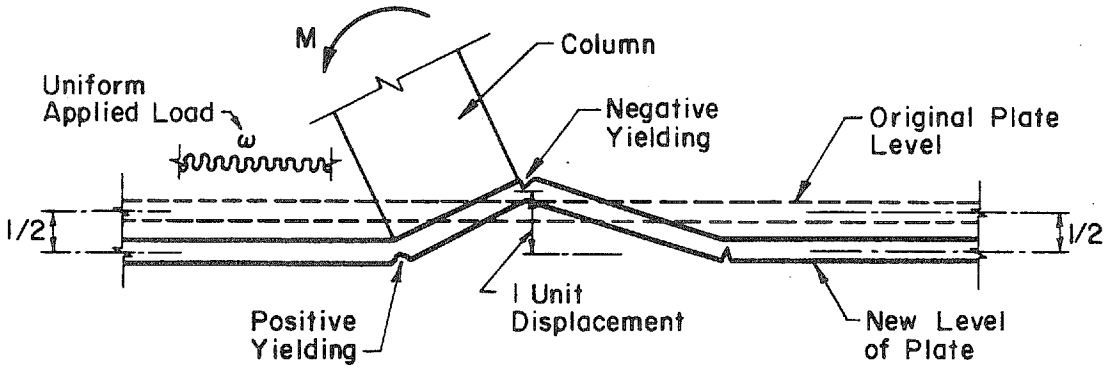

Section Through Mechanism Section A-A

Fig. B.6 Local Yield Line Pattern
(Gesund and Goli)

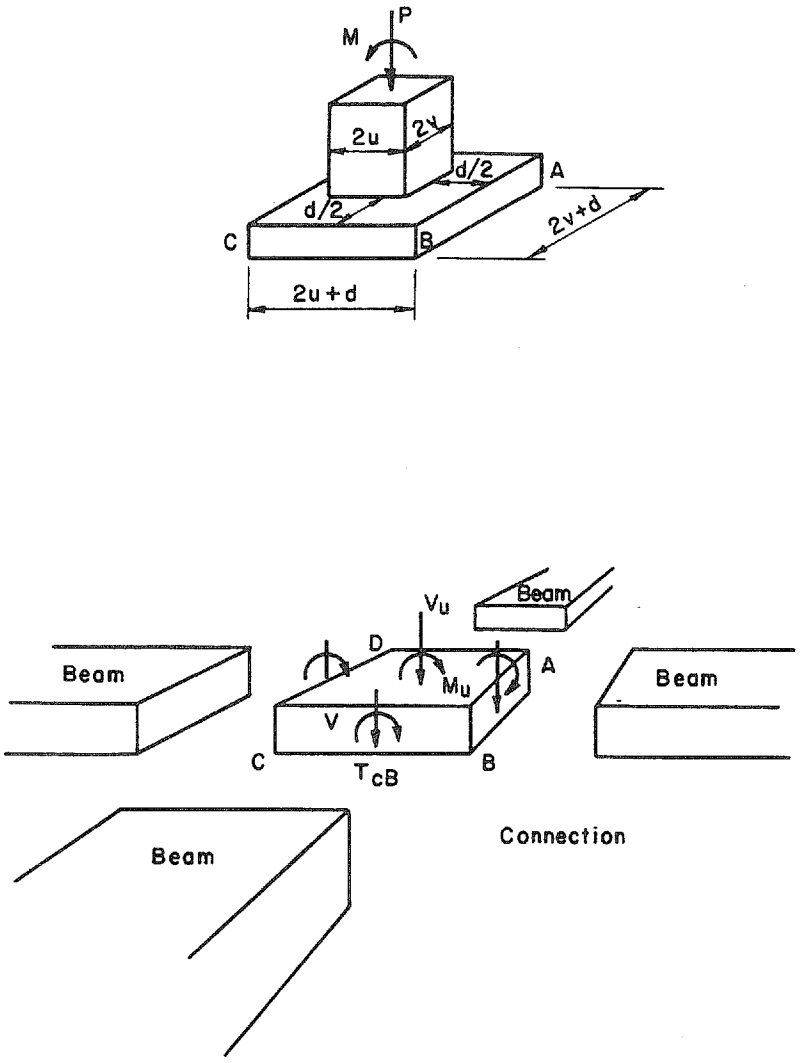

Fig. B.7 Description of Beam-Analogy

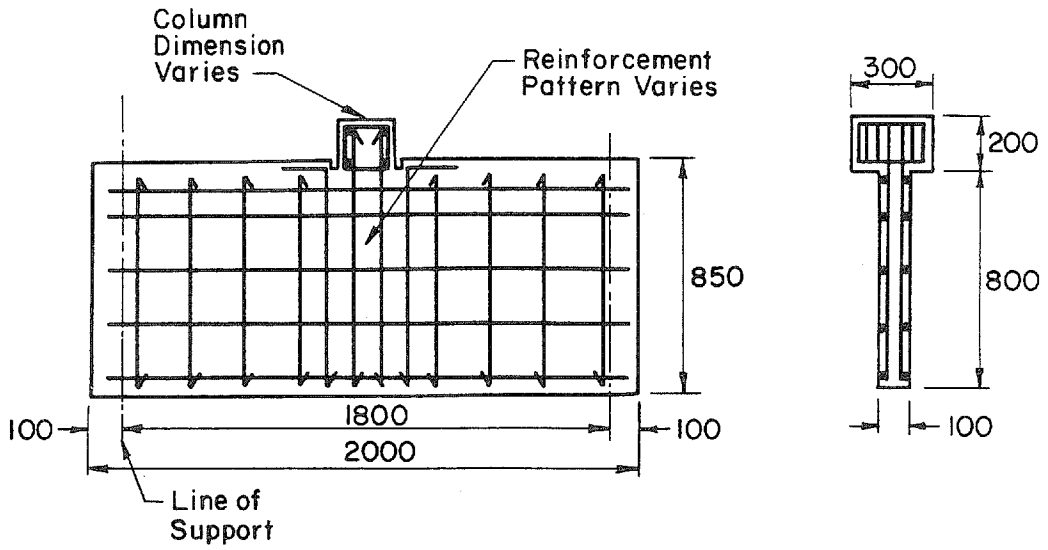

Plan of Plate

Section Through Plate

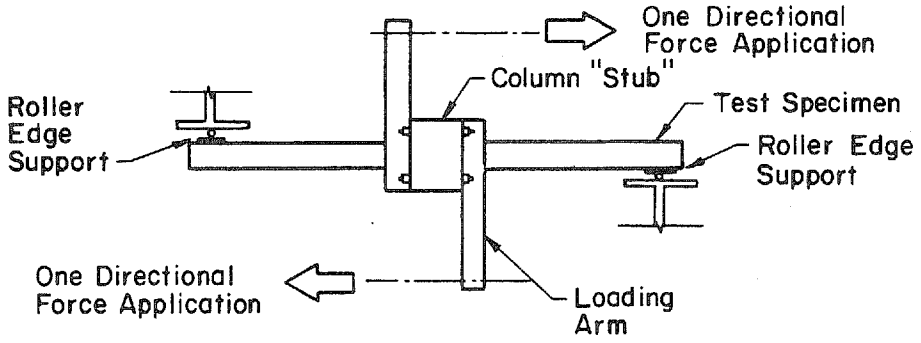

Loading Set-up

All Dimensions
Are In mm

Fig. B.8 Test Setup (Kanoh and Yoshizaki)

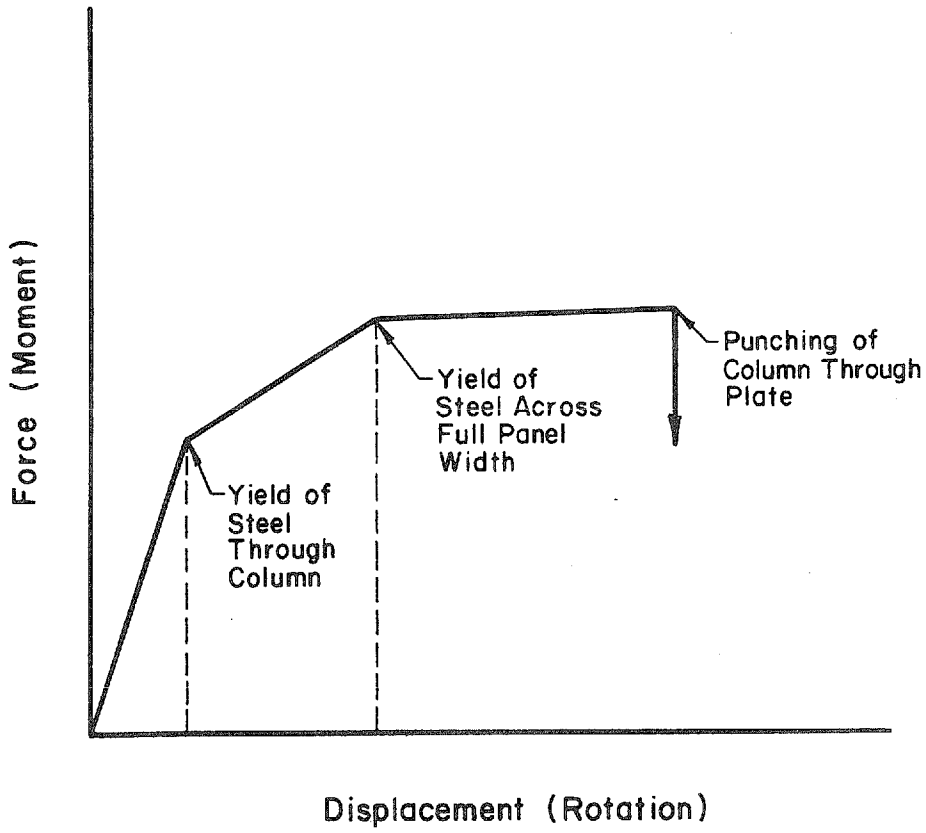

Fig. B.9 Possible Changes in Idealized Moment-Rotation Relationship

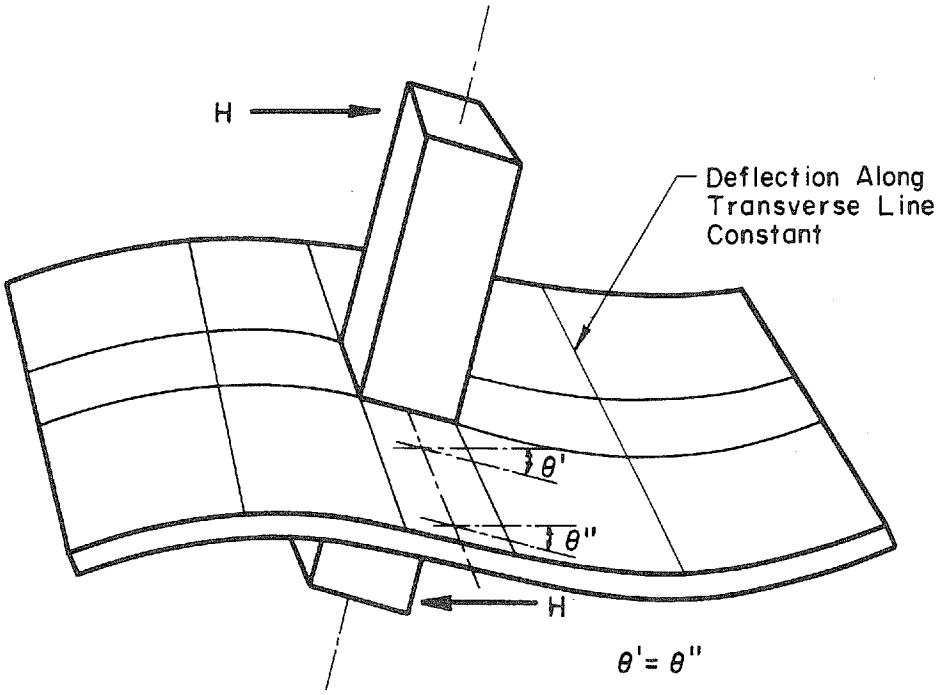

Typical Deflected Shape of Beam-Column Element

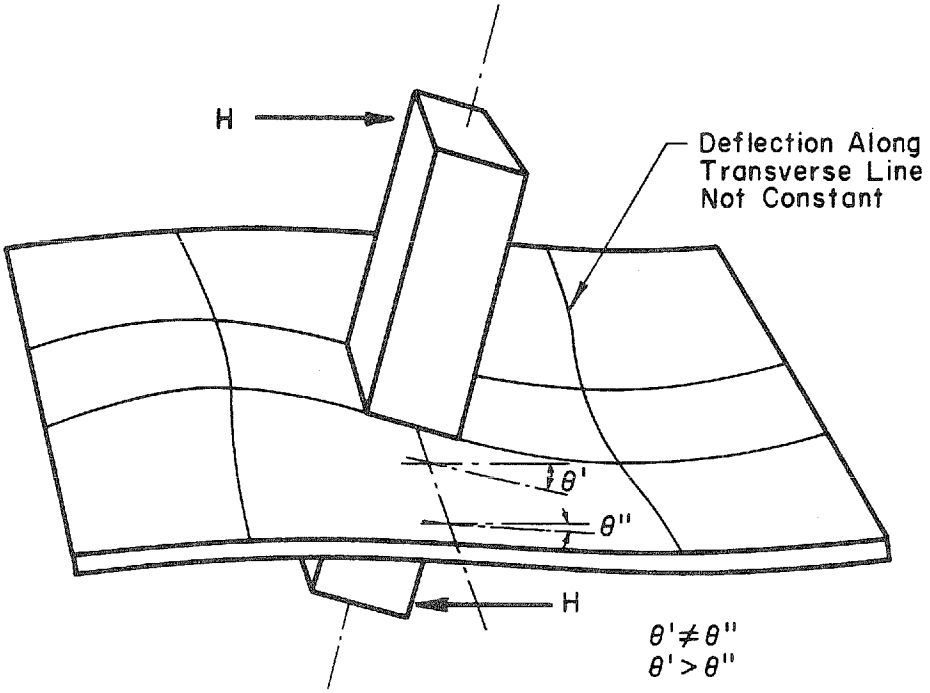

Typical Deflected Shape of Plate-Column Element

Fig. B.10 Difference in Deformation of Beam-Column and Plate-Column Connections

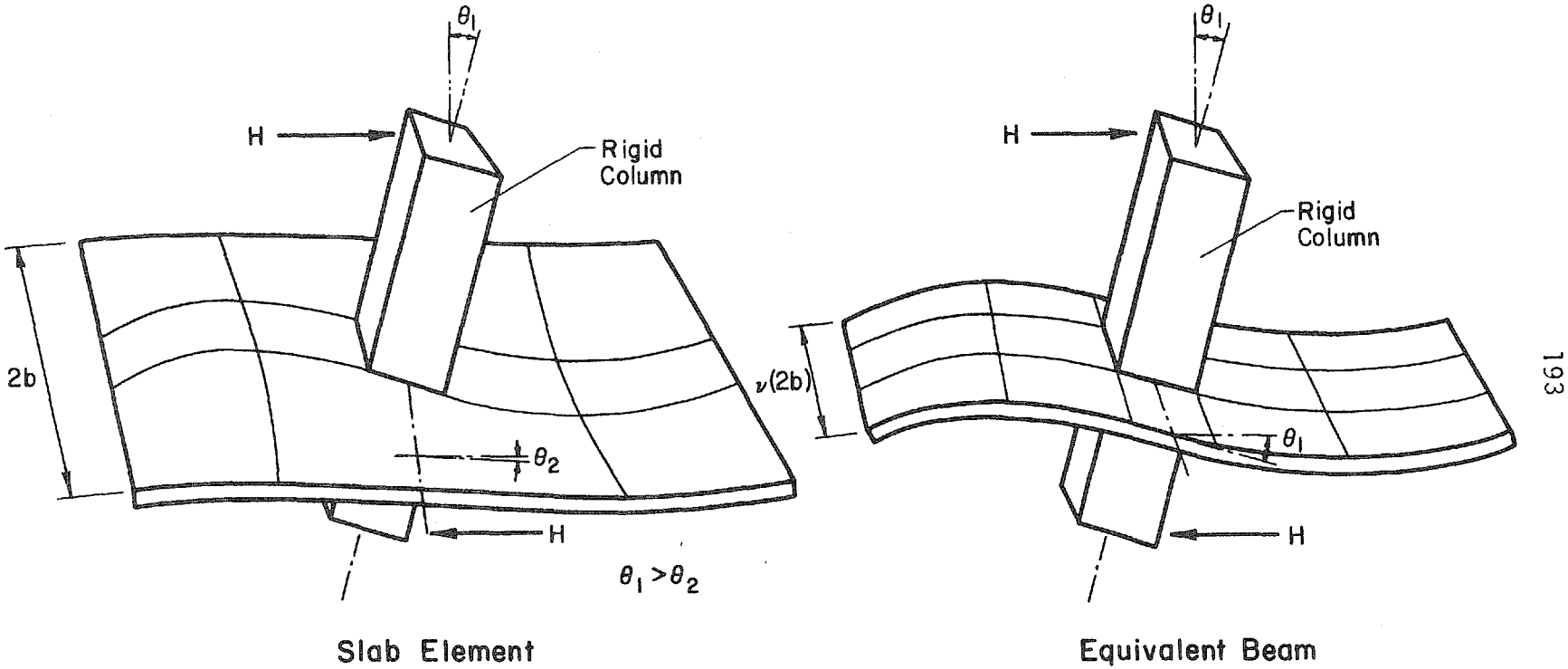

Fig. B.11 Definition of "Equivalent Width" ("ν") Factor

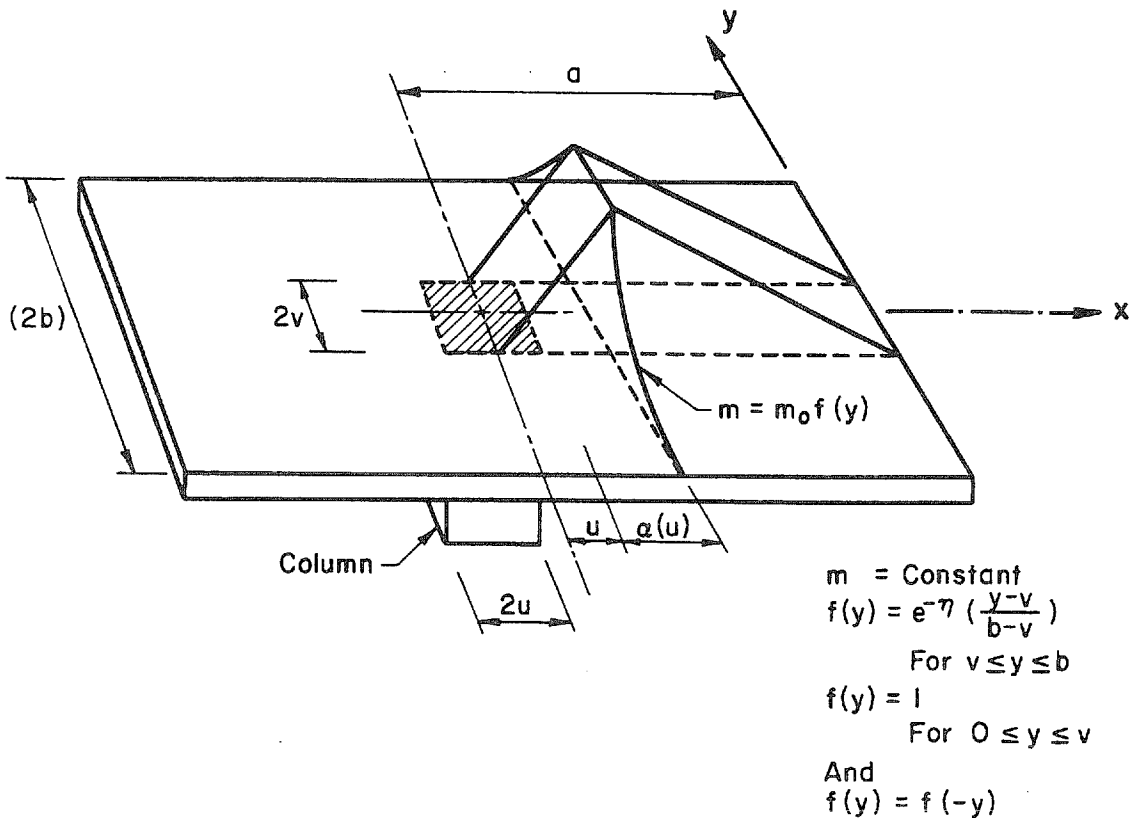

Fig. B.12 Assumed Moment Distribution (Elias)

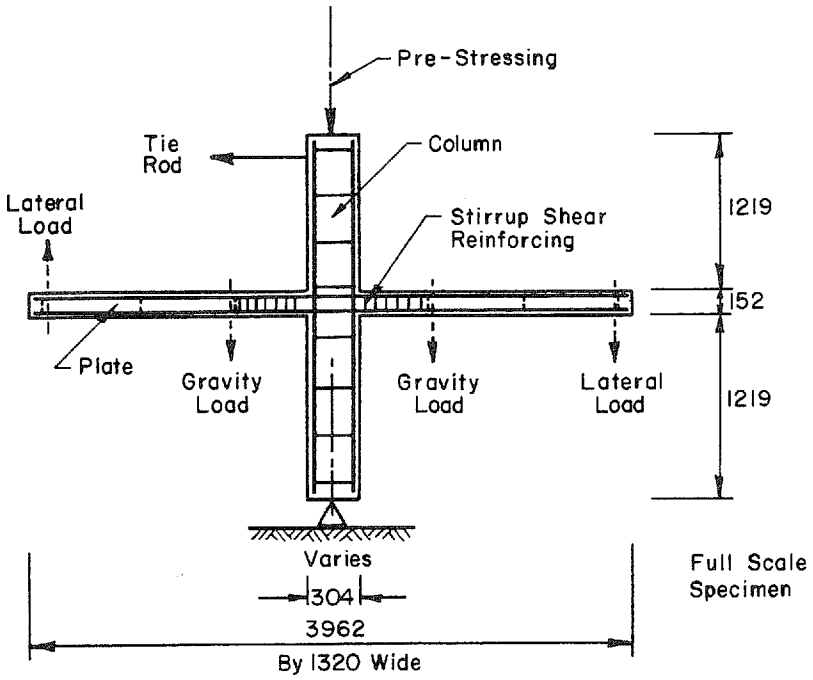

Specimen Type A
(After Hawkins et al 1977)

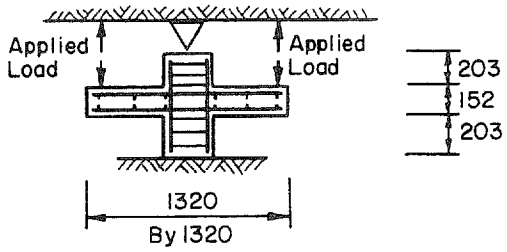

Specimen Type B
(After Hawkins et al 1977)

Fig. B.13 Illustration of Loading Methods
(Hawkins et al)

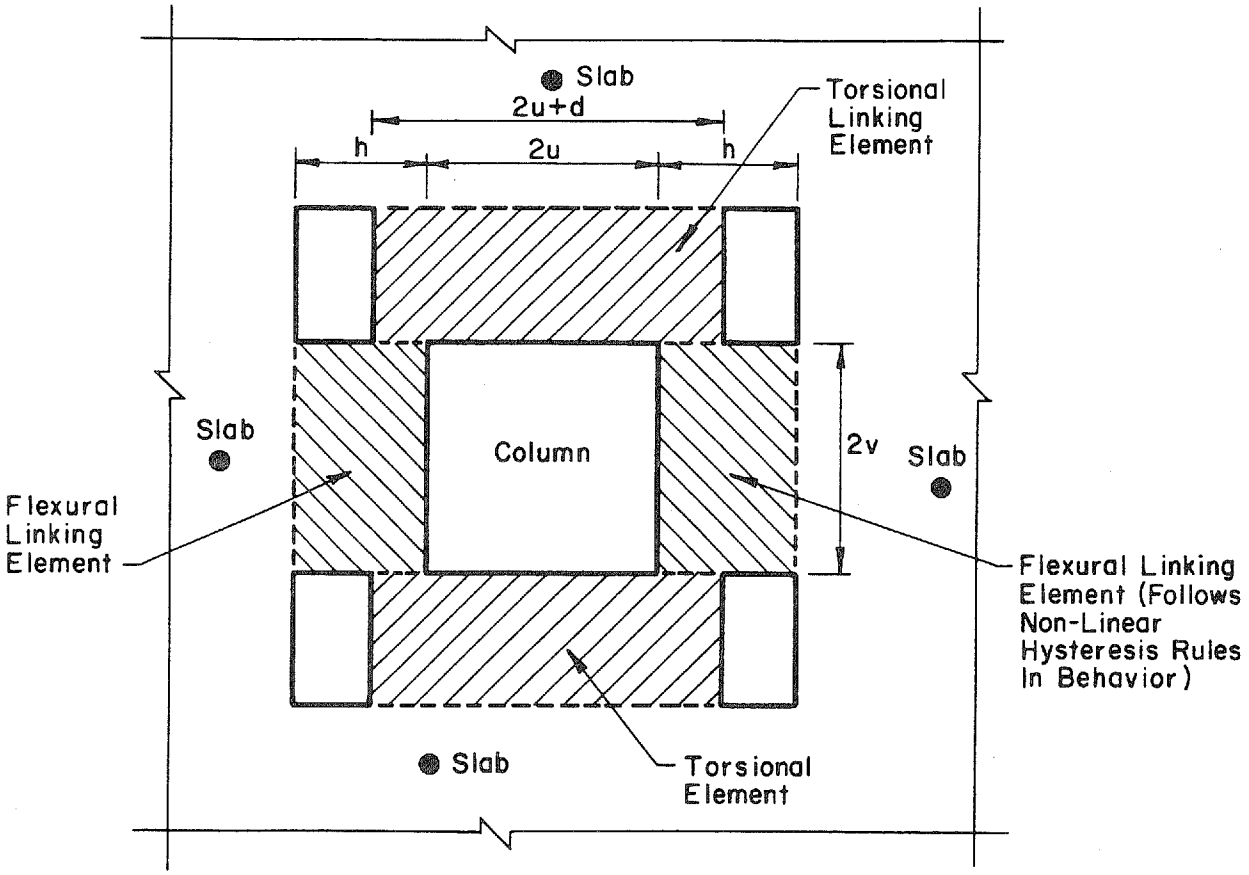

Fig. B.14 Definition of Components in Stiffness Model (Hawkins et al)

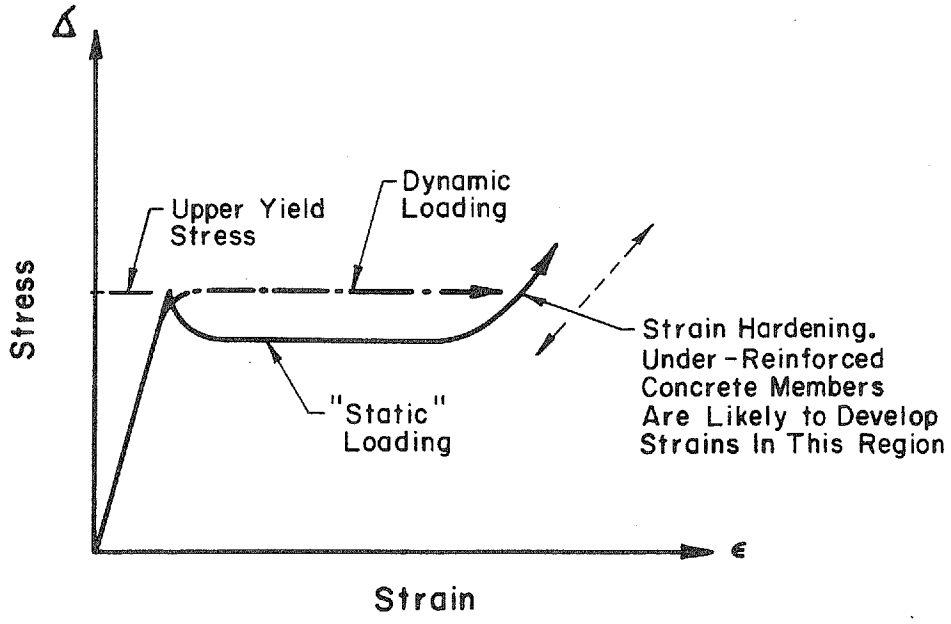

(b) Steel

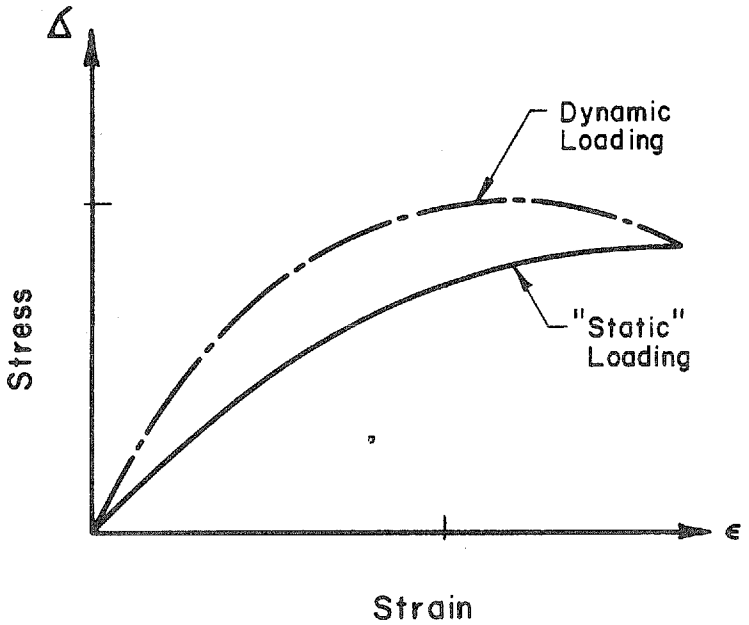

(a) Concrete

Fig. B.15 Idealized Stress-Strain Relationships

APPENDIX C

OUTLINE OF EXPERIMENTAL WORK: STATIC TESTS

C.1 Static Tests: Test Specimen

Plan and elevation of the test specimen are shown in Fig. C.1. The specimen comprised a 76-mm thick slab and a 305*305mm column. Figure C.2 shows the basic specimen in the test setup while Fig. C.3 shows a specimen with added load on slab. The nominal plan dimensions of the slab were 1829 by 1829 mm. However, to permit attachment of supports, the length of the concrete slab in the direction of loading was reduced from 1829 to 1652 mm. The nominal length of the column between hinges used for support and load application was 1118 mm. Both column and slab sections were symmetrically reinforced. The column was much stiffer and stronger than the slab and may be considered rigid in evaluating overall response of the assembly.

The horizontal load was applied by a servo-controlled ram (deflection control) at the hinge point on top of the column. The edges of the slab, perpendicular to the direction of loading, were supported by three hinged columns on each side to approximate a line of contraflexure in the slab. All vertical reactions from applied vertical and horizontal load were measured.

A total of five slab-column assemblies were tested. Two of these had added load on the slab as described in Table C.1.

The thickness and effective depths for the slab given in Table C.2 were based on 6 measurements for each specimen. The measurements were made within 200 mm of the column face on a line perpendicular to the direction of loading.

Different spacings of the No. 2 deformed bars were 38 (1.5), 51 (2), and 76 (3) mm (in.) as illustrated in Fig. C.4, C.5 and C.6.

Column reinforcement consisted of four No. 8 bars (Fig. C.14).

C.2 Static Tests: Materials

Type III Portland Cement, river sand and a gravel of 0.953 cm (3/8 inch) maximum size were used for all the specimens. All specimens and cylinders were cast using the same concrete mix design. Mix proportions, by weight, were 1.00: 3.51: 2.63 (cement: sand: gravel). The water-to-cement ratio was 0.8:1.0. For each specimen a single batch of concrete weighing approximately 9 kN (2024 lb) was mixed in a horizontal rotating type (9.8 kN or 2200 lb capacity) mixer.

Nine standard 15.2 by 30.5 cm (6 by 12 in.) concrete cylinders were taken from each batch. Of these, three cylinders were tested at the age of 1 week, and the remaining six on the day of testing of the particular specimen. Compressive and tensile strengths listed in Table C.2 are averages of the results obtained from three cylinders. Splitting tensile strengths of concrete listed in Table C.2 are also averages from the results obtained from three cylinders. A typical stress-strain curve for the concrete is shown in Fig. C.7.

Slab reinforcement was cut from No. 2 deformed bar stock from the same heat of steel. Measured mechanical characteristics of coupons cut from steel used in each specimen are listed in Table C.4. Each reported value represents the mean of three measurements. A typical stress-strain curve for the reinforcement is shown in Fig. C.8.

C.3 Static Tests: Fabrication of Specimens

Three types of slab reinforcing mats were fabricated as shown in Figs. C.4 through C.6. Strain gauges were attached to the bars at selected locations as indicated in the same figures. The strain gauges for steel were attached on the steel surface using the following procedure:

1. Remove the rust from the surface where the measurement is to be made. Then lightly polish the surface with sandpaper (#200) and wash with acetone.
2. Mount the gauge using bonding cement, M-BOND 200 ADHESIVE kit. Place one drop on the clean bar surface. Place the gauge and cover it with a plyethylene sheet. Then apply uniform pressure of approximately 5 to 10 N for 10 to 30 seconds at room temperature.
3. Check the gauge resistance and insulation with an electronic resistance meter and with an applied voltage lower than 50v DC.
4. Solder gauge terminals to lead wires.
5. Coat the gauge and the soldered joints with M-COAT BT.
6. Moisture-proof by using the MIRACLE SEAL covered by wrappings of High-Bond Tape.
7. Coat the wrapped gauge with M-COAT BT again.

Of the 90 gauges mounted using this procedure, none was damaged by moisture. Two were lost during installation of the specimen in the test setup because of accidental pulling-off of the lead wires. A 305 x 305 x 25 mm (12 x 12 x 1 in.) steel plate was welded to the bottom end of the column reinforcement cage. The column reinforcement cage was positioned in the center of the form. Following this, the bottom of the slab reinforcement mat was placed on steel spacers on the slab form, and dropped over the column reinforcement. The bars passing through the column were added to complete the bottom mat. Similarly the top mat, with the bars passing through the column initially omitted, was dropped over the column

reinforcement and held in position by chairs above the bottom mat. The bars required to complete the top mat were placed subsequently (Fig. C.15(a)).

The specimens were cast in a form primarily made of wood, the base and two opposite sides of the slab, and the column form work was constructed in wood. The remaining two sides of the slab form were provided by 25 mm x 76 mm x 1829mm(1x 3 x 72 in.) steel plates with eight bolt holes to allow connecting of end supports at a later stage (Fig. C.15 (b)).

Concrete for the specimens was compacted with an electric vibrator. The top plate of the column was set in place by using a cement paste once the specimen had reached an age of three days, and welded to the main reinforcement the following day.

The specimens and cylinders were cured under wet burlap and plastic for one week, then stripped and stored in the laboratory until the testing date.

C.4 Static Tests: Test Setup

A schematic diagram of the test setup is shown in Fig. C.1 through C.3.

The lateral load was applied to the top of the column by a servo-controlled hydraulic ram. The jack was of the push-pull type and it was capable of applying a load of $\pm$ 111.2 KN (25 kips) and had a stroke of $\pm$ 76 mm (3 in.).

In two specimens (S4 and S5) "dead load" was applied at four points in the slab by hanging steel weights as indicated in the photograph in Fig. C.3.

The loading points were located on diagonal axes of the slab plan. The center of each loading point was at a distance of 467 mm from the closest corner of the column. The column base and two sides of the slab at right angles to the direction of loading were supported by hinge supports corresponding to the points of contraflexure of the horizontally loaded structure.

Reaction forces at all seven vertical supports were measured by load cells. Ideally, there was no horizontal reaction at the six exterior supports. The horizontal reaction at the interior support was transferred to a steel plate on rollers which permitted measurement of the vertical force without distorting the load cell.

The lateral support for the loading ram was provided by a steel reaction frame (Fig. C.3). The steel reaction frame was braced diagonally to minimize sidesway.

C.5 Static Tests: Instrumentation

Each test specimen was instrumented to provide detailed data on its behavior throughout its entire loading history. Measurements were made of loads, displacements and strains.

(a) Loads: The force in the jack was monitored by an X-Y recorder using a load cell attached to the ram. All vertical reactions were monitored using load cells positioned at the locations indicated in Fig. C.9. The six load cells along the edges of the slab were prestressed to a load of approximately 44.5 KN (10 kips) so as to counteract any uplift. The load cells had a linear range of 89 KN (20 kips) and a sensitivity of 0.1 KN (23 lb).

(b) Displacement: Four linear voltage differential transformers (LVDT) were used to determine the horizontal displacements of the slab and the column with respect to independent frames fixed to the laboratory floor. The positions for those LVDT's are shown in Fig. C.9. They are identified by numerals 1,4,5, and 10. The movement of the top and bottom plate of the column were measured using a piano wire attached centrally to the top and bottom plates, extending around a pulley and activating a potentiometer positioned horizontally above the laboratory floor.

(c) Vertical Deflections and Twisting Angles: Vertical deflections of slab were measured by two LVDT's (2 and 3) as shown in Fig. C.9. The distribution of the deflections along the E-W centerline were measured by ten dial gages located above the top surface of the slab at the positions shown in Fig. C.10.

Twisting angles of the slab in N-S direction were measured by ten dial gauges. The locations are shown in Fig. C.10. All the dial gauges and the two LVDT's (2 and 3) were attached to a specially designed frame which was supported by a hinge at the ends of the slab (Fig. C.11). A deflection profile of the slab could be determined within 0.025 mm (0.001 in.), and the dial gauges for measuring twisting angles could be determined within 0.013 mm (0.0005 in).

(d) Rotations: The rotations of the slab with respect to the column were measured by LVDT's identified by numerals 6, 7, 8 and 9 (Fig. C.9).

(e) Strains: Electrical resistance strain gauges were used to determine strains at selected locations on the reinforcing steel and concrete. Eighteen, 2-mm (0.08 in.) long, gauges were placed on specific flexural reinforcing bars of the slab. The locations of these gauges are

indicated in Figs C.4 through C.6. The gauges on the top and bottom bars were placed in corresponding positions. These gauges designated KFR-02-C1-11, were manufactured by Kyowa, Electronic Instruments Ltd., Tokyo, Japan. Eight, 25 mm (1 in.) long SR-4 gauges were placed on the top and bottom surface of the concrete slab adjacent to the column at the locations shown in Fig. C.10.

C.6 Static Tests: Data Acquisition and Reduction System

The data acquisition system is shown in photograph of Fig. C.12. The LVDT's were regulated by a six-volt power supply. Electrical impulses from the load cells, strain gauges and LVDT's were received by a VIDAR data acquisition system and sent to a teletype where voltage readings were punched on paper tape. The tape was later fed into a teletype tape reader and stored on a permanent storage disk. Data from each file was then reduced and plotted using CALCOMP subroutines. Curves of applied load versus displacements, slab deflections, moments and slab rotation and etc. were plotted.

C.7 Static Tests: Test Procedure

All specimens were tested by applying lateral displacement reversals. The maximum load for each cycle was controlled by the column rotation angle (practically, the displacement of the top of the column). Three load levels were applied, each consisting of 5 cycles, corresponding to a rotation angle of 1/400, 1/200 and 1/100, respectively. Thereafter two large cycles were applied corresponding to the rotation angle of 1/50. After that the specimens were loaded to failure. The loading pattern is shown diagrammatically in Fig. C.13.

Displacements, loads, deflections, rotations and strains were measured after each increment or decrement of displacement during any cycle of load. Crack patterns for the slab were recorded at the first cycle to a given maximum level. The eighteen dial gauges were also read at the first cycle to a new maximum load level, and during the last incremental loading to failure. The tests were monitored by plotting the applied load versus displacement at the top of the column level on a X-Y recorder.

Each test was completed within approximately seven hours.

C.8 Static Tests: General

Detailed descriptions of the specimen dimensions, fabrication of specimens and test apparatus are presented in this section.

The detail of the specimen dimensions is shown in Fig. C.14. The fabrication of a specimen is shown in Fig. C.15(a) through (d) (photograph).

The steel chair (for top bar) and #3 bar (for bottom bar) were used as the spacer (Fig. C.15 (a)). The 3/4 x 9 in. bolts were used for connecting slab edges and edge supports (Fig. C.15 (b)). Strain gauges for top and bottom steel were attached on the cross-section (Fig. C.15 (c)). The top of the column was cleaned after casting and the steel plate was welded to main steels three days after casting (Fig. C.15 (d)).

The six edge supports were prestressed to counteract uplift effects on the load cells. Those support systems were calibrated individually. The calibration factors of each support is shown in Table C.5. Sixteen steel weights for dead load were arranged under specimen S4 and S5. The arrangement is shown in Fig. C.16.

TABLE C.1 Test Program

SPECIMEN	SLAB REINFORCEMENT RATIO (%)	DEAD LOAD
S1	0.65	Self Weight
S2	0.98	Self Weight
S3	1.31	Self Weight
S4	0.98	Self Weight + 27.82 KN
S5	0.98	Self Weight + 59.31 KN

TABLE C.2 Properties of Test Specimens

Mark	SLAB			COLUMN		STEEL	
	Thickness	Effective Depth		Comp. Strength	Tens. Strength**	Yield Stress	Spacing
		Top Reinf.*	Bottom Reinf.				
	mm	mm	mm	MPa	MPa	MPa	mm
S1	76	60	64	48.5	2.85	323	38
S2	77	62	65	35.1	2.29	330	51
S3	76	58	64	33.9	2.18	340	76
S4	76	58	64	34.9	2.55	317	51
S5	76	60	64	35.2	2.43	366	51

*Reinf. = Reinforcement

**From Splitting Tests

TABLE C.3 Measured Properties of Concrete

PARAMETER	TEST STRUCTURE				
	S1	S2	S3	S4	S5
Age at Testing (days)	51	64	59	59	48
Slump (mm)	76	114	127	146	171
Compressive Strength, f'_c (MPa)	45.8	35.1	33.9	34.9	35.2
Secant Modulus, E_c ($* 10^4$ MPa)	* 3.22	** 2.98	** 2.84	*** 2.84	*** 2.74
Tensile Strength, f_{sp} (MPa)	2.85	2.29	2.18	2.55	2.43
Compressive Strength at 1 week (MPa)	31.3	20.6	21.3	22.7	21.3

* Measured at compressive stress = 14.6 MPa
** Measured at compressive stress = 9.7 MPa
***Measured at compressive stress = 12.2 MPa

TABLE C.4 Measured Properties of Reinforcement

	S1	S2	S3	S4	S5
Yield Stress f_y (MPa)	323	330	335	317	340
Yield Strain ε_y	0.0016	0.0016	0.0017	0.0016	0.0018
ε_h	0.0201	0.0195	0.0218	0.0168	0.0140
Maximum Stress f_u (MPa)	459	474	469	460	514
Strain at Maximum Stress ε_u	0.121	0.153	0.150	0.150	0.160
Fracture Strain ε_b	0.237	0.257	0.244	0.209	0.243

ε_y: measured yield strain (extensometer, 25 mm gage length)

ε_h: strain at initiation of strain hardening

TABLE C.5 Calibration Factors of Supports

SUPPORT NUMBER	CALIBRATION FACTOR (μ volt/kip)**	
	Tension	Compression
1	56.9	85.0
2	47.5	83.5
3	80.1	84.5
4	54.9	89.0
5	61.6	88.0
6	75.1	84.5
*7	203.2	--

*Center support, compression only

**Range (Compression 0 - 0.85 - 1.708 kips
Tension 0 - 2.5 - 5.0 kips

Reading (Compression → increase
Tension → reduce

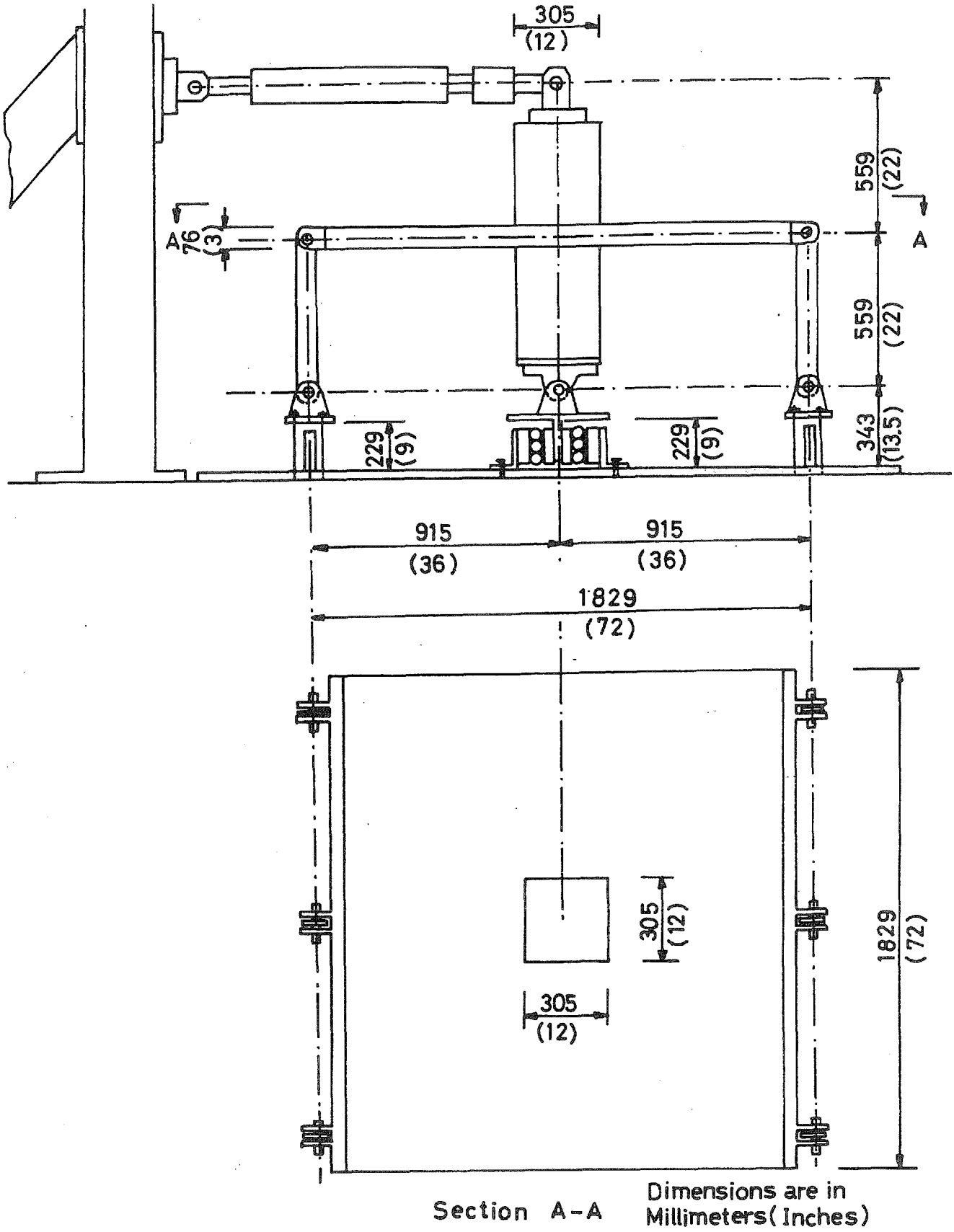

Fig. C.1 Plan and Elevation of Test Specimen

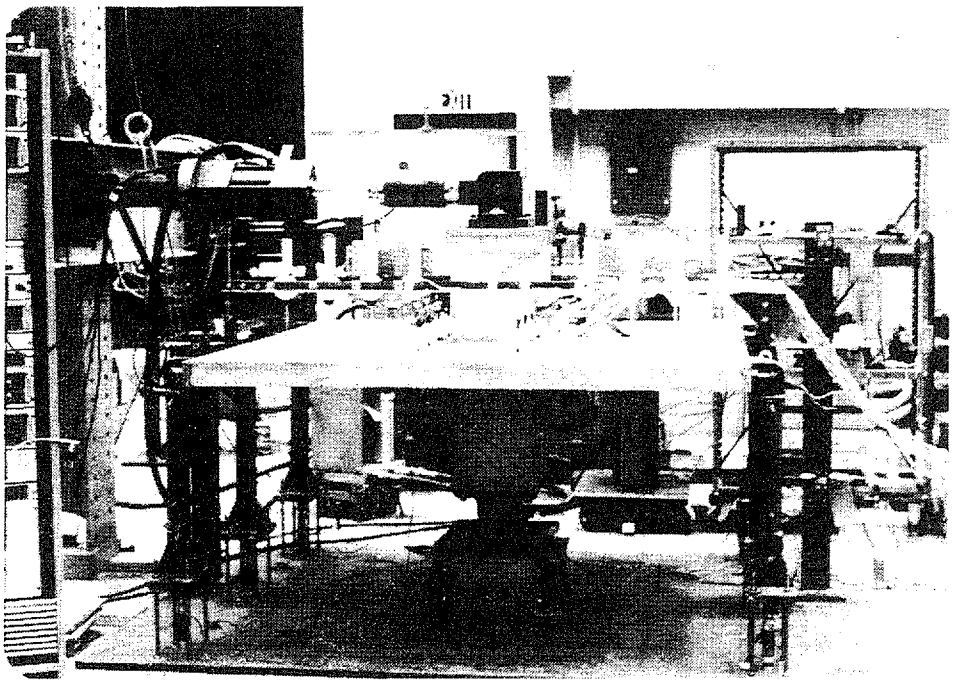

Fig. C.2 Test Setup (self weight only)

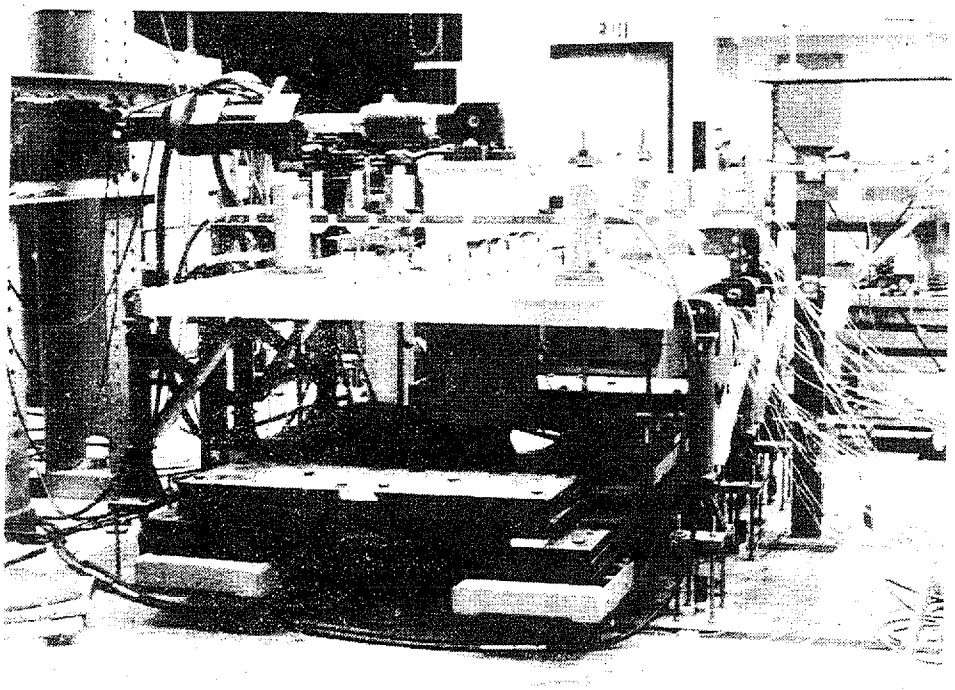

Fig. C.3 Test Setup (applied dead load)

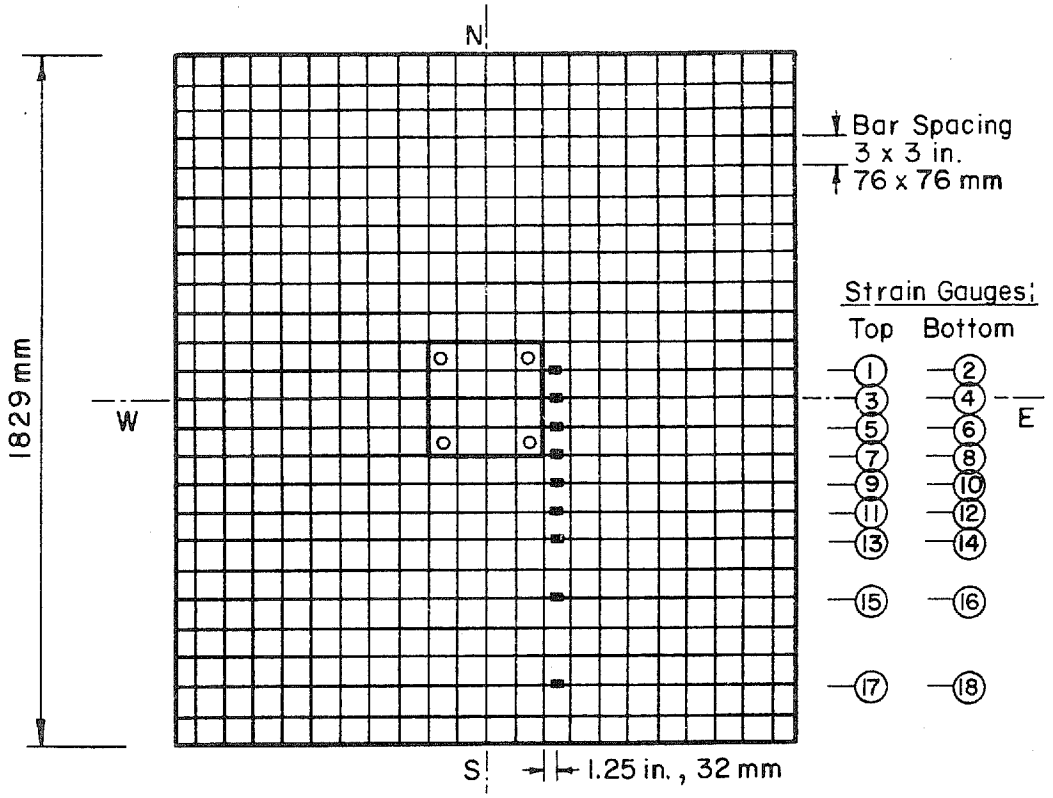

Fig. C.4 Reinforcement Layout, S1

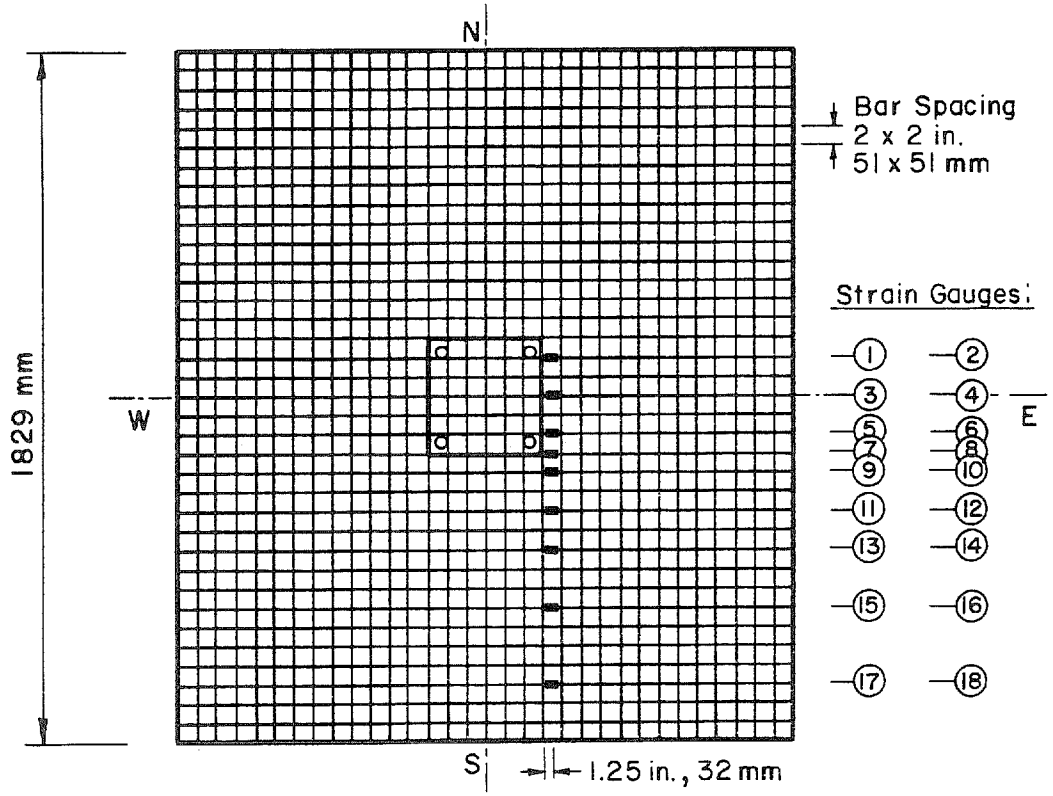

Fig. C.5 Reinforcement Layout, S2

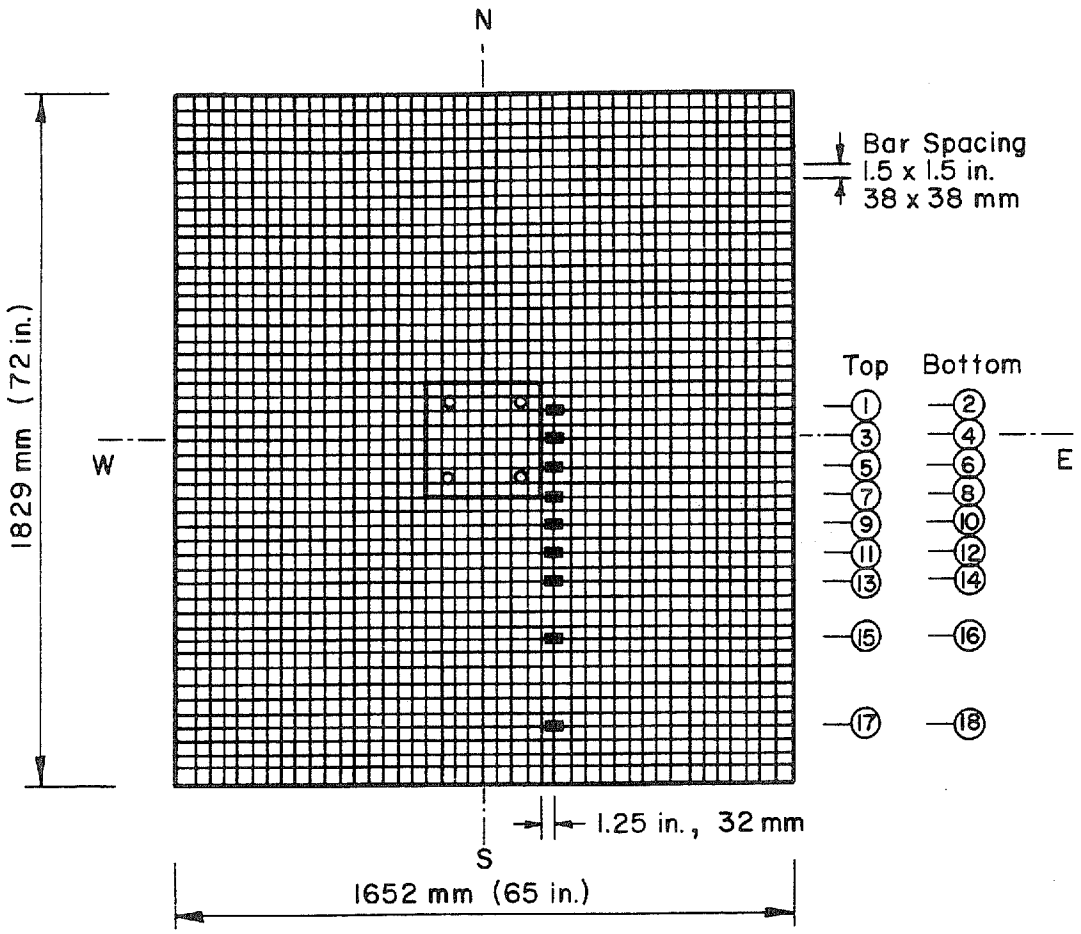

Fig. C.6 Reinforcement Layout, S3

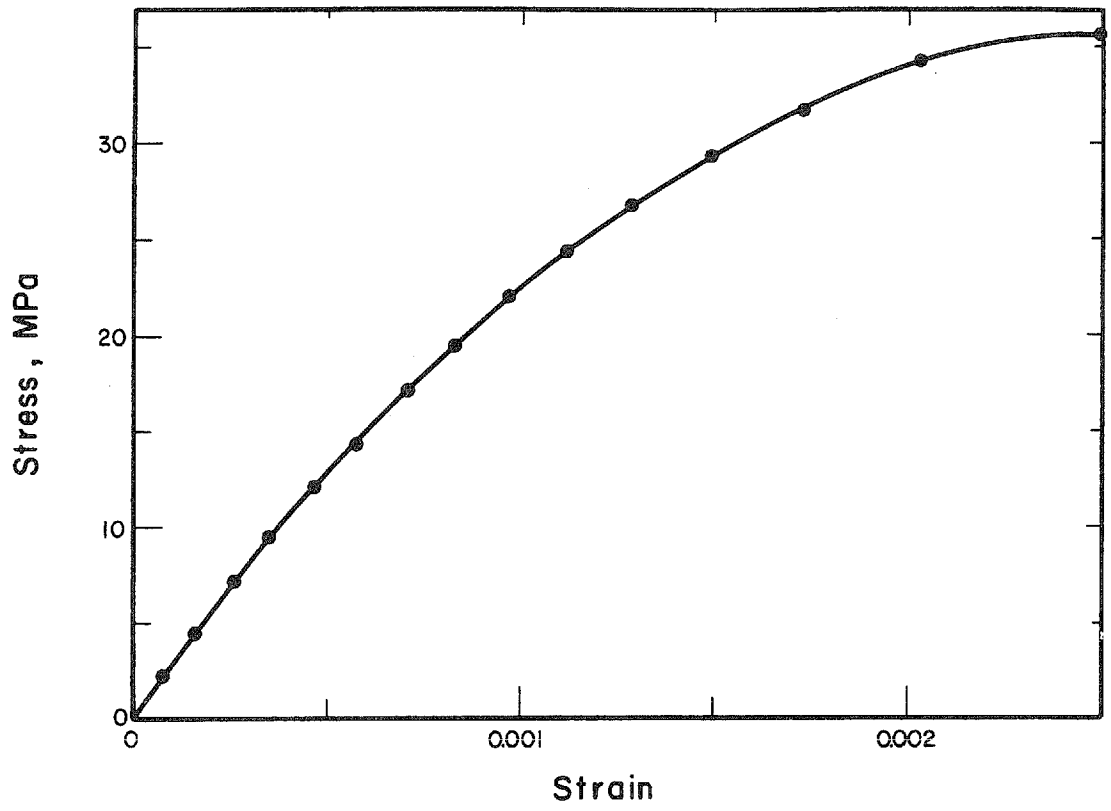

Fig. C.7 Typical Concrete Stress-Strain Relationship

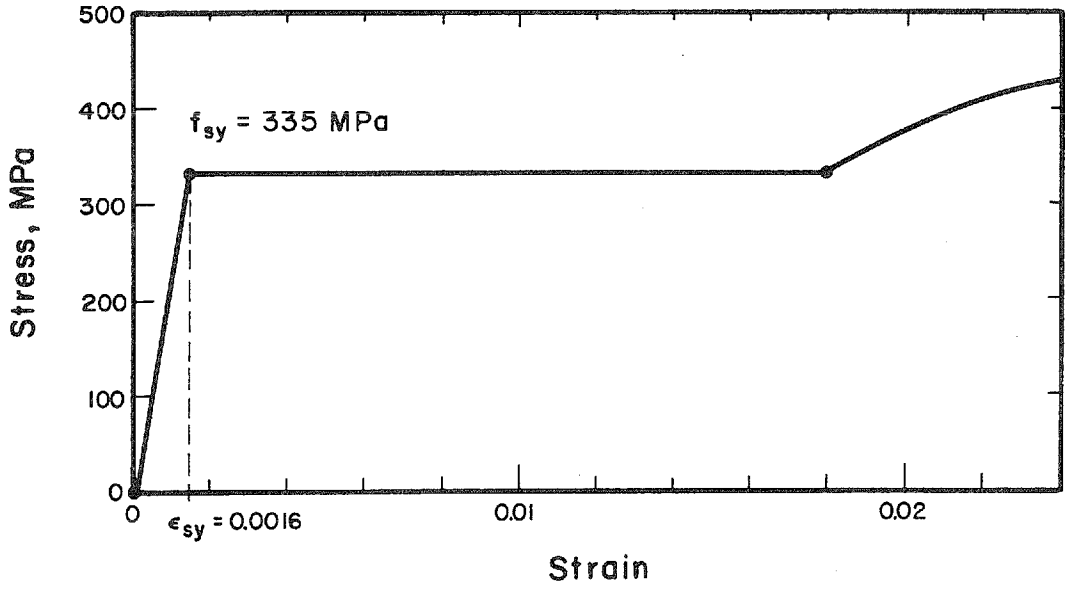

Fig. C.8 Typical Steel Stress-Strain Relationship

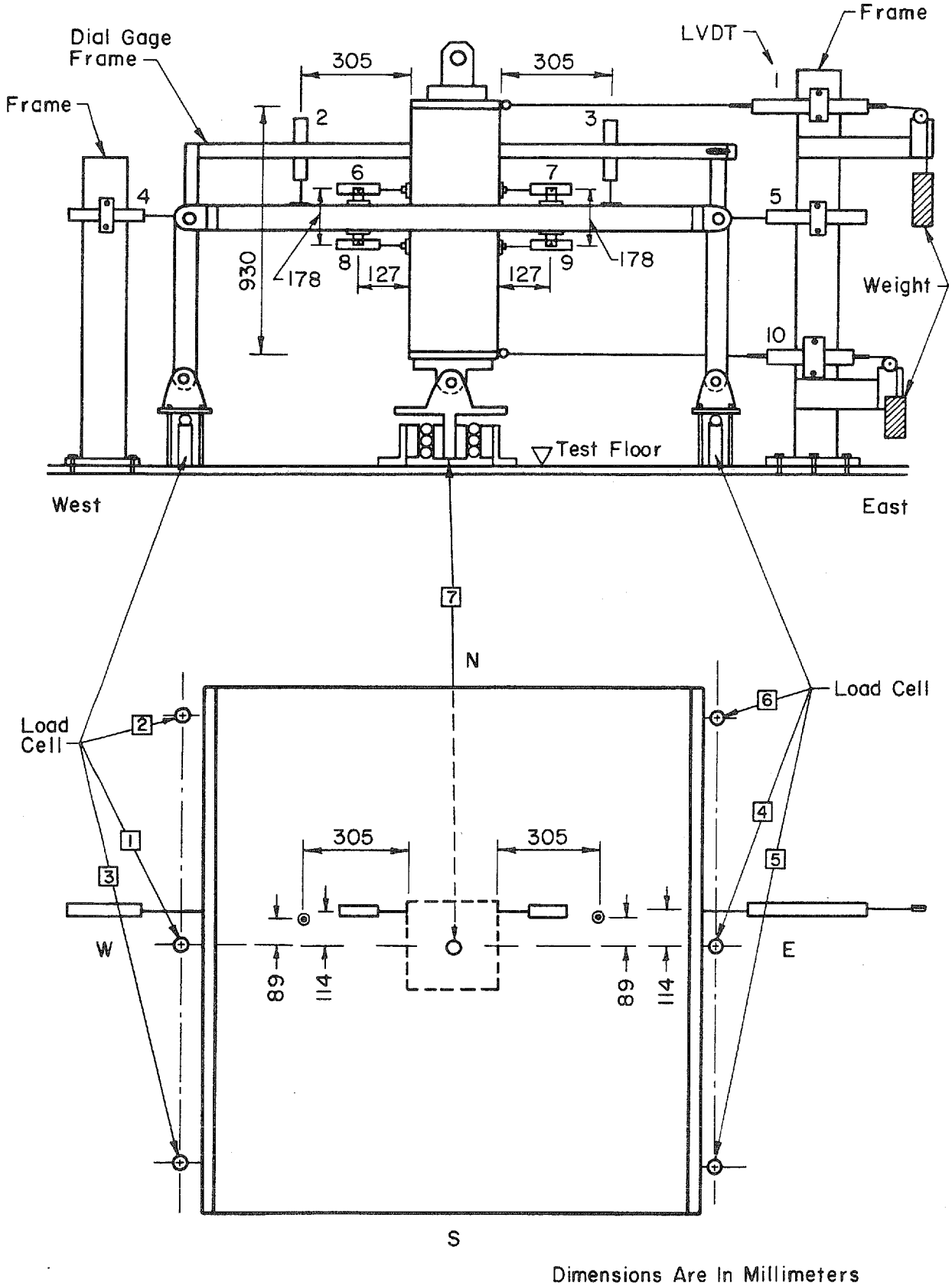

Fig. C.9 Positions of LVDT's and Load Cells

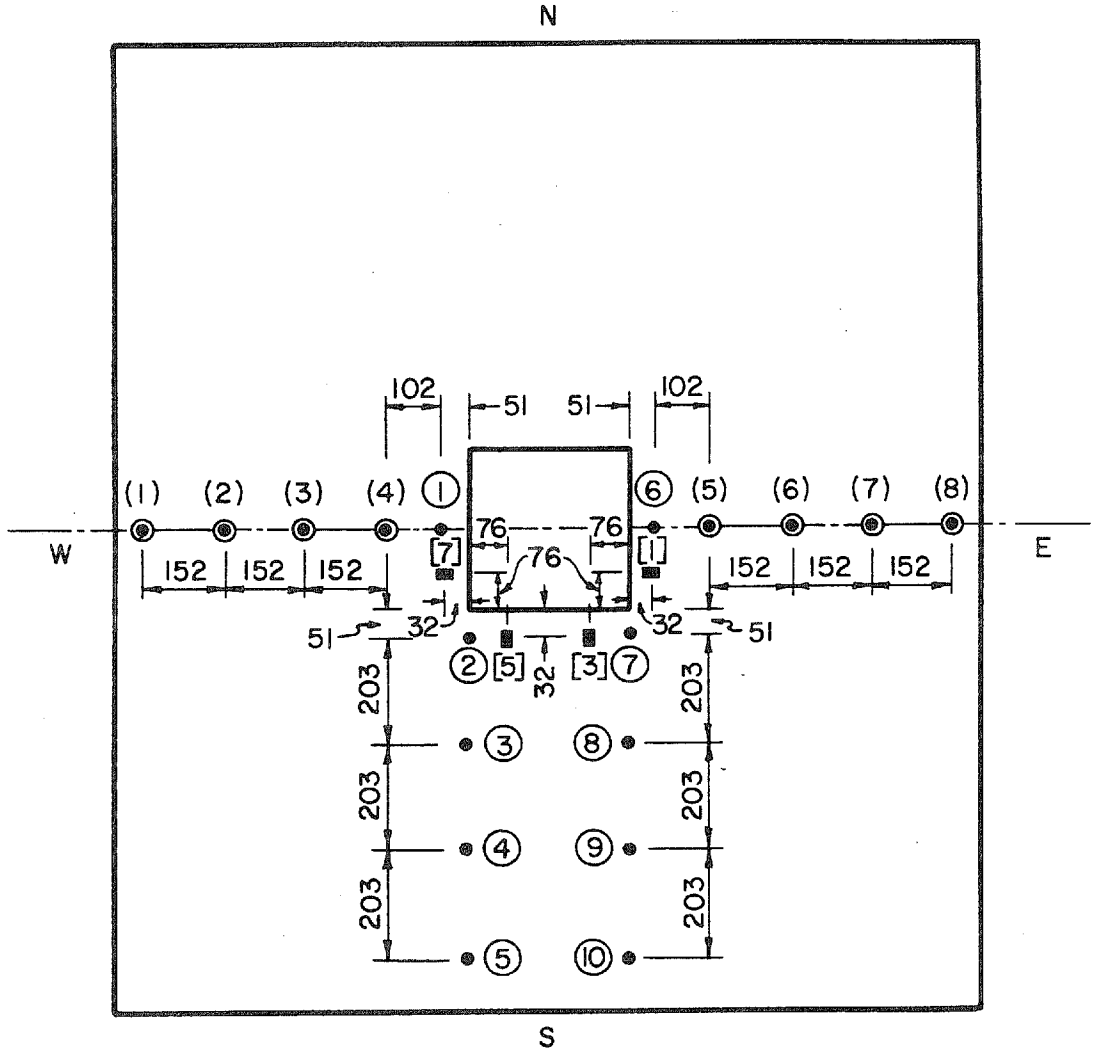

◉ (1) Dial Gauge
• ① Dial Gauge
▬ [1] Strain Gauge

Dimensions Are In Millimeters

Concrete Gauge		
Top	Bottom	
[1]	[2]	East
[3]	[4]	Side - East
[5]	[6]	Side - West
[7]	[8]	West

Fig. C.10 Positions of Dial and Strain Gauges

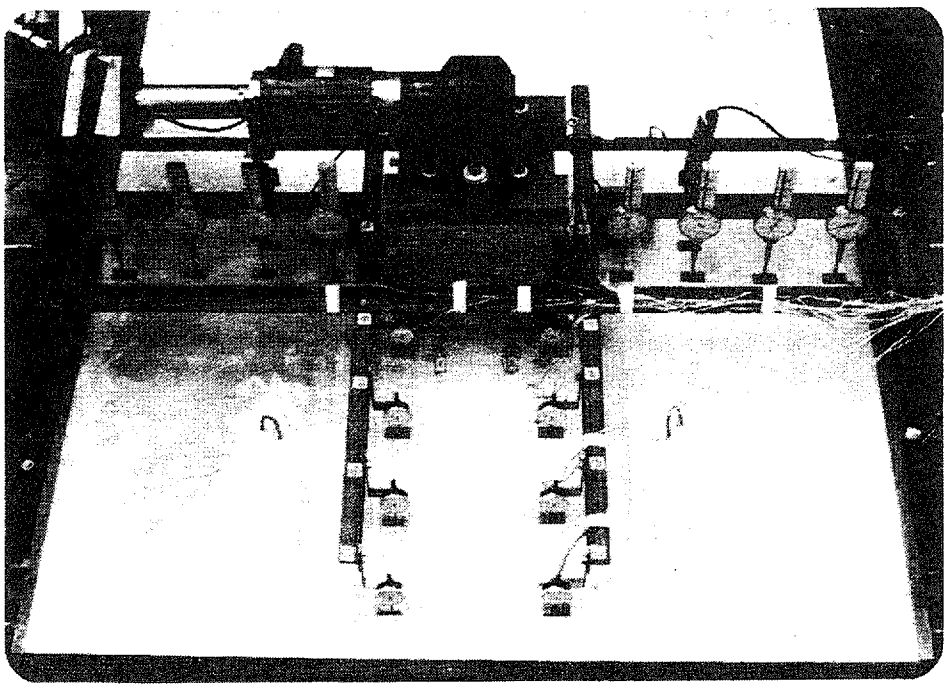

Fig. C.11 Dial Gauge Frame

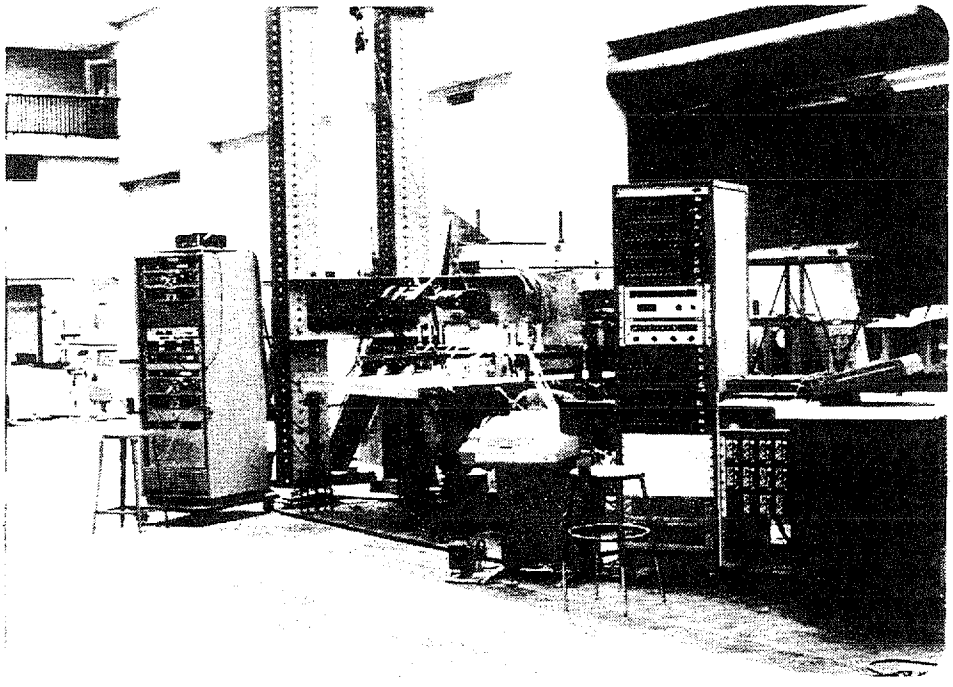

Fig. C.12 Data Acquisition System

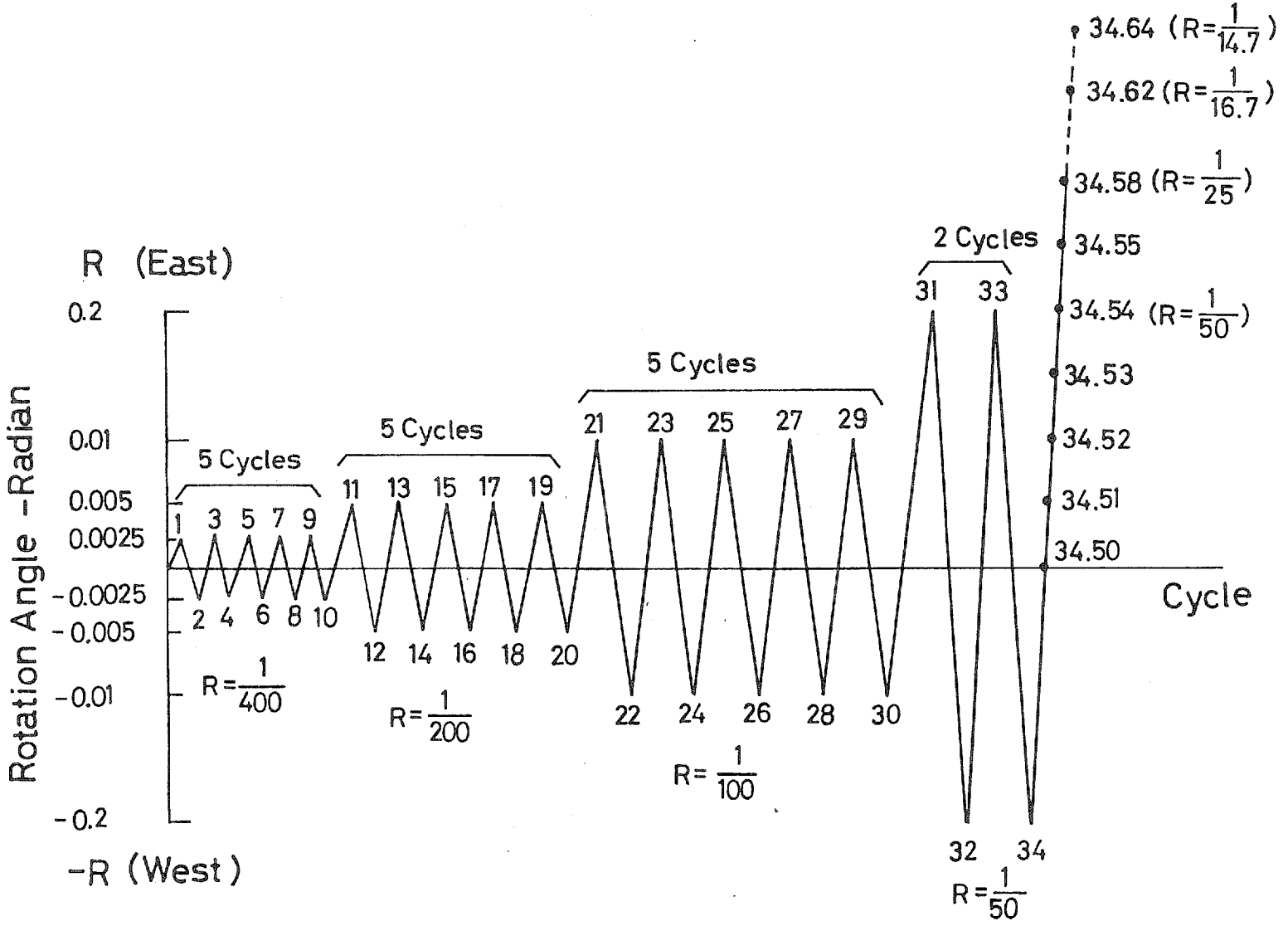

Fig. C.13 Loading Pattern

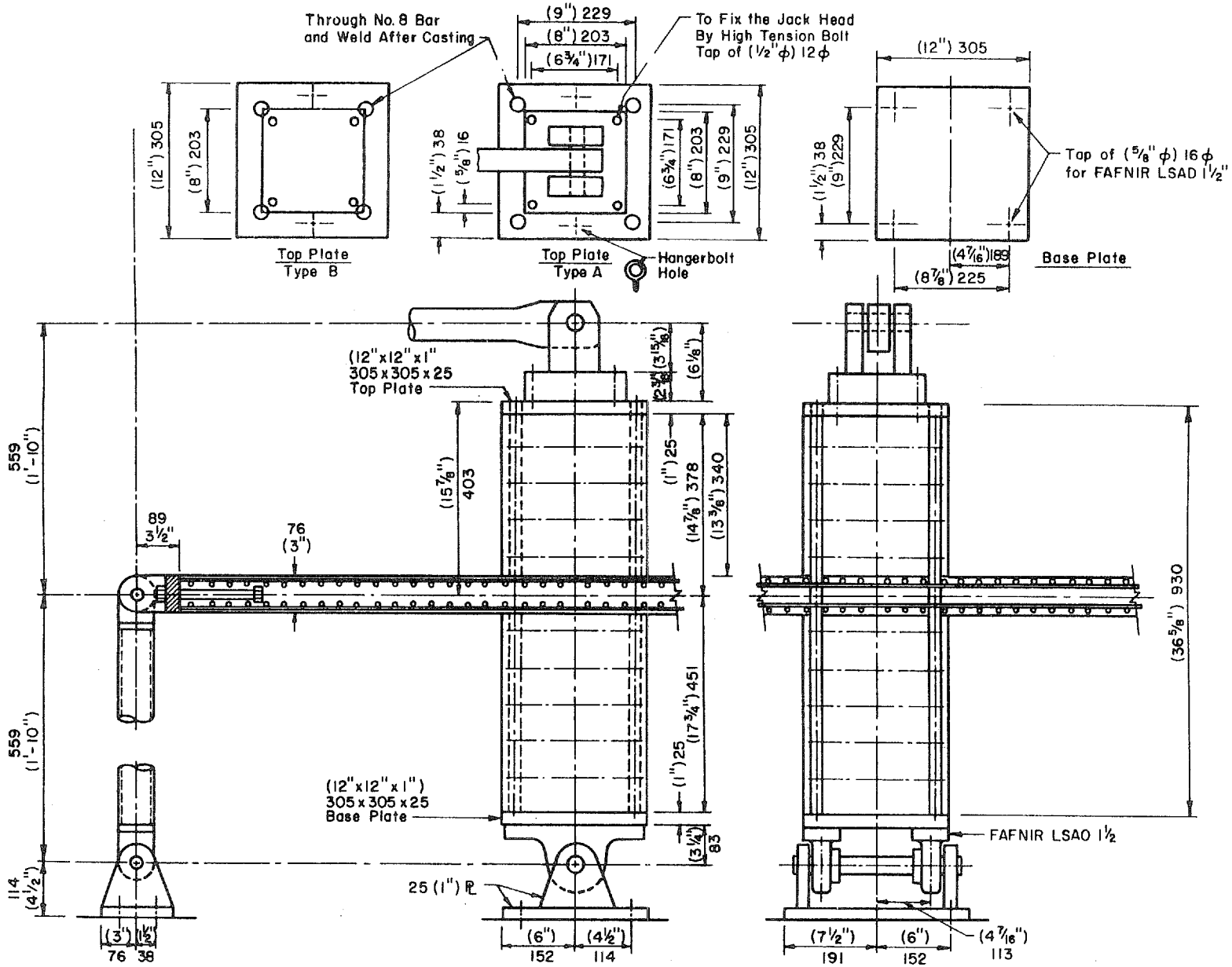

Fig. C.14 Details of Specimen

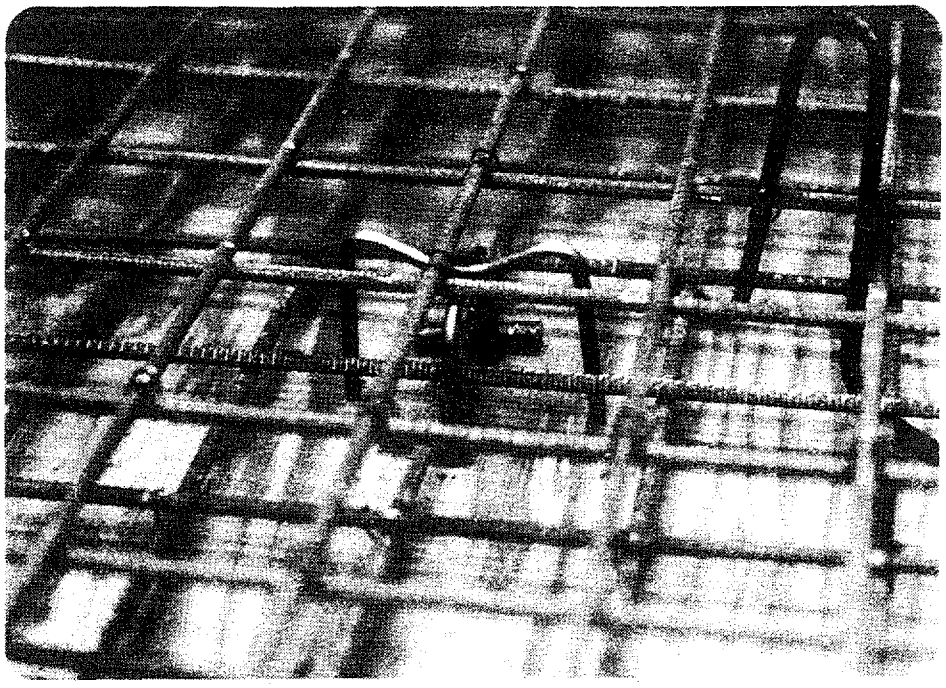

(a) Spacers

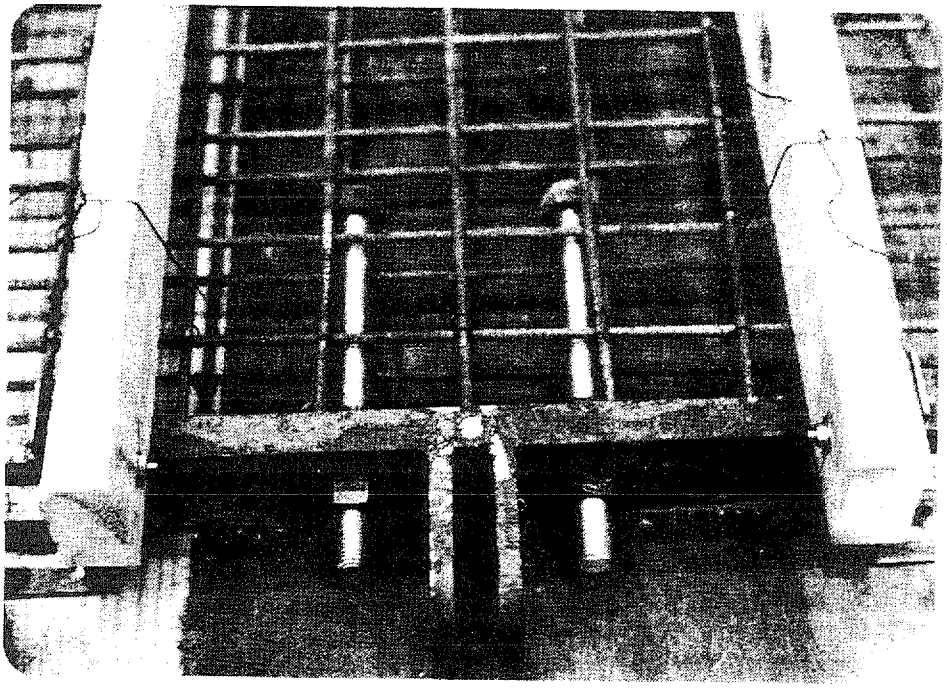

(b) Connecting Bolts

Fig. C.15 Fabrication of Specimen

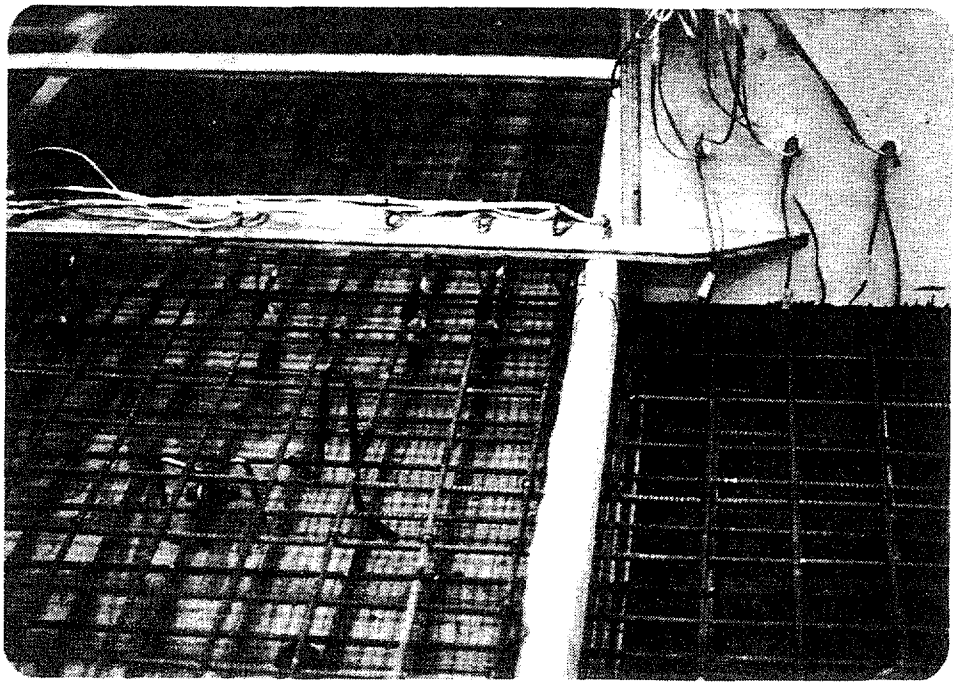

(c) Attached Gages

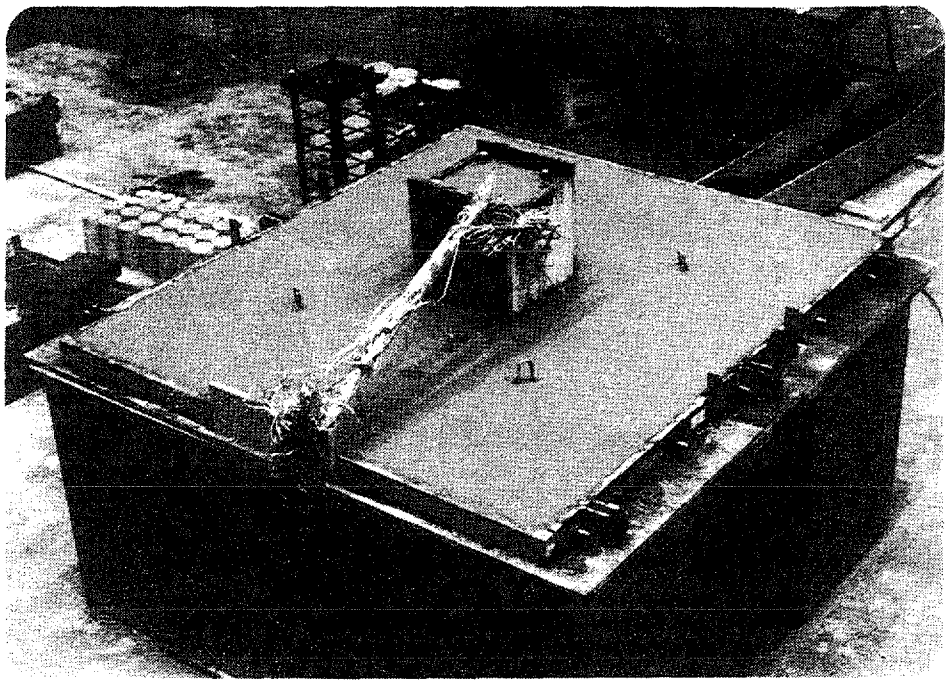

(d) After Casting

Fig. C.15 (contd.) Fabrication of Specimen

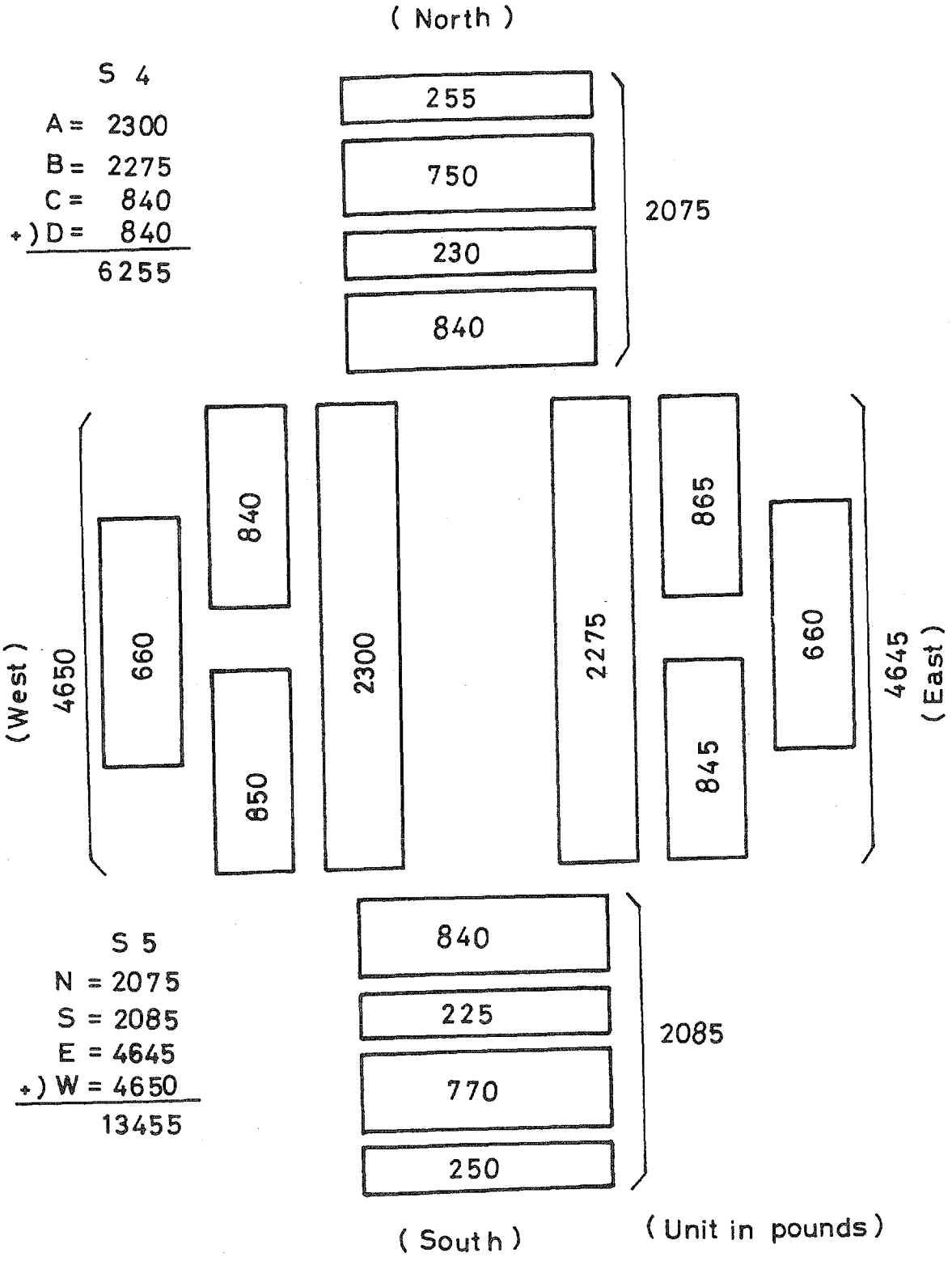

Fig. C.16 Arrangement of Steel Weight

APPENDIX D

OUTLINE OF EXPERIMENTAL WORK: DYNAMIC TESTS

D.1 Dynamic Tests: Test Specimen

The specimens that were tested dynamically--on the earthquake simulater at the University of Illinois (44)--were reproductions of those tested statically. Three specimens were constructed to match the range of reinforcement ratios in the statically tested specimens; these dynamically tested column-slab connections corresponded to statically tested specimens S1, S2 and S3.

The appearance of the dynamically tested specimens would, at a first glance, seem identical to those tested statically; overall slab dimensions were the same; the column cross section was also 305mm x 305mm (12 in. x 12 in.); bolts were cast to protrude from the longitudinal edge of the slab for assembling support along that boundary; a steel plate at the base of the column provided the required connection point to the hinge at the column base. (Details in Fig. D.1.)

On closer inspection the top portion of the column would betray the difference in testing procedures; the dynamically tested specimens had a longer column with a shaft cast at the same height above the slab as that at which the jack force was applied in the static case. (See Fig. D.2.) The shaft through the column allowed masses to be hung on either side of the column creating significant inertial forces during the dynamic testing.

Reinforcing bars used in the specimens were taken from the same heat as those used in the statically tested slab-column connections. The column reinforcement comprised four No. 8 (25mm) bars (Grade 60), and stirrups of

No. 2 (6mm) bars spaced at not more than 100mm. Stirrups were positoned at 50mm spacings for 150mm on either side of the shaft passing through the column. This accommodated local stresses at the shaft. In casting, a 76mm thick slab was called for; as can be seen in Fig. D.3, the as-built dimension was very close to this value.

D.2 Dynamic Tests: Materials

With respect to the materials used in construction, the statically and dynamically tested specimens were alike.

The resulting characteristics of the 1.00:3.51:2.63 (cement:sand: gravel) and 0.8:1.0 (water:cement) concrete mix are reported in Table D.1. The listed values were obtained from nine standard (6 by 12 in.) cylinders. Three were used to find the compressive strength of the concrete at 7 days; six were tested on completion of the experimental procedure, three to obtain tensile splitting stress, and three for stress-strain relationships. A typical stress-strain curve for the concrete is shown in Fig. D.4.

Table D.2 shows the results obtained from testing three reinforcing bar coupons from each specimen. The No. 2 deformed bars were taken from the same heat of steel as those used in the static test specimens. For the steel an idealized stress-strain curve is shown in Fig. D.5.

D.3 Dynamic Tests: Fabrication of Specimens

The same design was used to make up formwork for both test series (dynamic and static).

Column reinforcement was partially made up--no stirrups were fixed above the slab level--and positioned in the formwork. The completed mat of lower-slab steel was dropped through the longitudinal column bars to rest on spacers on the slab formwork; the mat of upper-slab reinforcing followed,

resting on spacer chairs. The average measured effective depth of the longitudinal reinforcement (measured after testing) was 64 mm for specimens D1 and D2, and 62 mm for specimen D3. By fixing the remainder of the column stirrups above slab level, the reinforcement cage was ready for the concrete placement.

Bolts, required for assembly of a specimen in the test setup, were positioned at appropriate locations in the longitudinal steel (25mm x 76mm x 1829mm) edges of the slab formwork prior to concreting. Also, before casting, the base plate of the column was carefully weighted down by adding steel weights to channels bolted to the underside of the base plate. In this manner the plate, and the column reinforcement attached to it, was held firm and level during the robust process of pouring and vibrating concrete; an acceptable fit in the experimental setup depended on a plumb column.

Casting of the reinforced concrete specimen took place in two pours; the first placed concrete in the slab and the column up to a level about 75mm above the slab; and last pour completed the column.

A capping plate was put on the top of the column, and welded to the longitudinal column reinforcement in a fashion described in the static specimen documentation.

The specimens and cylinders were cured under wet burlap and plastic sheets for a week, at which time they were uncovered and kept in the laboratory until the test day.

D.4 Dynamic Tests: Test Setup

A schematic view of the specimen on the University of Illinois shake table is provided in Fig. D. 6. A photograph of the actual assembly is shown in Fig. D.7.

The dominant feature of the assembly on the shake table is the attached mass system comprised of equal masses on either side of the column. A front view of the mass is shown in Fig. D.8, and from this angle cross-bars can be seen that were used to position the two halves. Longer cross-bars provided the means of adding further mass during testing by guiding such masses into position.

Also apparent in Fig. D.8 is the cross-bracing between the support legs along the front edge of the assembly. Cross-bracing was used to restrict movement transverse to the principal direction of motion.

Another motion that would jeopardize the validity of test readings is slippage between the column base plate and the column hinge. Fig. D.9 shows this hinge connection, and Fig. D.10 shows the hinge after angles have been welded to the column base plate (at each corner). The prupose of the angles was to counter slippage by tightening bolts, mounted in the angles, up against the hinge.

A very important characteristic of a specimen undergoing dynamic testing is its mass. The measured weight of each specimen with the fittings it had during testing is shown in Table D.4. (It was mentioned previously, and viewed in Fig. D.8. that additional masses were hung on the sides of the column to create significant inertial forces.) As the relatively heavily reinforced slab in specimen D3 was expected to resist higher loads, provision was made to add more mass to the specimen during testing. Total weights for the different combinations of masses used on either side of the column are listed in Table D.3.

It is reassuring to notice in Fig. D.11 that the levels of crucial parts in the specimens were very close to target values. Listed in

Fig. D.11 are the results of readings derived from a sophisticated Wild level, before testing of a specimen had taken place. As the various instrument mountings were located at these levels, observed data could be evaluated with confidence when the position at which it was taken was of interest.

D.5 Dynamic Tests: Instrumentation

Absolute accelerations and relative displacements were measured at points on the structure. In some instances measurements were used to monitor the success of the modelling. In all, 26 instrument positions were used. These were divided into two independent sets of 13 readings each. During testing, two different tape-drives were used to record the two groupings.

D.5.1 "Tape 1" The information contained on this tape contained the main output of an experiment. A schematic drawing (Fig. D.12) is used to show the position of the differential transformers (LVDT's) and accelerometers.

Channel 1 measured the input acceleration, and was used for synchronization in the process of data reduction.

LVDT measurement positons 2 and 3 were at the level of the attached masses. They provided a check on one another during data reduction; they should not indicate significant differences. Were differences observed, it would mean that the column had twisted; an undesirable motion. For the same reason LVDT locations 4 and 5 would be a way of picking up any in-plane twisting motion that the slab might undergo. The combined observations of LVDT's 2 and 4, for example, indicated very clearly whether the column was behaving as a rigid member; the reading taken at instrument 4 should

be half of that at position 2. Once the rigid behavior of the column was proven, the two locations 2 and 4 could be used--if necessary--to subtract off any unwanted column-hinge slippage (top reading (2) - slab reading (4) times 2 = "purified" top reading). The remaining LVDT, channel 6, was at the theoretical position above the hinge at which all the mass of a specimen would have to be concentrated to provide an equivalent kinetic energy for the specimen. (In other words, if it were physically possible to combine the structure's mass with that of the attached mass and lump it at one location.)

Accelerometer records at positions 8 and 7 correspond to LVDT measuring levels; the LVDT provided deformation information and the accelerometers the amount of inertial force in the longitudinal direction. For the same reason an accelerometer was placed at position 12, in line with LVDT 6. The accelerometer at the base of the column hinge, position 11, was required to gauge the input base motion that the assembly was subjected to; analyses from steady-state tests demanded it, as well as the calculation of response spectra. Completing the array of accelerometers were those at position 9 and 10 giving a measure of the transverse acceleration experienced by the slab.

D.5.2 "Tape 2" This "tape" furnished insurance for some vital measurements recorded on "tape 1." In this sense--referring to Fig. D.12--accelerometers at positions 2, 3 and 13 duplicate records at the centroid of the attached mass, the slab level and the base of the specimen.

Accelerometer positon 4 gave more lateral acceleration information. The remaining instruments, the vertically mounted LVDT's, could be used to gain additional information of the slab behavior (LVDT's 5 to 12).

D.6 Dynamic Tests: Data Acquisition and Reduction System

Readings obtained from the instruments discussed in the previous section were recorded on two tapes for each particular specimen; the data was in analogue form. An audio channel on each tape was used to make comments on during the testing, and also to identify progress in the procedure. An automatic process recorded sufficient portions of each step in the test.

After testing had been completed, the raw data in its analogue format was copied and processed creating a new tape of digital data. This tape--containing the raw data in digital fashion--was used to obtain calibration factors necessary for each step in the testing sequence. With the appropriate calibration factor a channel of data could be transformed from its voltage reading on the raw data tape to a physical vlaue, and stored on magnetic tape for further use (such as plotting).

The Cyber 175 of the Computer Department at the University of Illinois (Urbana-Champaign) was used for data handling and manipulation.

D.7 Dynamic Tests: Test Procedure

Response to three types of motion were recorded during the testing of a specimen; simulated earthquake, steady-state and free-vibration runs were introduced.

The simulated earthquake base motion was that of the 1940 North-South El Centro record. In the steady-state testing a sinusoidal base excitation was performed; the input frequency was incremented to span the range of response from before the resonance of the specimen to after this occurrence. By connecting a wire to the steel capping plate on the column and hanging

weights at the other end of the wire, a free-vibration motion was introduced when the weights were released instantaneously.

As far as was possible, the described motions were performed in the same sequence for each of the dynamically tested specimens. This idealized test program is listed in Table D.5.

Specimen D2 was the first in the dynamically tested series, and deviated from the idealized test sequence in some respects (Table D.7). Relatively low intensity base motions were used to gauge the conduct of the column hinge; hence, the large number of sequence steps in the test. Column-hinge slippage was eliminated as described in Section D.4 and Fig. D.9 to D.10. The positioning of the instruments was such that slippage--were it to occur--could be extracted from the records.

Specimen D1 followed schedule very closely. (See Table D.6.) The steady state tests were, on occassions, done in groups of 3. Consider, for example, steady-state 2.1, 2.2 and 2.3 to compose steady-state 2. A low amplitude steady-state test was planned (steady-state 2.1) before a large amplitude test (steady-state 2.2). The third component (steady-state 2.3) was also a small displacement steady-state test. In this fashion the large amplitude test--which could possibly surpass the maximum displacement previously undergone by the specimen--was sandwiched between two steady-state tests that could monitor damage which may occur. A worthwhile comparison between large and small amplitude steady-state tests was also afforded by the described pattern.

D3, too, employed a test sequence close to the idealized sequence of Table D.5. In the comments on Table D.8 two positions are indicated at which mass was added to the attached column mass; the first addition took place after free-vibration No. 6, and the second after free-vibration No. 8.

TABLE D.1 Measured Properties of Concrete

PARAMETER	TEST STRUCTURE		
	D1 ρ = .0065	D2 .0098	D3 .0131
Age at Testing [Days]	60	23	79
Slump [mm]	127	178	127
Compressive Strength f'_c [MPa]	36.3	33.9	36.5
Secant Modulus $E_c * 10^4$[MPa] (calculated at 9.76 MPa)	3.37	2.93	3.20
Tensile Strength f_{sp} [MPa]	3.3	2.3	3.0
Compressive Strength at 1 week [MPa]	24.4	24.5	24.4
Modulus of Rupture [MPa]	6.8	7.2	6.7

TABLE D.2 Measured Properties of Reinforcement

PARAMETER	TEST STRUCTURES					
	D1		D2		D3	
	* $\bar{x}$	(c.o.v.)	* $\bar{x}$	(c.o.v.)	* $\bar{x}$	(c.o.v.)
Yield Stress f_y [MPa]	290	(0.04)	327	(0.05)	355	(0.05)
Yield Strain						
ε_y	0.0015	(0.09)	0.0015	(0.25)	0.0015	(0.04)
ε_h	0.0113	(0.10)	0.0200	(0.09)	0.0182	(0.17)
Maximum Stress f_u [MPa]	464	(0.02)	477	(0.05)	492	(0.03)
Strain at Max. Stress ε_u	0.165	(0.03)	0.146	(0.05)	0.138	(0.18)
Fracture Strain ε_b	0.280	(0.09)	0.208	(0.18)	0.172	(0.22)

* $\bar{x}$ = mean value

c.o.v.= coefficient of variance

TABLE D.3 Total Weight of Attached Mass

MEASUREMENT	TEST STRUCTURE			COMMENTS
	D1	D2	D3	
BASIC ASSEMBLY	13.789 kN	13.789 kN	13.789 kN	2/228mm Thick Masses Complete with bars and nuts.
BASIC ASSEMBLY with 2/76mm Thick masses added.	-	-	18.103 kN	2/228mm Thick + 2/76mm Thick Masses Complete with bars and nuts.
BASIC ASSEMBLY + 2/76 mm Thick Masses. +2/50 mm Thick Masses.	-	-	21.039 kN	2/228 mm Thick +2/76 mm Thick +2/50 mm Thick Masses Complete with bars and nuts.

TABLE D.4 Total Weight of Specimens

MEASUREMENT	TEST STRUCTURE			COMMENTS
	D1	D2	D3	
WEIGHT OF SPECIMEN	9.341 kN	9.488 kN	9.621 kN	Weight includes fixtures, bearings, steel edge plates, instrument frame.

TABLE D.5 Idealized Testing Sequence

SEQUENCE	SIMULATED EARTHQUAKE RUN No.	FREE VIBRATION No.	STEADY STATE No.	COMMENTS
1		1		
2	1			
3		2		
4	2			
5		3		
6			1	
7		4		
8	3			
9		5		
10			2	
11		6		
12	4			
13		7		
14			3	
15		8		
16	5			
17		9		
18			4	
19		10		
20	6			
21		11		
22			5	

TABLE D.6 Test Sequence: D1

SEQUENCE	SIMULATED EARTHQUAKE RUN No.	FREE VIBRATION No.	STEADY STATE No.	COMMENTS
1		1		
2	1			
3		2		
4	2			
5		3		
6			1	
7		4		
8	3			
9		5		
10.1			2.1	
10.2			2.2	
10.3			2.3	
11		6*		*Lost, Electrical Fault.
12	4*			
13		7		
14.1			3.1	
14.2			3.2	
14.3			3.3	
15		8		
16	5			
17		9		
18.1			4.1	
18.2			4.2	
18.3			4.3	
19		10		
20	6			
21		11		
22			5	

TABLE D.7 Test Sequence: D2

SEQUENCE	SIMULATED EARTHQUAKE RUN No.	FREE VIBRATION No.	STEADY STATE No.	COMMENTS
1		1		
2	1			
3		2		
4	2			
5		3		
6	3			
7		3.1		
8			1	
9		4*		*Lost, Electrical Fault.
10	3.1			
11		5		
12			2	
13		6		
14	4**			**Hinge Difficulty
15		7		
16			3	
17		8		
18	5**			**Hinge Difficulty
19		9		
20			4	
21		10		
22	6**			**Hinge Difficulty
23	7			
24		11		
25			5	
26	8			
27		12		
28	9			
29			6	
30	10			
31			7	

TABLE D.8 Test Sequence: D3

SEQUENCE	SIMULATED EARTHQUAKE RUN No.	FREE VIBRATION No.	STEADY STATE No.	COMMENTS
1		1		
2	1			
3		2		
4	2			
5		3*		*Lost, Elec. Fault.
6			1	
7		4		
8	3			
9		5		
10.1			2.1	
10.2			2.2	
10.3			2.3*	*Lost, Elec. Fault.
11		6		
11.1		6.1**		**Additional Attached Mass.
12	4			
13		7*		*Lost,Elec. Fault.
14.1			3.1	
14.2			3.2	
14.3			3.3	
15		8		
15.1		8.1***		***More Mass Attached.
16	5			
17		9		
18.1			4.1	
18.2			4.2	
18.3			4.3	
19		10		
20	6			Elec. = Electrical
21		11		
22	7			
23	8			

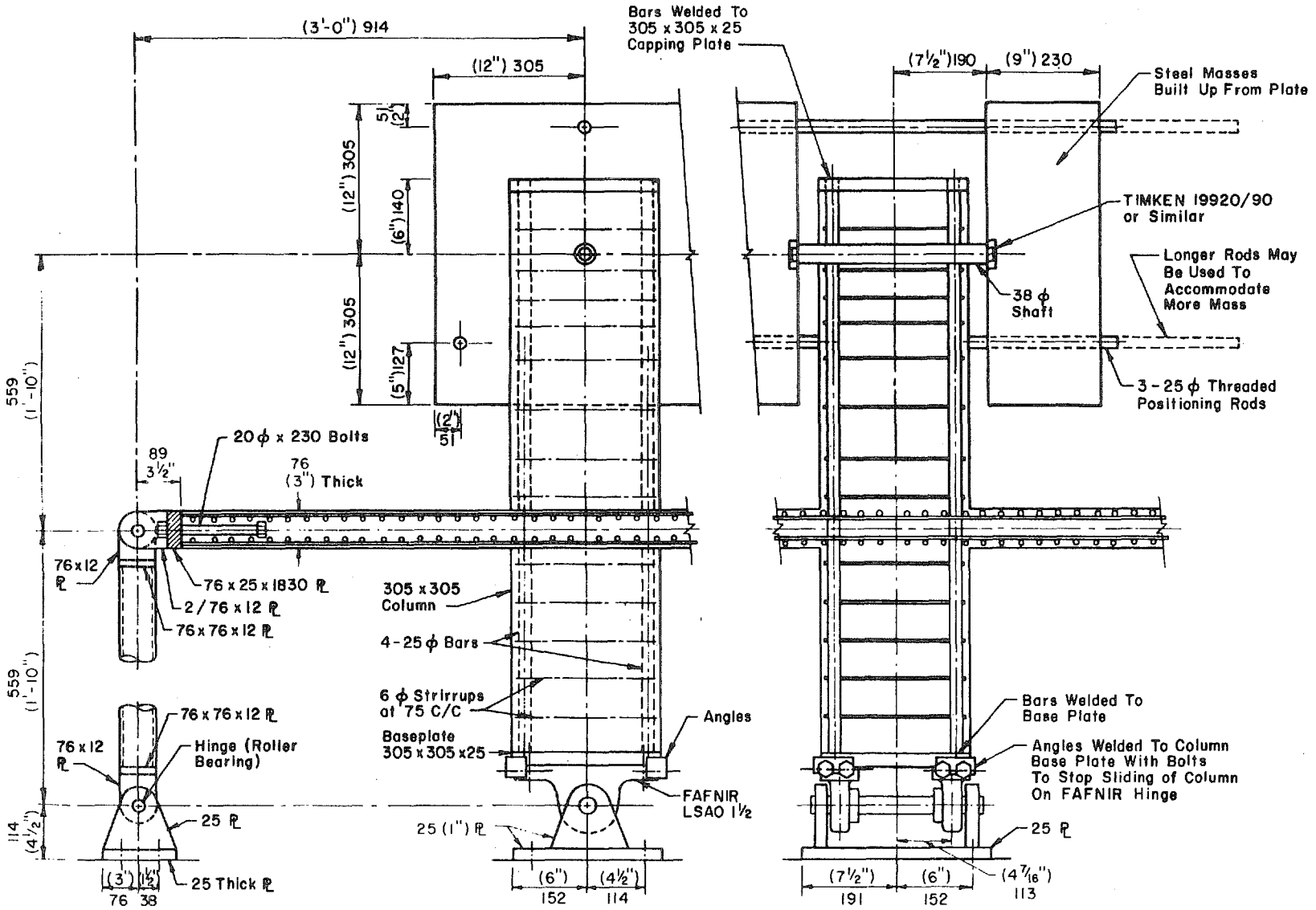

Fig. D.1 Typical Details of Specimens

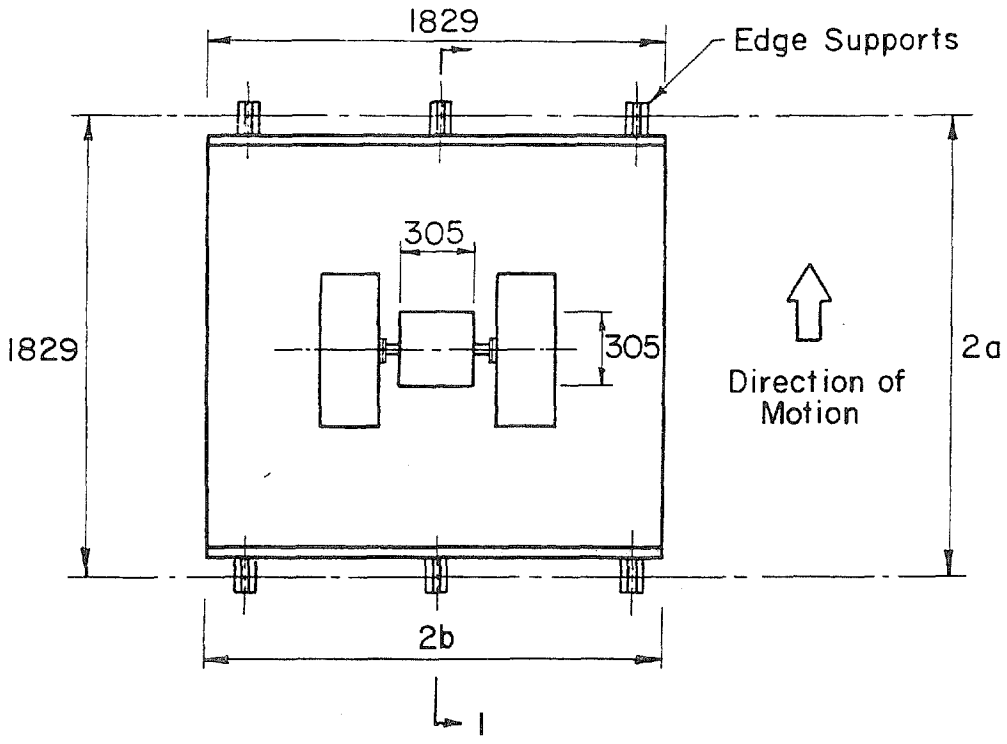

Plan of Plate

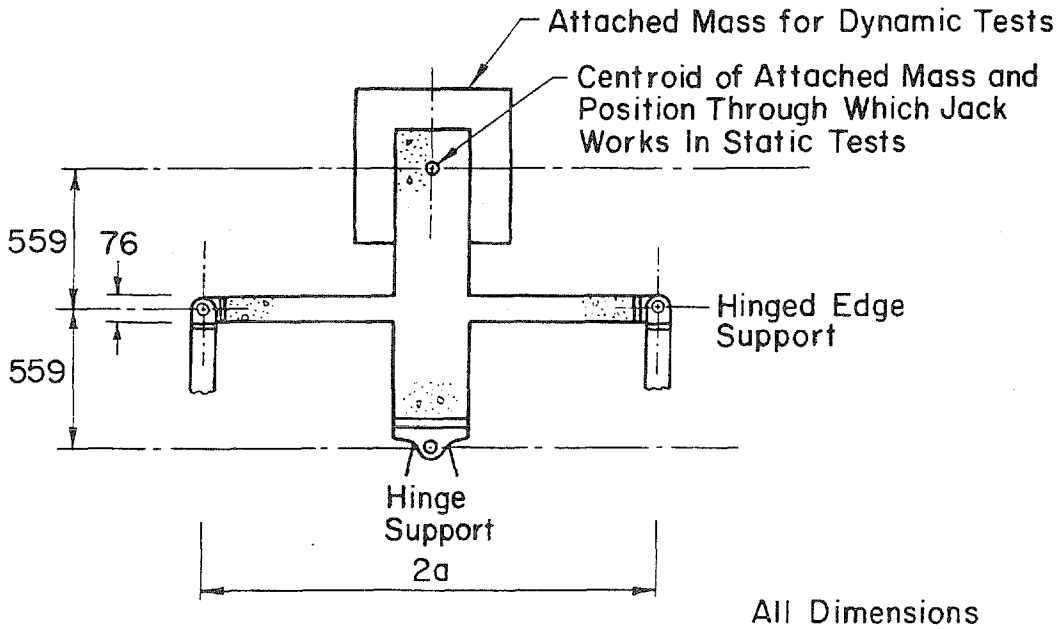

Section I-I

Fig. D.2 Specimen Plan and Section

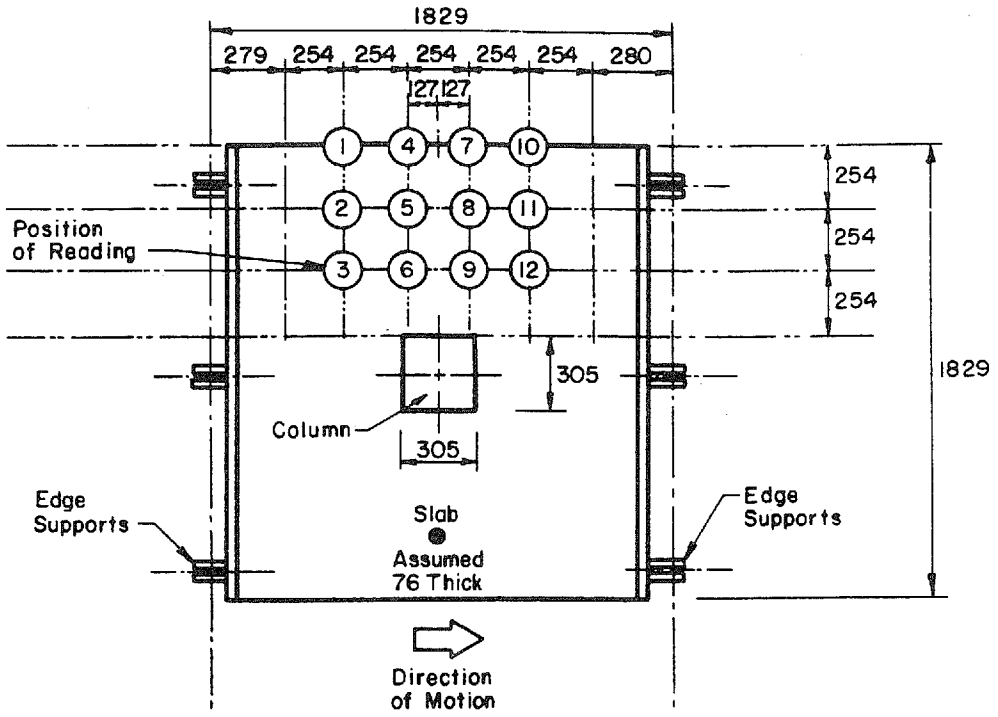

Plan of Column-Slab Specimen Indicating Thickness Measurement Points

THICKNESS OF SLAB (MM)			
POSITION	SPECIMEN: D1	D2	D3
1	77.1	--	--
2	75.2	77.5	77.3
3	75.3	77.5	78.0
4	76.7	78.0	77.9
5	77.6	77.0	77.3
6	76.2	77.2	77.9
7	76.1	77.2	77.3
8	76.4	77.7	77.9
9	75.1	77.3	78.2
10	75.3	--	--
11	74.5	77.1	77.1
12	73.8	77.1	77.3
AVERAGE	75.8	77.4	77.6

Fig. D.3 Measurements of Slab Thickness

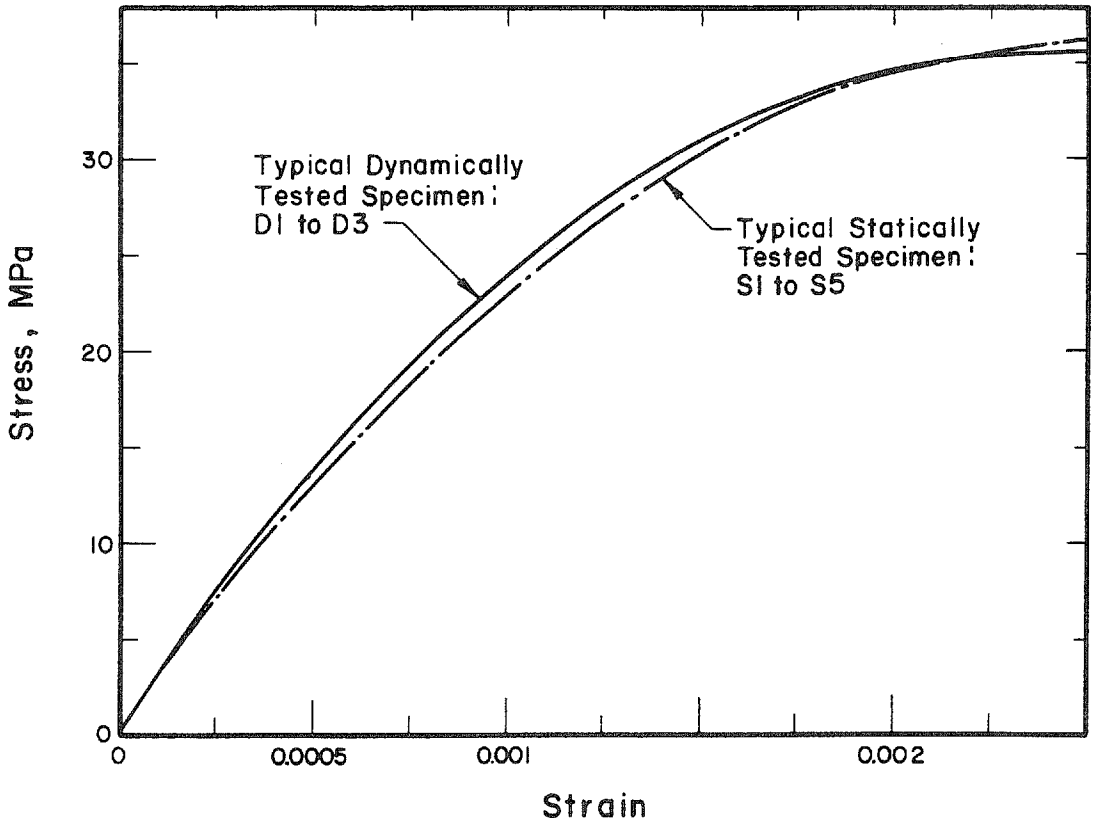

Fig. D.4 Typical Concrete Stress-Strain Relationship

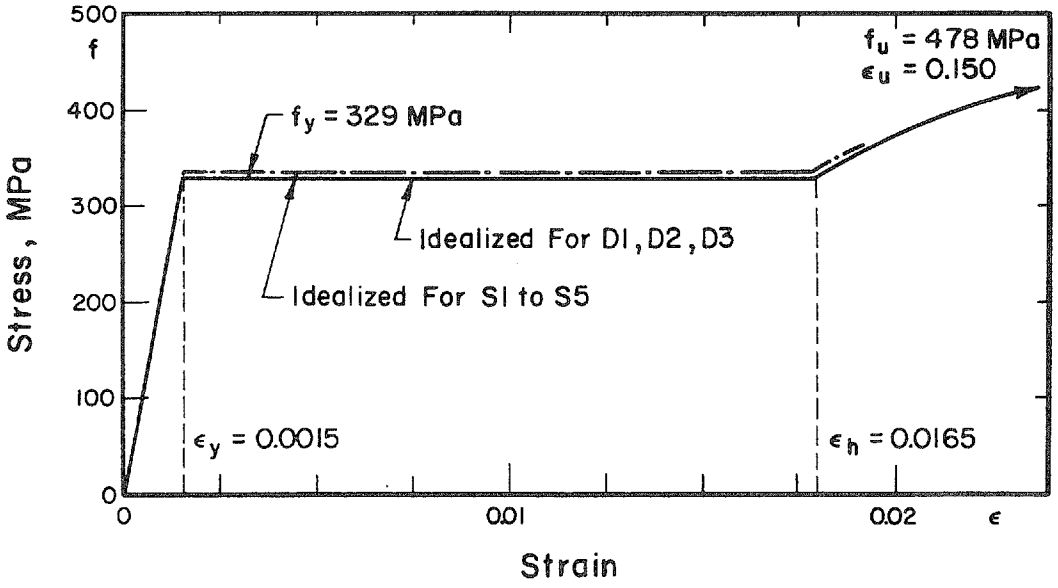

Fig. D.5 Typical Steel Stress-Strain Relationship

(All Dimensions In Meters)

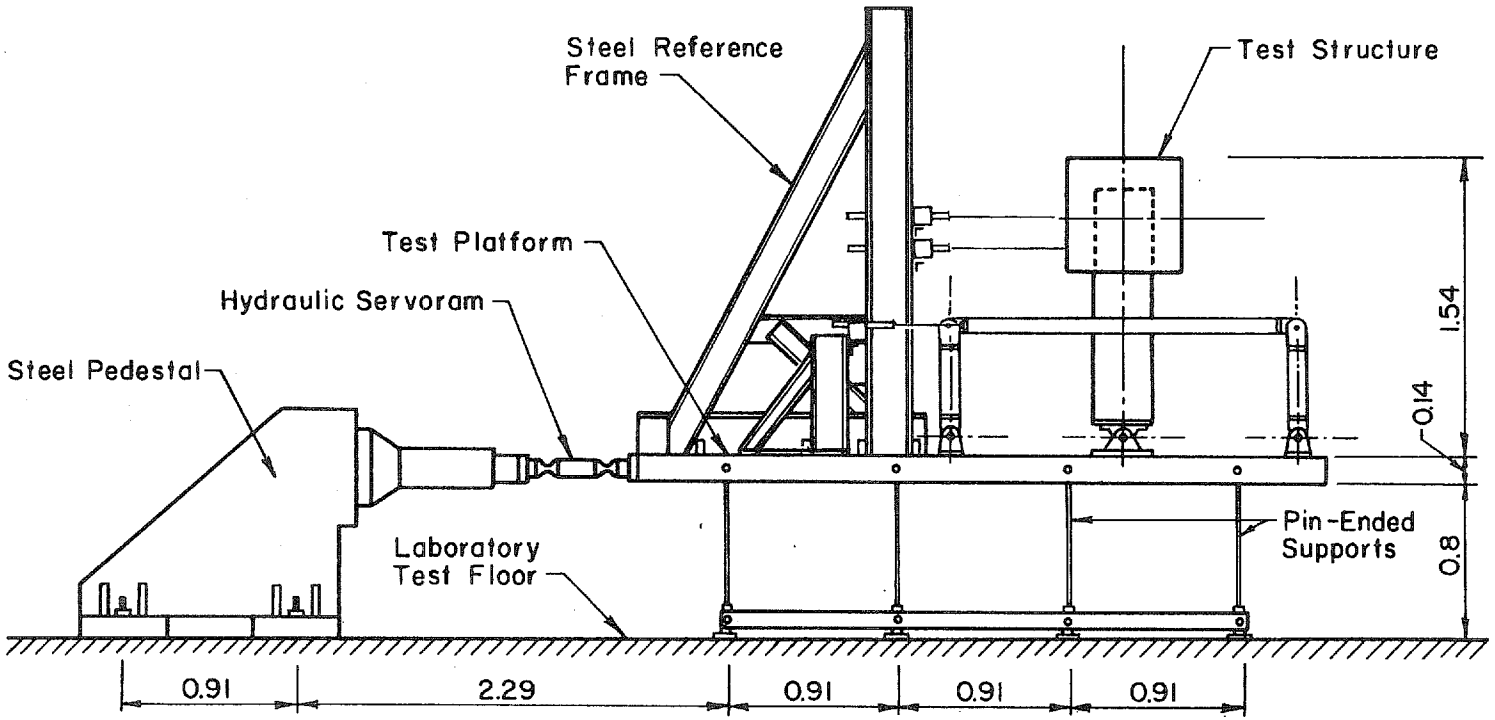

Fig. D.6 Test Setup

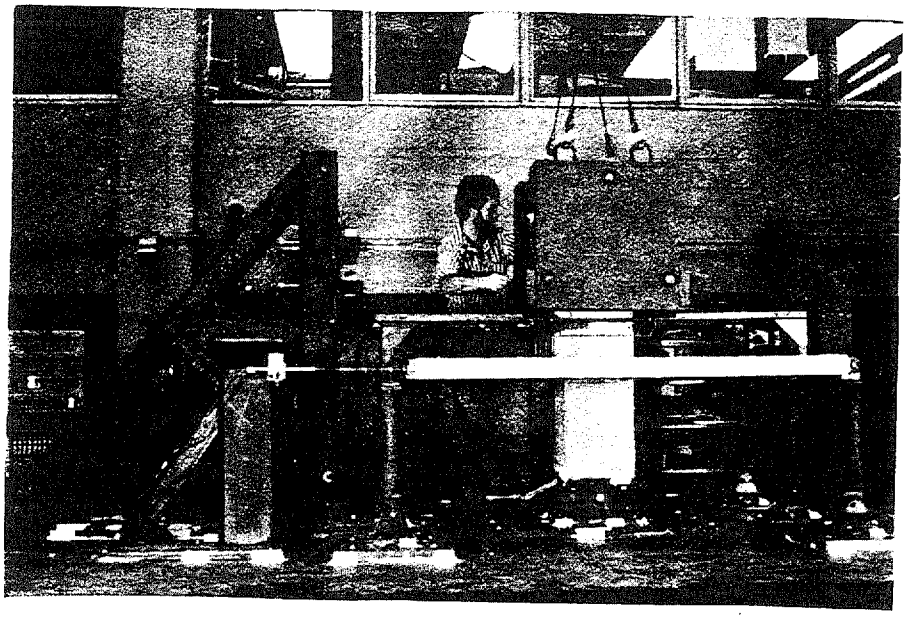

Fig. D.7 Test Assembly

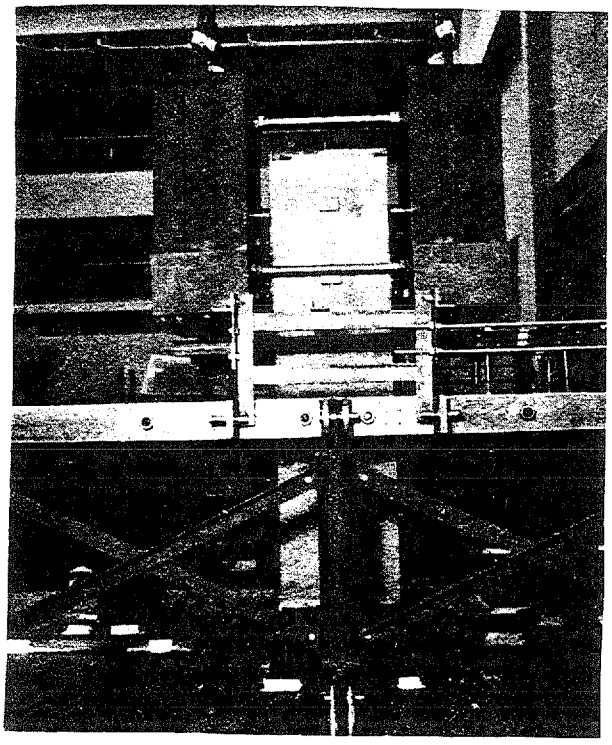

(a) Detail of Attached Mass

Fig. D.8 Front Elevation of Assembly

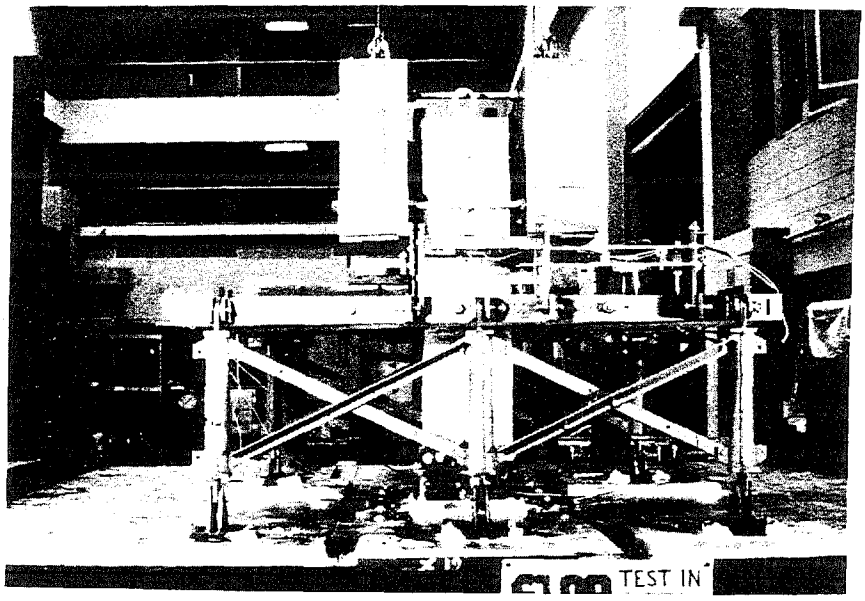

(b) Test Assembly

Fig. D.8 (contd.) Front Elevation of Assembly

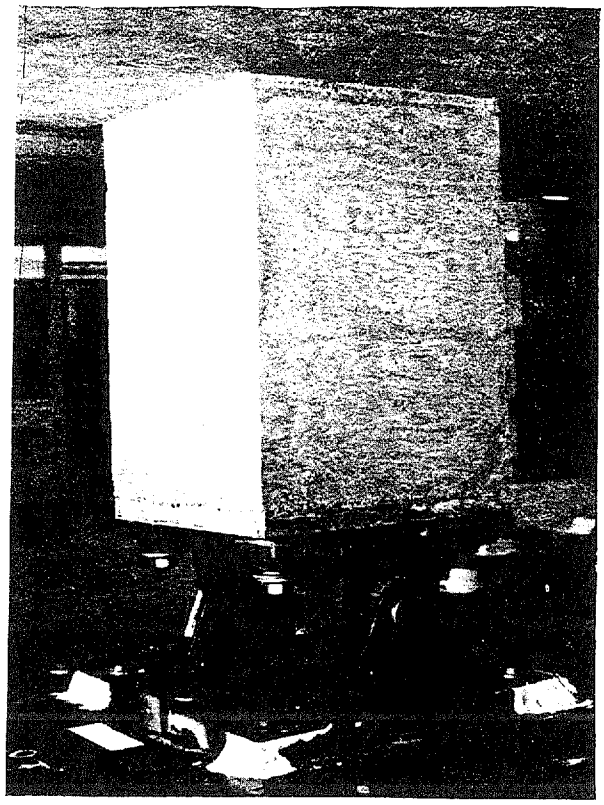

Fig. D.9 Central Hinge

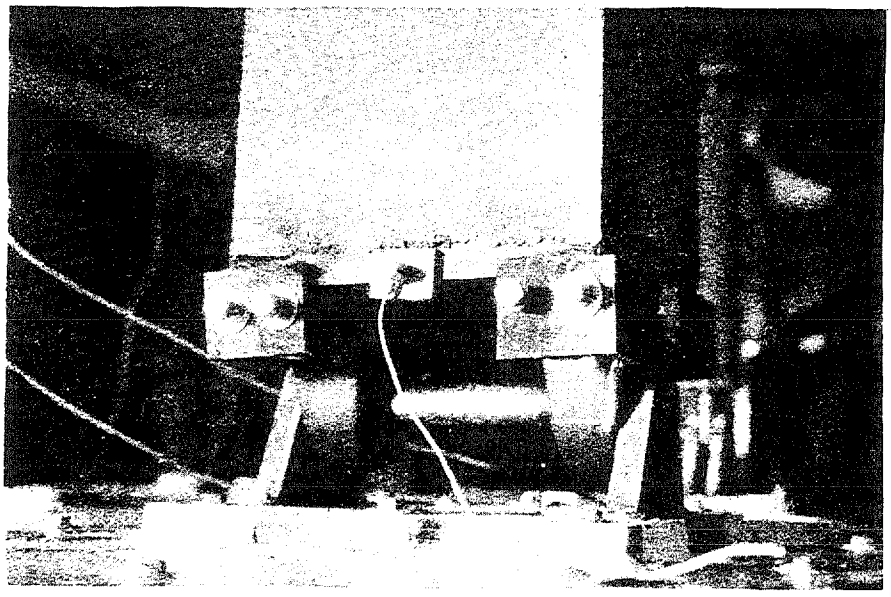

Fig. D.10 Central Hinge with Angles

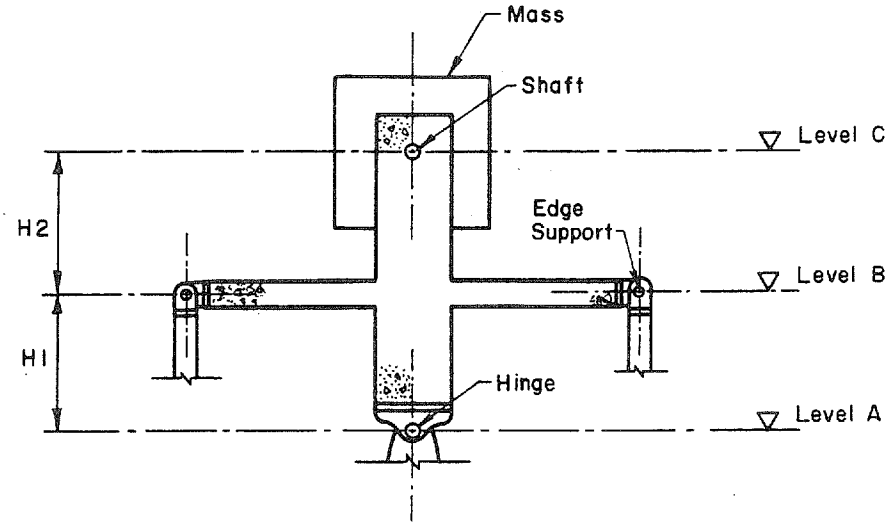

Section Through Specimen

MEASURE-MENT	SPECIMEN			COMMENTS
	D1	D2	D3	
	[mm]	[mm]	[mm]	
LEVEL A	0.0	0.0	0.0	REDUCED ZERO LEVEL
LEVEL B	558.0	559.0	559.0	TARGET DIMENSION = 559 mm
DIMENSION H1	558.0	559.0	559.0	
LEVEL C	1116.3	1117.2	1118.0	TARGET DIMENSION = 559 mm
DIMENSION H2	558.3	558.2	559.0	

Fig. D.11 Measured Levels of Important Positions on Specimens

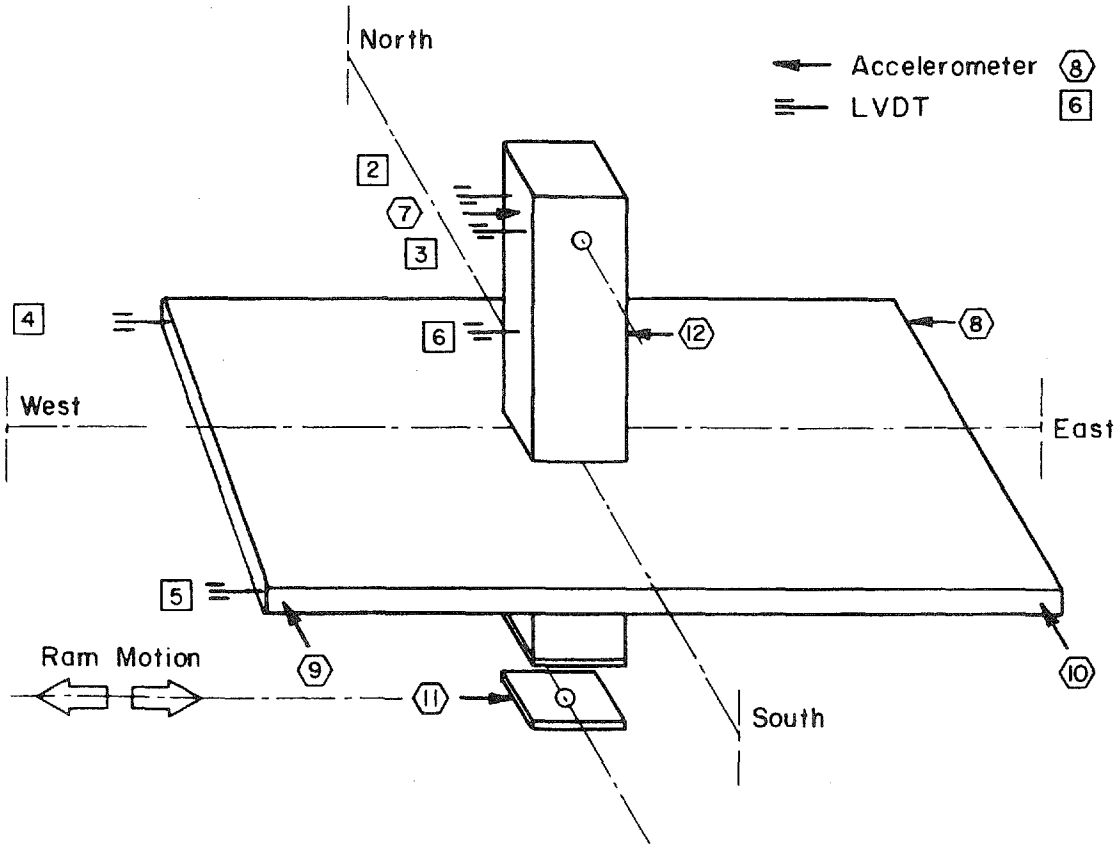

CHANNEL No.	TYPE	DESCRIPTION
1	ACCELEROMETER	INPUT
2	LVDT	LONGITUDINAL COLUMN DISPLACEMENT, TOP NW
3	LVDT	LONGITUDINAL COLUMN DISPLACEMENT, TOP SW
4	LVDT	LONGITUDINAL SLAB DISPLACEMENT, NW
5	LVDT	LONGITUDINAL SLAB DISPLACEMENT, SW
6	LVDT	LONGITUDINAL COLUMN DISPLACEMENT, CENTROID
7	ACCELEROMETER	LONGITUDINAL COLUMN ACCELERATION, TOP W
8	ACCELEROMETER	LONGITUDINAL SLAB ACCELERATION, NE
9	ACCELEROMETER	LATERAL SLAB ACCELERATION, SW
10	ACCELEROMETER	LATERAL SLAB ACCELERATION, SE
11	ACCELEROMETER	LONGITUDINAL TABLE ACCELERATION, BASE W
12	ACCELEROMETER	LONGITUDINAL COLUMN ACCELERATION, CENTROID
13	DISPLACEMENT	LONGITUDINAL RAM DISPLACEMENT

Fig. D.12 Instrument Positions ("Tape 1")

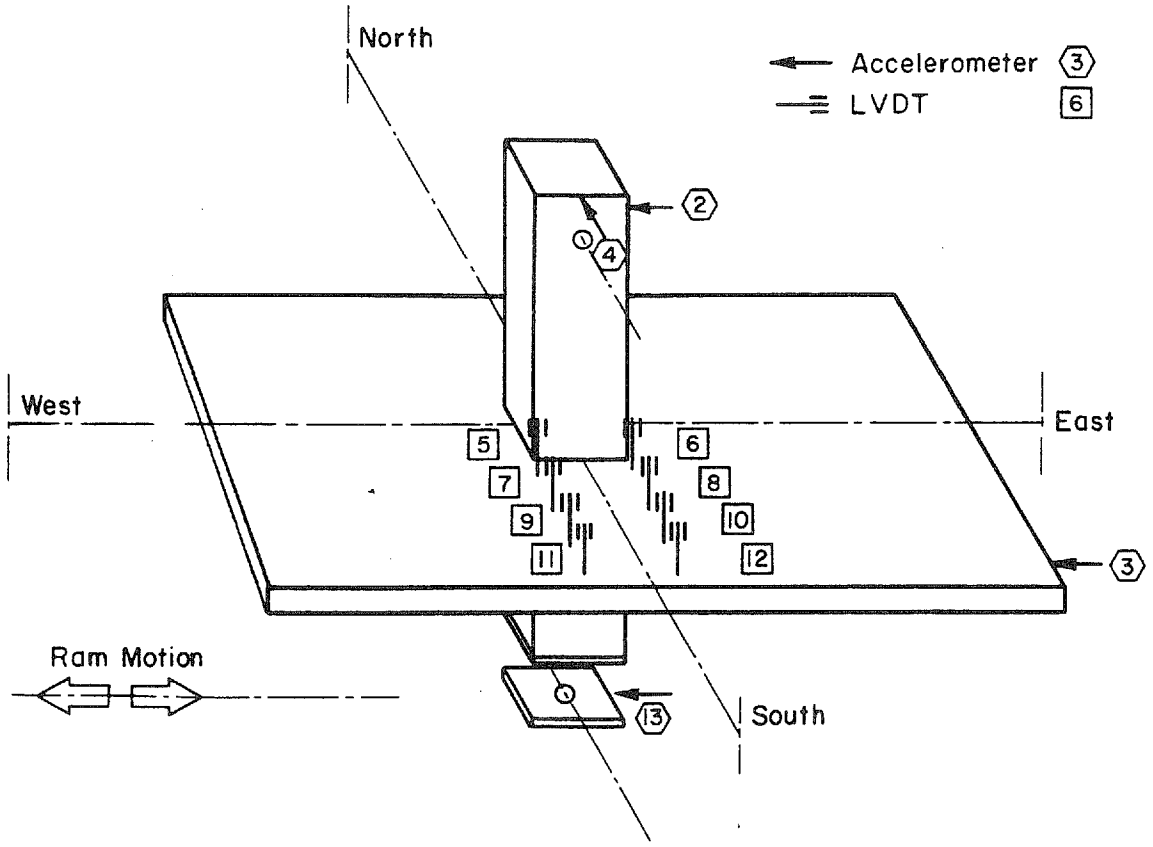

CHANNEL No	TYPE	DESCRIPTION
1	ACCELEROMETER	INPUT
2	ACCELEROMETER	LONGITUDINAL COLUMN ACCELERATION, TOP E
3	ACCELEROMETER	LONGITUDINAL SLAB ACCELERATION, SE
4	ACCELEROMETER	LATERAL COLUMN ACCELERATION, TOP S
5	LVDT	VERTICAL SLAB DISPLACEMENT, LVDT A
6	LVDT	VERTICAL SLAB DISPLACEMENT, LVDT B
7	LVDT	VERTICAL SLAB DISPLACEMENT, LVDT C
8	LVDT	VERTICAL SLAB DISPLACEMENT, LVDT D
9	LVDT	VERTICAL SLAB DISPLACEMENT, LVDT E
10	LVDT	VERTICAL SLAB DISPLACEMENT, LVDT F
11	LVDT	VERTICAL SLAB DISPLACEMENT, LVDT G
12	LVDT	VERTICAL SLAB DISPLACEMENT, LVDT H
13	ACCELEROMETER	LONGITUDINAL TABLE ACCELERATION, BASE E

Fig. D.13 Instrument Positions ("Tape 2")